

THE UNIVERSITY OF HULL

An investigation into the regulation of cellular homeostasis through
modulation of cell-surface tissue factor

Thesis submitted to the University of Hull towards the degree of
Doctor of Philosophy

by

Yahya Awaji Madkhali

August 2020

Abstract

In recent years it has become evident that cell-derived microvesicles (MV) influence the recipient cells through inducing signalling mechanisms which lead to cell proliferation or apoptosis. In addition, the excessive release of procoagulant MV during chronic diseases including cancer, sepsis and cardiovascular disease, appears to advance the severity of these diseases. MV released in response to inflammatory stimuli, mostly carry the proteins tissue factor (TF), coagulation factor VIIa (fVIIa) and negatively charged phospholipids. The formation of the TF-fVIIa complex is known to activate protease activated receptor 2 (PAR2) which in turn promotes the release of additional TF-containing MV by cells. In this study, the ratio of fVIIa:TF carried on the surface of MV was measured and its influence on cell proliferation, apoptosis and PAR2 activation was assessed. Incubation of cells with MV containing the highest ratios of fVIIa:TF (38:1 and 54:1) were shown to be proliferative, while at lower ratios (10:1), the MV were shown to be pro-apoptotic. To investigate the requirements for the activation of PAR2 on cell lines and endothelial cells, the cDNA for PAR2 was cloned and expressed as a hybrid protein, in tandem with either mCherry or mEmerald. The digestion of PAR2 resulted in the release of the fluorescent group into the media which was then measured using a fluorescence plate-reader. Analysis of the cell lines and endothelial cells treated with procoagulant MV indicated that the activation of PAR2 on the surface of the transfected cells was proportionately dependent on the fVIIa:TF ratio. Furthermore, incubation of the transfected endothelial cells with either the MV, or combinations of fVIIa and recombinant TF confirmed the dependence of PAR2 activation on the fVIIa:TF ratio with which the cells come into contact. In the final section of the study, the association of TF-fVIIa complex with PAR2 and also with the caveolae on the cell surface was investigated, and alternative mechanisms for clearance of TF were explored. Knock-down of fVII using specific siRNA prevented the association of TF with PAR2 as examined by the proximity ligation assay (PLA). In addition, incubation of cells with excess amounts of Texas Red labelled-recombinant TF indicated the association of TF with lipid rafts as identified by NBD-cholesterol loading. The exogenous recombinant TF also co-localised with caveolin-1 as determined by PLA.

Disruption of lipid rafts using methyl- β -cyclodextrin (M β CD) enhanced the pro-apoptotic influence of the TF in endothelial cells indicating that the TF associated with lipid rafts is maintained in a functionally inactive form. Additionally, a series of experiments indicated the potential of the currently used direct oral anticoagulant Apixaban, to reduce the damage arising from the procoagulant MV. In conclusion, this study has shown that cellular regulation of TF by cells determines the fate of the cells following injury. This is dependent on the ratio of fVIIa and TF carried on MV, which may lead to growth or clearance of cells. In addition, cells regulate the level of TF by two separate mechanisms, both of which are dependent on PAR2 signalling. While these mechanisms ensure the survival of cells following injury and trauma, the exhaustion of the cellular capacity, overwhelmed during chronic diseases, appears to be an underlying cause of vascular deterioration, but there is potential to modulate these interactions for therapeutic benefit. Finally, the study indicated the potential of Apixaban to reduce the damage arising from the procoagulant MV.

Acknowledgment

First and foremost, I thank my God for the health, family and all blessing that he bestows upon me. I would like to thank my supervisor Dr Camille Ettelaie for her supervision, encouragement and endless support during the course of my PhD. I would also like to thank my second supervisor Prof. John Greenman for his advices and unconditional helps as well as Prof. Anthony Maraveyas. I was and always will be grateful to you for your support. My special thanks go to my Mom for her continuous support, encouragement and inspiration throughout my PhD. It is my pleasure to express my thanks to the Saudi Ministry of Higher Education and Saudi Cultural Bureau in London for the scholarship and financial support of this research. I am very thankful to all my colleagues especially Ali, Sophie, Mohammad and Naima for their support and help. Special thanks go to my friends Adeeb, Erriche, Mossad and Esam for their supports and advices.

Publication and presentation

Papers

Madkhali, Y., Featherby, S., Collier, M., Maraveyas, A., Greenman, J. and Ettelaie, C. (2019) The Ratio of Factor VIIa:Tissue Factor Content within Microvesicles Determines the Differential Influence on Endothelial Cells. *TH Open*, 03(02), 132-145.

Featherby, S., Madkhali, Y., Maraveyas, A. and Ettelaie, C. (2019) Apixaban Suppresses the Release of TF-Positive Microvesicles and Restrains Cancer Cell Proliferation through Directly Inhibiting TF-fVIIa Activity. *Thrombosis and Haemostasis*, 119(09),1419-1432.

Ethaeb, A., Mohammad, M., Madkhali, Y., Featherby, S., Maraveyas, A., Greenman, J. and Ettelaie, C. (2019) Accumulation of tissue factor in endothelial cells promotes cellular apoptosis through over-activation of Src1 and involves β 1-integrin signalling. *Apoptosis*, 25(1-2),29-41.

Abstracts

Madkhali Y, Greenman J, Ettelaie C (2017) The synergy between tissue factor-containing microvesicles and PAR2 activation in the induction of apoptosis is dependent on the properties of the cancer-derived microvesicles (poster). Presented at annual conference of extracellular vesicles. Cambridge, UK.

Madkhali Y, Maraveyas A, Greenman J, Ettelaie C (2017) Cancer cell-derived microvesicles induce endothelial cell apoptosis mediated through tissue factor, factor VII and PAR2 activation (poster). Presented at the 9th international conference on thrombosis & hemostasis issues in cancer. University of Bergamo, Italy.

Madkhali Y, Greenman J, Ettelaie C (2017) The synergy between tissue factor-containing microvesicles and PAR2 activation in the induction of apoptosis is dependent on the properties of the cancer-derived microvesicles (poster). Presented in BSHT Annual Scientific Meeting. University of Warwick, UK.

Madkhali Y, Maraveyas A, Greenman J, Ettelaie C (2018) Investigation of Mechanism of Tissue Factor-Mediated Cell Apoptosis (poster). Presented in BSHT Annual Scientific Meeting. University of Warwick, UK.

Madkhali Y, Maraveyas A, Greenman J, Ettelaie C (2019) The ratio of factor VIIa:tissue factor content within microvesicles determines the differential influence on endothelial cells (poster). Presented at congress of the international society on thrombosis and haemostasis. Melbourne, Australia.

Madkhali Y, Maraveyas A, Greenman J, Ettelaie C (2019) Excess tissue factor is preferentially cleared from endothelial cells through microvesicle release and then, by caveolae-mediated internalisation, through a mechanism requiring fVIIa (poster). Presented at congress of the international society on thrombosis and haemostasis. Melbourne, Australia.

Madkhali Y, Maraveyas A, Greenman J, Ettelaie C (2019) The ratio of factor VIIa:tissue factor content within microvesicles determines the differential influence on endothelial cells (poster). Presented at European Congress on Thrombosis and Haemostasis. Glasgow, UK.

Presentations

Madkhali Y, Featherby S, Maraveyas A, Greenman J, Ettelaie C (2018) Cancer Cells Release Active TF-fVIIa Complex Which Can Be Directly Inhibited by Apixaban. Presented in BSHT Annual Scientific Meeting. University of Warwick, UK.

To my family

Thank you for supporting me all over my life

Table of content

Abstract.....	ii
Acknowledgment.....	iv
Publication and presentation.....	v
Table of content.....	viii
Table of figures.....	xv
Table of tables.....	xix
List of Symbols and Abbreviations.....	xx
Chapter 1 General introduction.....	1
1.1 Introduction.....	2
1.1 Tissue factor.....	3
1.2 Factor VII.....	5
1.3 The role of tissue factor in haemostasis.....	7
1.4 Tissue factor and cell signalling.....	8
1.5 Protease-activated receptors.....	12
1.6 The structure and cellular source of microvesicles (MV).....	13
1.6.1 Formation of MV.....	15
1.6.2 Functions of MV.....	17
1.7 Endothelial cells.....	19
1.8 Cellular apoptosis.....	20
1.9 Caveolae.....	25
1.10 Endocytosis.....	28
1.11 Aims.....	32
Chapter 2 Materials and methods.....	34
2.1 Materials.....	35
2.2 Methods.....	41
2.2.1 Cell culture.....	41

2.2.2	Harvesting, subculturing and counting of cells	42
2.2.3	Cryopreservation and recovery of cells	42
2.2.4	Cells lysis.....	43
2.2.5	SDS-polyacrylamide gel electrophoresis (SDS-PAGE).....	43
2.2.6	Western blot analysis.....	44
2.2.7	Preparation of microvesicles from conditioned media derived from cell lines.....	44
2.2.8	Measurement of the density of isolated MV	46
2.2.9	Apoptosis assay	46
2.2.10	Measurement of fVII antigen by ELISA assay	49
2.2.11	Determination of cell numbers using the crystal violet staining assay.....	50
2.2.12	Measurement of TF antigen by ELISA assay.....	55
2.2.13	Measuring TF-fVIIa activities using fXa generation assay.....	55
2.2.14	Measurement of the concentration and purity and of the isolated nucleic acid.....	57
2.2.15	Statistical Analysis	57
Chapter 3	The ratio of factor VIIa:tissue factor content within microvesicles determines the differential influence on endothelial cells.....	60
3.1	Introduction.....	61
3.1.1	Aims.....	64
3.2	Methods.....	66
3.2.1	Isolation of total RNA	66
3.2.2	Measurement of the amount of fVII mRNA by real-time PCR (RT-PCR).....	66
3.2.3	Examination of the ability of direct oral anticoagulants to prevent cellular apoptosis in endothelial cells induced by MV	67
3.2.4	Examining the ability of apixaban and rivaroxaban to inhibit the proteolytic activity of fVIIa.....	70

3.2.5	Examination of the influence of DOAC on cofactor activity of TF and the proteolytic activity of purified fVIIa and MV-associated fVIIa	70
3.3	Results.....	71
3.3.1	Analysis of the expression of fVII/fVIIa protein in cancer cell lines by western blot.....	71
3.3.2	Examination of the expression of fVII mRNA in cancer cell lines using real-time RT-PCR.....	71
3.3.3	Measurement of MV-associated TF using ELISA assay.....	73
3.3.4	Measurement of MV-associated fVII/fVIIa using ELISA assay.....	73
3.3.5	Calculation of the molar ratio of fVIIa:TF within MV derived from cancer cell lines.....	77
3.3.6	Measurement of TF and fVIIa activity using the fXa-generation assay....	77
3.3.7	Examination of the influence of cancer cell-derived MV on endothelial cells.....	81
3.3.8	The effect of different ratios of exogenous fVIIa:TF on HCAEC proliferation.....	86
3.3.9	Examination of the influence of exogenous fVIIa on MV-induced apoptosis in endothelial cells.....	89
3.3.10	MV-induced cell proliferation and apoptosis is mediated through PAR2 receptor.....	89
3.3.11	Examination of the involvement of TF-fVIIa complex in endothelial cells apoptosis and proliferation.....	96
3.3.12	Measurement of the exposure of fVII on the surface of endothelial cells in response to TF and PAR2 activation.....	100
3.3.13	Examination of the ability of direct oral anticoagulants to prevent MV-induced apoptosis in endothelial cells	101
3.3.14	Examination of the ability of DOAC to block the proteolytic activity of fVIIa.....	107
3.3.15	Examination of the ability of apixaban to block fVIIa and MV-associated fVIIa activity in the presence of recombinant TF	107

3.4	Discussion.....	113
Chapter 4	Investigation of PAR2 activation in response to TF:fVIIa complex using a novel hybrid protein.....	118
4.1	Introduction	119
4.1.1	Aims.....	123
4.2	Methods	125
4.2.1	Measurement of PAR2 activation on the cell surfaces.....	125
4.2.2	Preparation of LB agar plates, LB broth and freeze medium.....	125
4.2.3	Bacterial transformation	126
4.2.4	Purification of plasmid DNA using the Wizard® Plus Midipreps kit.....	126
4.2.5	Isolation of plasmid DNA using the miniprep kit	128
4.2.6	Ethanol precipitation of plasmid DNA.....	129
4.2.7	Analysis of plasmid DNA by agarose gel electrophoresis	129
4.2.8	Design of DNA primers for PCR amplification of full- and short-length PAR2 DNA.....	131
4.2.9	PCR amplification of PAR2 cDNA.....	131
4.2.10	Restriction digestion of the empty expression plasmids and the amplified PAR2 cDNA.....	133
4.2.11	Purification of DNA following the restriction reactions	133
4.2.12	Ligation of the PAR2 DNA inserts into the mCherry2-C1 and mEmerald-C1 plasmids.....	138
4.2.13	Examination and identification of sub-cloned inserts into the plasmids.	138
4.2.14	Transfection of primary cells and cancer cell lines with plasmid DNA..	139
4.2.14.1	Transfection of HDBEC and HCAEC using Viromer® RED reagent.	140
4.2.14.2	Transfection of HDBEC and HCAEC using TransIT®-2020 reagent.	140
4.2.15	Determination of transfection efficiency by flow cytometry	140
4.2.16	Determination of plasmid DNA transfection by fluorescence microscopy..	141
4.2.17	Measurement of PAR2 auto-activation on cancer cell surfaces	141

4.2.18	Measurement of MV release by PAR2 auto-activation in the transfected cancer cells.....	142
4.2.19	Measurement of PAR2 activation in HDBEC in response to TF-fVIIa complex.....	142
4.2.20	Assessment of the influence of cell line-derived MV on PAR2 activation in HDBEC.....	142
4.3	RESULTS.....	143
4.3.1	Optimisation of digestion of the plasmids and the amplified PAR2 cDNA with <i>HindIII</i> and <i>BamHI</i> restriction enzymes	143
4.3.2	Sub-cloning of the PAR2 cDNA into the vector	143
4.3.3	Validation of the sub-cloning of the insert into the plasmid	147
4.3.4	Assessment of DNA transfection efficiency into HCAEC and HDBEC...153	
4.3.4.1	Examination of Viromer RED transfection efficiency in HDBEC.....	153
4.3.4.2	Examination of TransIT-2020-mediated transfection efficiency in HDBEC.....	156
4.3.5	Measurement of PAR2 activation on the surface of cells and MV release using cell lines expressing the mCherry2-short-length PAR2 construct	160
4.3.6	Examination of the influence of TF-fVII complex on the activation of PAR2 in HDBEC.....	160
4.3.7	Examination of the influence of MV isolated from cell lines on PAR2 activation in HDBEC	163
4.4	Discussion.....	166
Chapter 5	Excess tissue factor is preferentially cleared from the surface of endothelial cells through microvesicle release and caveolae-mediated internalisation.....	172
5.1	Introduction	173
5.1.1	Aim	175
5.2	Methods.....	176
5.2.1	Optimization of the knockdown of fVII expression using siRNA.....	176
5.2.2	<i>In situ</i> Proximity ligation assay (PLA) using the Duolink® kit	176

5.2.3	Examination the association of TF, fVII and PAR2 proteins.....	179
5.2.4	Examination of the association of fVII and TF within caveolin-1 in HCAEC.....	180
5.2.5	Optimisation of the depletion of cell-membrane cholesterol in HCAEC..	181
5.2.6	Optimization the M β CD:cholesterol molar ratios for labelling lipid rafts in HCAEC.....	181
5.2.7	Labelling human recombinant TF using the Lightning-Link [®] Rapid Texas Red [®] conjugation kit.....	182
5.2.8	Analysis of the co-localisation of TF on the surface of HCAEC by confocal microscopy	182
5.2.9	Evaluating the influence of cell-membrane cholesterol on preventing TF inducing apoptosis in HCAEC	183
5.3	Results.....	184
5.3.1	Examination of the interactions of fVII, TF and PAR2 in cancer cells using PLA.....	184
5.3.2	Optimization of the silencing of fVII expression in MDA-MB-231 cell line.....	184
5.3.3	Examination of the influence of fVII on the association of TF and PAR2 protein.....	187
5.3.4	Confirmation of the lack of TF expression in MDA-MB-231 TF knock out cell line.....	191
5.3.5	Examination of the association of fVIIa and PAR2 protein in the absence of TF.....	191
5.3.6	Examination of the association of fVII and caveolae in HCAEC	192
5.3.7	Examination of the association of TF and caveolin-1 in HCAEC	198
5.3.8	Optimization of the depletion and exchange of cell-membrane cholesterol in HCAEC.....	198
5.3.9	Analysis of the incorporation of Texas-Red labelled TF into cell membrane.....	200

5.3.10	Examination of the co-localisation of TF with the lipid rafts within HCAEC membrane by confocal microscopy.....	200
5.3.11	Examination of the influence of cell-membrane cholesterol on TF- mediated cell apoptosis.....	203
5.4	Discussion.....	207
Chapter 6	Discussion.....	212
Chapter 7	References.....	223

Table of figures

Figure 1.1 The schematic representation of the structure of TF domains	4
Figure 1.2 Schematic representation of the structural domains of factor VII.....	6
Figure 1.3 Schematic representation of the coagulation system.....	9
Figure 1.4 The roles of TF in coagulation and cell signalling.....	11
Figure 1.5 The activation of PARs by the coagulation proteases.....	13
Figure 1.6 Schematic diagram of MV structure.....	15
Figure 1.7 Postulated mechanism for MV formation	17
Figure 1.8 Schematic representation of functions of endothelial cells	21
Figure 1.9 Schematic representation of the extrinsic and intrinsic pathways of apoptosis	24
Figure 1.10 Schematic representation of the structure of the caveolae	26
Figure 1.11 Proposed mechanism of caveolae-dependent endocytosis	31
Figure 2.1 The measurement of microvesicles using the Zymuphen MP Activity kit	47
Figure 2.2 An example standard curve for MV concentration measured by the Zymuphen MP kit	48
Figure 2.3 Standard curve for the fVII concentration.....	51
Figure 2.4 Standard curve for the determination of HCAEC cell numbers.....	52
Figure 2.5 Standard curve for the determination of HepG2 cell numbers.....	53
Figure 2.6 Standard curve for the determination of MDA-MB-231 TF knock out cell numbers	54
Figure 2.7 Standard curve for the TF concentration.....	56
Figure 2.8 Standard curve of TF activity using the fXa generation assay	58
Figure 2.9 Standard curve of fVIIa activity using the fXa generation assay	59
Figure 3.1 Analysis of the expression of fVIIa protein in cancer cell lines by western blot..	72
Figure 3.2 Assessment of expression of fVII mRNA in cancer cell lines using real time RT-PCR.....	74
Figure 3.3 Measurement of MV-associated TF antigen by ELISA	75
Figure 3.4 Measurement of MV-associated fVII/fVIIa antigen by ELISA	76
Figure 3.5 Molar ratio of fVIIa:TF within MV derived from cancer cell lines	78
Figure 3.6 Measurement of TF activity within MV derived from cancer cell lines using the fXa generation assay	79
Figure 3.7 Measurement of fVIIa activity within MV isolated from cancer cell lines using the fXa-generation assay.....	80

Figure 3. 8 Assessment of the influence of MV derived from cancer cell lines on endothelial cell proliferation.....	82
Figure 3. 9 The rate of endothelial cells proliferation induced by cancer cell-derived MV shown as percentages of the untreated cells.....	83
Figure 3. 10 Examination of the influence of MV isolated from cancer cell lines on endothelial cell apoptosis.....	84
Figure 3. 11 The rate of endothelial cells apoptosis induced by cancer cell-derived MV shown as percentages of the untreated cell population	85
Figure 3. 12 Assessment of the influence of exogenous TF and fVIIa on endothelial cell numbers.....	87
Figure 3. 13 Examination of the influence of exogenous fVIIa and TF on endothelial cell numbers.....	88
Figure 3. 14 Examination of the influence of exogenous fVIIa on the pro-apoptotic effect of MV	90
Figure 3. 15 Assessment of the involvement of PAR2 in endothelial cells proliferation.....	92
Figure 3. 16 Examination of the involvement of PAR2 in endothelial cells apoptosis.....	93
Figure 3. 17 The influence of the over-activation of PAR2 on the induction of apoptosis by MV	94
Figure 3. 18 High concentrations of 786-O-derived MV induce PAR2 internalisation in endothelial cells through over-activation of the receptor	95
Figure 3. 19 MV-associated TF promotes endothelial cells apoptosis through pro-coagulant activity.....	97
Figure 3. 20 Neutralisation of fVIIa within 786-O-derived MV abolishes the promotion of apoptosis in endothelial cells	98
Figure 3. 21 Neutralisation of fVIIa within HepG2 cell-derived MV prevents the promotion of endothelial cells proliferation	99
Figure 3. 22 Examination of the alteration in endothelial cell-surface fVII antigen levels in response to TF.....	102
Figure 3. 23 Examination of the alteration in endothelial cell-surface fVII antigen levels in response to PAR2-AP	103
Figure 3. 24 Examination of the alteration in endothelial cell-surface fVII antigen in response to repeated treatment with recombinant TF	104
Figure 3. 25 Quantification of the release of MV-associated fVII antigen following multiple treatments with TF	105

Figure 3. 26 Examination of the ability of DOAC on blocking the pro-apoptotic effect of MV on endothelial cells	106
Figure 3. 27 Measurement of the proteolytic activity of exogenous fXa and fVIIa using two chromogenic substrates	109
Figure 3. 28 Examination of the influence of DOAC on the proteolytic activity of fVIIa....	110
Figure 3. 29 Examination of the influence of apixaban on the proteolytic activity of fVIIa in combination with recombinant TF	111
Figure 3. 30 Examination of the effectiveness of DOAC in blocking the proteolytic activity of fVIIa within MV	112
Figure 3. 31 Schematic representation of the outcomes of the ratio of fVIIa:TF on endothelial cells	117
Figure 4. 1 The proposed study for by which PAR2 signalling induces MV release and the activation of recipient cells.	124
Figure 4. 2 Schematic of the strategy for measuring PAR2 activation.....	127
Figure 4. 3 The DNA map of the mEmerald-C1 mammalian plasmid.....	130
Figure 4. 4 The DNA map of mCherry2-C1 mammalian plasmid	130
Figure 4. 5 The cDNA sequence of the human PAR2 and the designed cloning primers.....	132
Figure 4. 6 The map of VersaClone plasmid containing hPAR2 cDNA.....	134
Figure 4. 7 Optimisation of digestion mCherry2-C1 plasmid with <i>HindIII</i> and <i>BamHI</i> restriction enzymes	144
Figure 4. 8 Optimisation of the ligation of the full-length PAR2 cDNA into the mEmerald-C1 plasmid.....	145
Figure 4. 9 Optimisation of the ligation of the short-length PAR2 cDNA into the mCherry2-C1 plasmid.....	146
Figure 4. 10 Analysis of the constructed plasmids by <i>HindIII</i> and <i>BamHI</i> restriction digestion	148
Figure 4. 11 Confirmation of cloning of PAR2 inserts by PCR amplification.....	149
Figure 4. 12 Alignment of the amplified PAR2 cDNA PCR product with the published PAR2 sequence.....	150
Figure 4. 13 Confirmation of the sub-cloning of the full-length PAR2 cDNA into the mEmerald-C1 plasmid	151
Figure 4. 14 Confirmation of the sub-cloning of the short-length PAR2 cDNA into the mCherry2-C1 plasmid.....	152

Figure 4. 15 Analysis of transfection efficiency using the Viromer RED-mediated.....	154
Figure 4. 16 Analysis of transfection efficiency using the Viromer RED-mediated.....	155
Figure 4. 17 Analysis of transfection efficiency using the TransIT-2020-mediated.....	157
Figure 4. 18 Analysis of transfection efficiency using the TransIT-2020-mediated.....	158
Figure 4. 19 Analysis of the expression of the mCherry2-short-length PAR2 construct by fluorescence microscopy.....	159
Figure 4. 20 Auto-activation of PAR2 on the surface of the transfected cancer cell lines....	161
Figure 4. 21 Measurement of the MV release from the transfected cell lines.....	162
Figure 4. 22 Measurement of the activation of PAR2 in HDBEC by combinations of exogenous TF and fVIIa	164
Figure 4. 23 The influence of isolated MV from cell lines on PAR2 activation on the surface of HDBEC.....	165
Figure 4. 24 The proposed role of TF-fVIIa complex on PAR2 activation.....	171
Figure 5. 1 The principle of Duolink® <i>in situ</i> proximity ligation assay reaction.....	178
Figure 5. 2 Interactions between fVII, TF and PAR2 as detected by PLA.....	185
Figure 5. 3 Optimization of the suppression of fVII expression.....	188
Figure 5. 4 The influence of fVIIa on the association of TF with PAR2	189
Figure 5. 5 Confirmation of the lack of TF expression in MDA-MB-231 TF KO cells by flow cytometry	193
Figure 5. 6 The influence of recombinant TF on MDA-MB-231 TF KO proliferation	194
Figure 5. 7 Analysis of the association of fVIIa and PAR2 in TF knock out cells.....	195
Figure 5. 8 Analysis of the proximity between fVII and caveolin-1 in HCAEC.....	196
Figure 5. 9 Analysis of the proximity between TF and caveolin-1 in HCAEC	199
Figure 5. 10 Analysis of cell viability for the optimisation of cholesterol depletion	201
Figure 5. 11 Optimisation of the ratio of M β CD:cholesterol complex for labelling lipid rafts on HCAEC.....	202
Figure 5. 12 Examination the incorporation of Texas-Red labelled TF into cell membrane by fluorescent microscopy	204
Figure 5. 13 Examination of the co-localisation of TF within lipid rafts in HCAEC.....	205
Figure 5. 14 The influence of cholesterol on the influence of TF on cell numbers.....	206
Figure 6. 1 Postulated cellular mechanisms for the management of excess TF	222

Table of tables

Table 2. 1 Primary and secondary antibody dilutions used in the western blot procedure.....	45
Table 3. 1 Real-time RT-PCR master mix.....	68
Table 3. 2 Real-time RT-PCR program	69
Table 4. 1 PCR master mix.....	135
Table 4. 2 Master mix for DNA digestion with restriction enzymes from Promega.....	136
Table 4. 3 Master mix for DNA digestion with high-fidelity restriction enzymes.....	137

List of Symbols and Abbreviations

α	Alpha
β	Beta
γ	Gamma
$^{\circ}\text{C}$	Degrees centigrade
μ	Micro
%	Percentage
Ala	Alanine
Apaf-1	Apoptotic protease activating factor-1
ATP	Adenosine triphosphate
ADP	Adenosine diphosphate
bp	Base pair
BSA	Bovine serum albumin
C	Cytosine
Ct	Threshold cycle
Ca^{+2}	Calcium
CaCl_2	Calcium chloride

cDNA	Complementary deoxyribonucleic acid
CO ₂	Carbon dioxide
DAPI	4',6-Diamidino-2-phenylindole dihydrochloride
dH ₂ O	Distilled water
DMEM	Dulbeco's modified essential medium
DMSO	Dimethyl sulphoxide
DNA	Deoxyribonucleic acid
dNTP	Deoxynucleotide triphosphate
EC	Endothelial cell
EGF	Epidermal growth factor
ELISA	Enzyme-linked immunosorbent assay
ERK1/2	Extracellular signal-regulated kinases 1/2
<i>E. coli</i>	<i>Escherichia coli</i>
EDTA	Ethylenediaminetetraacetic acid
FACS	Fluorescence-activated cell sorting
FCS	Foetal calf serum
FICT	Fluorescein isothiocyanate

FVII	Factor VII
FVIIa	Activated factor VII
FX	Factor X
FXa	Activated factor FX
g	Gram
<i>g</i>	Gravity
G	Guanine
GAPDH	Glyceraldehyde-3-phosphate dehydrogenase
Gly	Glycine
h	Hour
HBS	HEPES-buffered saline
HCL	Hydrochloric acid
HCAEC	Human coronary artery endothelial cells
HRP	Horseradish peroxidase
IgG	Immunoglobulin G
IL	Interleukin
JNK	c-Jun N-Terminal Kinase

Kb	Kilo base
L	Litre
LB	Luria Bertani medium
Log	Logarithm
M	Molar
m	Milli
mA	Milliamps
M β CD	Methyl- β -cyclodextrin
MAPK	Mitogen-activated protein kinase
min	Minute
mol	Mole
MV	Microvesicle
mRNA	Messenger ribonucleic acid
n	Nano
NaCl	Sodium chloride
NO	Nitric oxide
p38	Protein 38

p53	Protein 53
PAR	Protease activated receptor
PAR2-AP	Protease activated receptor2-activating peptide
PBS	Phosphate buffered saline
PCR	Polymerase chain reaction
PLA	Proximity ligation assay
PS	Phosphatidylserine
RNA	Ribonucleic acid
RNase	Ribonuclease
rpm	Revolutions per minute
RT-PCR	Reverse transcription-polymerase chain reaction
s	Second
SD	Standard deviation
SDS	Sodium dodecyl sulphate
SDS-PAGE	Sodium dodecyl sulphate polyacrylamide gel electrophoresis
SEM	Standard error of mean
siRNA	Short interfering RNA

T	Thymine
TBE	Tris borate-EDTA
TBST	Tris buffered saline tween 20
TEMED	N,N,N',N'-Tetramethylethylenediamine
TF	Tissue factor
TFPIs	Tissue factor pathway inhibitors
TMB	3,3',5,5'-Tetramethylbenzidine
TNF	Tumour necrosis factor
UV	Ultra violet
U	Unit
V	Volt
v/v	Volume to volume
w/v	Weight to volume

Chapter 1

General introduction

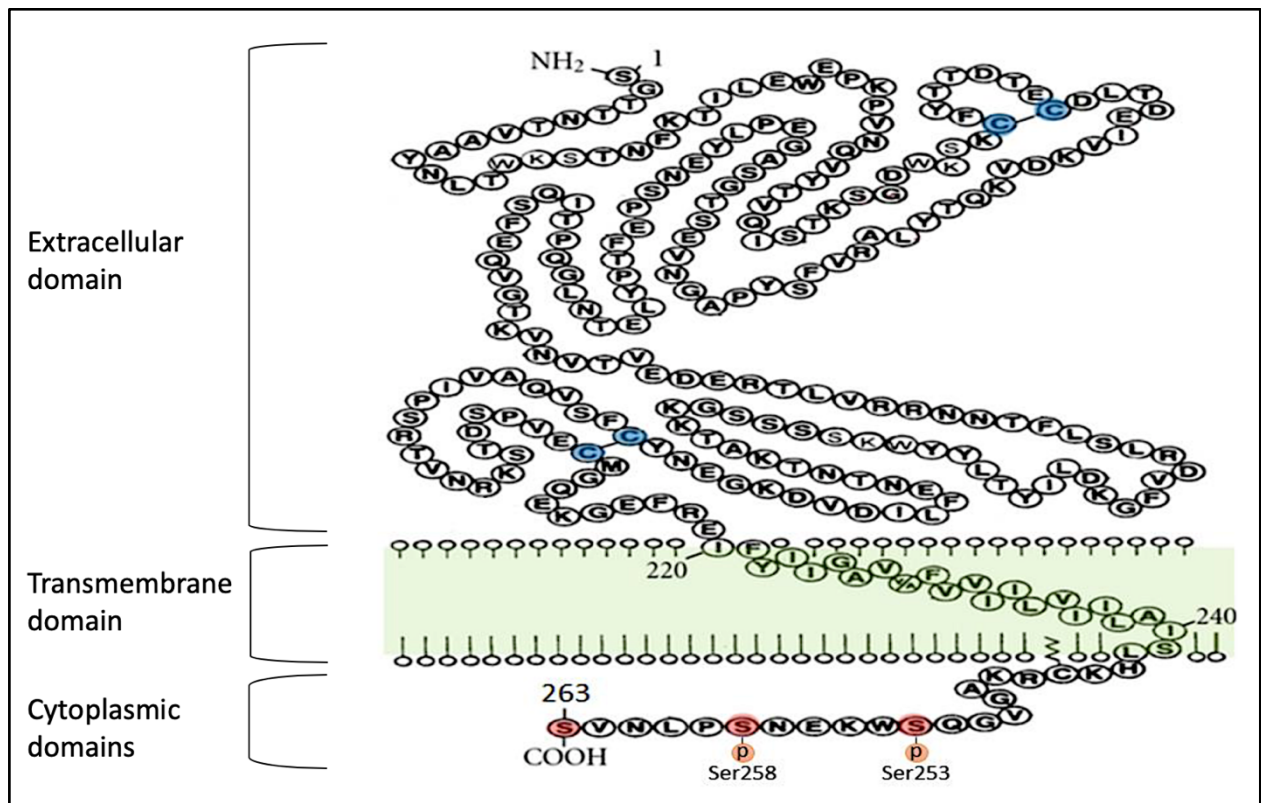
1.1 Introduction

The relationship between thrombosis and cardiovascular complications is well established and has been associated with increased morbidity and mortality in many chronic diseases (Kim et al., 2016; Wattanakit et al., 2012; Prandoni et al., 2003; Meijers and de Boer, 2019; Fernandes et al., 2019). It has recently become evident that procoagulant microvesicles (MV) may exacerbate the development of vascular complications associated with many diseases (Chen et al., 2018). Elevated levels of procoagulant MV have been reported in patients with chronic diseases such as diabetes, hypertension, cancer or following myocardial infarction (Manly et al., 2010; Badimon et al., 2017). MV express a number of proteins on the external surface and among these proteins is tissue factor (TF). TF is known to be the key protein responsible for the procoagulant activity associated with MV (Owens and Mackman, 2011). In addition to acting as the main initiator of the coagulation system (Lasne et al., 2006), TF is involved in other biological processes such as angiogenesis (Abdulkadir et al., 2000; Cimmino and Cirillo, 2018), inflammation (Cunningham et al., 1999) and induction of MV release (Collier and Ettelaie, 2011). TF can also promote endothelial cell proliferation (Collier and Ettelaie, 2010; Ettelaie et al., 2011). Furthermore, the accumulation of TF in endothelial cells induces cellular apoptosis (Elkeeb et al., 2015; Ethaeb et al., 2019) which can lead to endothelial dysfunction (Hadi et al., 2005; Yau et al., 2015). During the course of this study, the influence of TF-positive MV from different cancer cells on cultured endothelial cells was examined. In addition, the effect of recombinant TF on endothelial cell proliferation and apoptosis were explored. Understanding these processes may allow the control of the detrimental effects of cancer cell-derived MV on the vascular system. It may also aid the understanding of the mechanisms through which cells manage to regulate excess TF in pathophysiological settings.

1.1 Tissue factor

Tissue factor (also known as thromboplastin, CD142, or coagulation factor III) is the main initiator of blood coagulation and is essential for correct haemostasis (Lasne et al., 2006; Grover and Mackman, 2018; Grover and Mackman, 2019). The gene for TF is located on chromosome 1 p21-22 (Butenas, 2012) which encodes for a 263 amino acid transmembrane glycoprotein with a molecular weight of 47 kDa (Figure 1.1). The protein is comprised of an extracellular domain, a transmembrane region and a cytoplasmic domain. The extracellular domain contains 219 amino acids (residues 1-219) and serves as the binding site for factor VII (fVII)/active fVIIa (fVIIa). The transmembrane domain contains 23 amino acids (residues 220-242) and stabilises TF within the membrane. The cytoplasmic domain consists of 21 amino acids that can be phosphorylated at Ser253 and Ser258 (Morrissey et al., 1987; Chu, 2011). TF is expressed by a number of cell types including fibroblasts, epithelial cells, kidney, brain and lung cells (Drake et al., 1989; Erlich et al., 1999). Furthermore, TF is synthesised by cells of the tunica intima and tunica adventitia within the blood vessel walls (Fleck et al., 1990). Under physiological conditions, endothelial cells and circulating blood cells do not express TF (Drake et al., 1989; Butenas et al., 2009; Østerud and Bjørklid, 2006; Akinmolayan et al., 2016). However, TF has been shown to be present in the blood circulation of healthy individuals at low levels (Albrecht et al., 1996; Menzies et al., 2009). In contrast, high levels of TF have been observed in the bloodstream of patients with atherosclerosis, diabetes, cancer or following infections (Williams and Mackman, 2012; Eisenreich et al., 2016; Witkowski et al., 2016). This circulating TF is shown to be associated with the surface of MV (Key and Mackman, 2010). In addition to its function in haemostasis, TF can also act as a modulator of blood vessel development (angiogenesis) and cellular proliferation (Abdulkadir et al., 2000; Cimmino and Cirillo, 2018).

Figure 1.1 The schematic representation of the structure of TF domains



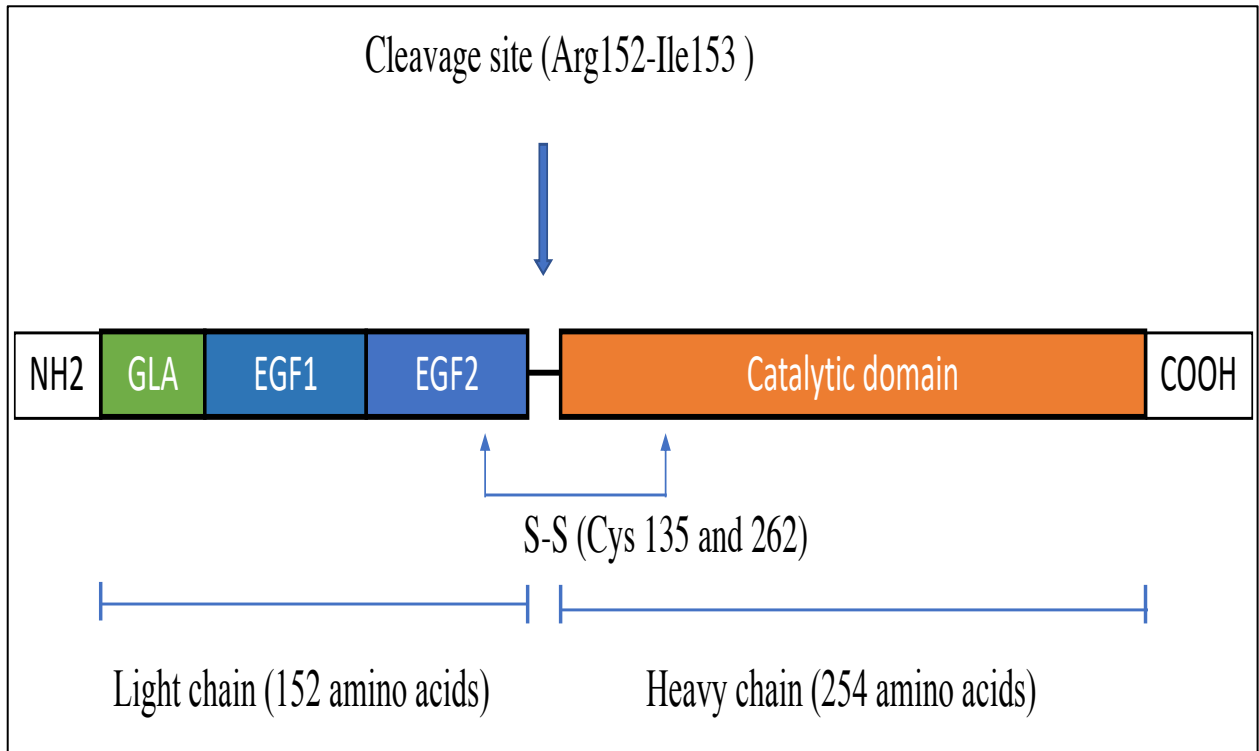
TF is a 47-kDa transmembrane glycoprotein. Human TF contains 263 amino acids comprised of an extracellular, a transmembrane and a cytoplasmic domains. The extracellular domain has 219 amino acids and provides a site for fVII/fVIIa binding. The transmembrane domain has 23 amino acids which connects the extracellular and intracellular domains and stabilises TF within the membrane. TF has a small cytoplasmic domain made up of 21 amino acids and contains three serine residues. The protein has been shown to be phosphorylated at Ser253 and Ser258 (adapted from Chu, 2011).

The mechanisms of TF-mediated signalling and the roles of TF in the regulation of cellular functions and coagulation are discussed below in this chapter.

1.2 Factor VII

Factor VII is a vitamin K-dependent coagulation factor that forms a complex with TF, thereby initiating the extrinsic pathway of the coagulation system (Grover and Mackman, 2019). The gene for human fVII is located on chromosome 13 and encodes for a single-chain protein that is composed of 406 amino acids. The mature protein has a molecular weight of 50 kDa (Broze and Majerus, 1980) and circulates in the plasma as a zymogen at a concentration of around 500 ng/ml with approximately 1% of the protein circulating in its active form (fVIIa) (Perera et al., 1999; Vadivel and Bajaj, 2012; Pongjantarasatian et al., 2019). FVII protein has a half-life of 2-3 h. The protein is made up of a gamma-carboxyglutamate (Gla) domain (residues 1-45), two epidermal growth factor (EGF-1 and -2) domains and a C-terminal catalytic domain (residues 153-406) (Figure 1.2). The Gla domain binds Ca^{2+} ions and allows fVII to associate with the negatively charged phospholipids on the membrane surface of activated cells. The EGF-1 (residues 47-84) and EGF-2 (residues 85-131) serve as the binding site for TF (Stenflo, 1999; Vadivel and Bajaj, 2012; Thiec et al., 2003). FVII is activated by proteases including Xa, IXa and XIIa, and auto-lytically by coming into contact with other TF-fVIIa complexes (Pike et al., 1999; Shahbazi and Mahdian, 2019). The activation to fVIIa occurs through the cleavage of the single peptide bond between Arg152 and Ile153, located at the boundary of the EGF-2 and C-terminal catalytic domains (Mirzaahmadi et al., 2011). The digestion of this bond results in the formation of a light chain (152 amino acids) and a heavy chain (254 amino acids) which are held together by a disulphide bond to stabilise the protein (Pike et al., 1999; Kembal-Cook et al., 1999; Shahbazi and Mahdian, 2019).

Figure 1. 2 Schematic representation of the structural domains of factor VII



The fVII protein is comprised of a Gla domain, two tandem EGF domains and a C-terminal domain which contains the catalytic region. FVIIa is activated through cleavage at a site between residues 152 (Arg) and 153 (Ile). The cleavage of fVII releases a light chain (152 amino acids) and a heavy chain (254 amino acids) which are held together by a disulphide bond (adapted from Shahbazi and Mahdian, 2019).

Elevated plasma levels of fVII/fVIIa have been observed in liver cirrhosis (Hollestelle et al., 2004) and in patients suffering from heart disease (Suzuki et al., 1991). Although liver cells are the main source of fVII, inflammatory modulators have been shown to trigger the expression of this protein in other cells including monocytes (Tsao et al., 1984; Wilcox et al., 2003). An *in vitro* study conducted by Tsao et al. (1984) demonstrated that monocytes and macrophages express fVII/fVIIa on their surfaces in response to lipopolysaccharide stimulation. Similarly, the expression of fVII/fVIIa was detected in human alveolar macrophages isolated from patients with sarcoid disease (Chapman et al., 1985). In addition to monocytes, fVII has been shown to be expressed in human keratinocytes, coronary artery smooth muscle cells (SMC) and fibroblasts (Wilcox et al., 2003). It has also been shown that cells from a range of cancers, including ovarian (Yokota et al., 2009), lung, liver, thyroid, prostate and stomach cancer (Koizume et al. 2006; Koizume and Miyagi, 2015) express the ectopic form of fVII/fVIIa protein. FVII/fVIIa may also be associated with and carried on the surface of cell-derived MV (Yokota et al., 2009; Featherby et al., 2019). The functions of TF-fVIIa complex in cell signalling are discussed in section 1.4.

1.3 The role of tissue factor in haemostasis

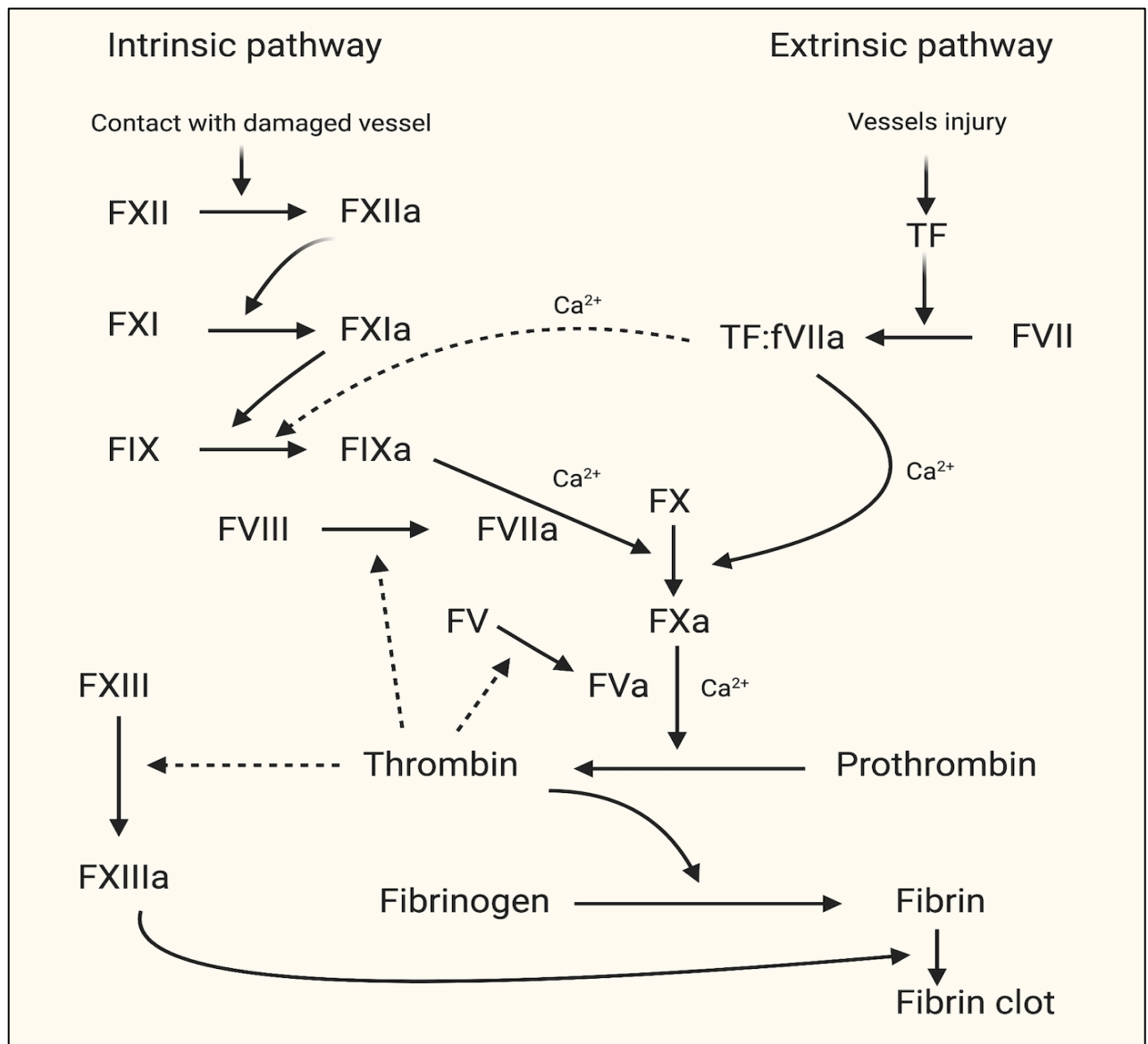
The haemostatic system is composed of cells and proteins which function to regulate blood clotting. This system responds to injury to blood vessels by creating a clot at the site of the wound in order to curtail the loss of blood (Patalakh, 2011; Palta et al., 2014; Göbel et al., 2018). The haemostatic system can be separated into the primary haemostasis, the coagulation pathways and the fibrinolysis (Palta et al., 2014). The focus of this study concerned the role of TF as the main initiator of coagulation pathway. The coagulation pathway can be divided into the extrinsic pathway (also known as the TF pathway) and the intrinsic pathway. These two pathways converge at a point which leads to the activation of the common pathway (Figure 1.3; Pallister and Watson, 2010; Palta et al., 2014).

The extrinsic pathway is the first step in the coagulation and is initiated by the exposure of TF from the sub-endothelial layer. Under normal physiological conditions, the vascular endothelium minimises the contact between TF and the blood (Lasne et al., 2006; Grover and Mackman, 2018). However, TF can become exposed to blood when the vascular wall is damaged. The exposure of TF to the blood leads to the binding of circulating fVII to the extracellular domain of TF and generation of activated fVIIa. The resulting TF-fVIIa complex in turn converts fX and fIX into their respective active forms, fXa and fIXa (Figure 1.3; Mackman et al., 2007; Owens and Mackman, 2010). The intrinsic pathway is initiated by the activation of fXII to fXIIa by various factors, including collagen and kallikrein (Wu, 2015). The activation of fXII (fXIIa) facilitates the catalytic conversion of fXI to fXIa. fXIa, in turn, activates fIX to activated fIXa which then digests fX to the activated form, fXa (Figure 1.3; Kumar et al., 2010; Grover and Mackman, 2019). Convergence of the two mechanism into the common pathway occurs at the point of fXa which subsequently activates prothrombin to thrombin. Consequently, thrombin activates both fV and fVIII into the respective active forms fVa and fVIIIa to intensify the coagulation system. In addition, thrombin cleaves soluble fibrinogen to insoluble fibrin monomers which polymerise to form a fibrin clot. Thrombin can also activate fXIII (also known as fibrin stabilizing factor) which cross-links the fibrin polymers to create a fibrin network (Figure 1.3; Palta et al., 2014; Kumar et al., 2010).

1.4 Tissue factor and cell signalling

In addition to its role in coagulation, TF has been shown to function as a cell signalling receptor (Rao and Pendurthi, 2005; Ruf et al., 2011; Zelaya et al., 2018). Most of TF signalling activities can be initiated through protease-activated receptor (PAR) 1 and PAR2 (López-Pedrerera et al., 2006). The binary TF-fVIIa complex is only capable of signalling through PAR2, whereas the ternary TF-fVIIa-fXa complex activates both PAR1 and PAR2 (Samad and Ruf, 2013; López-Pedrerera et al., 2006). TF signalling is involved in a number of physiological and pathological

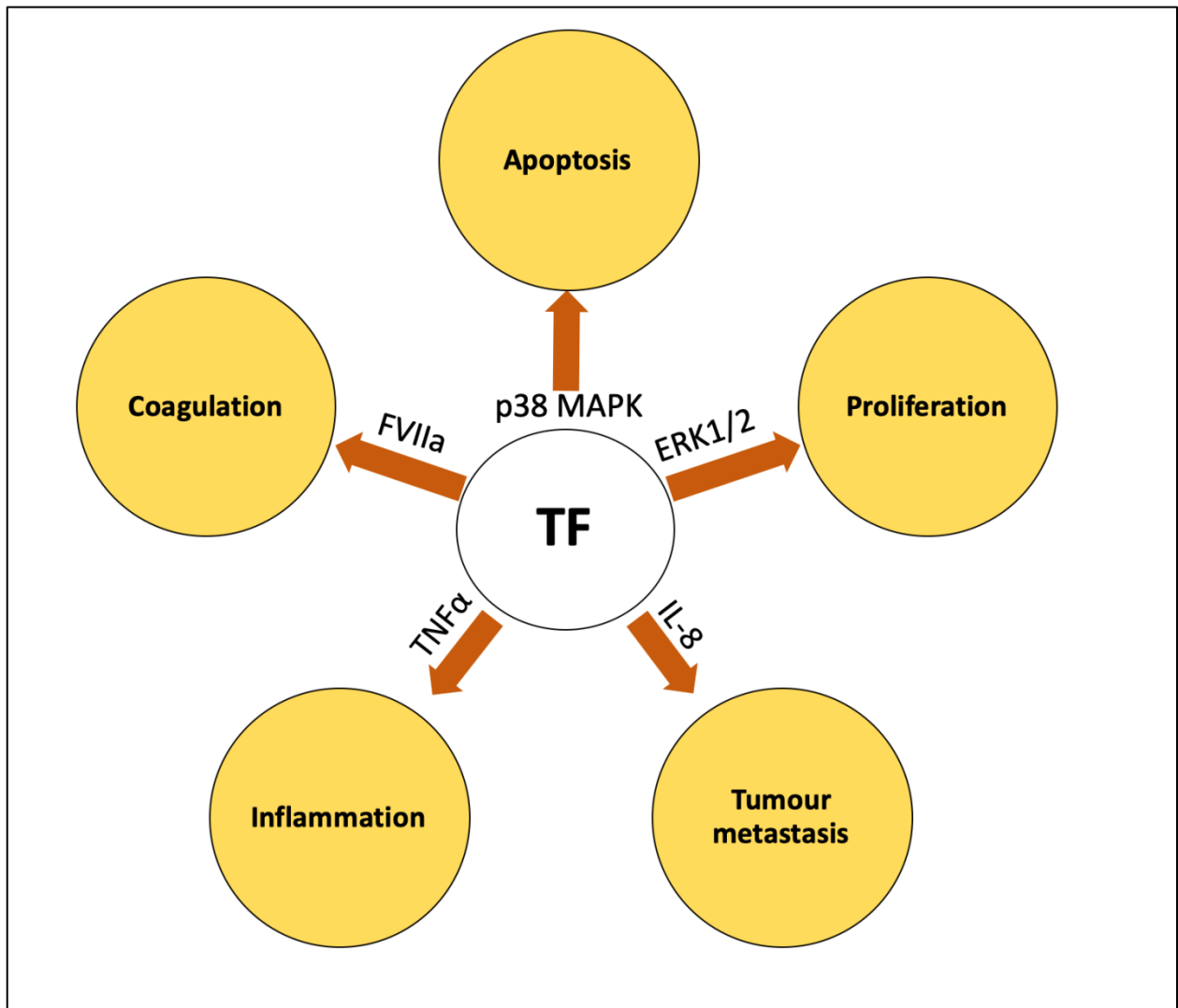
Figure 1. 3 Schematic representation of the coagulation system



The extrinsic pathway is triggered upon vessel injury when fVII binds with TF and form a complex. The intrinsic pathway is initiated by the activation of factor XII by various factors, including collagen. The intrinsic and extrinsic pathways converge to initiate the common pathway, leading to the activation of fX (fXa). The conversion of prothrombin to thrombin by fXa leads to the conversion of fibrinogen to insoluble fibrin (adapted from Palta et al., 2014).

processes (Figure 1.4; Rao and Pendurthi, 2005; Ruf et al., 2011). For example, TF signalling can promote cellular proliferation. In support of this, TF-fVIIa complex has been shown to induce proliferation in smooth muscle cells (SMC) through activation of the MAP kinase (ERK 1/2) (Cirillo et al., 2004). Similarly, incubation of recombinant TF or TF-containing MV with human coronary artery endothelial cells appears to promote cellular proliferation through the activation of the ERK1/2 pathway (Collier and Ettelaie, 2010). However, Elkeeb et al. (2015) showed that the accumulation of TF in endothelial cells induces cellular apoptosis mediated through the p38 MAPK pathway. In addition, Ethaeb et al. (2019) reported that TF induced apoptosis of endothelial cells through Src1 signalling, which also involved the interaction of TF with β 1-integrin. TF signalling has also been implicated in complications associated with a number of pathological conditions. For instance, TF-fVIIa complex signalling has been shown to enhance tumour angiogenesis accelerating the tumour growth (Fernandez and Rickles, 2002; Versteeg et al., 2008). In support of this finding, blocking of the signalling initiated by TF-fVIIa complex using recombinant nematode anticoagulant protein c2 (rNAPc2) prevented the level of tumour angiogenesis and the rate of tumour growth in mice (Hembrough et al., 2003). TF signalling also appears to enhance the rate of tumour invasion and metastasis and TF-fVIIa signalling has been reported to induce IL-8 overexpression in the MDA-MB-231 cell line through the activation of PAR2. Overexpression of IL-8, in turn, enhances invasion and migration in MDA-MB-231 cells (Hjortoe et al., 2004; Morris et al., 2006; Li et al., 2001; Singh and Varney, 2000). In addition, signalling arising from TF, and regulated through protease-activated receptors can promote the expression of pro-inflammatory cytokines such as interleukins and tumour necrosis factor (Chu, 2011). For example, it has been demonstrated that the expression of tumour necrosis factor-alpha (TNF α) is significantly reduced in TF-KO mice with steatohepatitis compared to the control mice with steatohepatitis (Luyendyk et al., 2010).

Figure 1. 4 The roles of TF in coagulation and cell signalling



TF is involved in many physiological and pathological processes. TF is known as the main initiator of the coagulation pathways. TF signalling can also induce cellular proliferation. In addition, high concentrations of TF are capable of promoting apoptosis through p38 MAPK pathway. Moreover, signalling arising from TF-fVIIa complex can enhance tumour metastasis. Furthermore, TF might also play a role in inflammation through enhancing the expression of proinflammatory mediators such as TNF- α .

1.5 Protease-activated receptors

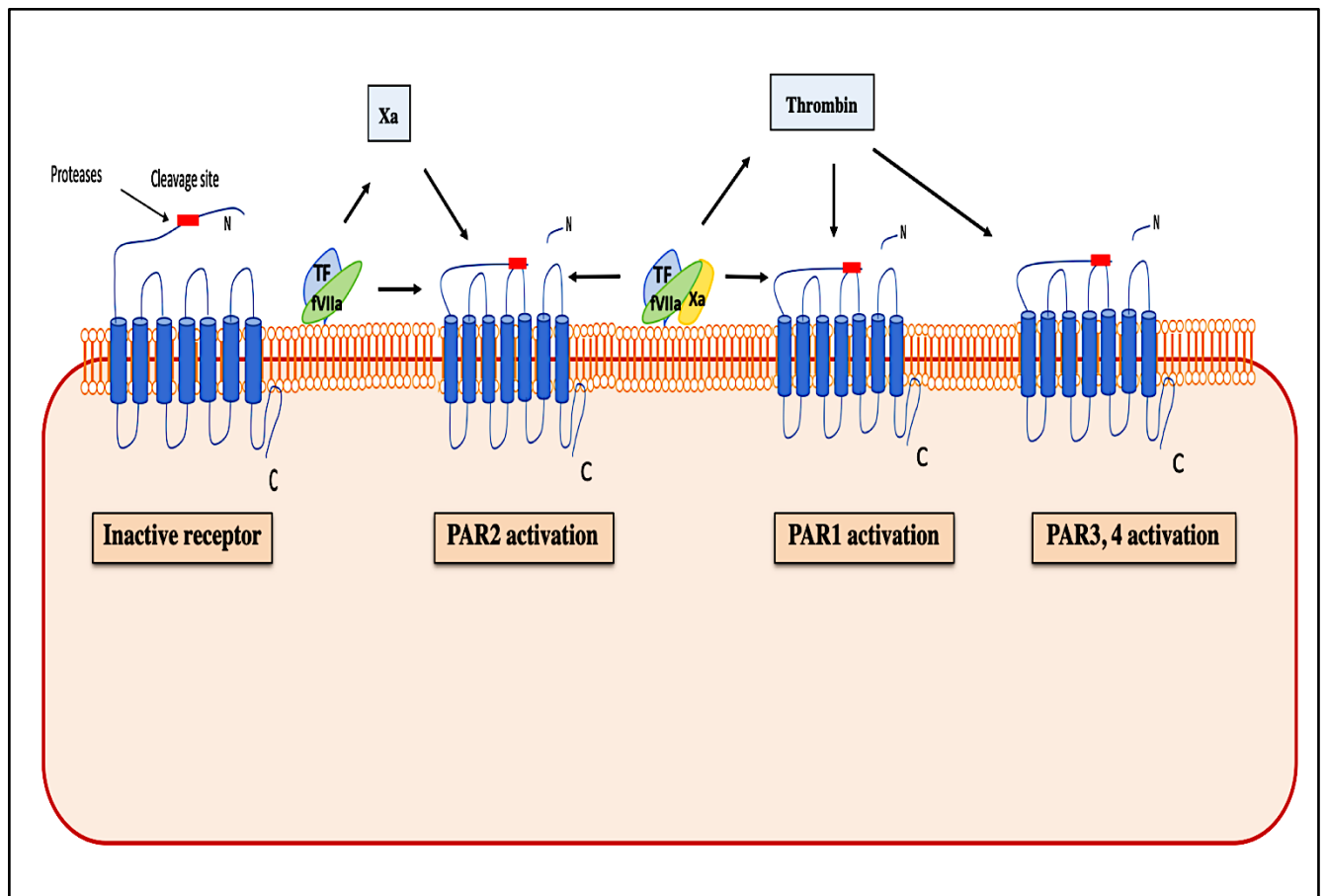
Protease-activated receptors (PARs) are a subfamily of G-protein-coupled receptors (GPCR) and to date four members of the PAR family have been identified. These receptors are highly expressed in platelets, endothelial cells, neurons and monocytes (Macfarlane et al., 2001; Heuberger and Schuepbach, 2019). The overexpression of PARs has also been reported in various types of cancer (Arora et al., 2007). PAR activation occurs through cleavage of its N-terminal extracellular domain, the removal of which exposes a tethered ligand which then binds to the second extracellular loop of the receptor. This interaction alters the configuration of the receptor thereby inducing intracellular signalling mechanisms (Coughlin, 1999; Zhao et al., 2014). PAR2 is activated by trypsin, fXa and the TF-fVIIa complex (Figure 1.5). Thrombin and fXa reportedly cleave PAR1, whereas PAR3 and PAR4 are mainly activated by thrombin (Macfarlane et al., 2001; Camerer et al., 2000; Rothmeier and Ruf, 2011; Zhao et al., 2014; Benelhaj et al., 2019). This study concentrates on the mechanisms of PAR2 activation and the contribution of PAR2 signalling to cell proliferation, apoptosis and MV release. PAR2 has been shown to signal through two separate mechanisms which are mediated by G-proteins, or alternatively through β -arrestin signalling. In the G-protein-mediated pathway, PAR2 activation can induce Ras, protein kinase C (PKC) and inositol trisphosphate (IP₃)-mediated pathways. In contrast, the association of PAR2 with β -arrestin can activate Raf and ERK1/2 cascades (Rothmeier and Ruf, 2011). PAR2 signalling is involved in a number of physiological processes (Feistritzer et al., 2005; Benelhaj et al., 2019; Darmoul et al., 2004). For instance, activation of PAR2 can promote MV release from cells (Ettelaie et al., 2012; Collier and Ettelaie, 2011; Das et al., 2018; Featherby et al., 2019). In support of this, a recent study reported a substantial increase in MV release by a panel of cancer cell lines following PAR2 activation (Ettelaie et al., 2016). In addition to the induction of MV release, activation of PAR2 induces the phosphorylation of the cytoplasmic domain of TF at Ser253. The phosphorylation

of TF at Ser253 has in turn been shown to be essential for the incorporation of TF into MV (Collier and Ettelaie, 2011). Signalling arising from PAR2 has also been implicated in pathological conditions (Cicala, 2002; Antoniak et al., 2013). For example, PAR2 activation can enhance the rate of proliferation of cancer cells (Su et al., 2009). In support of this, activation of PAR2 with either trypsin or PAR2-AP induced colon cancer cell proliferation via the phosphorylation of ERK1/2 (Darmoul et al., 2004). PAR2 may also promote angiogenesis through enhancing the expression of vascular endothelial growth factor (VEGF) (Shibuya, 2011). For example, it has been reported that the activation of PAR2 in a panel of cancer cell lines using PAR2-activating peptide (PAR2-AP), trypsin or fVIIa increased the expression of VEGF (Liu and Mueller, 2006; Ikeda et al., 2003). The mechanism of VEGF expression was shown to be regulated through ERK1/2 and p38 pathways (Liu and Mueller, 2006). This angiogenesis, in turn supplies tumours with oxygen and nutrients allowing rapid growth (Nishida et al., 2006). Other studies have also shown the involvement of PAR2 in inflammatory responses (Shpacovitch et al., 2002; Rothmeier and Ruf, 2012; Heuberger and Schuepbach, 2019). To examine the role of PAR2 signalling in inflammation, Crilly et al. (2012) conducted a study using a mouse model of collagen-induced arthritis. The authors reported substantially less cartilage damage and cell infiltration into the joints of the mice, following the injection of a PAR2-inhibitory monoclonal antibody called SAM11, compared to the control mice (Crilly et al., 2012).

1.6 The structure and cellular source of microvesicles (MV)

Microvesicles (MV) also known as microparticles, are small membrane-bound vesicles which can be released from the plasma membrane following cell activation or apoptosis (Wolf, 1967; Hargett and Bauer, 2013). MV are heterogeneous in content and size, and their diameters range from 100 nm to 1,000 nm (Figure 1.6; Badimon et al., 2017). MV can be produced by a variety of cell types, including red blood cells (RBC), monocytes, cancer cells and endothelial cells

Figure 1. 5 The activation of PARs by the coagulation proteases



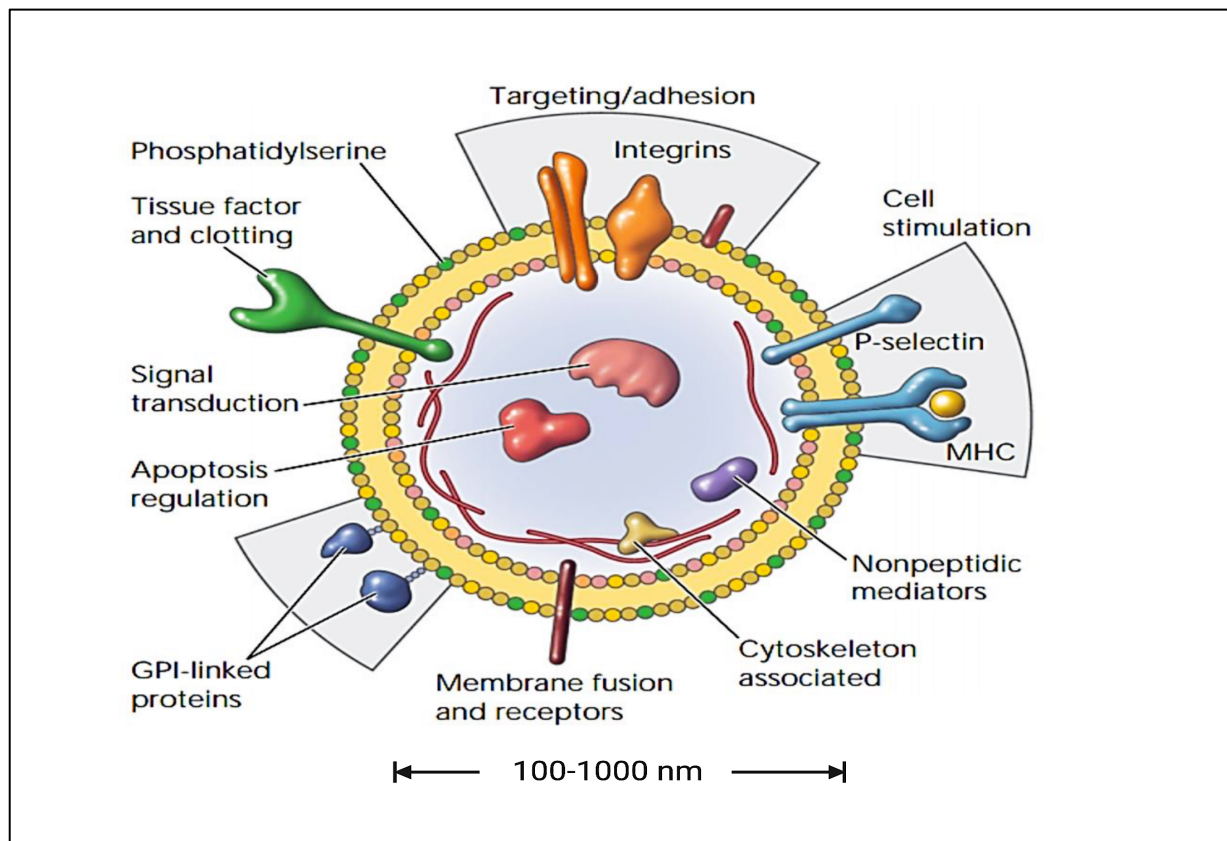
PAR activation occurs by the cleavage of the protein at specific sites within the N-terminal of the proteins. The digestion of the proteins results in the formation of tethered ligand, which alters the configuration of the receptor and promotes intracellular signalling. PAR2 can be activated by coagulation proteases, such as fXa and TF-fVIIa complex. Thrombin activates PAR3 and PAR4 and PAR1 may be activated by thrombin or fXa.

(Burnier et al., 2009; Omoto et al., 2002; Geddings and Mackman, 2013; Badimon et al., 2017). The membranes of MV are composed of a phospholipid bilayer and contain transmembrane and cytoplasmic proteins derived from their cells of origin (Hugel et al., 2005). MV can carry a number of different components, including nucleic acids (Badimon et al., 2017), negatively charged phospholipids (Morel et al., 2006; Freyssinet and Toti, 2010; Gardiner et al., 2015; Date et al., 2013; Hron et al., 2007; Thaler et al., 2014; Auwerda et al., 2011), TF protein (Collier and Ettelaie, 2011) and functional fVIIa (Yokota et al., 2009; Koizume et al., 2006; Featherby et al., 2019). While circulating MV are found at low levels in healthy individuals, these are often more abundant in the bloodstream of patients with cancer, diabetes and hypertension as well as those who have suffered from myocardial infarction (Baran et al., 2009; Herring et al., 2013; Badimon et al., 2017).

1.6.1 Formation of MV

The exact mechanisms of MV release are not entirely understood. However, it has been suggested that MV are released when cells are activated or undergo apoptosis (Distler et al., 2005; Hugel et al., 2005; Martinez et al., 2011). The release of MV is preceded by the disruption of the asymmetry of plasma membrane phospholipids. In the resting state, the cells maintain membrane asymmetry by maintaining phosphatidylserine (PS) and phosphatidylethanolamine (PE) on the inner leaflet of the cell membrane, and phosphatidylcholine and sphingomyelin on the external leaf of the cell membrane (Morel et al., 2011). This process is regulated by three membrane enzymes, called flippase, floppase and scramblase. Flippase is an ATP-dependent enzyme that transfers PS and PE from the extracellular surface of the cell membrane to the cytoplasmic side. Floppase is also an ATP-dependent enzyme and transfers phospholipids from the intracellular layer of the cell membrane to the extracellular surface (Herring et al., 2013). Scramblase is an ATP-independent enzyme that facilitates the redistribution of phospholipids in both directions (Hugel et al., 2005; Hankins et al., 2014). Following cellular stimulation, an

Figure 1. 6 Schematic diagram of MV structure



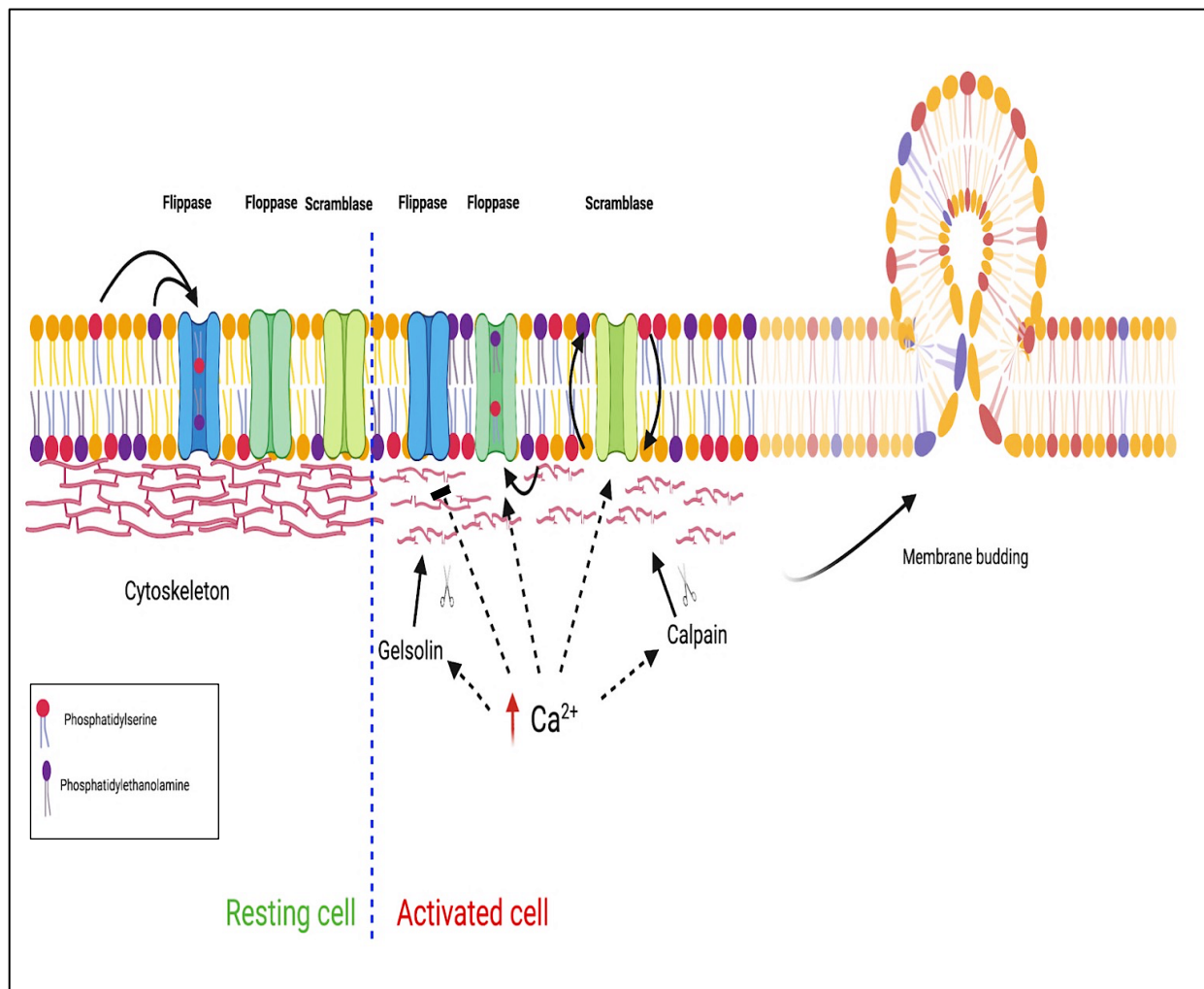
Microvesicles are small membrane-bound vesicles which are released from the plasma membrane following cell activation or apoptosis. The diameter of MV range from 100 nm to 1,000 nm. The membrane of MV is composed of a phospholipid bilayer which contains cytoplasmic and transmembrane proteins derived from their cells of origin. MV can carry distinct components such as tissue factor (TF), selectins and also contain phosphatidylserine within the membrane (adapted from Hugel et al., 2005).

increase in cytosolic Ca^{2+} ion level activates floppase and scramblase activity and blocks the activity of flippase (Figure 1.7; Burnier et al., 2009). Upon disruption of membrane asymmetry, both PS and PE are exposed on the extracellular surface of the plasma membrane. The increased cytosolic Ca^{2+} ion level also activates two enzymes called calpain and gelsolin which disrupt the cytoskeleton (Piccin et al., 2007; Morel et al., 2011; Herring et al., 2013). These changes to cell membrane phospholipid asymmetry, together with the local break down in the cytoskeleton initiate membrane budding which leads to MV release (Zwaal and Schroit, 1997; Hugel et al., 2005; Herring et al., 2013).

1.6.2 Functions of MV

MV have been shown to carry various types of macromolecules, such as membrane receptors, adhesion molecules and nucleic acids (Hugel et al., 2005; Burnouf et al., 2015; Maurer-Spurej et al., 2016). The proteins may facilitate the participation of MV in various physiological and pathological processes (Geddings and Mackman, 2013; Nomura, 2008) including haemostasis, angiogenesis and inflammation (Hugel, et al., 2005; Piccin et al., 2007; Morel et al., 2008). Importantly, MV allow the formation of coagulation complexes, accelerating the rate of coagulation (Piccin et al., 2007). In addition to sustaining the coagulation mechanisms, MV have also been shown to support platelet adhesion (Piccin et al., 2007; Herring et al., 2013). For example, MV-associated von Willebrand factor (vWF) derived from endothelial cells have been shown to enhance platelet aggregation and clot stability (Jy et al., 2005). In addition, MV derived from RBC and platelets have been shown to enhance the coagulation by activating factor XII (Van Der Meijden et al., 2012). Similarly, MV isolated from patients with sickle cell disease have been shown to trigger coagulation pathways by activating factor XI (Van Beers et al., 2009; Rubin et al., 2013). MV can also transfer their cargo to recipient cells (Badimon et al., 2017; Date et al., 2017). For example, incubation of activated platelets with TF-containing MV from monocytes resulted in the incorporation of TF into the activated platelets

Figure 1. 7 Postulated mechanism for MV formation



In resting cells, flippase maintains membrane asymmetry by transferring PS and PE to the inner leaflet of the cell membrane. However, increases in cytosolic Ca^{2+} ion following stimulation activates floppase and scramblase activity and blocks flippase activity, which results in the exposure of both PS and PE on the extracellular surface. Furthermore, cytosolic Ca^{2+} ion activates calpain and gelsolin which disrupt the local cytoskeleton. These changes to cell membrane asymmetry and the cytoskeleton result in membrane budding and the release of MV (adapted from Hugel et al., 2005 and Morel et al., 2011). The figure was created using BioRender.com

del Conde et al., 2005; Osterud and Bjorklid, 2012). Similarly, TF-containing MV may be internalised by endothelial cells (Collier and Ettelaie, 2011). MV can also carry proteins that influence other functions in the recipient cells (Hoyer et al., 2010). These influences include the induction of cellular proliferation by MV (Rackov et al., 2018). For example, incubation of neural stem cell with platelet-derived MV which contained VEGF, increased the rate of cellular proliferation in a process that involved the phosphorylation of ERK and Akt (Hayon et al., 2012). In contrast, MV have also been shown to promote cellular apoptosis. For example, Elkeeb et al. (2004) showed that treatment of endothelial cells with cancer cell-derived MV which contained TF, resulted in activation of p53 through the p38 MAPK signalling. This aberrant over-activation of p53 resulted in the upregulation of Bax protein and the subsequent cellular apoptosis (Elkeeb et al., 2014). Similarly, MV isolated from human blood and shown to contain caspase-3 promoted apoptosis in pancreatic (AsPC3) and oesophageal (KYSE-270) cell lines (Schneider et al., 2012).

1.7 Endothelial cells

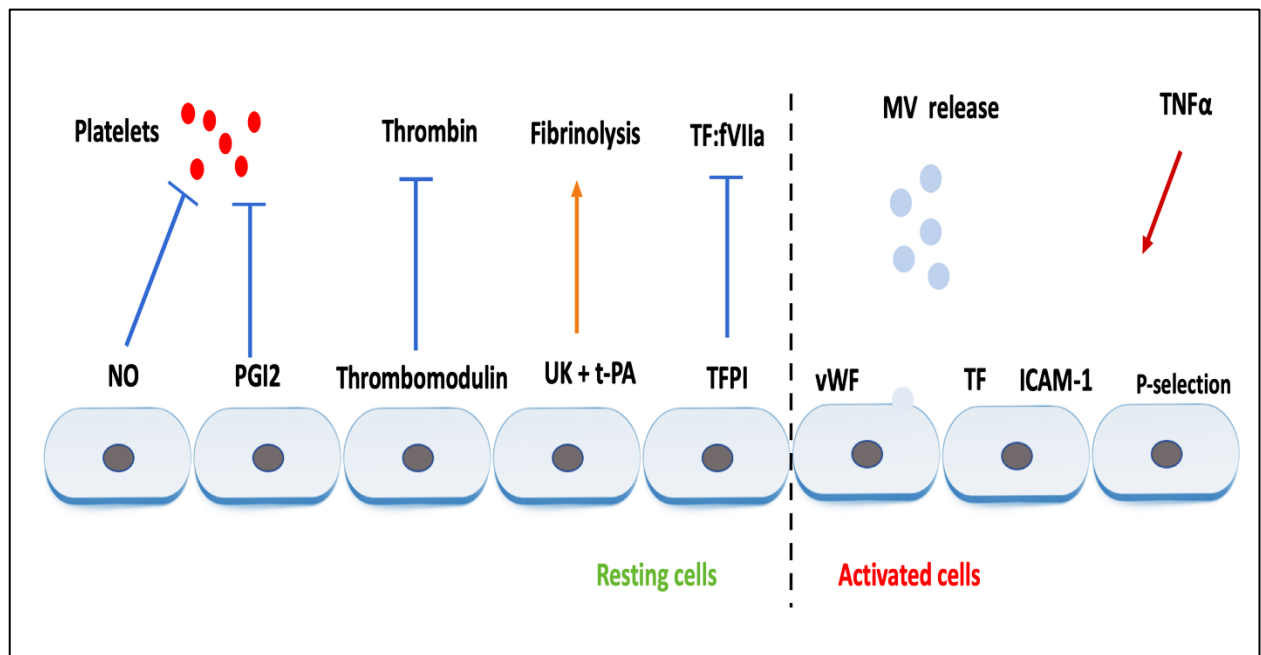
Endothelial cells cover the inner surfaces of lymphatic and blood vessels. These cells form an elongated cell monolayer which is oriented in the direction of blood flow. Endothelial cells act as a barrier to separate the blood from the surrounding tissue (Alberts et al., 2002; Sumpio et al., 2002; Pepper and Skobe, 2003). The main function of endothelial cells is to regulate and maintain vascular tone and blood flow (Michiels, 2003). Under normal conditions, healthy endothelial cells suppress clot formation by expressing proteins such as tissue factor pathway inhibitor (TFPI), thrombomodulin, tissue-type plasminogen activator (t-PA) and urokinase (UK), that suppress coagulation. In addition, endothelial cells synthesise antiplatelet factors such as nitric oxide and prostacyclin on the surface to prevent platelet aggregation (Figure 1.8) (Kato, 2002; Michiels, 2003). Following injury, endothelial cells synthesise and release factors

that promote blood coagulation including TF, fVIII and factor V (Michiels, 2003; Turner and Moake, 2015). Concurrently, the endothelial cells express vWF and P-selectin on the surface to promote platelet adhesion (Denis, 2002; Michiels, 2003). Endothelial cells can also be activated by inflammatory mediators such as cytokines (Pearson, 1999). Following activation, endothelial cells express adhesion molecules such as intercellular adhesion molecule 1 (ICAM-1) and vascular cell adhesion molecule 1, in addition to selectins to promote the adherence of leucocytes at the site of inflammation (Figure 1.8) (Sprague and Khalil, 2009). Furthermore, endothelial cells can release TF-bearing MV when exposed to inflammatory stimuli (Morel et al., 2004; Morel et al., 2006). A number of studies have suggested a direct correlation between the level of circulating MV and the extent of endothelial dysfunction in patients with diabetes, hypertension, and heart disease, or those who have suffered myocardial infarction (Boulanger et al., 2001; Badimon et al., 2017; Silambanan et al., 2019). In support of this observation, MV derived from T lymphocytes have been shown to induce endothelial dysfunction through suppressing the expression of endothelial nitric oxide synthase (eNOS) (Martin et al., 2004). Such endothelial dysfunction is thought to be as a result of cellular apoptosis. As mentioned above, MV-associated TF have been shown to induce endothelial cell apoptosis (Elkeeb et al., 2014; Ethaeb et al., 2019). Therefore, investigation of the influence of MV may explain the endothelial cell degeneration that accompanies many chronic diseases.

1.8 Cellular apoptosis

Apoptosis, also known as programmed cell death is a highly regulated cellular mechanism in which cells are eliminated without releasing harmful material into the surrounding environment (Reed, 2000; Singh et al., 2019). Apoptosis is a physiological process and occurs in every multi-cellular organism. Apoptosis plays a vital role in development and homeostasis by removing unhealthy or unwanted cells (Jacobson et al., 1997; Zhang et al., 2005). However, apoptosis can also be triggered during pathological conditions by external stimuli such as viral

Figure 1. 8 Schematic representation of functions of endothelial cells



Endothelial cells express anticoagulant factors including tissue factor pathway inhibitor (TFPI), thrombomodulin, tissue-type plasminogen activator (t-PA) and urokinase (UK). Endothelial cells also synthesise antiplatelet factors such as nitric oxide (NO) and prostacyclin (PGI2) on the surface to prevent platelet aggregation. In addition, endothelial cells can synthesise and release factors such as TF and von Willebrand factor (vWF) that participate in blood coagulation and platelet adhesion. Endothelial cells also release MV and express adhesion molecules such as P-selectin and ICAM-1 on the cell surface in response to inflammatory stimuli such as tumour necrosis factor α (TNF- α) (adapted from Michiels, 2003).

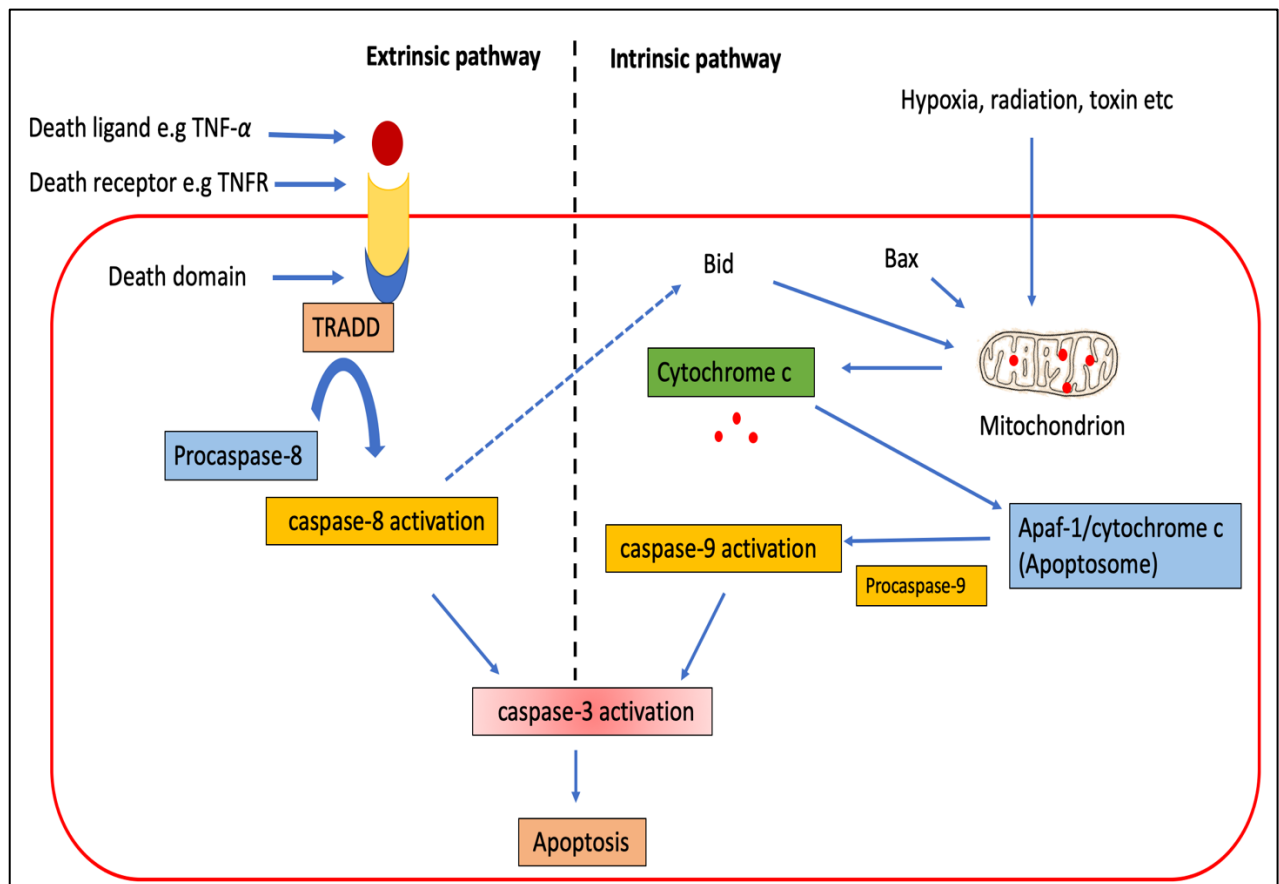
infection (Thomson, 2001), growth factor withdrawal (Verheij and Bartelink, 2000) and hypoxia (Sendoel and Hengartner, 2014). In addition, chemotherapeutic drugs have been shown to eliminate cancer cells by inducing apoptosis (Pucci et al., 2000). The morphological changes associated with apoptosis include chromatin condensation, membrane blebbing, cell shrinkage and DNA fragmentation (Danial and Korsmeyer, 2004). The mechanisms of both apoptosis are interlinked with those of cell proliferation and are highly regulated.

Cell cycle checkpoints are a control system which ensure the integrity of DNA and progression of cell division during cell cycle. The major regulatory checkpoints are at G1/S, G2/M and the spindle checkpoint. G1/S is one the main regulatory checkpoint where the cells may become arrested in the cell cycle, or continue with the cell division. DNA damage activates the checkpoint control system that cause cell cycle arrest in order to allow the cell to attempt to repair the damage. Once the damage is repaired, the cell cycle may resume. However, the cell will undergo apoptosis if the damage is irreparable (Pucci et al., 2000). Apoptosis can occur via the extrinsic (death receptor) pathway or the intrinsic (mitochondrial) pathway and both of these pathways lead to the activation of the enzyme, caspase-3 (Figure 1.9) (Elmore, 2007; Singh et al., 2019). In the extrinsic apoptosis pathway, death activators such as Fas ligand or tumour necrosis factor α (TNF- α) interact with their corresponding death-receptors on the cell surface. The engagement of the death-receptor with its ligand leads to recruitment of adaptor proteins such as FAS-associated death domain (FADD) and TNFR-associated death domain (TRADD). The adaptor protein then induces the dimerization and activation of caspase-8. Activated caspase-8 in turn activates caspase-3 and initiates the extrinsic pathway of apoptosis (Chinnaiyan et al., 1995; Kumar et al., 2005; Elmore, 2007; Wali et al., 2013; McIlwain et al., 2015; Savitskaya and Onishchenko, 2015). Additionally, caspase-8 can initiate the intrinsic pathway of apoptosis through cleavage of Bid protein. Bid is a pro-apoptotic member of Bcl-2 family (Figure 1.9; McIlwain et al., 2015). The intrinsic pathway of apoptosis is activated by

various types of cellular stress including viral infection, growth factor withdrawal and hypoxia (Loreto et al., 2014). The activation of the intrinsic pathway can damage the mitochondrial membrane and increases the permeability of the inner membrane, resulting in the release of mitochondrial proteins such as cytochrome *c* into the cytoplasm. Cytochrome *c* binds to a protein called the apoptotic protease activating factor-1 (Apaf-1) forming what is called the apoptosome. The apoptosome binds and activates procaspase-9 (Savitskaya and Onishchenko, 2015) which in turn activates caspase-3 (Figure 1.9). Once caspase-3 is activated, it can trigger DNA degradation through activating the inhibitor of caspase activated DNase (ICAD) protein, which results in dissociation of DNase from ICAD. The release of DNase in turn, causes DNA degradation and fragmentation (Kitazumi and Tsukahara, 2010). In addition, the increased cytosolic Ca^{2+} ion levels during apoptosis induces cytoskeleton degradation and membrane blebbing as mentioned above. Other proteins are also released from mitochondria which include a protein termed the second mitochondrial-derived activator of caspases (SMAC). SMAC binds to and blocks the function of inhibitors of apoptosis proteins (IAP) (Fulda and Debatin, 2006; Elmore, 2007). IAP proteins have key roles in preventing apoptosis through binding and inhibiting caspases-3, -7 and -9 activation (Deveraux et al., 1998).

The intrinsic pathway is also regulated by Bcl-2 family of proteins which are comprised of both pro-apoptotic and anti-apoptotic regulators. The anti-apoptotic proteins, such as Bcl-2, Bcl-xl and Mcl-1 inhibit caspase activity and prevent the release of cytochrome *c* from mitochondria. In contrast, the pro-apoptotic proteins such as Bax, Bak and Bad enhance the release of cytochrome *c* (Chao and Korsmeyer, 1998; Reed, 2000; Wali et al., 2013). Dysregulation of the balance of apoptosis leads to disease conditions. For instant, a relatively high rate of apoptosis may lead to atrophy of the tissue whereas defects in apoptotic mechanisms permits uncontrolled cell proliferation which consequently contributes to the occurrence of tumours (Pucci et al., 2000).

Figure 1. 9 Schematic representation of the extrinsic and intrinsic pathways of apoptosis



Apoptosis can occur through the extrinsic and intrinsic mechanisms. In the extrinsic pathway of apoptosis, the engagement of the death activator and its corresponding receptor leads to dimerization and activation of caspase-8 with the recruitment of adaptor protein (TRADD). Activated caspase-8 then directly activates caspases-3. In addition, caspase-8 can initiate intrinsic pathway through activation of Bid protein. The intrinsic pathway is activated by various types of cellular stresses such as viral infection. Such stimuli increase the permeability of the inner mitochondrial membrane resulting in the release of cytochrome *c* into the cytoplasm. Cytochrome *c* then binds with the apoptotic protease activating factor-1 (Apaf-1) to form the apoptosome which activates caspase-9. Caspase-9 in turn activates caspase-3 which promotes cell apoptosis through inducing inhibitor of caspase activated DNase (ICAD) cleavage which releases the active DNase enzyme. Pro-apoptotic proteins such as Bax can also induce the intrinsic pathway by promoting the release of cytochrome *c* from mitochondria (adapted from McIlwain et al., 2015).

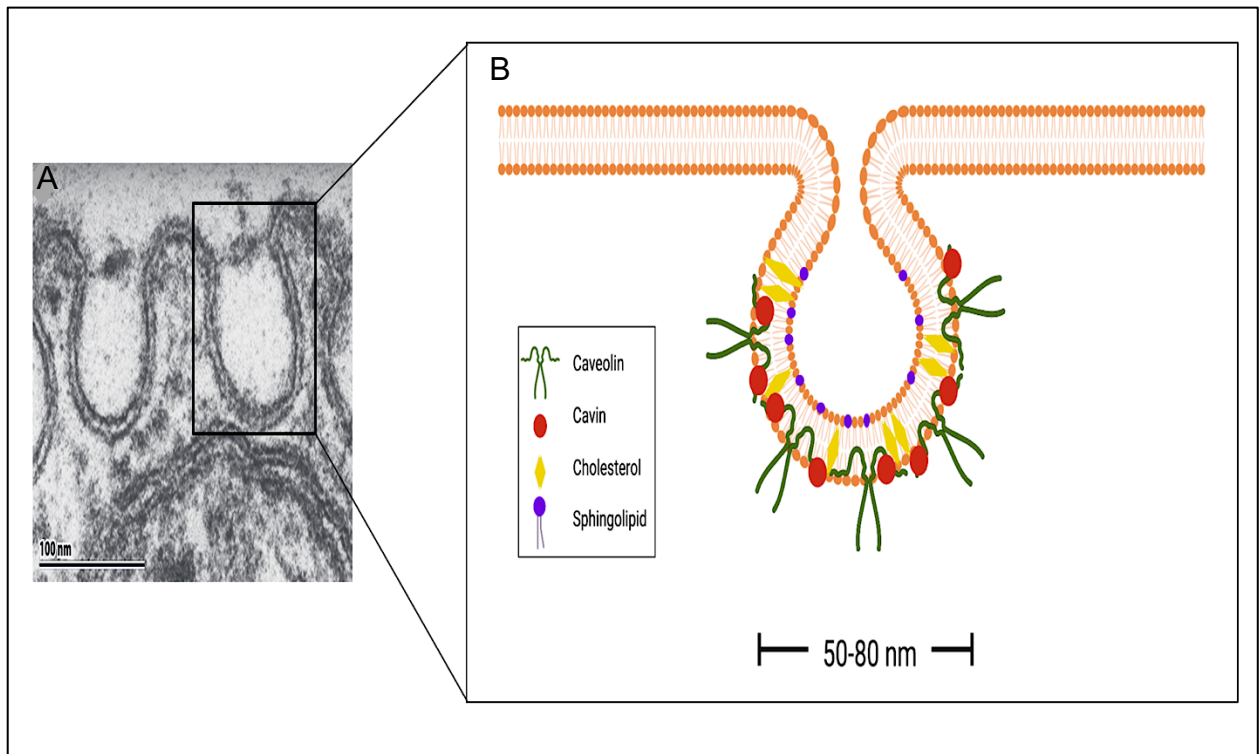
pro-apoptotic and anti-apoptotic regulators. The anti-apoptotic proteins, such as Bcl-2, Bcl-xl and Mcl-1 inhibit caspase activity and prevent the release of cytochrome *c* from mitochondria. In contrast, the pro-apoptotic proteins such as Bax, Bak and Bad enhance the release of cytochrome *c* (Chao and Korsmeyer, 1998; Reed, 2000; Wali et al., 2013). Dysregulation of the balance of apoptosis leads to disease conditions. For instant, high rate of apoptosis may lead to atrophy of the tissue. In contrast, defects in apoptotic mechanisms permits uncontrolled cell proliferation which consequently contributes to the occurrence of tumours (Pucci et al., 2000).

1.9 Caveolae

Caveolae (derived from the Latin for ‘little caves’) are small invaginations of plasma membrane microdomains with diameters of between 50 nm and 80 nm. Although caveolae can be found in many cell types, these are most prevalent in endothelial cells, adipocytes and SMC (Nixon et al., 2007; Parton and Simons, 2007; Parton, 2018). Caveolae are rich in cholesterol and glycosphingolipids and also contain a number of integral membrane proteins termed caveolins, which are essential for the formation of caveolae. A single caveolae may contain up to 144 caveolin protein molecules (Figure 1.10; Pelkmans and Zerial, 2005). Three distinct caveolin proteins have been identified of which caveolin-1 and caveolin-2 are mainly expressed in endothelial cells and adipocytes. Caveolin-3 has been shown to be more abundantly expressed in cardiac and skeletal muscle (Chidlow and Sessa, 2010; Nixon et al., 2007). Other proteins are also associated with caveolae including cavin proteins.

There are four cavin proteins which are essential in the formation and stabilisation of caveolae structure. Cavins regulate the function and organisation of caveolin proteins by acting as the molecular scaffold for these proteins (Hansen and Nichols, 2010;). However, it has been reported that cavin 3 might also be involved in the formation of caveolae-derived endosomal

Figure 1. 10 Schematic representation of the structure of the caveolae



A) Electron micrograph of caveolae showing invaginations in an endothelial cell. Caveolae are small invaginations of plasma membrane microdomains. They range in size from a diameter of 50 to 80 nm. B) Caveolae contain caveolin and cavin proteins and are rich in cholesterol and sphingolipids (adapted from Shibata et al., 2009 and Bastiani and Parton, 2010). The figure was created using BioRender.com

vesicles (Chidlow and Sessa, 2010). Caveolae are involved in a variety of cellular processes including lipid homeostasis and endocytosis (Thomas and Smart, 2008). For example, it has been demonstrated that the over-expression of caveolin-1 in cells increases cellular levels of free cholesterol and increases with fatty acid uptake by cells (Parton and Simons, 2007). In contrast, low expression of caveolin-1 has been shown to result in the reduction in cholesterol synthesis in mice (Frank et al., 2006). Caveolae are also involved in cell signalling (Chidlow and Sessa, 2010; Bastiani and Parton, 2010; de Almeida, 2017). In support of this, Liao et al. (2009) demonstrated that caveolae provide a platform for the assembly of the signalling complex by VEGFR2, following engagement of VEGF, which leads to ERK1/2 signalling and endothelial cell proliferation. The study also reported that the disruption of the structure of caveolae using methyl- β -cyclodextrin resulted in the elimination of VEGF signalling and reduced the rate of cell proliferation (Liao et al., 2009). Caveolae may also play an essential role in a variety of pathological process since they are expressed by the majority of cells (Thomas and Smart, 2008; Frank, 2010). Currently, there is contrasting literature that suggests the opposite influence of caveolae on the regulation of tumour formation and growth (Tahir et al., 2001; Fong et al., 2003; Thomas and Smart, 2008; Thompson et al., 2009). For example, Capozza et al. (2003) reported that mice lacking caveolin-1 showed a high rate of tumour growth and incidence, compared to wild-type mice. In contrast, down-regulation of caveolin-1 expression significantly decreased tumour growth and metastasis of prostate xenografts in mice (Williams et al., 2005). Such dissimilar behaviours may arise from the ability of caveolae to harbour a number of different soluble proteins and receptors (Sevinsky et al., 1996). Importantly, several studies have suggested that TF, either alone or in complex with fVIIa, may become associated with the caveolae (Liu et al., 1997; Sevinsky et al., 1996; Mulder et al., 1996; Mandal et al., 2006; Awasthi et al., 2007). Therefore, the regulation of both the

procoagulant and the signalling activities of TF by caveolae were examined in the current study.

1.10 Endocytosis

Endocytosis is an essential, energy dependent process performed by eukaryotic cells that consists of the engulfment and internalisation of substances such as macromolecules, receptor proteins and even other cells from the surrounding medium (Cooper, 2020; Kumari et al., 2010; Lakoduk and Schmid, 2016; Aguilar and Wendland, 2005; Marcel et al., 2018). The substance to be internalised is surrounded by part of the plasma membrane which forms a pocket (invagination). This pocket then buds off into the cytoplasm to form a vesicle containing the endocytosed material. These endosomal vesicles are critical for many physiological processes including nutrient uptake, cell adhesion, membrane remodelling, cell signalling and also involved in pathogen entry (Kaksonen and Roux, 2018). The most common types of endocytosis is called phagocytosis (meaning “cell eating”), pinocytosis (meaning “cell drinking”), receptor-mediated endocytosis (also known as clathrin-mediated endocytosis) (Ellinger and Pietschmann, 2016; Kumari et al., 2010; Mayor et al., 2014) and caveolae/raft-dependent endocytosis (Hansen and Nichols, 2009). In this study, the focus is on the caveolae-dependent endocytosis.

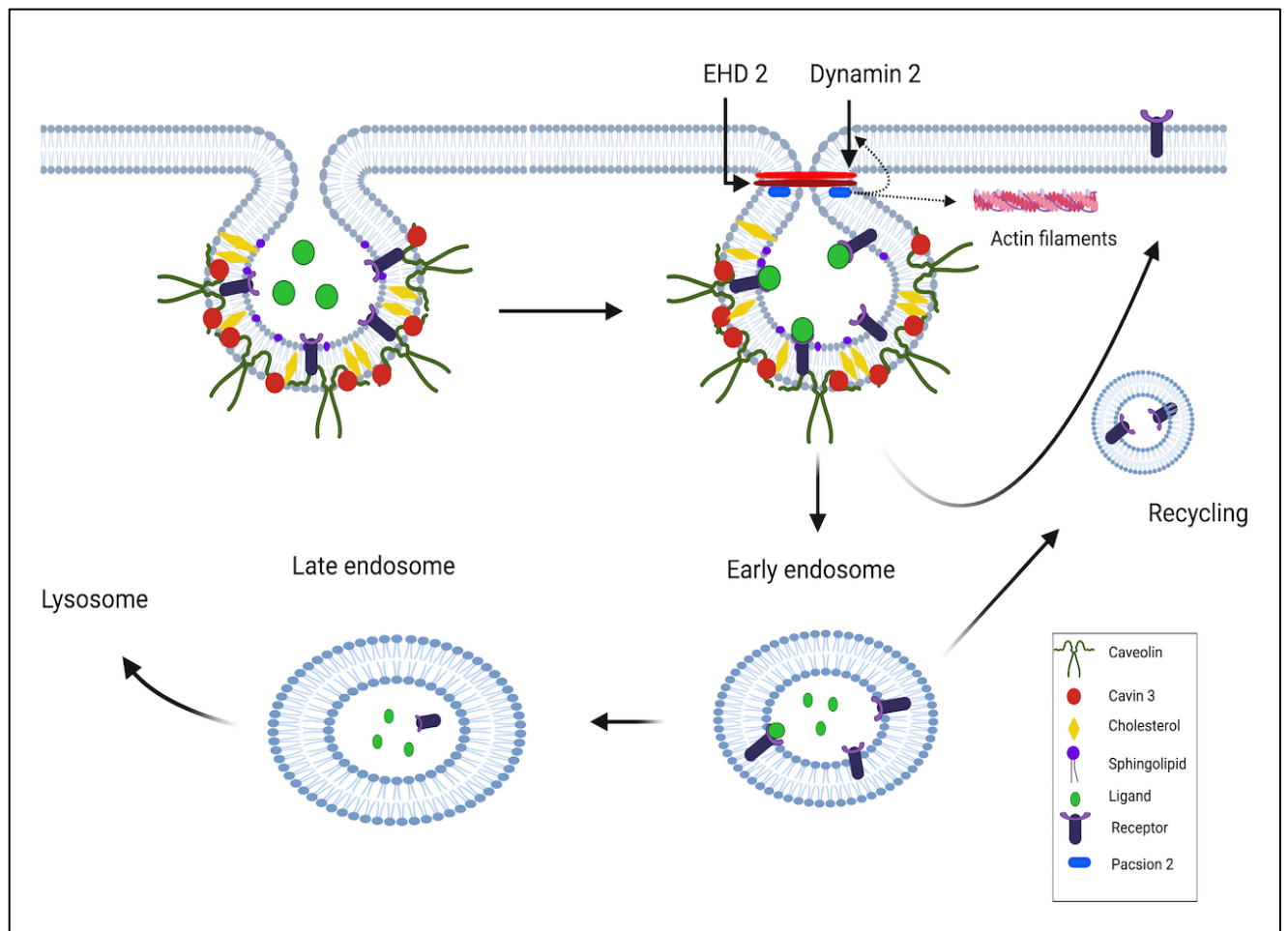
A number of previous studies have demonstrated the role of caveolae in endocytosis (Mellman, 1996; Nabi and Le, 2003; Cooper, 2020; Mayor et al., 2014) including the uptake of proteins such as albumin (Schnitzer et al., 1994), nutrients such as folic acid (Anderson et al., 1992) and receptors such as the insulin receptor (Chen et al., 2019). The caveolae endocytosis is also implicated in infections such as those by the human immunodeficiency virus (Campbell et al., 2001) and influenza virus (Nunes-Correia et al., 2004). The TF-fVIIa complex has previously been reported to be endocytosed through clathrin-independent endocytosis (Hansen et al.,

2001). However, Collier et al. (2013) reported that inhibition of the dynamin protein slowed down, but did not prevent, the internalisation of MV-associated TF by endothelial cells. The authors suggested that TF may be endocytosed through both clathrin-dependent and independent mechanisms (Collier et al., 2013). While the results of recent studies suggest a possible role of caveolae in endocytosis, the link between caveolae and endocytosis remains controversial (Parton and Howes, 2010; Cheng and Nichols, 2016). It has even been suggested that caveolin proteins can themselves be taken up through clathrin endocytosis. For example, the overexpression of caveolin-1-green fluorescent protein (GFP) results in its degradation within the late endosomal compartments (Shvets et al., 2015). This finding suggests that take up of cargo is processed through clathrin endocytosis pathway rather than caveolae (Shvets et al., 2015). In addition, Simian virus 40 (SV40), which is considered a caveolar endocytosis marker, has also been shown to be internalised through clathrin endocytosis pathway (Pelkmans, et al., 2004).

The exact mechanism of caveolar endocytosis is not yet fully understood (Mellman, 1996; Nabi and Le, 2003; Cooper, 2020; Mayor et al., 2014; Cheng and Nichols, 2016). For example, it has been suggested that caveolae may rely on dynamin for endocytosis (Henley et al., 1998). However, the involvement of dynamin in caveolar endocytosis is also disputed (Corrotte et al., 2013). The mechanism of caveolar endocytosis is thought to be mediated through cavin 3 and scission proteins (Shvets et al., 2015) and is initiated when a ligand binds to its corresponding receptor (Yao et al., 2005). Unlike the other cavins, cavin 3 destabilizes caveolae which promotes the budding and release of caveolae (Shvets et al., 2015; Cheng and Nichols, 2016). Initially, oligomerisation of EHD2 protein forms a ring around the neck of caveolae and also recruits pacsin 2, which links the caveolae membrane to actin filaments. Pacsin 2 then recruits dynamin-2 which assembles around the neck of the caveolae forming helical rings that cleave the caveolae vesicles and release them into the cytoplasm (Figure 1.11; Hansen et al., 2011;

Cheng and Nichols, 2016; Oh et al., 1998). After the budding of the caveolae-derived endosomal vesicles from the plasma membrane, the vesicles may fuse back into the plasma membrane or develop into early endosomes. These may then mature into late endosomes some of which are broken down in the lysosome (Branza-Nichita et al., 2012; Chen et al., 2019; Huotari and Helenius, 2011; Naslavsky and Caplan, 2018). As mentioned above, TF may be endocytosed by different mechanism involving clathrin or caveolae. In addition, the TF associated with caveolae is shown to remain in an encrypted form (Dietzen et al., 2004). Therefore, in this study, the involvement of caveolae in the regulation of the procoagulant and signalling functions of TF was investigated.

Figure 1. 11 Proposed mechanism of caveolae-dependent endocytosis



Receptor-ligand binding in caveolae results in disruption of the cytoskeleton and initiation of caveolar endocytosis. Cavin 3 destabilizes the caveolae. EHD 2 proteins then oligomerize and form a ring around the neck of the caveolae and also recruit pacsin 2 protein. Pacsin 2, associated with EHD 2, links caveolae membrane to actin filaments and also recruits dynamin 2. Dynamin 2 proteins then assemble around the neck of caveolae, forming a helical ring which results in the release of caveolae into the cytoplasm. The caveolae-derived endosomal vesicles then either fuse back into the plasma membrane or develop into early endosomes. These then mature into late endosomes some of which are broken down in lysosomes (adapted from Chen et al., 2019 and Echarri and Del Pozo, 2015). The figure was created using BioRender.com

1.11 Aims

MV can contain TF, functional fVIIa and negatively charged phospholipids. Elevated levels of MV-associated TF can be detected in patients with chronic diseases such as cancer, diabetes and cardiovascular disease and may be involved in the progression of these conditions. TF signalling plays a vital role in many physiological and pathological functions and the exposure of endothelial cells to high levels of TF can induce cellular apoptosis resulting in vasculature damage and dysfunction. Therefore, the aim of this study was to examine the mechanisms by which cells clear excess TF, to avoid the detrimental effects of TF accumulation. The main objectives of the study are outlined below.

- To examine if MV derived from a panel of cancer cell lines (HepG2, 786-O, BxPC-3, MDA-MB-231 and MCF-7) mediate distinct and dissimilar effects on endothelial cells by evaluating the outcome on cellular apoptosis and proliferation.
- To examine the mechanisms underlying the cellular outcomes observed above, by examining the relationship between PAR2 activation and MV release in both tumour cell lines and endothelial cells.
- To investigate the ability of caveolae to harbour and regulate the function of the TF-fVIIa complex through
 - Examining the requirements for the association of TF and fVII/fVIIa with caveolin-1 in endothelial cells.
 - Investigating the co-localisation of labelled TF with caveolae on the surface of endothelial cells by confocal microscopy.
 - Assessing the influence of cholesterol-depletion of cell-membrane on TF-mediated signalling.

- To investigate the ability of rivaroxaban and apixaban to block the proteolytic activity of purified fVIIa or cancer cell-derived MV-associated fVIIa, and to examine the influence of these two compounds on induction of cell apoptosis and proliferation by TF.

Chapter 2

Materials and methods

2.1 Materials

Ambion® by life technologies™ , Loughborough, UK

Silencer® Select Pre-designed siRNA (fVII)

Silencer® Select Pre-designed siRNA (PAR2)

Silencer® Select Negative Control #1 siRNA

Abcam, Cambridge, UK

Rabbit anti-factor VIIa polyclonal antibody (ab7053)

Rabbit anti-human TF polyclonal antibody

Beckman Coulter, High Wycombe, UK

1.5 ml ultracentrifuge tube

TLA-100 rotor

TL-100 Ultracentrifuge

Eppendorf Ltd, Stevenage, UK

Eppendorf µCuvette G1.0

Eppendorf BioSpectrometer®

BD Bioscience, Oxford, UK

Becton Dickinson FACS Calibur flow cytometer

CellQuest software version 3.3

Falcon FACS tubes

BDH, Pool, UK

SDS (sodium dodecyl sulphate)

Glycerol

Magnesium chloride

Sodium acetate

Sodium hydroxide

Bioline Ltd, London, UK

Molecular grade agarose

Bio-Rad, Hemel Hempstead, UK

iCycler real-time thermal cycle

Nitrocellulose membrane

Mouse anti-human TF antibody (10H10)

Mouse anti-human PAR2 antibody (SAM11)

Promega Corporation, Southampton, UK

GoTaq® 1-Step RT-qPCR System

Midipreps DNA purification system

TBE Buffer; 0.9 M Tris-borate (pH 8.3), 25 mM EDTA

TMB stabilised substrate for horse raddish peroxidase

Western blue stabilised substrate for alkaline phosphatase

Qiagen, Manchester, UK

QuantiTect beta-actin primers

QuantiTect human coagulation fVII primers

BMG lab Tech, Offenburg, Germany

POLAR star OPTIMA Plate reader

Thermo Fisher scientific, Loughborough, UK

GeneRuler 1 kbp DNA ladder

Multicolour broad range protein ladder (10-260 kDa)

Mouse anti-human TF antibody (HTF-1)

Glycine

NaCl

Tris Base

DAPI (4',6-diamidino-2-phenylindole), NucBlue™ Fixed Cell

Flowgen Bioscience, Nottingham, UK

Horizontal electrophoresis tank

Proto FlowGel (acrylamide: bisacrylamide)

Proto FlowGel, resolving buffer (1.5 M Tris-HCl (ph 8.8), 0.4% (w/v) SDS.)

Proto FlowGel staking buffer

FMC Corporation, Philadelphia, USA

SYBR Green I DNA stain

Gibco- Invitrogen Corporation, Paisley, UK

Opti-MEM® I reduced serum medium

TrypLE™ Select Enzyme (10X), no phenol red

Endothelial cell serum-free medium

Greiner Bio-One Ltd, Gloucestershire, UK

6, 12, 48 and 96 well culture plates

25 and 75 cm² cell culture flasks

Hofer, Inc, San Francisco, USA

TE 50X protein transfer tank

<http://imagej.nih.gov/ij/>

ImageJ program

LGC-ATCC, Teddington, UK

MDA-MB-231 breast cancer cell line (HTB-26)

BxPC-3 pancreatic cancer cell line (CRL-1687)

MCF-7 breast cancer cell line (HTB-22)

CLS, Hamburg, Germany

HepG2 liver cancer cell line (330198)

Lonza, Basel, Switzerland

DMEM medium (4.5 g/L Glucose with L-Glutamine)

RPMI-1640 medium (with L- Glutamine)

EMEM medium (without L- Glutamine)

Foetal calf serum (FCS)

LOXO, Dossenheim, Germany

fVII chromogenic substrate

Mirus Bio LLC, Madison, USA

Trans IT® -2020 transfection reagent

New England Biolab, Hitchin, UK

Monrach plasmid miniprep kit

Monrach PCR & DNA cleanup kit

DNA ligase master mix

BamHI- high fidelity restriction enzyme

HindIII-high fidelity restriction enzyme

Quick load purple DNA ladders

SOC Outgrowth Medium

Addgene, Massachusetts, USA

mCherry2-C1 plasmid

mEmerlad-C1 plasmid

PromoCell, Heidelberg, Germany

Endothelial cell growth medium (MV)

Endothelial cell growth supplement pack

Human coronary artery endothelial cells (HCAEC)

Human dermal blood endothelial cells (HDBEC)

R&D Systems, Abingdon, UK

Escherichia coli TB-1 strain

Human Coagulation Factor III/Tissue Factor Quantikine ELISA

TiterTACS *In Situ* Detection Kit - Colorimetric

Mouse anti-human fVII antibody (321621)

Goat anti-human fVII polyclonal antibody

Mouse anti-human fX antibody

Santa Cruz Biotechnology, Heidelberg, Germany

Donkey anti-goat alkaline phosphatase-conjugated antibody

Goat anti-GAPDH polyclonal antibody

Goat anti-mouse alkaline phosphatase-conjugated antibody

GeneTex, Irvine, USA

Rabbit anti-human caveolin 1 antibody

Sigma Chemical Company, Poole, UK

Ammonium persulphate

Antibiotic antimycotic solution (Penicillin - Streptomycin - Kanamycin
Solution) (100X)

Bovine serum albumin (BSA)

Cycloheximide

Hydrogen peroxide solution (H₂O₂) 37%

Laemmli electrophoresis buffer (4% (w/v) SDS, 20% (w/v) glycerol, 10% (w/v)
2-mercaptoethanol, 0.004% (w/v) bromophenol blue and 0.125 M Tris-HCl, pH 6.8)

N,N,N',N'-Tetramethylethylenediamine (TEMED)

Phosphate buffered saline (PBS) solution (10X)

Powder microbial growth medium LB agar (Lennox)

Powdered microbial growth medium LB Broth (Luria Broth)

Proteinase-activated receptor 2-activating peptide (PAR2-AP)

Nuclease-free water

Trypsin/EDTA solution (1X)

Methyl- β -cyclodextrin

Tween 20

TCS Cellworks, Claydon, UK

DMSO freeze medium

UVP LTD, Cambridge, UK

3 UV-transilluminator

WPA, Cambridge, UK

UV-Visible spectrophotometer

AssayPro, Missouri, USA

Human Factor VII ELISA Kit

Lipocalyx GmbH, Weinbergweg, Germany

Viromer Red transfection reagent

VWR, Lutterworth, UK

RiboZol RNA Extraction Reagent

Severn Biotech, Kidderminster, UK

Chromogenic substrate (NH₂-Asn-Leu-Thr-Arg-pNA)

- 786-O renal cancer cell line was a gift from Dr. L. Nikitenko and MDA-MB-231 tissue factor knock out was provided by Dr. A. Rondon.

2.2 Methods

2.2.1 Cell culture

To minimise the risk of infection, all cell culture procedures were conducted in a biosafety class II laminar flow cabinet under sterile conditions. The cabinet was cleaned with diluted Dettol and 70% (v/v) industrial methylated spirit (IMS) and only sterile plasticware was used. All the media and reagents were warmed in a 37°C water bath prior to use.

Eight types of cells were used throughout this study:

- Human breast cancer cell line (MDA-MB-231).
- Human breast cancer tissue factor knock out cell line (MDA-MB-231 TF KO).
- Human breast cancer cell line (MCF-7)
- Human pancreatic cancer cell line (BxPC-3)
- Human renal carcinoma cell line (786-O)
- Human hepatocellular carcinoma cell line (HepG2)
- Human dermal blood endothelial cells (HDBEC).
- Human coronary artery endothelial cells (HCAEC).

I. Culture of cell lines

The MDA-MB-231 and MDA-MB-321 TF KO cells were cultured in DMEM medium. The BxPC-3 and 786-O cell lines were cultured in RPMI 1640 medium, and the MCF-7 and HepG2 cell lines were cultured in EMEM medium. All media were also supplemented with 10% (v/v) foetal calf serum (FCS) and 1% (v/v) antibiotic (penicillin (5 unit/ml), streptomycin (5 µg/ml) and amphotericin (25 ng/ml)). The cell lines were maintained in a humidified incubator at 37°C and in a 5% CO₂ atmosphere. All the media were replaced every 2 to 3 days with fresh medium as explained in 2.2.2.

II. Culture of primary cells

HDBEC and HCAEC cells were cultured in endothelial cell growth medium (MV) supplemented with 5% (v/v) FCS, epidermal growth factor (10 ng/ml), endothelial cell growth supplement (4 µl/ml), hydrocortisone (0.2 µg/ml) and heparin (90 µg /ml). The cells were kept in a humidified incubator at 37°C under 5% CO₂ atmosphere. All the media were replaced every 3 days with fresh medium.

2.2.2 Harvesting, subculturing and counting of cells

To harvest the cells, the medium was removed from the flask and the cells were washed twice with sterile phosphate buffer saline (PBS; pH 7.2) to remove any traces of the serum. Approximately 3 ml of trypsin/EDTA solution was added into the flask and then incubated for 5 min at 37°C. When detaching primary cells, 2 ml of TrypLE solution was used instead of trypsin/EDTA solution to prevent damage to the cells. The flask was then tapped gently to release the cells and complete media was added into the flask to deactivate the trypsin or TrypLE. The suspended cells were then transferred into a fresh 20 ml tube and centrifuged at 200 g for 5 min. The supernatant was then removed and the cells re-suspended in fresh medium. To measure the density of cells, 20 µl of the cell suspension was loaded into haemocytometer and the number of cells were counted in 1 mm² squares. The average was taken and multiplied by 10⁴ to estimate the cell number present in 1 ml of cell suspension. The cell suspension was then diluted to the desired density for sub-culturing, freezing or experimentation.

2.2.3 Cryopreservation and recovery of cells

Cells were harvested and counted as in 2.2.2 and were suspended in fresh medium. The cells were then centrifuged at 200 g for 5 min. The supernatant was discarded and the cell pellet re-suspended in DMSO freezing medium at a density of 10⁶ cell/ml. The cell suspension was then distributed to labelled cryovials (3 x 10⁵ cell/vial). The vials were placed in the freezing

container filled with isopropyl alcohol and frozen at -80°C overnight. The vials were then transferred into liquid nitrogen for long term storage. In order to start a new cell culture, a vial of frozen cells was thawed quickly in the water bath at 37°C for 1-2 min and then transferred into the cell culture flask containing the correct pre-warmed medium.

2.2.4 Cells lysis

In order to extract proteins from the cells for western blot analysis, cells were collected in eppendorf tubes (1.5 ml) by centrifugation at speed 300 g for 5 min. The supernatant was discarded and the cells were lysed in 200 μl of Laemmli's buffer. The samples were then heated at 95°C for 10 min to ensure protein denaturation.

2.2.5 SDS-polyacrylamide gel electrophoresis (SDS-PAGE)

A 12% (w/v) polyacrylamide resolving gel was used for the separation of proteins by denaturing electrophoresis (Laemmli, 1970). The gel was prepared by mixing 4 ml acrylamide solution (30% (w/v) acrylamide, 0.8% (w/v) bisacrylamide), 2.6 ml resolving buffer (1.5 M Tris-HCl pH 8.8, 0.4% (w/v) SDS), 3.3 ml dH_2O and 100 μl of 10% (w/v) ammonium persulphate. The mixture was mixed well and 8 μl of N,N,N',N'-tetramethylethylenediamine (TEMED) was added to begin the polymerisation. The mixture was mixed thoroughly and then poured between the electrophoresis glass plates and covered with a layer of butanol. To ensure complete polymerisation, the gel was left for 1 h at room temperature. After the gel had set, the butanol was discarded and a 4% (w/v) stacking gel was poured on top. The gel was made by mixing 0.65 ml of the acrylamide solution, 1.3 ml stacking buffer (0.5 M Tris-HCl pH 6.8, 0.4% (w/v) SDS), 3 ml dH_2O and 100 μl of 10% (w/v) ammonium persulphate (10% w/v). The mixture was thoroughly mixed and 6 μl of N,N,N',N'-tetramethylethylenediamine (TEMED) was added. The mixture was then poured on top of the resolving gel. An appropriate comb was then inserted and the gel was allowed to set for 1 h. After polymerisation, the comb was

removed and the complete gel was placed in the electrophoresis tank. Electrophoresis buffer (25 mM Tris-HCl pH 8.3, 192 mM glycine, 0.035% (w/v) SDS) was poured into the electrophoresis tank until the gel was completely submerged. 6 µl of molecular-weight protein markers (10-260 kDa) was loaded in the first well and then 15 µl of the protein sample was placed in the following wells. The electrophoresis was carried out at 110V for 2 h to separate the proteins.

2.2.6 Western blot analysis

Following electrophoresis, the proteins were transferred onto a nitrocellulose membrane. First, blotting papers and nitrocellulose membrane were soaked for 3 min in the transfer buffer (20 mM Tris-HCl pH 8.3, 150 mM glycine, 20% (v/v) methanol) and then placed in the holding cassette. The gel was placed in between the nitrocellulose membrane and blotting paper and the cassette was placed in a transfer tank containing the transfer buffer. The protein bands were transferred at 300 mA for 70 min at 4°C. Once the proteins were transferred, the nitrocellulose membrane was blocked with TBST (150 mM NaCl, 10 mM Tris-HCl pH 7.4, 0.05% Tween 20(w/v)) for 2 h at room temperature with shaking. The membrane was then incubated with the appropriate primary antibody (Table 2.1) diluted in TBST at 4°C overnight, with shaking. The membrane was then washed two times (10 min each time) with TBST and incubated with an appropriate secondary antibody for 90 min (Table 2.1). The membrane was finally washed two times with TBST (10 min each time) and developed with Western Blue-stabilised substrate for alkaline phosphatase. The images were taken and the visualised bands were analysed using the ImageJ program.

2.2.7 Preparation of microvesicles from conditioned media derived from cell lines

To isolate cell-derived microvesicles (MV) from BxPC-3, HepG2, MDA-MB-231, MCF-7, and 786-O cell lines, the cells were cultured separately in T-25 or T-75 flasks and permitted to

Table 2. 1 Primary and secondary antibody dilutions used in the western blot procedure

Primary antibodies	Dilution antibodies: TBST (v/v)	Secondary antibodies	Dilution antibodies: TBST (v/v)
Goat polyclonal anti-human fVII antibody	1:2000	Donkey anti-goat antibody alkaline phosphatase-conjugated	1:6000
Goat polyclonal anti-human fVII antibody	1:4000	Donkey anti-goat antibody alkaline phosphatase-conjugated	1:4000
Mouse anti-human fVII antibody	1:2000	Goat anti-mouse antibody alkaline phosphatase-conjugated	1:4000
Goat anti-human GAPDH antibody	1:6000	Donkey anti-goat alkaline phosphatase-conjugated antibody	1:6000

reach 75-80% confluence. The cells were then washed twice with PBS and 2 ml of serum-free medium was added to the cells and incubated for 1 h at 37°C. The medium was then collected and centrifuged at 8000 g for 10 min. The supernatant was then transferred into 1.5 ml Beckman ultracentrifuge tubes and centrifuged at 100,000 g for 1 h at 20°C (Collier et al., 2013). Following centrifugation, the supernatants were discarded and the pellets resuspended in Tris-HCl buffer (50 mM) pH 7.0. The samples were collected and stored at -20°C until required.

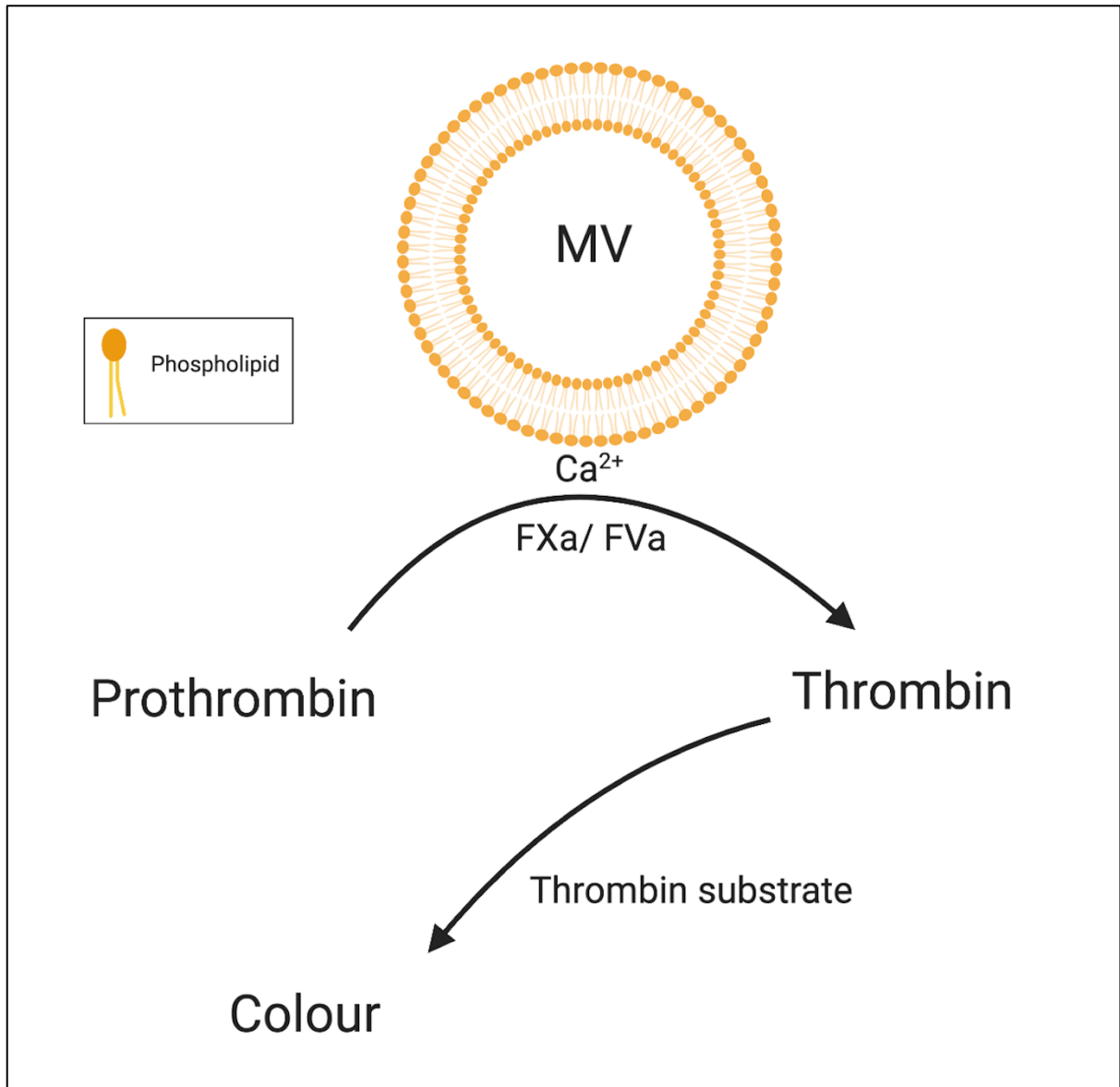
2.2.8 Measurement of the density of isolated MV

The density of the isolated MV samples was quantified by measuring the potential for thrombin generation using the Zymuphen MP Activity kit (Figure 2.1). According to the manufacturer's protocol, all the reagents were incubated at 37°C before use. To maintain the correct pH, 45 µl Tris-HCl buffer (50 mM) pH 7.0 was added to each well of 96-well plate followed by the isolated MV samples. A standard curve was created by using a range of concentrations of MV (0-0.78 nM) provided by the kit (Figure 2.2). To each sample, 40 µl of R1 reagent containing bovine FXa, FVa, and calcium was added. Next, 20 µl of provided R2 reagent containing prothrombin was added to each well. The plate was then incubated for 10 min at 37°C and chromogenic thrombin substrate (50 µl) was added to each well. The plate was again incubated at 37°C until the colour developed. The reaction was finally stopped by adding stop solution (50 µl) containing citric acid 2% (w/v) and the absorptions measured at 410 nm using a plate reader.

2.2.9 Apoptosis assay

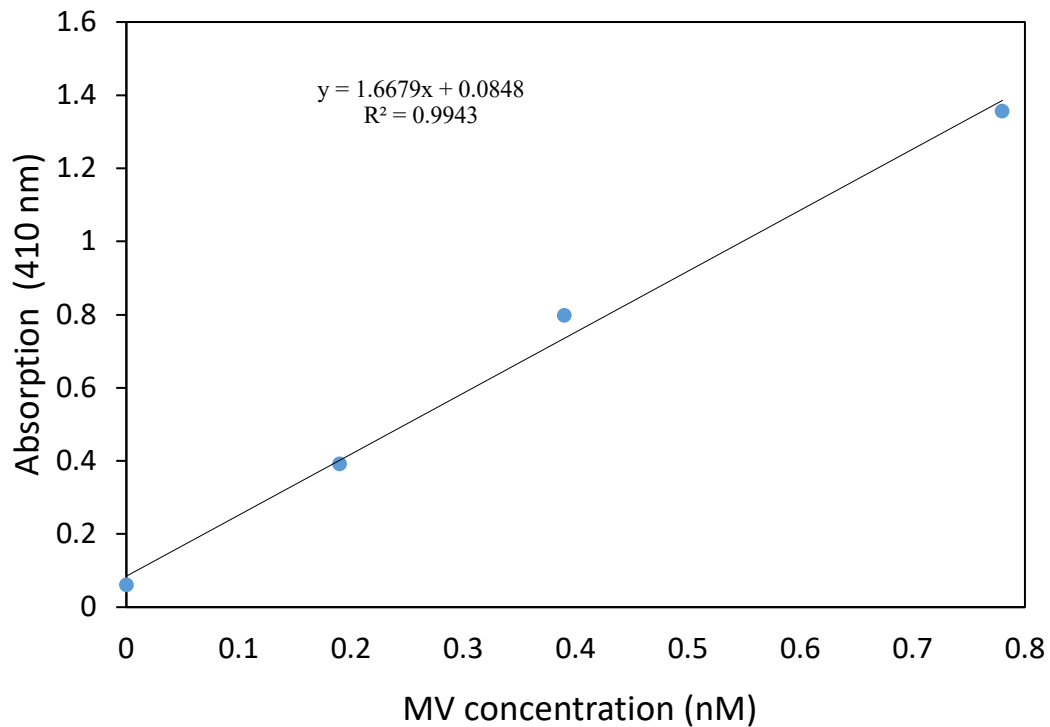
DNA degradation is a key feature of the process of cellular apoptosis which occurs through by the action of endonucleases. In this study, a TUNEL assay based on end-labelling of DNA fragments was applied to detect apoptotic cells by using TiterTACS Colorimetric Kit. HCAEC were seeded into 96-well plates and allowed to adhere. The cells were then treated with test

Figure 2. 1 Microvesicles measurement principle



The Zymuphen MP Activity kit measures MV concentrations based on the direct relationship between the phospholipid concentration and thrombin generation. The combined activity of fXa, fVa and calcium, which requires the presence of phospholipids, converts prothrombin to thrombin. A specific thrombin substrate can be used to determine the concentration of thrombin, which can be extrapolated to indicate the MV concentration.

Figure 2. 2 An example standard curve for MV concentration measured by the Zymuphen MP kit



Serial dilution of MV was made to prepare a range of concentrations (0-0.78 nM) in Tris-HCl buffer (50 mM) pH 7.0). 50 μ l of each diluted standard was then added into 96-well plate followed by adding 40 μ l of R1 reagent containing bovine FXa, FVa and calcium ion. 20 μ l of R2 reagent containing prothrombin was then added to each well then incubated for 10 min at 37°C. Following the incubation, 50 μ l of chromogenic thrombin substrate was added to each well and incubated at 37°C until the colour developed. The reaction was stopped by stop solution (50 μ l) containing citric acid 2% (w/v) and the absorption of the samples was measured at 410 nm using a plate reader (n=2).

reagents as described in the Results sections. In addition, sets of cells were treated with TNF α (1 ng/ml) and used as a positive control. The samples were then incubated for 24 h at 37°C. According to the manufacturer's protocol, the cells were washed two times with pre-warmed PBS and fixed with 4% (v/v) formaldehyde for 15 min. The cells were then washed with PBS and further treated with 100% methanol and incubated for 20 min before washing again with PBS. The cells were then permeabilised by incubation with cytonin provided with the kit (50 μ l) for 15 min. The cells were then washed twice with dH₂O and incubated with 2.5% (v/v) hydrogen peroxide (50 μ l) in 100% methanol for 5 min. The cells were washed again with dH₂O and TdT labelling buffer (150 μ l) was added and incubated for 5 min after which the solutions were discarded. Labelling reaction mixture was prepared by mixing 1X TdT labelling buffer with TdT dNTP Mix (0.35 μ l), 50X Mn²⁺ (1 μ l), and TdT enzyme (0.35 μ l). The mixture (150 μ l) was added to each well and incubated for 1 h at 37°C. After the incubation, 150 μ l of TdT stop buffer was added to each well and incubated for 5 min to stop the labelling reaction. The wells were then washed twice with PBS. Streptavidin-HRP solution was prepared by diluting strep-HRP in blue-strep diluent (1:1250 (v/v)) and 50 μ l of the solution was added to each well and incubated for 10 min. The wells were washed four times with PBS containing 0.1% (v/v) Tween 20 and 100 μ l of chromogenic substrate (TACS-Sapphire) was added to each sample and incubated for 30 min at room temperature in the dark. The reaction was then stopped by adding 100 μ l of 2 N hydrochloric acid (HCl) then the absorptions were measured at 450 nm using a plate reader. DNA fragmentation was measured based on the generated colour and used as a measure of cell apoptosis.

2.2.10 Measurement of fVII antigen by ELISA assay

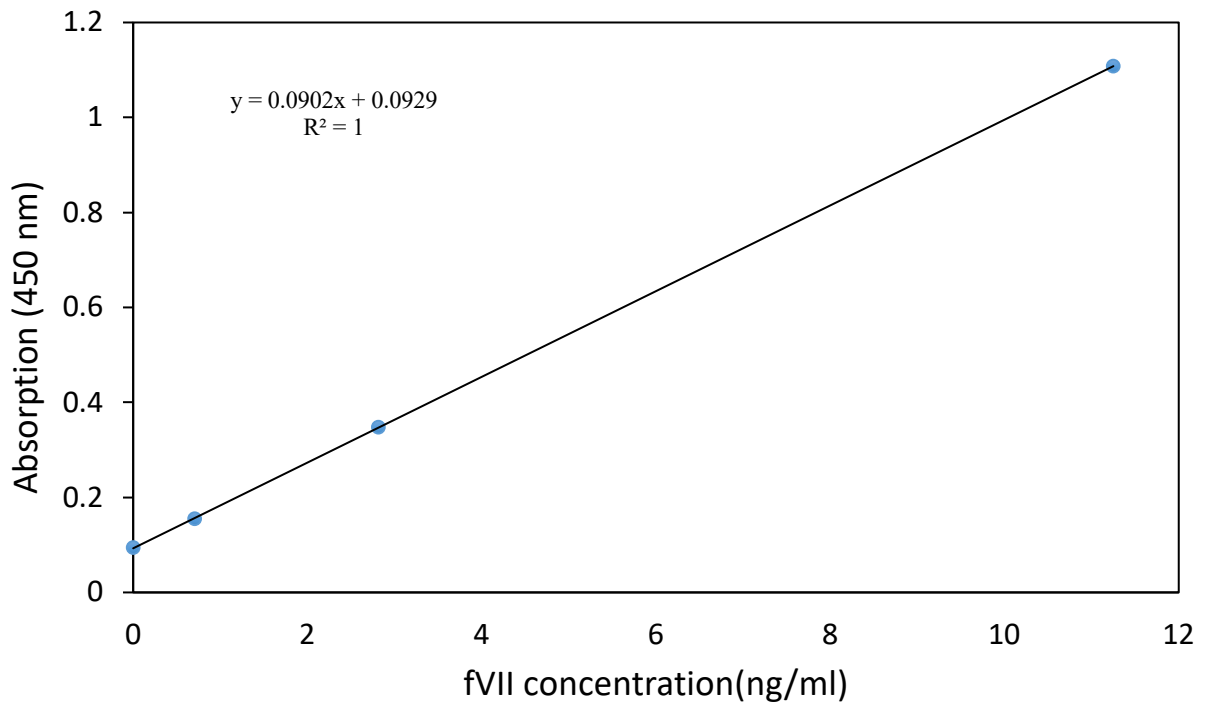
To determine the concentration of fVII antigen, the AssayPro ELISA kit was used. According to manufacturer's recommendation, the reagents were allowed to reach room temperature prior to use. 50 μ l of each sample was added to the provided human fVII antibody coated 96-well

plate. A standard curve was prepared using a range of concentration of human fVII (0-11.25 ng/ml) (Figure 2.3). The wells were then covered within an adhesive strip and incubated for 2 h. The wells were washed five times with the provided wash buffer and 50 µl of biotinylated human factor VII antibody (fVII) was added and incubated for 1 h. The wells were washed a further five times after which streptavidin-peroxidase conjugate reagent provided with the kit (50 µl) was added to each well. The samples were then incubated for 30 min at the room temperature in the dark. The wells were washed five times with the wash buffer and 50 µl of chromogenic substrate was added to each well and incubated for exactly 12 min in the dark. The reaction was stopped by stop solution (50 µl) and the absorptions were measured at 450 nm using a plate reader.

2.2.11 Determination of cell numbers using the crystal violet staining assay

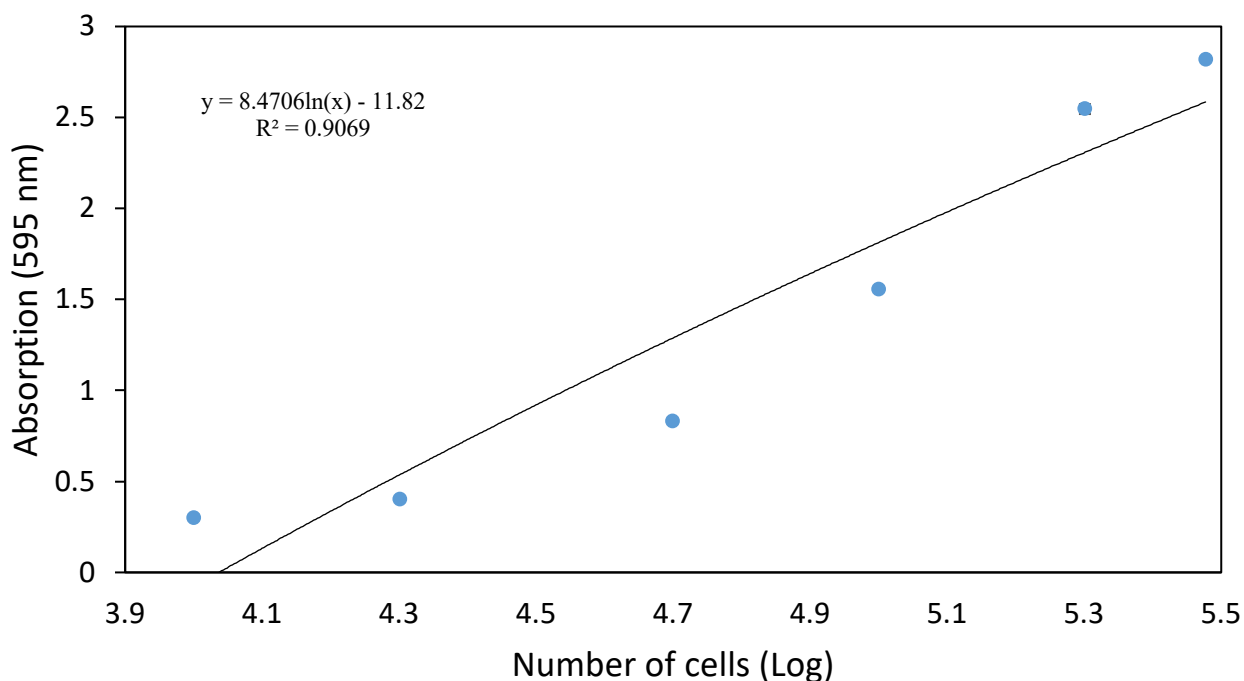
Crystal violet staining assay is a common method for measuring viable cell numbers based on DNA staining. During the washing step, dead cells are detached from cell culture plate and only adherent cells can be stained. The colour intensity of the eluted stain can be then measured to determine cell numbers (Chiba et al., 1998). Cells were seeded into 24 or 96 well-plates and allowed to adhere. The cells were then treated with reagents as described in the Results sections. Following the crystal violet assay procedure, the cells were washed twice with PBS and fixed with 4% (w/v) glutaraldehyde for 15 min on shaker. The cells were then washed twice with dH₂O and incubated with 1% (v/v) crystal violet solution for 15 min. The cells were washed another two times with dH₂O and the stain eluted by addition of 1% (w/v) SDS solution (100 µl) which was incubated for 20 min on shaker. The eluted stain was diluted with dH₂O at ratio 1:1 and the absorptions measured at 595 nm using a plate reader. Cell numbers were determined using a separate standard curve for each cell line because each cell lines can have different number of chromosomes (Figures 2.4-2.6). Standard curve was prepared against the Log cell numbers.

Figure 2. 3 Standard curve for the fVII concentration



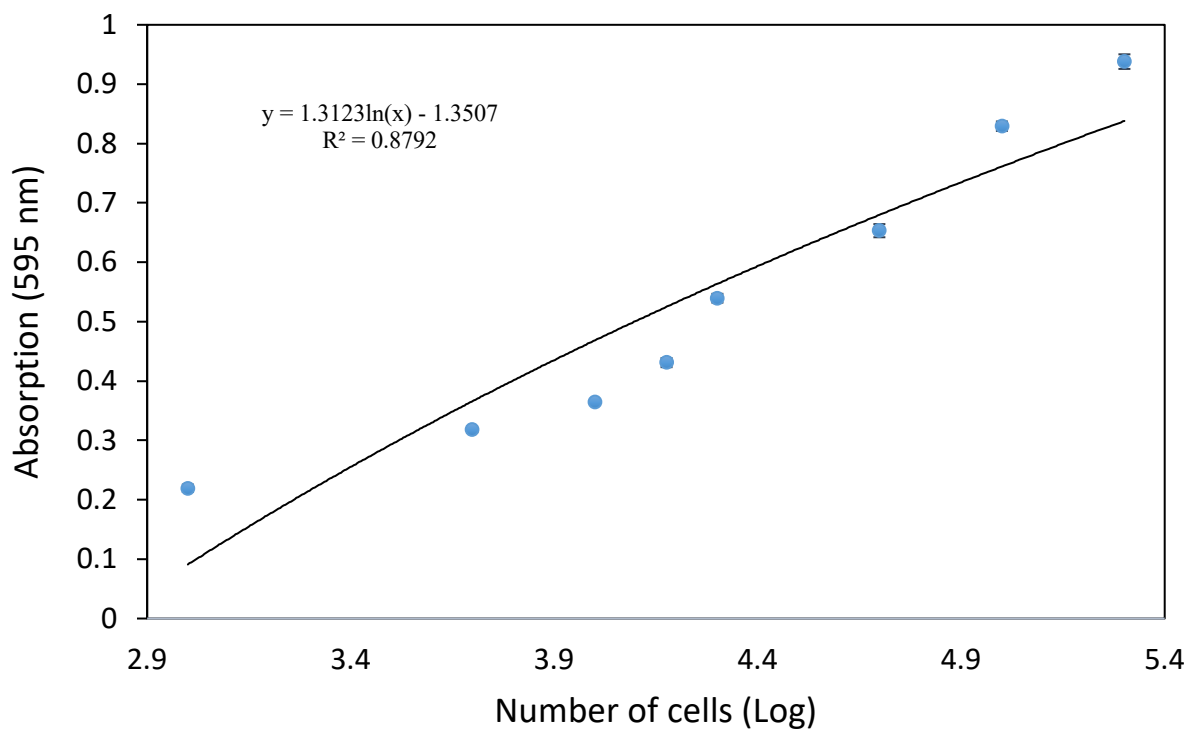
To create a standard curve for fVII antigen assay using ELISA, serial dilution of human factor VII protein was made to prepare a range of concentration (0-11.25 ng/ml) in the provided diluent. 50 μ l of each sample was placed into 96-well plates and covered within an adhesive strip and incubated for 2 h. Following the incubation, the wells were washed five times with the provided wash buffer and 50 μ l of biotinylated human factor VII antibody (fVII) was added to each well. The plate was then incubated for 1 h. The wells were washed five times with the wash buffer and 50 μ l of streptavidin-peroxidase conjugate was added and incubated for 30 min at the room temperature in the dark. After the incubation, the wells were washed five times with the wash buffer and the chromogenic substrate (50 μ l) was added to each well and incubated for exactly 12 min. The reaction was stopped by adding stop solution (50 μ l) and the absorption of the samples was measured at 450 nm using a plate reader (n=2).

Figure 2. 4 Standard curve for the determination of HCAEC cell numbers



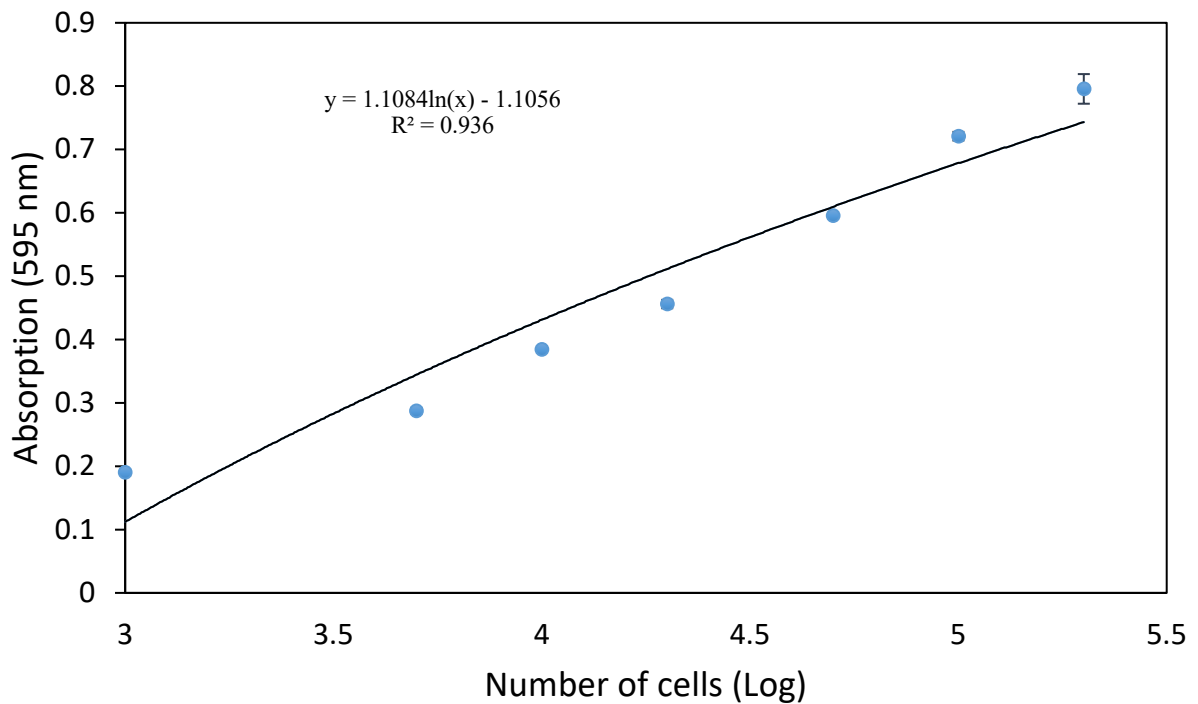
HCAEC ($0-3 \times 10^5$) were seeded into 24-well plates and allowed to adhere. The cells were washed twice with PBS and fixed with 4% (w/v) glutaraldehyde for 15 min. The cells were then washed twice with dH₂O and incubated with 1% (v/v) crystal violet solution for a further 15 min. The cells were washed two times with dH₂O and then treated with 1% (w/v) SDS solution for 15 min. The absorption for each sample was measured at 595 nm by a plate reader and a standard curve was constructed (n=4).

Figure 2. 5 Standard curve for the determination of HepG2 cell numbers



HepG2 cells ($0-2 \times 10^5$) were seeded into 24-well plates and permitted to attach. The cells were washed twice with PBS and fixed with 4% (w/v) glutaraldehyde for 15 min. The cells were then washed twice with dH₂O and incubated with 1% (v/v) crystal violet solution for a further 15 min. The cells were washed two times with dH₂O and then treated with 1% (w/v) SDS solution for 15 min. The absorption for each sample was measured at 595 nm by a plate reader and a standard curve was constructed (n=4).

Figure 2. 6 Standard curve for the determination of MDA-MB-231 TF knock out cell numbers



MDA-MB-231 TF KO ($0-2 \times 10^5$ cells) were seeded into 24-well plates and allowed to adhere. The cells were washed twice with PBS and fixed with 4% (w/v) glutaraldehyde for 15 min. The cells were then washed twice with dH₂O and incubated with 1% (v/v) crystal violet solution for a further 15 min. The cells were washed two times with dH₂O and then treated with 1% (w/v) SDS solution for 15 min. The absorption for each sample was measured at 595 nm by a plate reader and a standard curve was constructed (n=4).

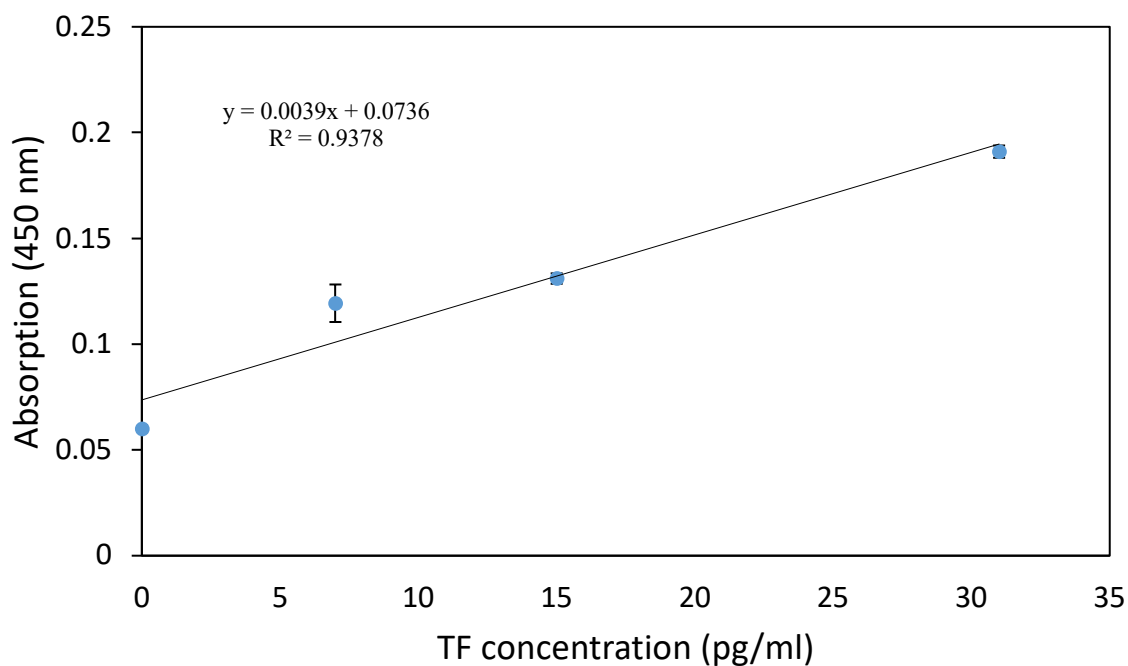
2.2.12 Measurement of TF antigen by ELISA assay

To determine the concentration of MV-associated TF antigen, TF antigen ELISA kit was used. The reagents were allowed to reach room temperature prior to use. According to the manufacturer's protocol, 100 µl of the provided assay diluent was added to human TF antibody coated 96-well plate followed by adding 50 µl of each sample. A standard curve was prepared using a range of concentration of recombinant TF (0-31.3 pg/ml) (Figure 2.7). The wells were then covered within an adhesive strip and incubated for 2 h with shaking. Following the incubation, the wells were washed three times with the provided wash buffer. 200 µl of coagulation factor III (TF) conjugate reagent was added to each well and incubated for 2 h with shaking. The wells were washed a further three times. Substrate solution was prepared by mixing provided colour reagents A with B at ratio 1:1 and incubated for 15 min. 200 µl of the substrate solution was added to each well and incubated for 30 min in the dark. The reaction was stopped by adding 50 µl of provided stop solution and the absorptions measured at 450 nm using a plate reader.

2.2.13 Measuring TF-fVIIa activities using fXa generation assay

TF-fVIIa activities of MV was measured by modification a procedure that described by Ettelaie et al. (2017). To measure TF activity, MV (0.10 nM) samples were incubated with HBS (pH 7.4) containing BSA (1% (w/v)) in 96-well plates. fVIIa (10 nM) was added to the reaction followed by fX (100 nM) and CaCl₂ (5 mM). The mixture was mixed properly and incubated for 30 min at 37°C. Following the incubation, fXa chromogenic substrate (0.2 mM) was added to the sample and incubated for 60 min at 37°C. The reaction was stopped by adding acetic acid (2% (v/v)) and the absorptions measured immediately at 410 nm. The MV-associated TF activities were determined using a standard curve prepared using a range of concentration of recombinant TF (0-5 U/ml) (Figure 2.8). To measure MV-associated fVIIa activity, fVIIa was excluded from the above reaction, and replaced with recombinant TF (1 U/ml). The MV-

Figure 2. 7 Standard curve for the TF concentration



Serial dilution of human TF protein was made to prepare a range of concentration (0-31.3 pg/ml) in distilled water. 100 μ l of assay diluent was placed into human TF antibody coated 96-well plates followed by 50 μ l of each sample. The wells were then covered within an adhesive strip and incubated at room temperature for 2 h with shaking. Following the incubation, the wells were washed three times with the provided wash buffer and 200 μ l of coagulation factor III (TF) conjugate reagent was added to each well and incubated at room temperature for 2 h with shaking. The wells were then washed a further three times and 200 μ l of substrate solution containing colour reagents A and B (1:1) was added and incubated for 30 min in the dark. The reaction was stopped by adding 50 μ l of stop solution and the absorptions measured at 450 nm using a plate reader (n=3).

associated fVIIa activities were determined using a standard curve prepared using a range of purified fVIIa (0-10 nM) (Figure 2.9).

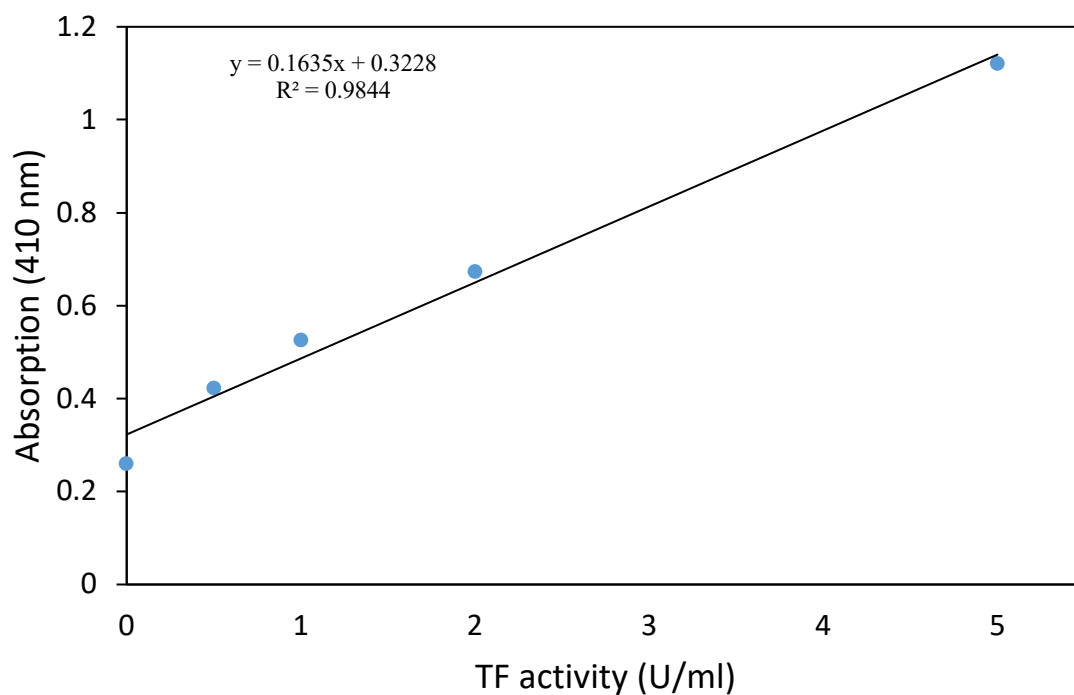
2.2.14 Measurement of the concentration and purity and of the isolated nucleic acid

To measure the concentration of the nucleic acids, 2 μ l of the sample was placed into Eppendorf μ Cuvette G1.0 and the concentration was determined at 260 nm against the nuclease-free water blank on an Eppendorf BioSpectrometer® instrument. To determine the sample purity, the ratio of the absorptions at 260 nm to the absorption at 280 nm was calculated. Any sample with a 260/280 ratio higher than 1.3 was considered sufficiently pure for further use.

2.2.15 Statistical Analysis

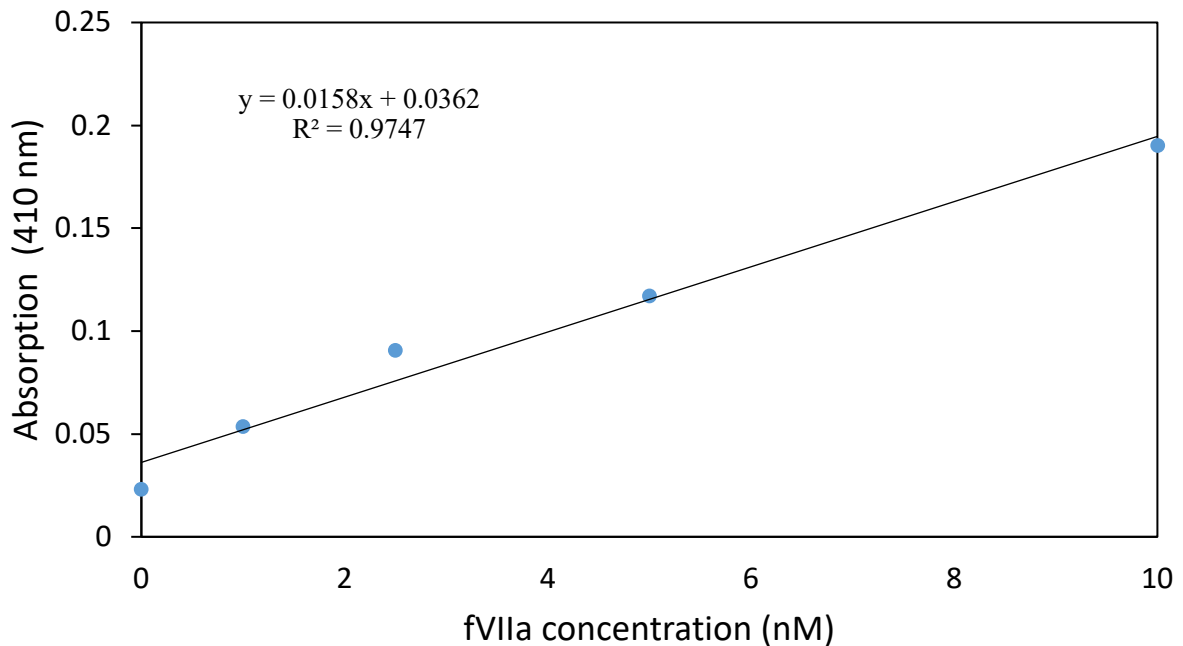
The data represent the calculated mean values from the number of experiments stated in each figure legend \pm the calculated standard error of the mean (SEM). The statistical analysis was performed using the Statistical Package for the Social Sciences program (SPSS). Significance differences in the variance compared to the control was determined using the One-Way ANOVA procedure and Tukey's honest significance test.

Figure 2. 8 Standard curve of TF activity using the fXa generation assay



To create a standard curve for TF activity, a range of concentration of human recombinant TF (0-5 U/ml) was used. Initially, the rec-TF was added to HBS (pH 7.4) containing BSA (1% (w/v)) in 96-well plate followed by adding fVIIa (10 nM) and fX (100 nM). CaCl_2 (5 mM) was added to the mixture mixed properly and incubated for 30 min at 37°C. To measure the activity of fXa generated by rec-TF, fXa chromogenic substrate (0.2 mM) was added to the samples and incubated for further 60 min at 37°C. The reaction was stopped by adding acetic acid (2% (v/v)) and the absorptions measured immediately at 410 nm using a plate reader (n=2).

Figure 2. 9 Standard curve of fVIIa activity using the fXa generation assay



To make a standard curve for fVIIa activity, a range of concentration of purified fVIIa (0-10 nM) was used. Initially, the fVIIa was added to HBS (pH 7.4) containing BSA (1% (w/v)) in 96-well plate followed by adding rec-TF (1 U/ml) and fX (100 nM). CaCl_2 (5 mM) was added to the mixture, mixed properly and incubated for 30 min at 37°C. To measure the activity of fXa generated by fVIIa, fXa chromogenic substrate (0.2 mM) was added to the samples and incubated for further 60 min at 37°C. The reaction was stopped by adding acetic acid (2% (v/v)) and the absorptions measured immediately at 410 nm by a plate reader (n=2).

Chapter 3

The ratio of factor VIIa:tissue factor content within microvesicles determines the differential influence on endothelial cells

3.1 Introduction

Tissue factor (TF) initiates the coagulation mechanism through the formation of a complex with factor VIIa (fVIIa), which then activates factors X and IX (Kirchhofer and Nemerson, 1996; Edgington et al., 1997). Under normal conditions, TF is kept from coming in contact with blood to prevent the risk of thrombosis. However, both vascular endothelial cells and circulating monocytes can express TF when activated by exposure to inflammatory stimuli (Butenas et al., 2009; Østerud and Bjørklid, 2006; Akinmolayan et al., 2016). The overexpression of TF protein has been reported in many pathological conditions such as atherosclerosis and diabetes (Williams and Mackman, 2012; Eisenreich et al., 2016; Witkowski et al., 2016), cancers, including prostate, breast, liver and brain (Chu, 2011), and inflammatory diseases, such as sepsis (Bode and Mackman, 2014). Similarly, the expression of fVII has been shown to be elevated in liver cirrhosis (Hollestelle et al., 2004) and heart disease (Suzuki et al., 1991). In addition, cancer cells including ovarian (Yokota et al., 2009), lung, liver, thyroid, prostate and stomach (Koizume et al. 2006) have been demonstrated to express ectopic fVII/fVIIa protein. As well as being expressed on the surface of the cells, TF can be released as cell-derived MV following cellular activation or apoptosis (Morel et al., 2006; Freyssinet and Toti, 2010; Gardiner et al., 2015; Date et al., 2013; Hron et al., 2007; Thaler et al., 2014; Auwerda et al., 2011) as can fVII/fVIIa protein (Yokota et al., 2009; Featherby et al., 2019). The MV-associated TF is capable of initiating cellular signals in recipient cells, while TF can induce auto-signalling in cells that express the protein. TF signalling has been shown to alter the cellular gene expression profile (Kask et al., 2014; Ramchandani et al., 2016) and has been demonstrated to require fVIIa activity and the involvement of protease-activated receptor 2 (PAR2) (Zelaya et al., 2018; McVey, 2016; Rothmeier et al., 2018; Fan et al., 2005; Cirillo et al., 2004; Hu et al., 2013; Gessler et al., 2009). Additionally, the interaction of TF with β -integrins has been directly implicated in inducing cell proliferation (Rothmeier et al., 2018;

Versteeg and Ruf, 2006; Kocaturk et al., 2013; Collier and Ettelaie, 2010; Ethaeb et al., 2019). Such TF signalling has been particularly associated with high proliferative capacity associated with cancer cells (Schaffner and Ruf, 2009; Bj et al., 2011). FVIIa protein also appears to be involved in the cellular proliferation mechanism. For example, eosinophils obtained from mice lacking fVII become more susceptible to apoptosis as compared to those obtained from wild type mice (Shinagawa et al., 2009). However, whilst this proliferative potential has been associated with the interaction of TF with fVIIa, data on the requirement for a proteolytic function of fVIIa remain inconsistent (Zelaya et al., 2018; McVey, 2016). As mentioned in the section 1.8, apoptosis occurs through two distinct, but interrelated pathways, the intrinsic and extrinsic pathways. The extrinsic apoptotic pathway is mediated through cell receptor signalling. It has been suggested that TF may trigger apoptosis through the extrinsic pathway in a death receptor-like manner (Frentzou et al., 2010). The incubation of the rat cardiomyocyte cell line H9c2 with a high concentration of recombinant TF resulted in cellular apoptosis via increased activity of caspase-3. The exposure of cells to low levels of recombinant TF alone is capable of promoting entry into the cell cycle (Pradier and Ettelaie, 2007). However, the exposure of cells to high levels of TF additionally causes cell cycle arrest at the G1/S checkpoint leading to cellular apoptosis (Pradier and Ettelaie, 2007; Frentzou et al., 2010; ElKeeb et al., 2015). In addition, the exposure of endothelial cells to monocyte-derived MV for up to 24 hours disrupted the cell membrane integrity and induced cellular apoptosis in these cells (Aharon et al., 2008). Therefore, it is possible that the magnitude of exposure to TF may be a determining factor in the outcome in the recipient cells.

The activation of PAR2 has been reported to be essential in the signalling processes that are initiated after the exposure of cells to TF (Schaffner and Ruf, 2008; Hjortoe et al., 2004). Formation of the TF-fVIIa complex is capable of directly triggering signals via PAR2 activation or alternatively, through the activation of factor Xa (fXa) and formation of a tertiary

complex (Camerer et al., 2000; Riewald and Ruf, 2001). As a consequence of inflammation or injury, large quantities of TF are released within MV (Boulanger et al., 2001; Morel et al., 2004; Morel et al., 2006; Morel et al., 2008). For example, such high levels of circulating MV have been detected in patients with cancers and cardiovascular disease (Enjeti et al., 2008; VanWijk et al., 2003; Badimon et al., 2017). These MV are likely to interact with endothelial cells and have been shown to be cleared from the bloodstream by endocytosis (Collier et al., 2013; del Conde et al., 2005; Osterud and Bjorklid, 2012). Moreover, ElKeeb et al. (2014) demonstrated that treatment of endothelial cells with TF-containing MV induced p38 MAPK signalling which resulted in increasing the level of p53 activation. This in turn resulted in upregulation of the expression of the Bax protein, leading to cellular apoptosis. More recently, it has been shown that the accumulation of TF within endothelial cells causes endothelial cell apoptosis in a mechanism that includes Src1 activation and β 1-integrin (Ethaeb et al., 2019). The inability to satisfactorily process TF appears to be detrimental to endothelial cells (ElKeeb et al., 2015), and exposure of these cells to TF can induce cellular apoptosis (Pradier and Ettelaie, 2007; Aharon et al., 2008). Therefore, exposure of endothelial layer to circulating TF-positive MV, over prolonged periods as seen in chronic diseases, may be a contributor to endothelial dysfunction associated with many chronic diseases (Date et al., 2013; Yang et al., 2008; Kuge et al., 2008). Interestingly, reports have shown the increases in the number of MV released correlated with endothelial dysfunction and the disruption of nitric oxide production (Boulanger et al., 2001; Badimon et al., 2017), which may subsequently promote the development of atherosclerosis (Davignon and Ganz, 2004).

It has previously been reported that the activation of PAR2 may enhance the release of procoagulant MV containing TF (Collier and Ettelaie, 2011) which may act as a mechanism by which the cells manage the excessive amounts of TF and prevent damage to the cells (ElKeeb et al., 2014; Ethaeb et al., 2019). The role of PAR2 activation in many

pathophysiological events such as cellular proliferation (Darmoul et al., 2004), inflammation (Feistritzer et al., 2005; Shpacovitch et al., 2002; Crilly et al., 2012), angiogenesis (Liu and Mueller, 2006; Ikeda et al., 2003; Shibuya., 2011) and MV release (Ettelaie et al., 2016; Das et al., 2018; Collier and Ettelaie, 2011; Ettelaie et al., 2012) has been established. PAR2 can be activated by proteases such as trypsin, fXa, fVIIa and the TF-fVIIa complex (Vergnolle et al., 1999; Rothmeier and Ruf, 2011; Zhao et al., 2014; Benelhaj et al., 2019). Therefore, blocking these proteases may abolish the PAR2 signalling. Featherby et al. (2019) reported that the incubation of MDA-MB-231 (breast cancer cell line) and AsPC1 (pancreatic cell line) with direct oral anticoagulants (DOAC) can inhibit the release of MV as well as reducing cell proliferation rate in response to purified fXa (10 nM) which occurs in a PAR2-mediated manner. DOAC comprise a recent group of drugs that can be used to either prevent or treat blood clots. Rivaroxaban and apixaban are two DOAC that act to inhibit the proteolytic activity of fXa (Hoffman et al, 2018). In addition, while incubation of the cells with apixaban reduced both the release of MV and cell proliferation, treatment with rivaroxaban only resulted in a decrease in release of MV. However, since no fXa was detected in the MV released by either of these cell lines, it was concluded that apixaban may inhibit proteases other than fXa (Featherby et al., 2019). Therefore, this property of the DOAC can be used as a tool to examine the mechanism(s) of the activation of PAR2 by endogenous TF-fVIIa and to differentiate this from that by fXa.

3.1.1 Aims

The aims of this study were to examine the effect of MV derived from a panel of cancer cell lines (HepG2, 786-O, BxPC-3, MDA-MB-321 and MCF-7) on endothelial cells proliferation and apoptosis. Also, the expression of ectopic fVII/fVIIa by these cell lines and release within MV was measured. Furthermore, the hypothesis that the activation of PAR2 by TF-fVIIa complex is involved in inducing cellular apoptosis or proliferation in endothelial cells was

investigated and the impact of molar ratios of fVIIa:TF on endothelial cell proliferation and apoptosis assessed. Finally, ability of rivaroxaban or apixaban to block the proteolytic activity of fVIIa was explored.

3.2 Methods

3.2.1 Isolation of total RNA

The following procedure was used to extract total RNA from cancer cell lines for use in real-time PCR (RT-PCR) to measure the amount of fVII mRNA. Cells (10^6) were collected separately from each cell line (HepG2, MDA-MB-231, MCF-7, BxPC3 and 786-O) in eppendorf tubes (1.5 ml) by centrifugation at 300 g for 5 min. To isolate the RNA, the supernatants were discarded and each cell pellet was resuspended with RiboZol solution (500 μ l). The mixtures were pipetted thoroughly several times to completely lyse the cells and ensure the homogeneity of the mixtures. The samples were then incubated for 10 min at room temperature. To separate the proteins from DNA and RNA, chloroform (100 μ l) was added to each sample and the samples were vortexed for 15 sec. The samples were then incubated for 3 min and then centrifuged at 12,000 g at 4°C for 15 min. Three layers developed after the centrifugation: red (contained proteins), white (contained DNA) and colourless (contained RNA). The upper colourless layer from each sample containing the RNA was transferred carefully into a new RNase-free tube and absolute isopropanol (200 μ l) was added and incubated for 10 min to precipitate the RNA. After the incubation, the samples were centrifuged at 12,000 g at 4°C for 10 min. The supernatants were discarded carefully without disrupting the RNA pellets. The pellets were then washed twice with 75% (v/v) ethanol (400 μ l), and each time, the samples were vortexed and centrifuged at 7,000 g at 4°C for 5 min. The pellets were dried by evaporation in a sterile environment and then resuspended in nuclease-free water (200 μ l) and stored at -20°C until required.

3.2.2 Measurement of the amount of fVII mRNA by real-time PCR (RT-PCR)

The expression of fVII was examined by using semi-quantitative qRT-PCR and specific primers for fVIIa. The values were normalised for comparing to the relative amounts of β -actin

which were amplified using appropriate primers set. All steps were conducted in a sterile environment and using only RNase-free water. 2.5 µl of combined forward and reverse primers (100 nM) for the fVII gene or the β-actin gene were added into each of six separate wells of a 96-well PCR plate, followed by the RNA samples (100 ng). The volume of each reaction was adjusted to 12.25 µl using RNase-free water. Finally, 12.5 µl of GoTaq® qPCR Master Mix provided with the kit was added to each RNA sample, followed by 0.25 µl of reverse transcriptase enzyme to make up the volume to 25 µl in each tube (see Table 3.1). The samples were mixed thoroughly and then centrifuged to remove any air bubbles. The RT-PCR was carried out using an iCycler thermal cycler RT-PCR machine according to the program shown in Table 3.2. The threshold number of amplification cycles (Ct) for each sample was determined and the relative amounts of fVII mRNA calculated using the $2^{-\Delta\Delta CT}$ method (Livak et al., 2001).

3.2.3 Examination of the ability of direct oral anticoagulants to prevent cellular apoptosis in endothelial cells induced by MV

Rivaroxaban and apixaban are DOAC that inhibit the proteolytic activity of fXa. The aim of this study was to examine the influence of these two compounds on preventing the apoptotic influence of cancer cell-derived MV on endothelial cell viability. HCAEC (2×10^4) were seeded into 96-well plates and permitted to adhere. The optimal concentration of MV (0.05 nM) isolated from the 786-O cancer cell line was pre-incubated with rivaroxaban (1.8 µM) or apixaban (1.8 µM) for 20 min prior to being added to the cells. The cells were then incubated for 24 h and the rate of apoptosis was determined using the TitreTACS chromogenic TUNEL assay as described in section 2.2.9.

Table 3. 1 Real-time RT-PCR master mix

Reagent	Volume per reaction (μ l)	Final concentration
DNA template	Variable	100 ng
Primers	2.5	100 nM
GoTaq® qPCR Master Mix	12.5	1X
Reverse transcriptase enzyme	0.25	1X
RNase-free water	Variable	-
Total	25	

Table 3. 2 Real-time RT-PCR program

Number of cycles	Temperature	Time	Step
1	48°C	30 min	Conversion of RNA to cDNA
	95°C	10 min	Degradation of RNA
40	95°C	15 sec	Denaturation
	60°C	1 min	Primers annealing
1	60-90°C Increase temp by 0.5°C		Dissociation Determining the melt temperature of the amplicons
Final hold	4°C		Final hold

3.2.4 Examining the ability of apixaban and rivaroxaban to inhibit the proteolytic activity of fVIIa

The specificity of activities of purified fVIIa and fXa towards a fVIIa chromogenic substrate were examined by assaying two different synthetic fVIIa substrates. fVIIa (5 nM) or fXa (10 nM) were added to Tris-HCl pH 7.4 (10 mM). A commercial chromogenic substrate for fVIIa, Pefachrome (1.6 mM) or a custom-synthesised chromogenic substrate NH₂-Asn-Leu-Thr-Arg-pNA (1.6 mM) (Baugh and Krishnaswamy, 1996) was added to each reaction mixture and incubated for 1 h at 37°C. The absorptions were then determined at 410 nm using a plate reader. To evaluate the ability of apixaban or rivaroxaban to inhibit the proteolytic activity of fVIIa, samples of purified fVIIa (5 nM) were pre-incubated with rivaroxaban (1.8 µM), apixaban (1.8 µM), an inhibitory polyclonal anti-fVIIa antibody (10 µg/ml), or a control isotype (10 µg/ml) and the fVIIa analysed as above.

3.2.5 Examination of the influence of DOAC on cofactor activity of TF and the proteolytic activity of purified fVIIa and MV-associated fVIIa

The aim of this study was to further investigate the influence of apixaban on the cofactor activity of TF and the proteolytic activity of purified fVIIa and MV-associated fVIIa by using an fVIIa chromogenic substrate. TF (1 U/ml) and fVIIa (5 nM) were mixed with Tris-HCl (10 mM; pH 7.4) in the presence or absence of apixaban (1.8 µM). Pefachrome fVIIa (1.6 mM) was added to the samples and the samples were incubated for 1 hr at 37°C. The absorptions of the samples were measured at 410 nm using a plate reader. In addition, samples of MV (0.05 nM), purified from the MDA-MB-231 cell line and shown to contain fVIIa, were pre-incubated with rivaroxaban (1.8 µM), apixaban (1.8 µM) or dimethyl sulfoxide (DMSO) prior to addition of the custom-fVIIa chromogenic substrate (NH₂-Asn-Leu-Thr-Arg-pNA; 1.6 mM). The reaction mixtures were incubated for 1h at 37°C and the absorption values for the samples were then determined at 410 nm using a plate reader.

3.3 Results

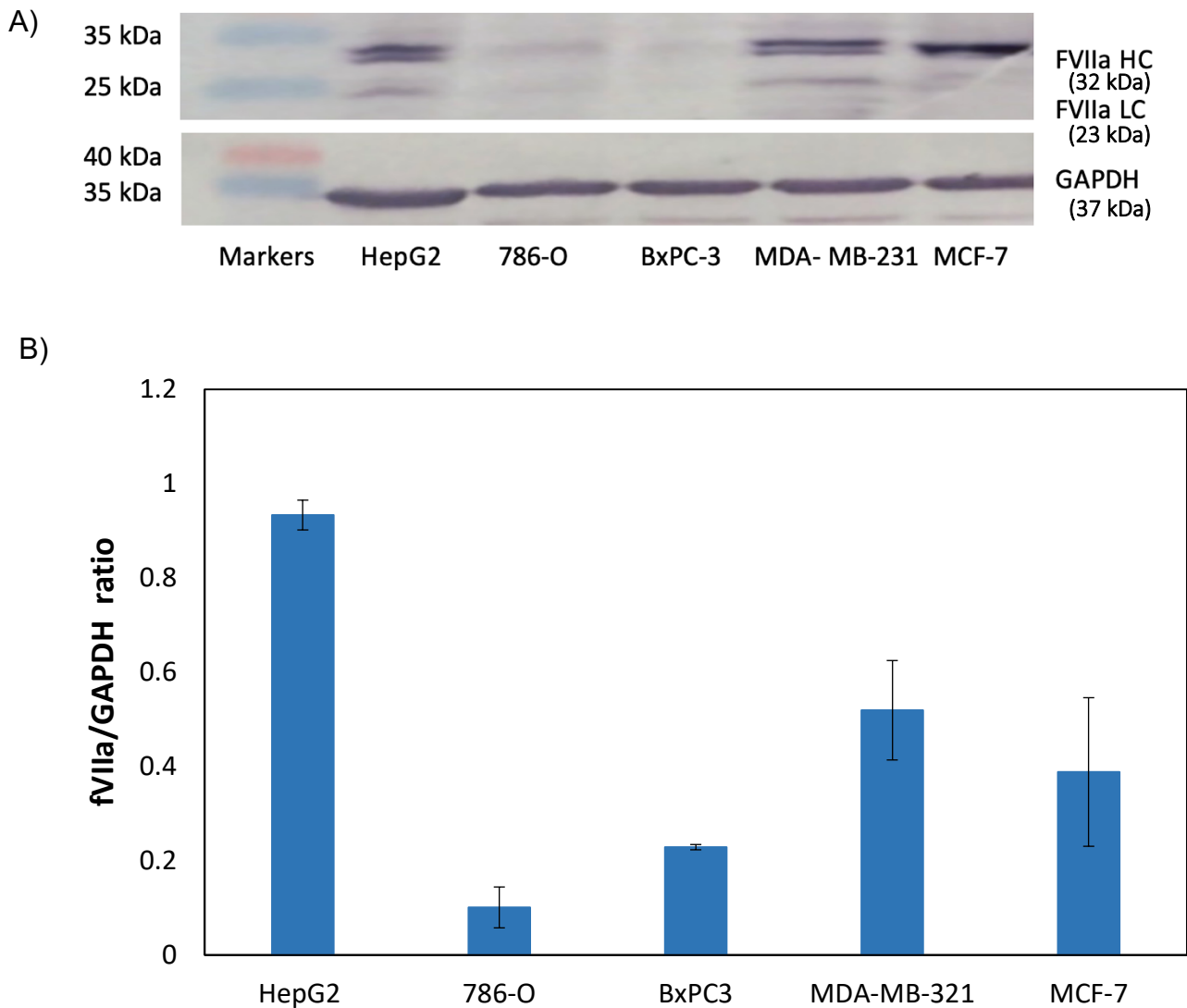
3.3.1 Analysis of the expression of fVII/fVIIa protein in cancer cell lines by western blot

The expression of the fVII/fVIIa protein in cancer cell lines was examined by western blot as described in section 2.2.8. The five cell lines tested were: HepG2, MCF-7, 786-O, BxPC-3 and MDA-MB-231. Following electrophoresis and transfer to the membrane, a mouse anti-fVII antibody was used as the primary antibody to ensure the detection of the non-active fVII, as well as both of the chains of the active fVIIa. In all the cell lines tested, bands of approximately 32 kDa and 23 kDa, corresponding to the heavy and light chains of the activated fVIIa were detected (Figure 3.1). In addition, to estimate the quantity of fVIIa protein expressed in each cell line, the intensity of the heavy chains bands was determined against the amount of GAPDH, using the ImageJ program. Analysis of the samples showed that HepG2 cells expressed the highest quantities of fVIIa, this is not surprising since liver cells are known to be major source of coagulation factors (Perera et al., 1999). Additionally, MDA-MB-231 and MCF-7 cell lines expressed similar and significant amounts of fVIIa protein, while 786-O and BxPC3 cell lines contained low levels of fVIIa protein.

3.3.2 Examination of the expression of fVII mRNA in cancer cell lines using real-time RT-PCR

Reverse transcription-polymerase chain reaction was performed to quantify the amount of fVII mRNA expressed in the five cell lines. Total RNA was isolated from the cell lines as described in section 3.2.1 and 100 ng of RNA from each sample was amplified. Analysis of the samples indicated that MDA-MB-231 and MCF-7 cell lines express the highest levels of fVII mRNA, whilst 786-O and BxPC3 cell lines expressed relatively low levels of mRNA (Figure 3.2). In agreement with the protein analysis, HepG2 cell line expressed the highest amounts of fVII

Figure 3. 1 Analysis of the expression of fVIIa protein in cancer cell lines by western blot



Cell samples were lysed and separated by 12% (w/v) SDS-PAGE. The bands were then transferred onto nitrocellulose membranes and blocked with TBST. The membranes were then probed with a mouse anti-fVII antibody diluted 1:2000 (v/v) in TBST and developed using an alkaline phosphatase-conjugated goat anti-mouse antibody diluted 1:4000 (v/v) in TBST. Additional sets of membrane were probed with a goat anti-human GAPDH antibody diluted 1:6000 (v/v) in TBST and developed using an alkaline phosphatase-conjugated donkey anti-goat antibody diluted 1:6000 (v/v) in TBST. **(A)** The bands were visualised using western blue stabilised substrate for alkaline phosphatase. **(B)** The bands were analysed using the ImageJ program and the protein expression quantified against GPADH bands (The results show the average of two separate experiments and expressed as the mean \pm SD).

mRNA which was four-fold higher than that of the MDA-MB-231 cells and is therefore not shown.

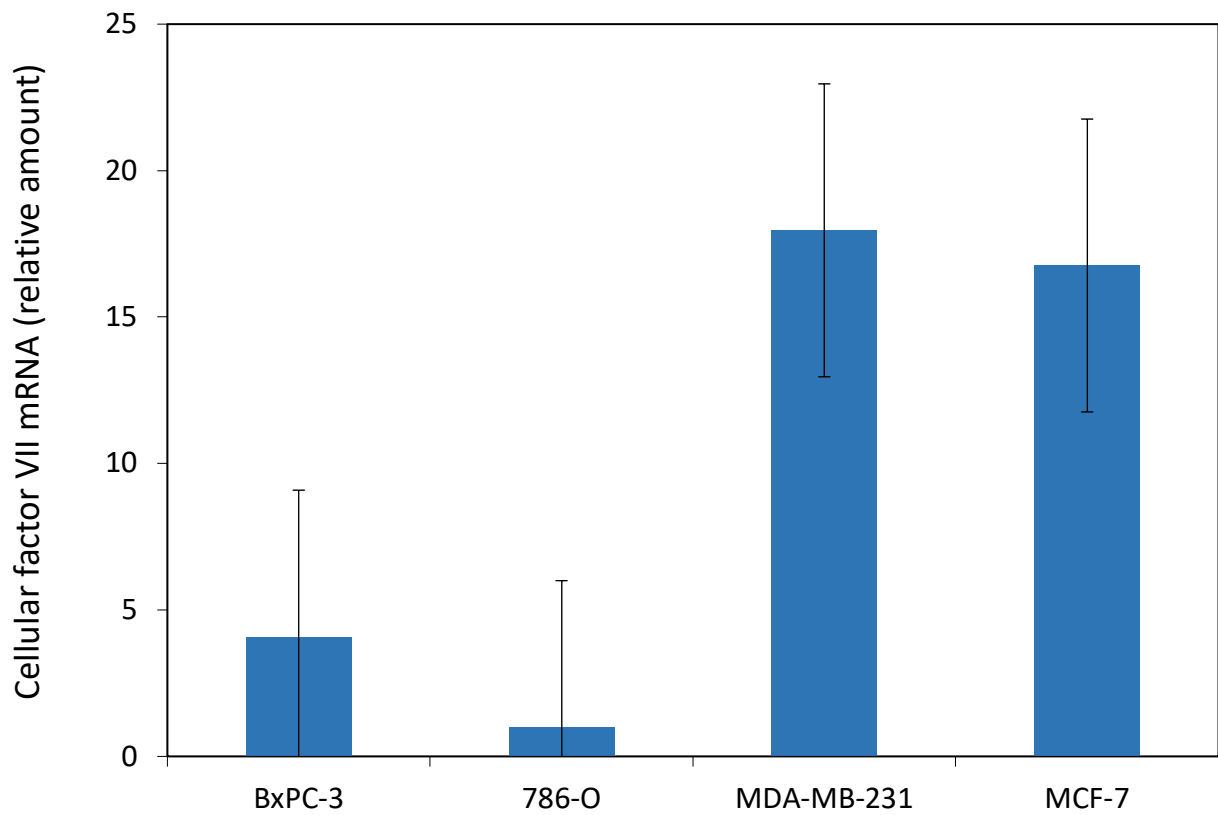
3.3.3 Measurement of MV-associated TF using ELISA assay

The following study aimed to quantify the amount of MV-associated TF released from the cells using an ELISA procedure described in section 2.2.10. MV were isolated from resting HepG2, BxPC-3, 786-O, MDA-MB-231 and MCF-7 cell lines as described in section 2.2.7 using 0.1 nM of each sample. MV isolated from BxPC-3 and MDA-MB-231 cell lines contained the highest levels of TF antigen (Figure 3.3) which is in agreement with previously published data (Ettelaie et al. 2016). In addition, MV isolated from HepG2, 786-O and MCF-7 cell lines contained comparable but lower levels of TF antigen compared to MDA-MB-231 and BxPC-3 cells (Figure 3.3).

3.3.4 Measurement of MV-associated fVII/fVIIa using ELISA assay

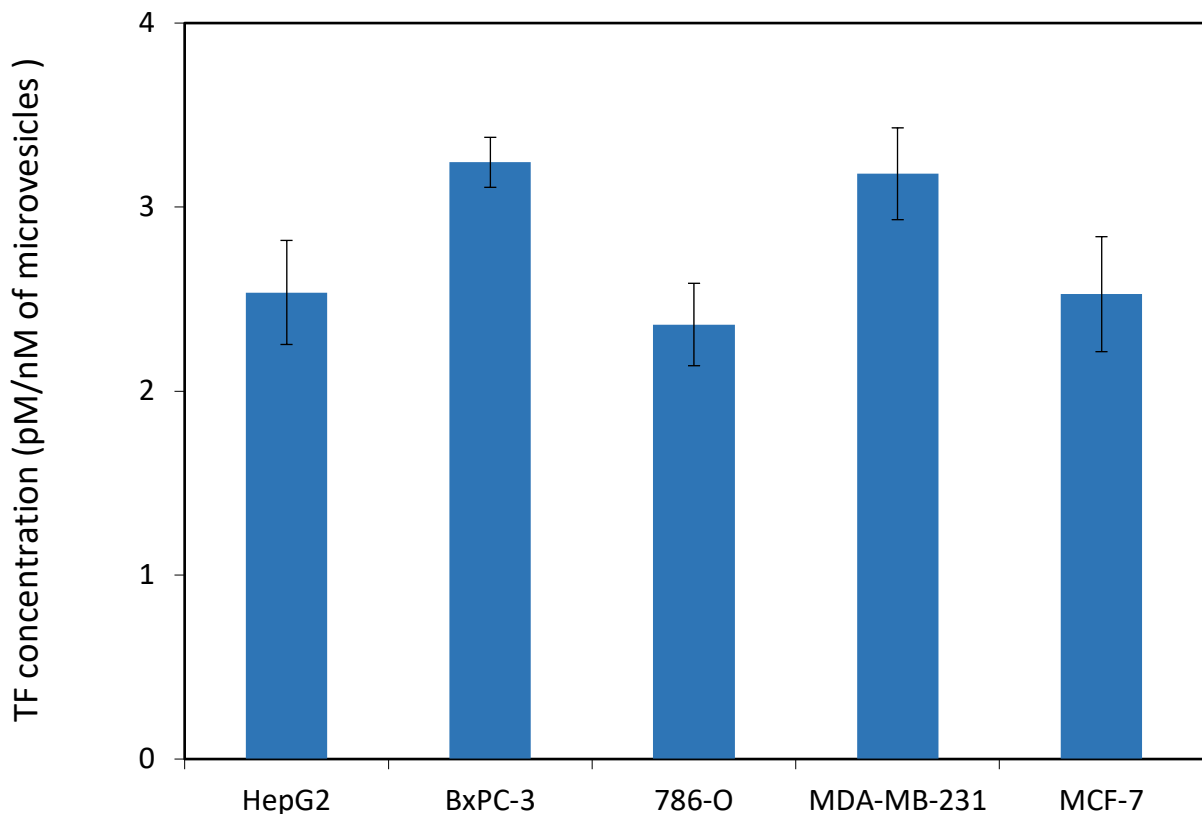
This study aimed to quantify the amount of MV-associated fVII/fVIIa released from the cells using an ELISA as described in section 2.2.10. MV were isolated from the 5 resting cells lines; 0.1 nM of each sample was used to examine the amount of MV-associated fVII/fVIIa. Analysis of the samples showed the highest level of fVII/fVIIa antigen within MV derived from HepG2 cell line (Figure 3.4). MV isolated from MCF-7 and MDA-MB-231 cell lines were shown to contain similar, moderate amounts of fVII/fVIIa protein. In contrast, MV isolated from BxPC-3 and 786-O cell lines exhibited lower levels of fVII/fVIIa antigen compared to HepG2 cell.

Figure 3. 2 Assessment of expression of fVII mRNA in cancer cell lines using real time RT-PCR



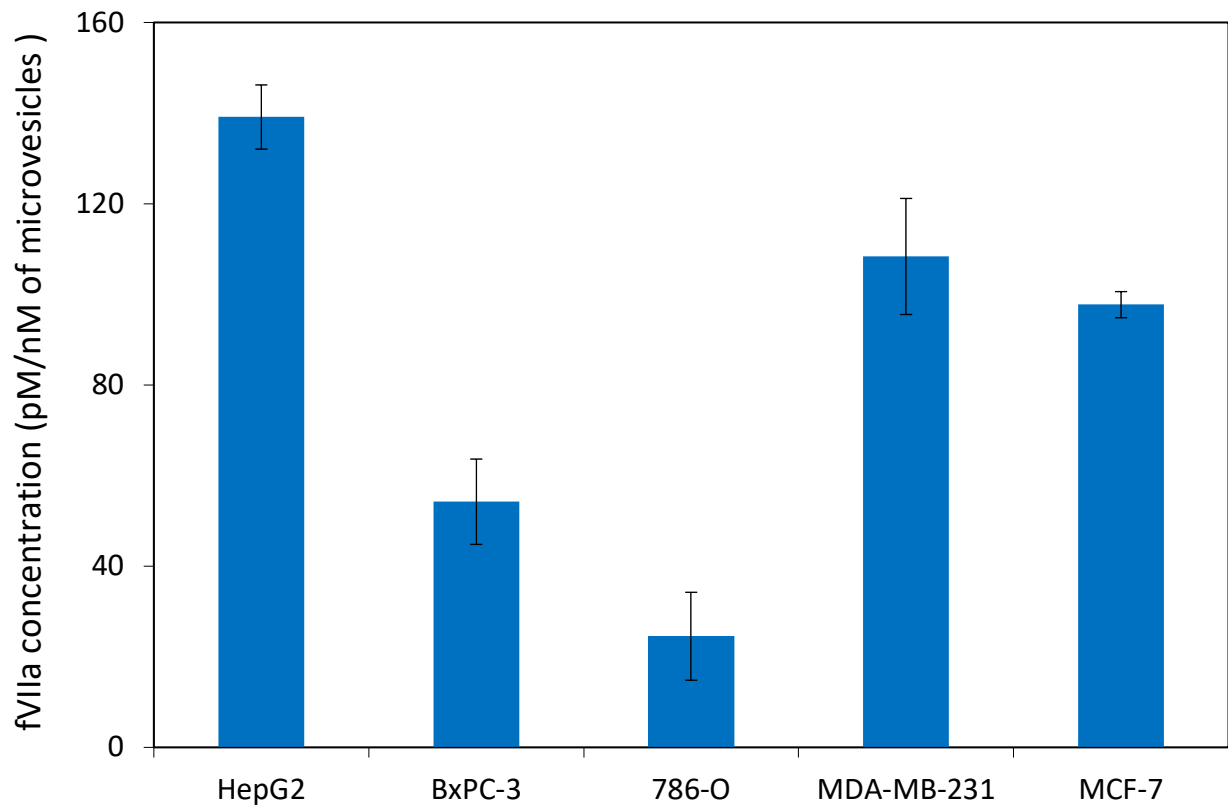
Total RNA was isolated from the cancer cell lines (HepG2, BxPC-3, 786-O, MDA-MB-231 and MCF-7) and the expression of fVII mRNA was measured in 100 ng of RNA from each sample, using real time RT-PCR. The Ct values were normalised against the respective β -actin mRNA in each sample and the relative amounts of fVII mRNA were calculated (The results show the average of three separate experiments and expressed as the mean \pm SEM).

Figure 3. 3 Measurement of MV-associated TF antigen by ELISA



MV were isolated from the media of resting cancer cell lines (HepG2, BxPC-3, 786-O, MDA-MB-231 and MCF-7) by ultracentrifugation. Samples (50 μ l) were placed into human TF antibody coated 96-well plates together with the assay diluent (100 μ l) supplied by the TF-ELISA kit. The wells were then covered with an adhesive strip and incubated for 2 h. The wells were then washed three times using the provided wash buffer and 200 μ l of coagulation factor III (TF) conjugate reagent was added to each well and incubated for 2 h. The wells were then washed a further three times and 200 μ l of substrate solution was added and incubated for 30 min, in the dark. The reaction was stopped by the addition of 50 μ l of stop solution and the absorption values were measured at 450 nm using a plate reader. A standard curve of human TF was prepared and used alongside to determine the TF antigen concentration within the MV (The results show the average of five separate experiments and expressed as the mean \pm SEM).

Figure 3. 4 Measurement of MV-associated fVII/fVIIa antigen by ELISA



MV were isolated from the media of resting cell lines (HepG2, BxPC-3, 786-O, MDA-MB-231 and MCF-7) by ultracentrifugation. Samples (50 μ l) were placed into human fVII antibody coated 96-well plates and covered with an adhesive strip and incubated for 2 h. The wells were then washed five times with the provided wash buffer and 50 μ l of biotinylated human factor VII antibody (fVII) was added to each well and incubated for 1 h. The wells were then washed five times with the wash buffer and 50 μ l of streptavidin-peroxidase conjugate was added and incubated for 30 min, in the dark. The wells were washed five times with the wash buffer and the chromogenic substrate (50 μ l) was added to each well and incubated for exactly 12 min. The reaction was stopped by adding stop solution (50 μ l) and the absorption values were measured at 450 nm using a plate reader. A standard curve of human factor VII protein was prepared and used alongside to determine MV-associated fVII/fVIIa antigen levels (The results show the average of five experiments and expressed as the mean \pm SEM).

3.3.5 Calculation of the molar ratio of fVIIa:TF within MV derived from cancer cell lines

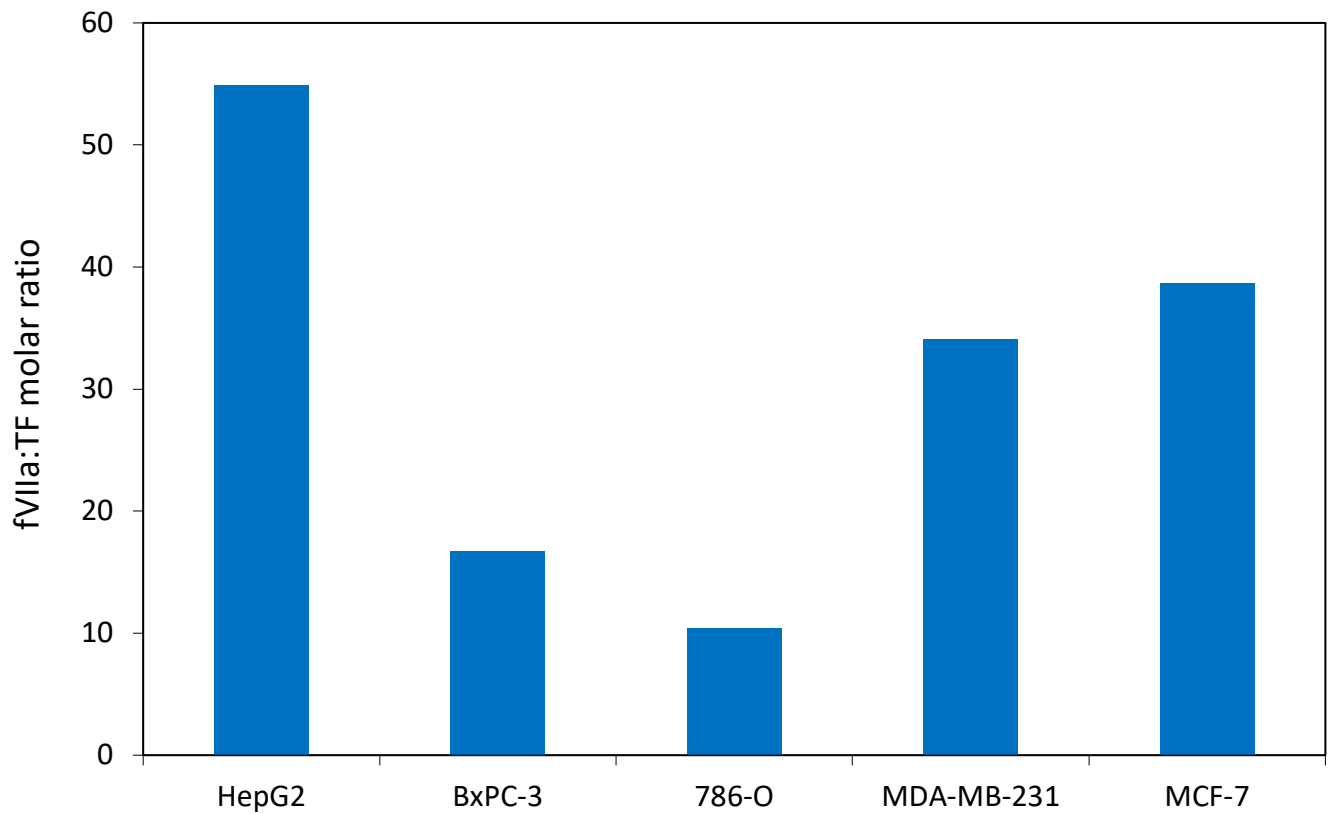
The data generated by measuring the levels of fVII/fVIIa and TF antigens within the MV was used to calculate the molar ratio of fVIIa to TF in MV isolated from the 5 cell lines (Figures 3.3 and 3.4). Analysis of the data showed that MV isolated from HepG2 cell line exhibited the highest fVIIa:TF molar ratio of 54:1 (Figure 3.5). MV isolated from MCF-7 and MDA-MB-231 cell lines exhibited lower ratios of fVIIa:TF which were 38:1 and 34:1, respectively. In contrast, MV derived from BxPC-3 and 786-O cell lines showed the lowest molar ratios; 16:1 and 10:1, respectively.

3.3.6 Measurement of TF and fVIIa activity using the fXa-generation assay

Since MV isolated from the 5 cell lines were shown to contain fVII/fVIIa as well as TF, in the next set of experiments the MV-associated TF and fVIIa activities were measured. The activities were measured by modification of the fXa-generation assay as described in section 2.2.13. Analyses of the MV samples showed that MV derived from BxPC-3 and MDA-MB-231 cell lines possessed substantial fXa-generation capacity, indicating high TF activity (Figure 3.6). In contrast, MV isolated from MCF-7, HepG2 and 786-O cell lines exhibited lower levels of TF activity and had a reduced fXa-generation capacity. On the whole, this finding reflected the measured TF antigens within the MV determined previously using the TF-ELISA (Figure 3.3).

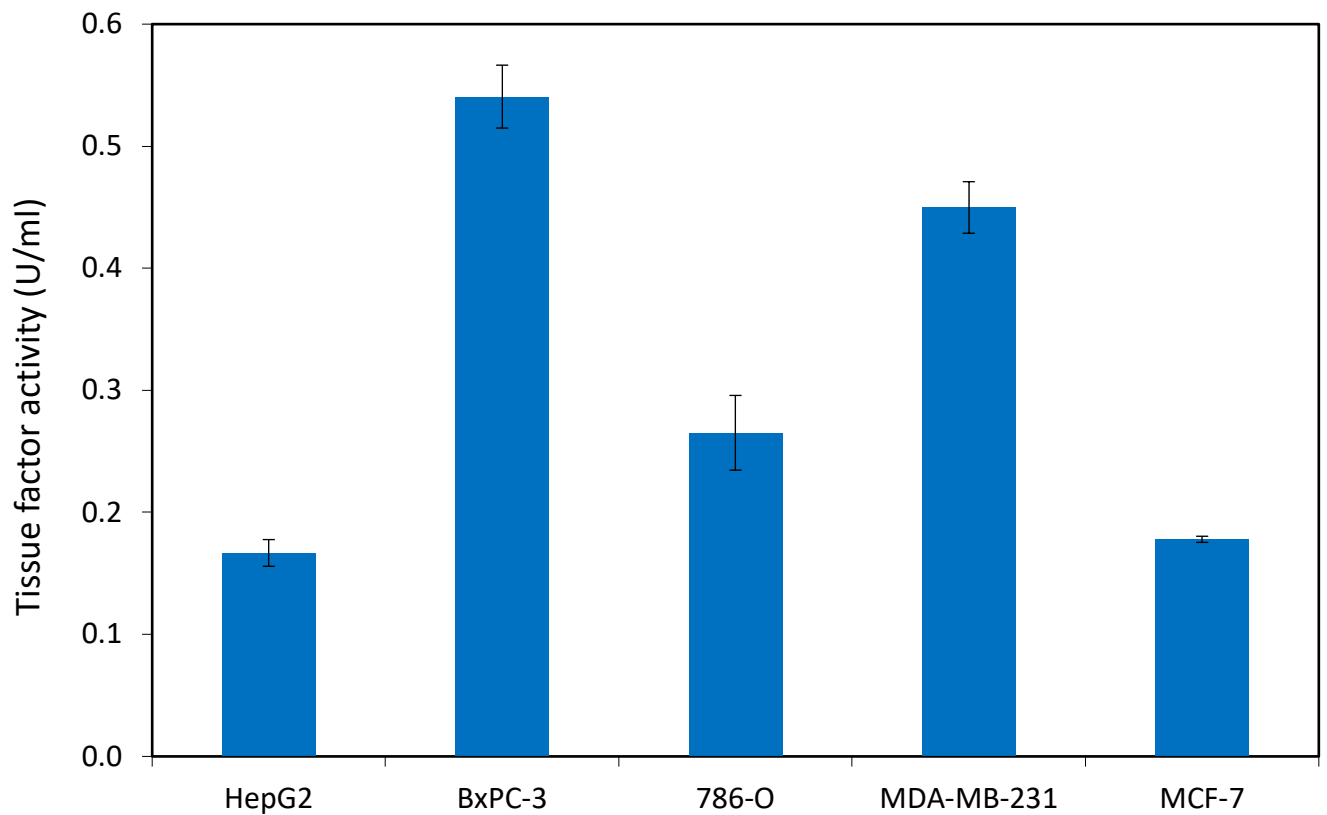
The activity of fVIIa associated with the isolated MV was also examined according to the procedure described in section 2.2.13. Analysis of the MV samples showed that MV isolated from HepG2, MDA-MB-231 and MCF-7 cell lines had higher levels of fVIIa activity (Figure 3.7). In contrast, MV isolated from BxPC-3 and 786-O cell lines exhibited lower fVIIa activity. This result also reflected the measured fVII/fVIIa antigens within the MV which were quantified previously using the fVII-ELISA (Figure 3.4).

Figure 3. 5 Molar ratio of fVIIa:TF within MV derived from cancer cell lines



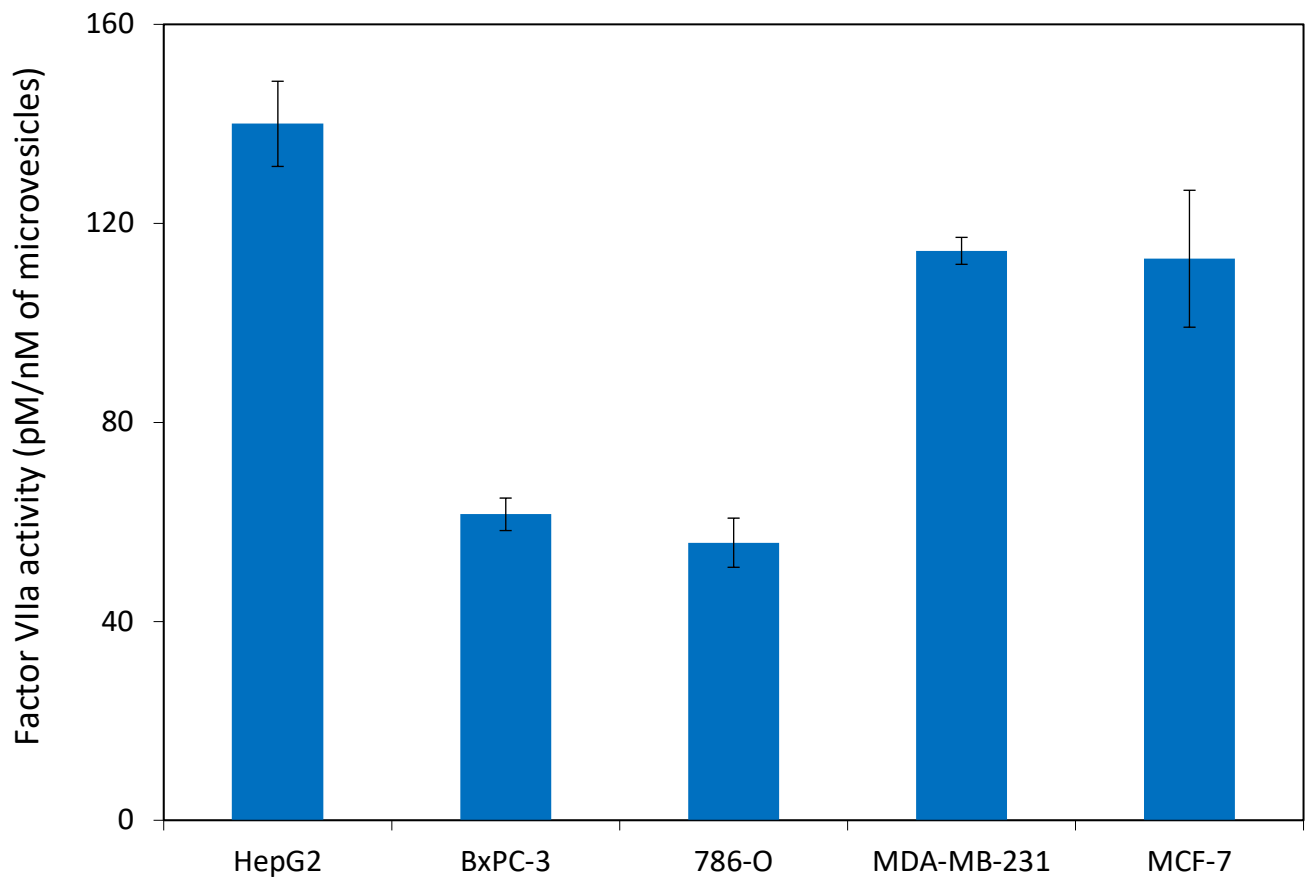
The molar ratio of fVIIa to TF in the MV isolated from HepG2, BxPC-3, 786-O, MDA-MB-231 and MCF-7 cell lines was calculated using the data generated by measuring the levels of fVII/fVIIa and TF antigens within the MV.

Figure 3. 6 Measurement of TF activity within MV derived from cancer cell lines using the fXa generation assay



MV (0.10 nM) isolated from the media of the 5 resting cell lines were supplemented with fVIIa (10 nM), fX (100 nM), and CaCl₂ (5 mM). The samples were mixed and incubated for 30 min at 37°C. To measure the amount of activated fXa generated by rec-TF, fXa chromogenic substrate (0.2 mM) was added to the samples and incubated for further 60 min at 37°C. The reaction was stopped by adding 2% (v/v) acetic acid and the absorptions were measured immediately at 410 nm. A standard curve prepared of recombinant TF (0-5 U/ml) was prepared and used alongside to measure the TF activities within the MV (The results show the average of five separate experiments and expressed as the mean ± SEM).

Figure 3. 7 Measurement of fVIIa activity within MV isolated from cancer cell lines using the fXa-generation assay



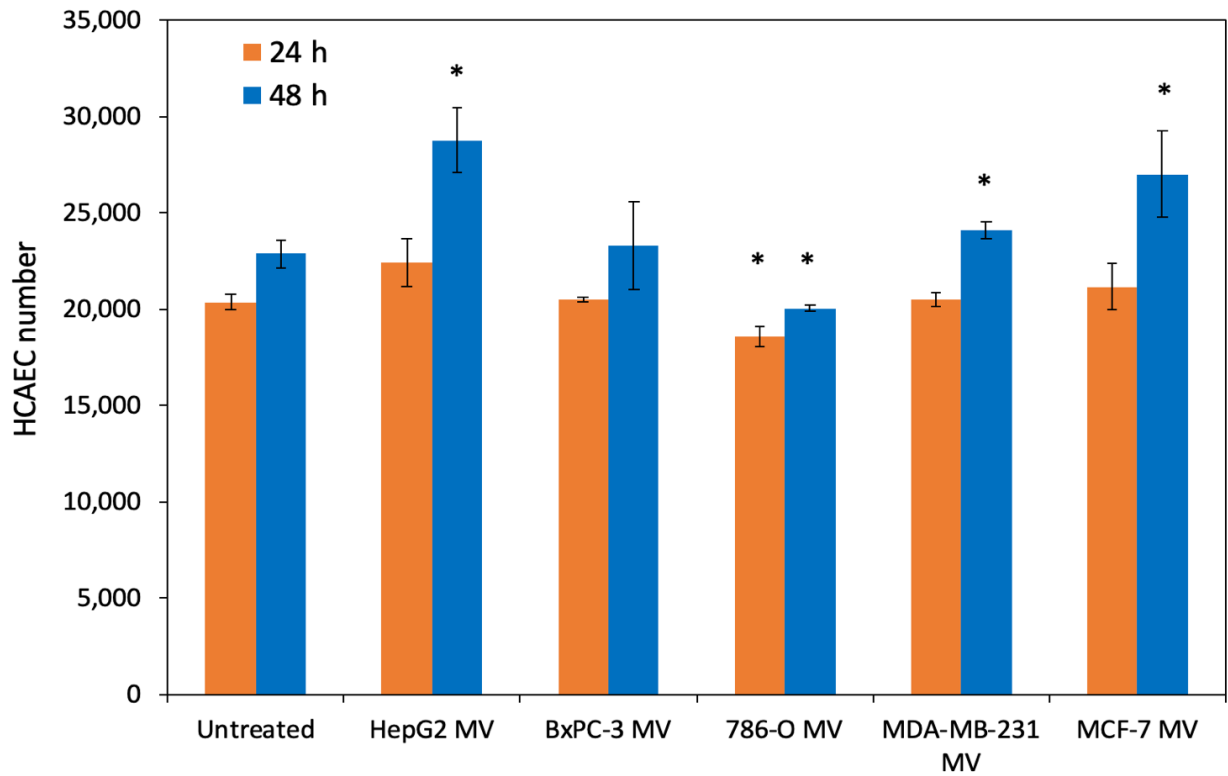
MV (0.10 nM) isolated from the media of the 5 resting cancer cell lines were supplemented with TF (1 U/ml), fX (100 nM) and CaCl₂ (5 mM). The samples were mixed and incubated for 30 min at 37°C. To measure the amount of activated fXa generated by fVIIa, fXa chromogenic substrate (0.2 mM) was added to the samples and incubated for further 60 min at 37°C. The reaction was stopped by adding 2% (v/v) acetic acid and the absorptions were measured immediately at 410 nm. A standard curve of purified fVIIa was prepared and used alongside to measure the fVIIa activities within the MV (The results show the average of five separate experiments and expressed as the mean ± SEM).

3.3.7 Examination of the influence of cancer cell-derived MV on endothelial cells

In the next study, the influence of MV isolated from the cell lines on the rate of proliferation and apoptosis in HCAEC was examined. To evaluate the effect of MV on HCAEC proliferation, the cells were seeded into 96-well plates and then incubated with MV (0.05 nM) isolated from different cell lines for up to 48 h. Cell numbers were then determined using the crystal violet assay as described in section 2.2.11. Analysis of the cell numbers showed that incubation of HCAEC with MV derived from HepG2 and MCF-7 cell lines resulted in significant increases in cell numbers (Figure 3.8 and 3.9). In addition, marginal increases in cell numbers were observed after incubation of HCAEC with MV isolated from MDA-MB-231 and BxPC-3 cells. In contrast, supplementation of HCAEC with MV derived from 786-O cell line resulted in the reduction in cell numbers compared to the untreated sample (Figure 3.8 and 3.9).

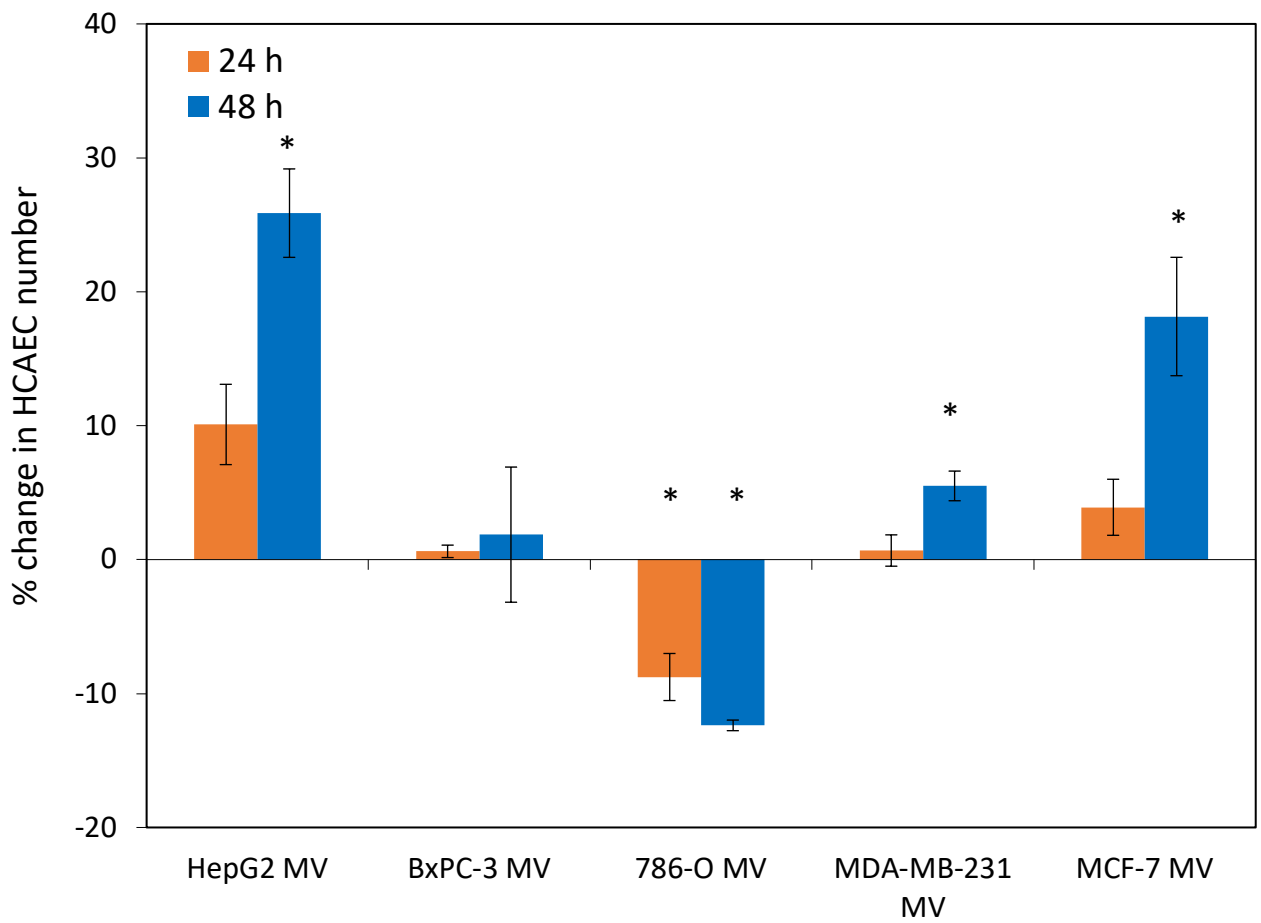
In addition to the cell numbers, the rate of induction of apoptosis was also examined after 24 h, in HCAEC incubated with MV derived from 786-O cells and compared to the outcome of incubation with MV derived from BxPC-3 cells. In each case, the cells were incubated with a range of concentrations of MV (0.025-0.130 nM) and the rate of apoptosis was then measured using the TiterTACS chromogenic TUNEL assay as described in section 2.2.9. Incubation of HCAEC with MV (0.05 nM) isolated from 786-O cell line resulted in a maximal level of cell apoptosis (Figures 3.10 and 3.11). In contrast, incubation of HCAEC with MV derived from BxPC-3 cell line did not induce significant amounts of cell apoptosis compared to the untreated sample (Figures 3.10 and 3.11).

Figure 3. 8 Assessment of the influence of MV derived from cancer cell lines on endothelial cell proliferation



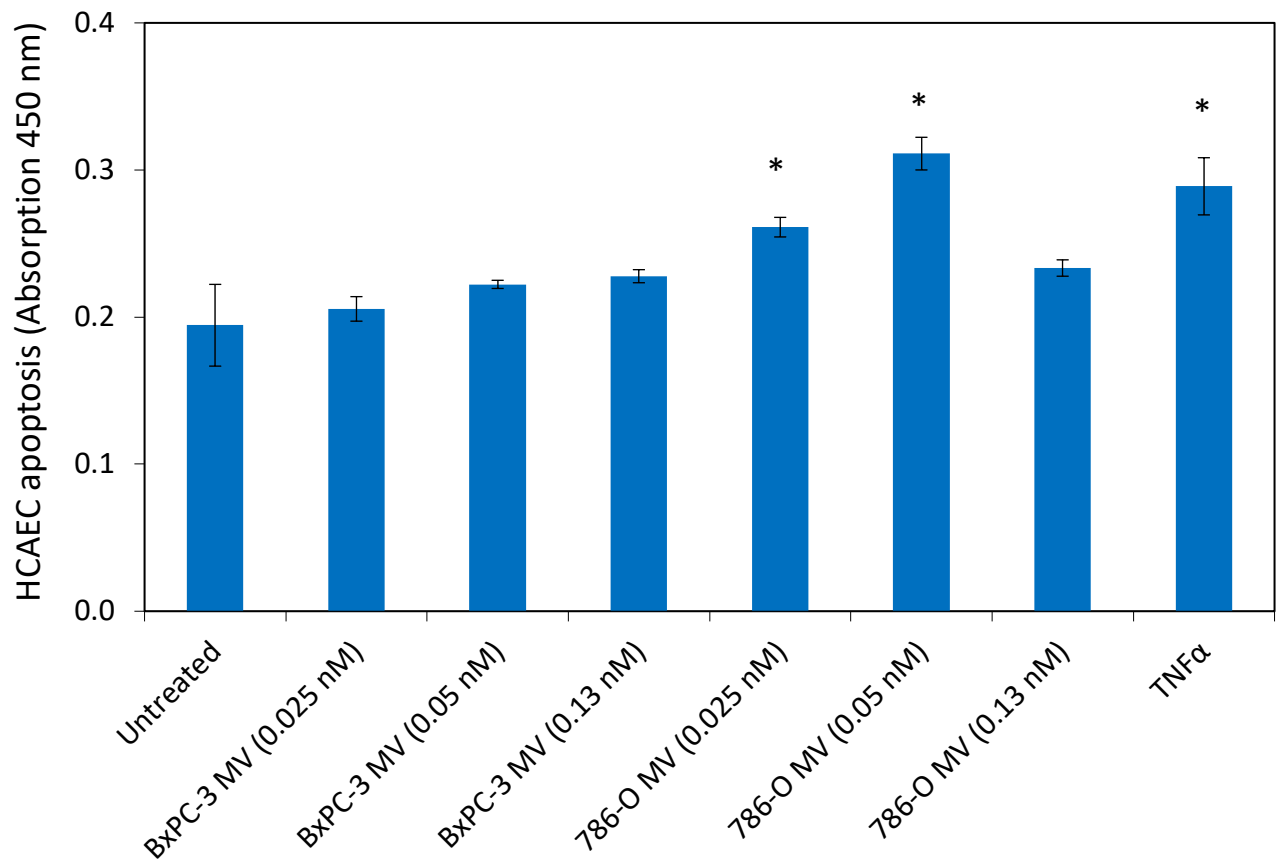
HCAEC (2×10^4) were seeded into 96-well plates and allowed to adhere. The cells were treated with MV (0.05 nM) purified from the 5 cell lines and incubated for up to 48 h. Cell numbers were determined using the crystal violet assay (The results show the average of five separate experiments and expressed as the mean \pm SEM; * = $p < 0.05$ compared to untreated cells).

Figure 3.9 The rate of endothelial cells proliferation induced by cancer cell-derived MV shown as percentages of the untreated cells



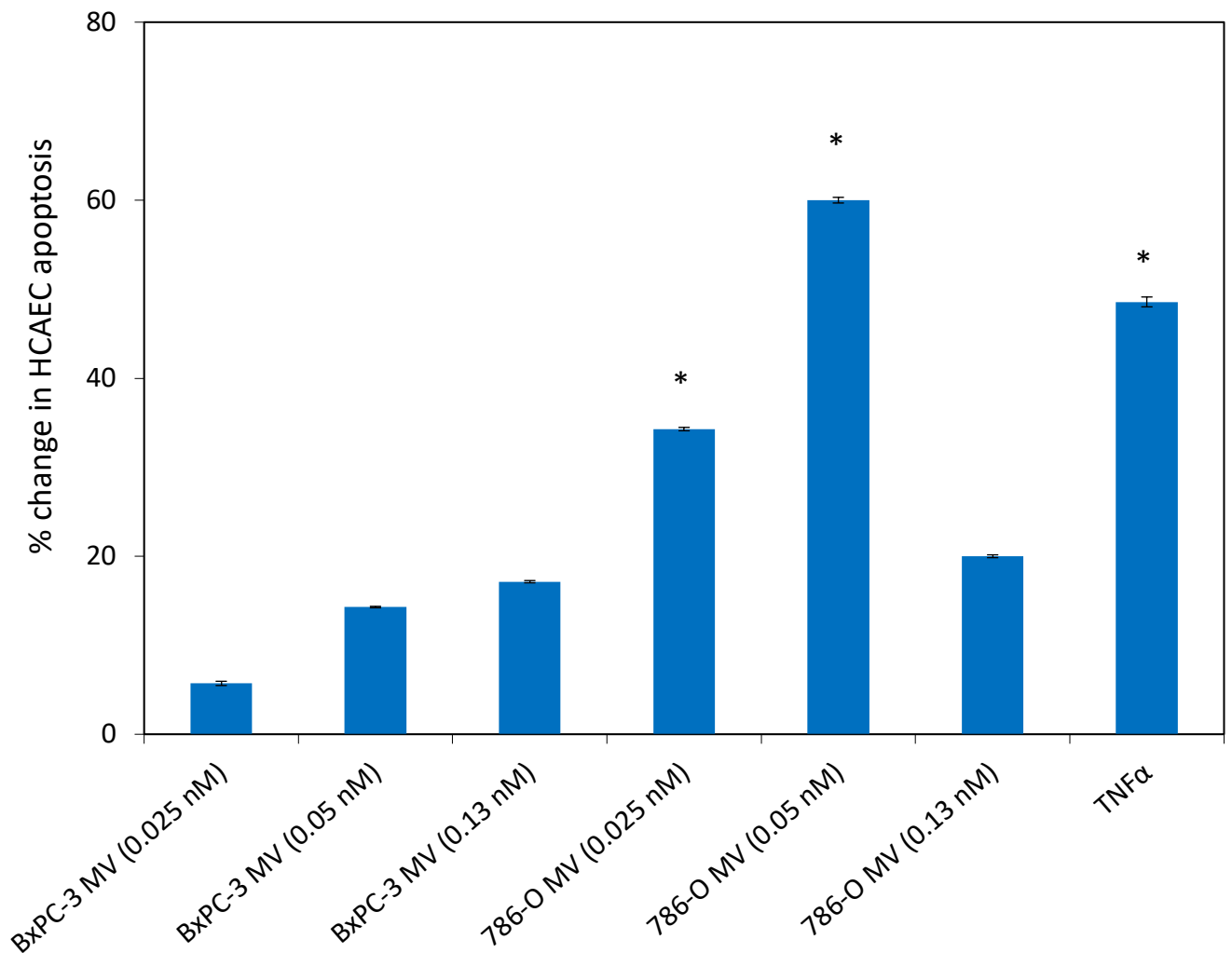
The percentage of cellular proliferation induced by MV purified from the 5 cancer cell lines was calculated against the untreated sample using the results presented in Figure 3.8. The change in the number of the endothelial cells was calculated as a percentage of the untreated cells (The results are the average of five separate experiments and expressed as the mean \pm SEM; * = $p < 0.05$ compared to untreated samples at each time point).

Figure 3. 10 Examination of the influence of MV isolated from cancer cell lines on endothelial cell apoptosis



HCAEC (2×10^4) were seeded into 96-well plates and allowed to adhere. The cells were then treated with different concentration of MV (0-0.130 nM) derived from the cell lines (786-O and BxPC-3) and incubated for 24 h. A set of cells were treated with TNF α (1 ng/ml) and used as a positive control. The rate of apoptosis was determined using the TiterTACS chromogenic TUNEL assay (The results are the average of five separate experiments and expressed as the mean \pm SEM; * = $p < 0.05$ compared to the untreated sample).

Figure 3. 11 The rate of endothelial cells apoptosis induced by cancer cell-derived MV shown as percentages of the untreated cell population



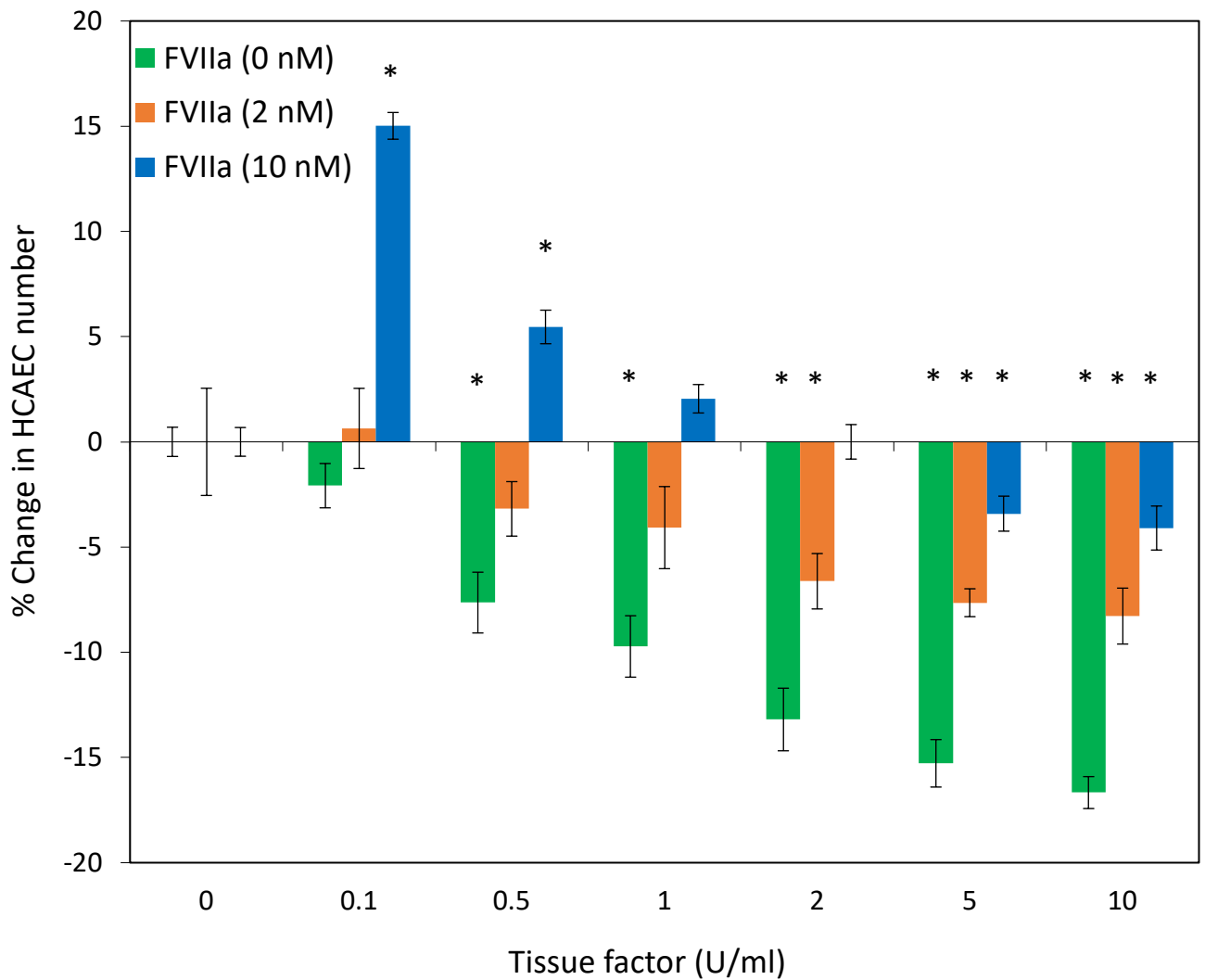
The percentage of cellular apoptosis induced by MV purified from two cancer cell lines (786-O and BxPC-3) was calculated against the untreated sample using the results presented in Figure 3.10. The change in the level of the cellular apoptosis was measured as a percentage of the untreated cells (The results show the average of five separate experiments and expressed as the mean \pm SEM; * = $p < 0.05$ compared to the untreated sample).

3.3.8 The effect of different ratios of exogenous fVIIa:TF on HCAEC proliferation

In section 3.1.7, incubation of HCAEC with MV derived from cancer cell lines indicated that the induction of cellular proliferation or apoptosis was based on the ratios of fVIIa:TF within these MV. Therefore, the next set of experiments were carried out to examine the influence of incubation with various combinations of purified fVIIa and recombinant TF on HCAEC cell numbers. HCAEC were seeded into 96-well plates and allowed to adhere. The cells were then incubated for 24 h with different combinations of recombinant TF (0-10 U/ml) and purified fVIIa (0-10 nM). Cell numbers were then measured using the crystal violet assay as described in section 2.2.11. Incubation of HCAEC with recombinant TF in the absence of any fVIIa resulted in a reduction in the number of viable cells (Figure 3.12). However, supplementation of the recombinant TF with purified fVIIa (2 nM) partially prevented the reduction in cell numbers, but it was ineffective at TF concentrations above 0.5 U/ml. Inclusion of 10 nM fVIIa restored the cell numbers up to 2 U/ml of TF and was proliferative when combined together with lower TF concentrations (0.1-1 U/ml). Finally, incubation of cells with fVIIa in the absence of TF had no detectable effect on cell numbers (Figure 3.12).

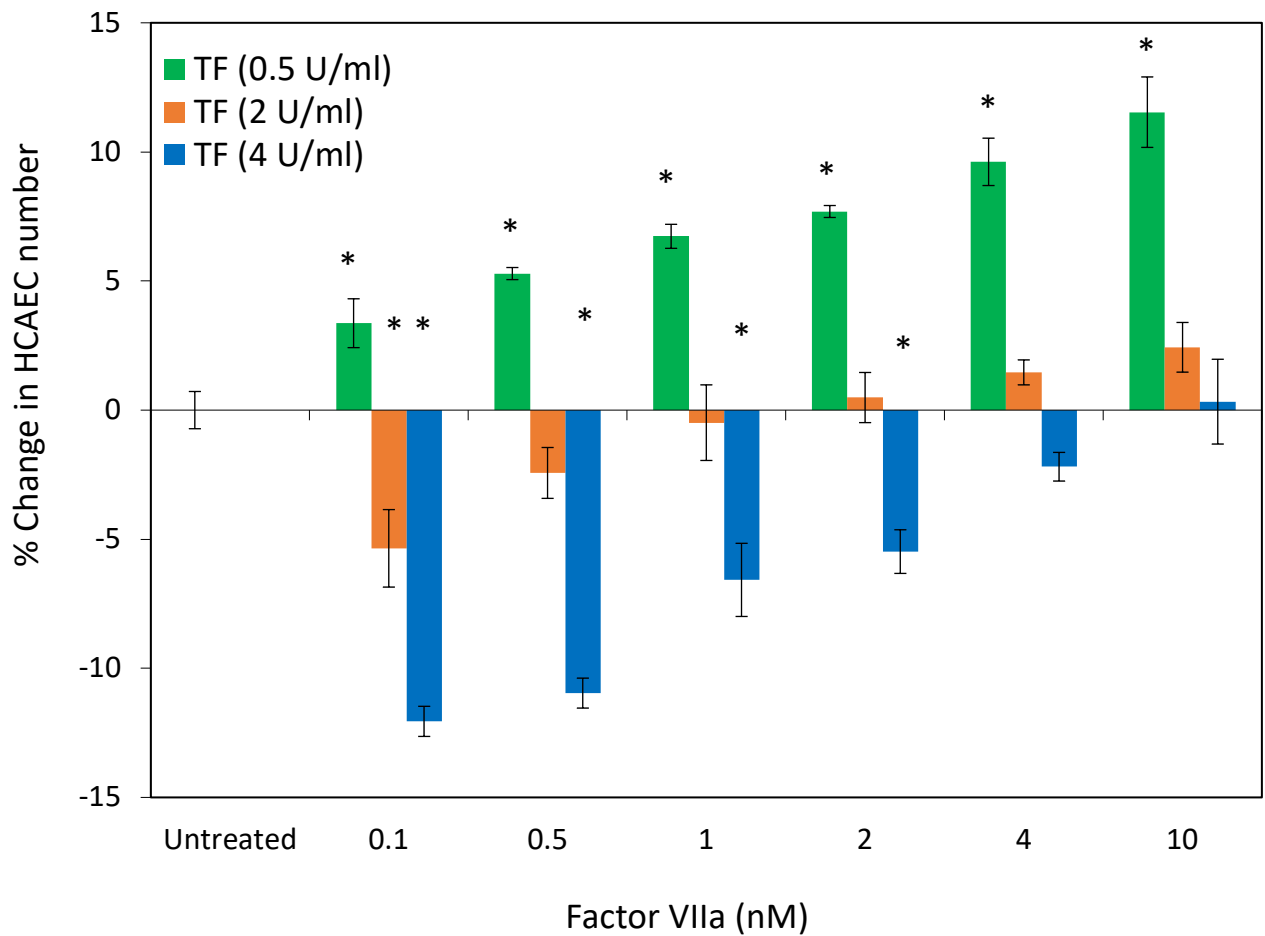
The above data were then confirmed by titrating a range of concentrations of purified fVIIa (0-10 nM) with three separate concentrations of TF (0-4 U/ml). On supplementation of HCAEC with 0.5 U/ml of TF, increased cell numbers were observed for all concentrations of fVIIa tested (Figure 3.13). However, on incubation of HCAEC with 2 U/ml TF to HCAEC, fVIIa concentrations of 1 nM or higher were required to preserve or increase cell numbers. Furthermore, in the presence of 4 U/ml TF, only 10 nM fVIIa was capable of preventing the reduction in cell numbers (Figure 3.13).

Figure 3. 12 Assessment of the influence of exogenous TF and fVIIa on endothelial cell numbers



HCAEC (2×10^4) were seeded into 96-well plates and allowed to adhere. The cells were then treated with a range of concentrations of recombinant human TF (0-10 U/ml), in the presence or absence of purified fVIIa (0-10 nM). The cells were incubated for 24 h and cell numbers were measured using the crystal violet staining assay. The changes in cell numbers were calculated as percentage of the original numbers (The results show the average of five separate experiments and expressed as the mean \pm SEM; * = $p < 0.005$ compared to the untreated sample).

Figure 3. 13 Examination of the influence of exogenous fVIIa and TF on endothelial cell numbers



HCAEC (2×10^4) were seeded into 96-well plates and allowed to adhere. The cells were then treated with a range of concentrations of purified fVIIa (0-10 nM), in the presence or absence of recombinant human TF (0-4 U/ml). The cells were then incubated for 24 h and cell numbers were measured using the crystal violet staining assay. The changes in cell numbers were calculated as percentages of the original numbers (The results show the average of five separate experiments and expressed as the mean \pm SEM; * = $p < 0.005$ compared to the untreated sample).

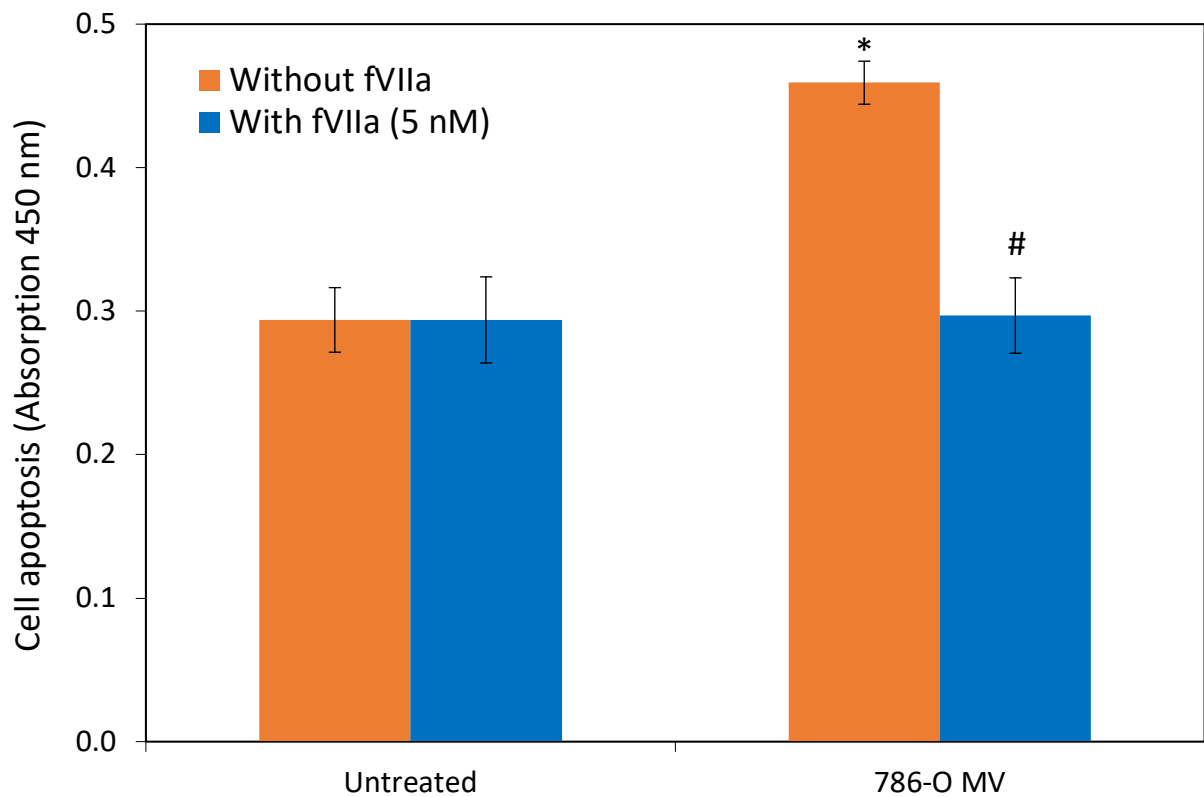
3.3.9 Examination of the influence of exogenous fVIIa on MV-induced apoptosis in endothelial cells

In the previous experiments, MV isolated from 786-O cells were shown to induce apoptosis in endothelial cells. In order to test the hypothesis that high levels of fVIIa may rescue cells from MV-induced apoptosis and enhance cell proliferation, HCAEC were seeded into 96-well plates and incubated with the optimal concentration of 786-O-derived MV (0.05 nM), in the presence or absence of exogenous fVIIa (5 nM). The rate of apoptosis was measured after 24 h using the TiterTACS chromogenic TUNEL assay. Inclusion of additional fVIIa completely eliminated the pro-apoptotic influence of MV derived from 786-O cell line on endothelial cells (Figure 3.14), reducing the level of apoptosis levels to those of the untreated cells.

3.3.10 MV-induced cell proliferation and apoptosis is mediated through PAR2 receptor

In the previous experiments, MV isolated from cancer cell lines were shown to contain TF and fVIIa proteins and induced either proliferation or apoptosis in endothelial cells according to the ratio of fVIIa to TF. TF-fVIIa complex is known to activate PAR2 receptor, as mentioned in section 1.4. Therefore, the aim of this experiment was to examine the involvement of PAR2 in HCAEC proliferation and apoptosis. The activation of PAR2 on the cells was blocked with an inhibitory antibody (SAM11; 20 µg/ml). The cells were then treated with MV isolated from HepG2 cells (0.05 nM), which was previously determined to be the optimal concentration for inducing cell proliferation, and incubated for 24 h. Cell numbers were then measured using the crystal violet assay. Inhibition of PAR2 activation reduced the increase in HCAEC numbers in response to the addition of HepG2 cell-derived MV to levels similar to the untreated cells (Figure 3.15).

Figure 3. 14 Examination of the influence of exogenous fVIIa on the pro-apoptotic effect of MV

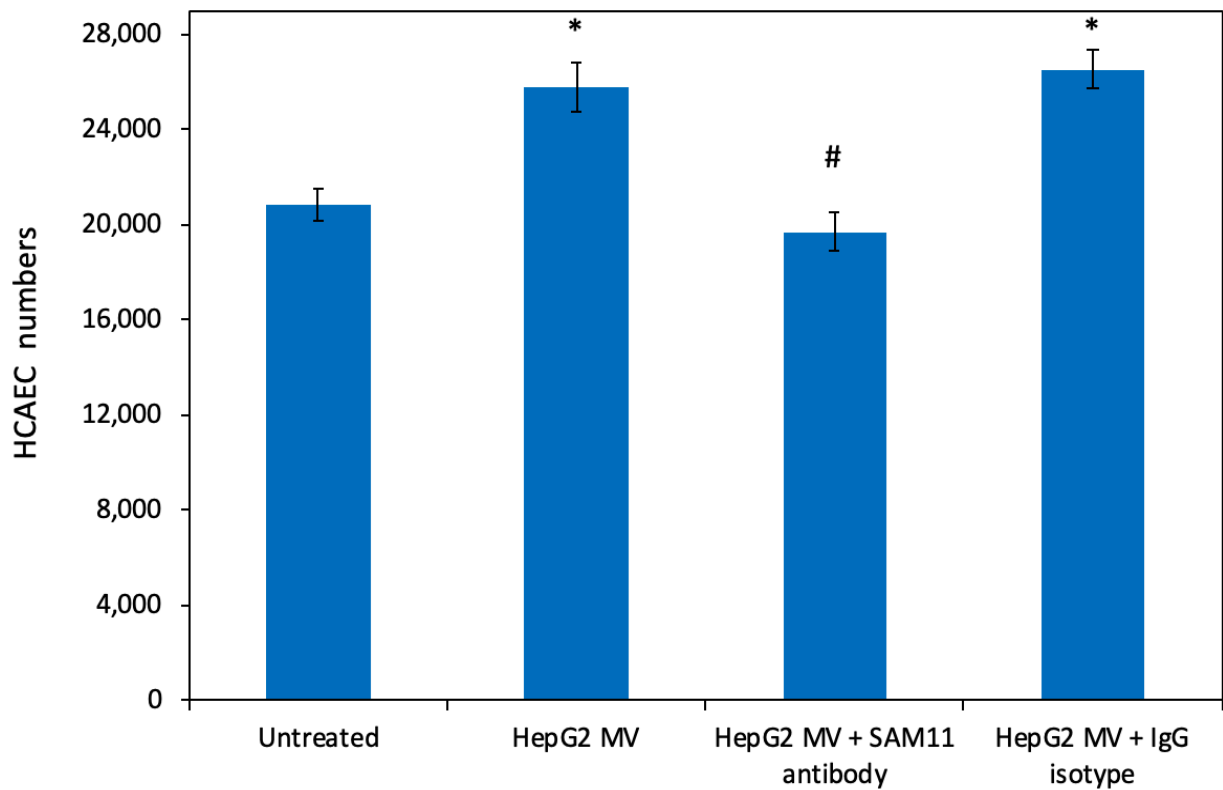


HCAEC (2×10^4) were seeded into 96-well plates and allowed to adhere. The cells were then treated with MV (0.05 nM) isolated from 786-O alone or in combination with exogenous fVIIa (5 nM) and incubated for 24 h. The rate of apoptosis was then determined using the TiterTACS chromogenic TUNEL assay (The results show the average of five separate experiments and expressed as the mean \pm SEM; * = $p < 0.05$ compared to the untreated sample; # = $p < 0.05$ compared to the sample without added fVIIa).

To examine the involvement of PAR2 in HCAEC apoptosis, PAR2 activation on the cells was blocked with an inhibitory antibody (SAM11; 20 µg/ml). The cells were then incubated with a concentration of 786-O cell-derived MV (0.05 nM) which was shown to induce optimal levels of apoptosis in HCAEC. The rate of apoptosis was then measured after 24 h using the TiterTACS chromogenic TUNEL assay. Analysis of the samples showed that blocking PAR2 activation abolished the pro-apoptotic influence of 786-O cell-derived MV (Figure 3.16). As a complementary experiment, the influence of the activation of PAR2 using a synthetic agonist, on preventing MV-induced apoptosis in HCAEC was investigated. PAR2 receptor in HCAEC was activated by PAR2-AP (20 µM) at the time of addition of the optimal concentration of 786-O cell-derived MV (0.05 nM). The cells were then incubated for 24 h and the rate of apoptosis was measured using the TiterTACS chromogenic TUNEL assay. Activation of PAR2 in HCAEC using PAR2-AP eliminated the pro-apoptotic influence of 786-O cell-derived MV (Figure 3.17).

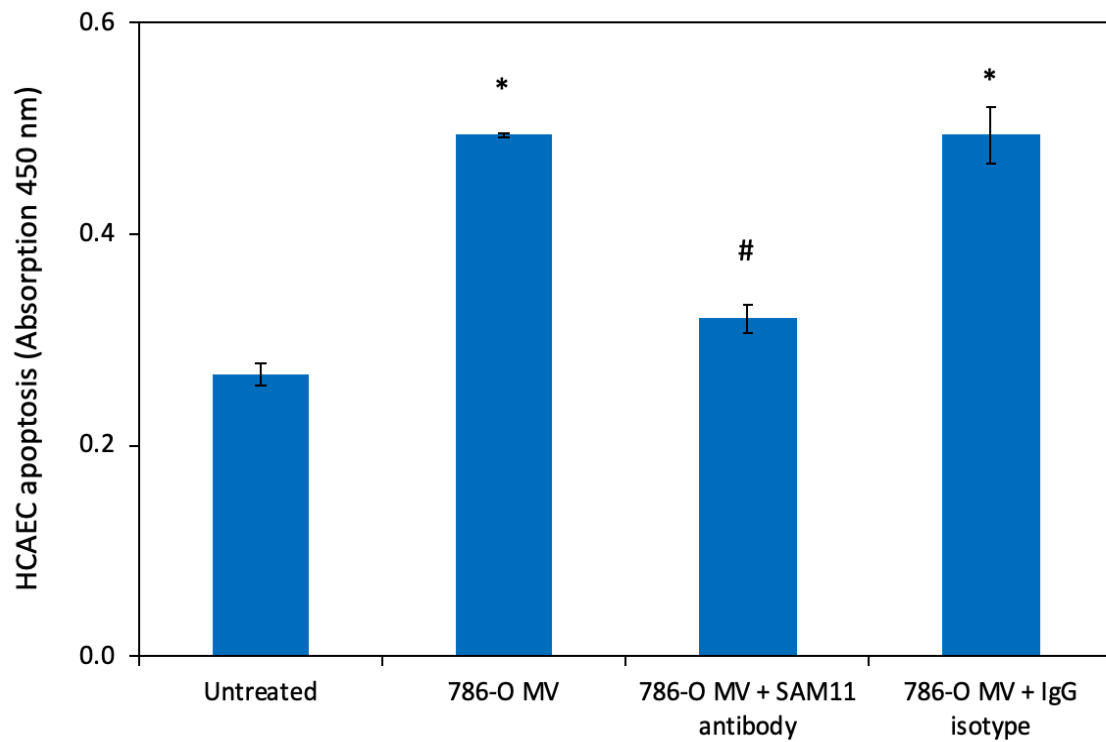
To further clarify these observations, the presence of PAR2 antigens on the surface of HCAEC were examined after being treated with PAR2-AP or MV isolated from 786-O at optimal or hyper-optimal concentration. HCAEC were seeded into 96-well plates, allowed to adhere and then incubated for 30 min with either PAR2-AP (20 µM), or 786-O-derived MV at the optimal (0.05 nM) or a hyper-optimal concentration (0.130 nM). The cells were fixed and probed with a mouse anti-human PAR2 antibody (SAM11; 20 µg/ml) and then with an HRP-conjugated goat anti-mouse antibody. Incubation of HCAEC with PAR2-AP (20 µM) or 0.130 nM 786-O cell-derived MV resulted in significant reductions in cell-surface PAR2 antigens (Figure 3.18). In contrast, cell-surface PAR2 antigen levels remained unchanged by the addition of 0.05 nM of MV isolated from 786-O cells compared to untreated cells. These results suggest that treatment of cells with PAR2-AP or high concentration of MV may induce the internalisation of PAR2 and consequently desensitize the cells to PAR2 signalling.

Figure 3. 15 Assessment of the involvement of PAR2 in endothelial cells proliferation



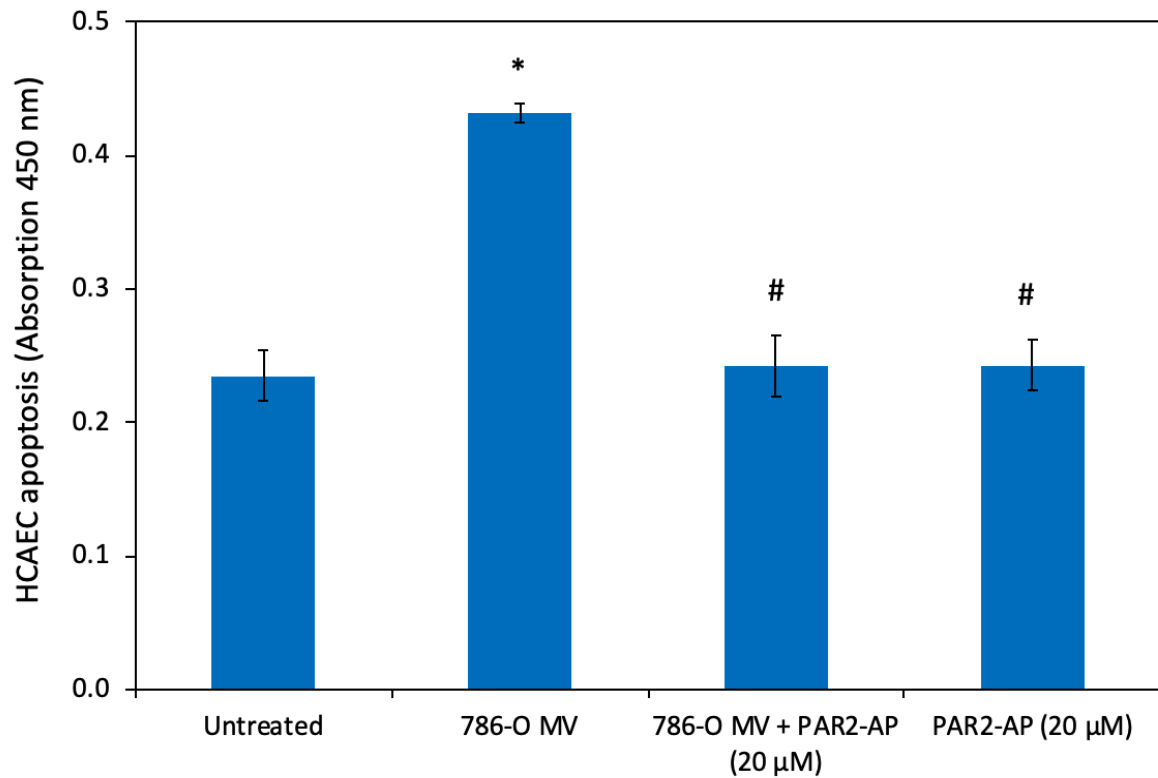
HCAEC (2×10^4) were seeded into 96-well plates and allowed to adhere. The cells were pre-incubated with an anti-PAR2 antibody (SAM11; 20 $\mu\text{g/ml}$) or a control isotype IgG (20 $\mu\text{g/ml}$). The cells were then incubated with HepG2 cell-derived MV (0.05 nM) for 24 h and cell numbers were determined using the crystal violet staining assay (The results show the average of five separate experiments and expressed as the mean \pm SEM; * = $p < 0.05$ compared to the untreated sample; # = $p < 0.05$ compared to the sample not treated with the antibody).

Figure 3. 16 Examination of the involvement of PAR2 in endothelial cells apoptosis



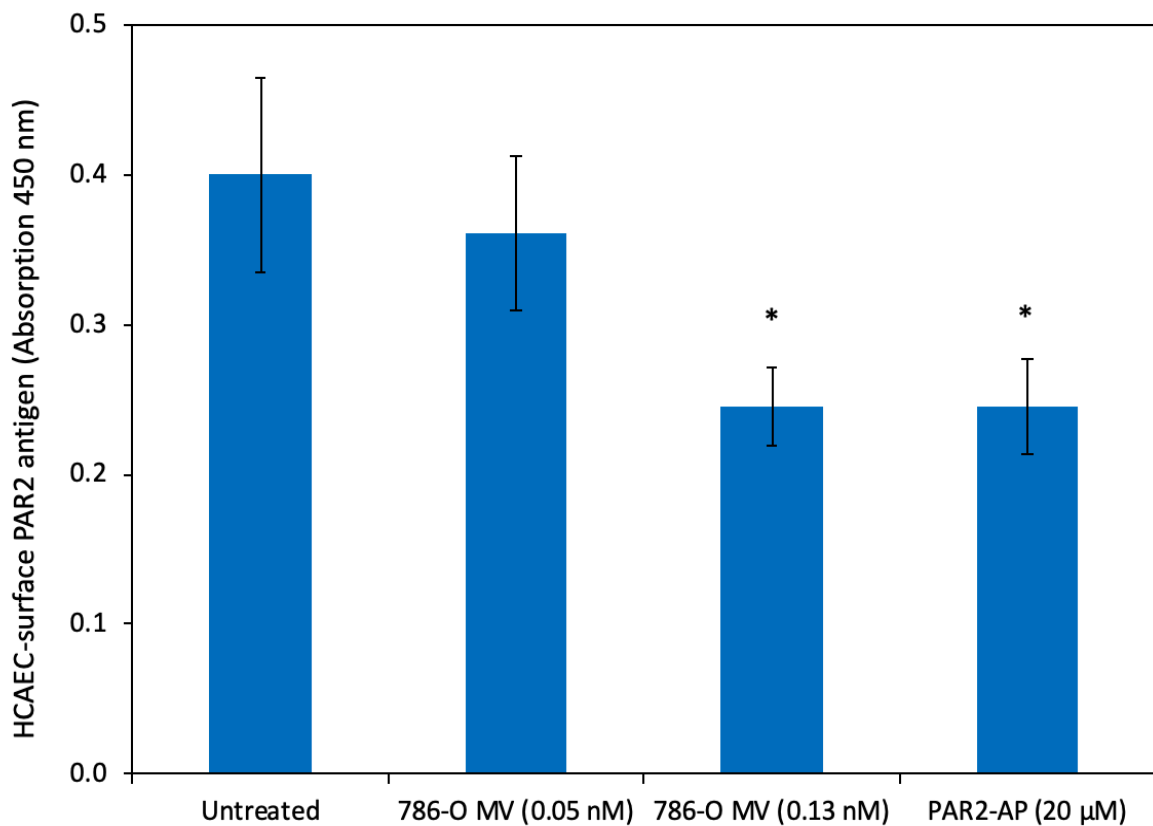
HCAEC (2×10^4) were seeded into 96-well plates and allowed to adhere. The cells were then pre-incubated with an anti-PAR2 antibody (SAM11; 20 $\mu\text{g/ml}$) or a control isotype IgG (20 $\mu\text{g/ml}$). The cells were then incubated with 786-O cell-derived MV (0.05 nM) for 24 h and the rate of apoptosis was then determined using the TiterTACS chromogenic TUNEL assay (The results show the average of five separate experiments and expressed as the mean \pm SEM; * = $p < 0.05$ compared to the untreated sample; # = $p < 0.05$ compared to the sample not treated with the antibody).

Figure 3. 17 The influence of the over-activation of PAR2 on the induction of apoptosis by MV



HCAEC (2×10^4) were seeded into 96-well plates and allowed to adhere. The cells were activated with PAR2-AP (20 μ M) at the time of addition of MV (0.05 nM) isolated from 786-O cells and incubated for 24 h. The rate of apoptosis was then measured using the TiterTACS chromogenic TUNEL assay (The results show the average of five separate experiments and expressed as the mean \pm SEM; * = $p < 0.05$ compared to the untreated sample; # = $p < 0.05$ compared to MV without the peptide).

Figure 3. 18 High concentrations of 786-O-derived MV induce PAR2 internalisation in endothelial cells through over-activation of the receptor



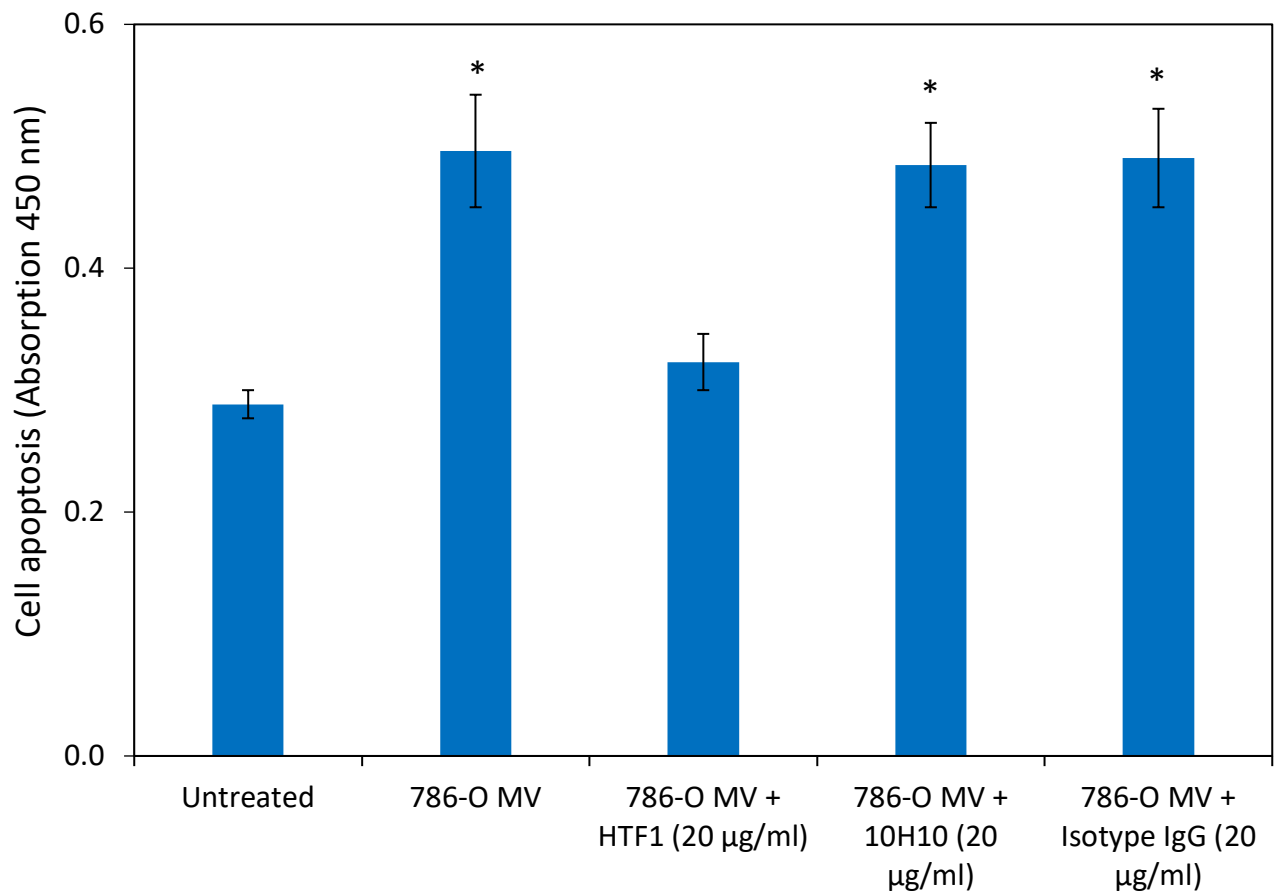
HCAEC (2×10^4) were seeded into 96-well plates and allowed to attach. The cells were then incubated with range of concentrations of 786-O cell-derived MV (0-0.130 nM) or PAR2-AP (20 µM) for 30 min. The cells were then fixed with 4% (v/v) formaldehyde and incubated with a mouse anti-human PAR2 antibody (SAM11; 20 µg/ml) and probed with an HRP-conjugated goat anti-mouse antibody diluted 1:1000 (v/v). The TMB substrate was then added to the samples and the relative amount of cell-surface PAR2 antigens were measured at 450 nm using a plate reader (The results show the average of five separate experiments and expressed as the mean \pm SEM; * = $p < 0.05$ compared to the untreated sample).

3.3.11 Examination of the involvement of TF-fVIIa complex in endothelial cells apoptosis and proliferation

In the previous experiments, MV isolated from cancer cells lines were shown to exhibit TF and fVIIa proteins and promoted either proliferation or apoptosis in endothelial cells. Therefore, this study aimed to investigate if these mechanism(s) (proliferation and apoptosis) are induced by TF-fVIIa signalling. HCAEC were seeded into 96-well plates and allowed to adhere. MV derived from 786-O cells (0.05 nM) were pre-incubated with HTF-1 anti-TF antibody that blocks the fVIIa binding site, 10H10 anti-TF antibody (20 µg/ml) to block TF signalling, or a mouse IgG isotype control (all at 20 µg/ml). The cells were then incubated with the MV samples for 24 h and the rate of apoptosis was determined using the TiterTACS chromogenic TUNEL assay. Blocking of procoagulant activity of TF in MV, using the HTF-1 anti-TF antibody, reduced the rate of cell apoptosis compared to MV treated with the isotype control antibody. However, inhibition of TF signalling by pre-incubation of 786-O cell-derived MV with the 10H10 anti-TF antibody did not influence the induction of cell apoptosis by the MV (Figure 3.19).

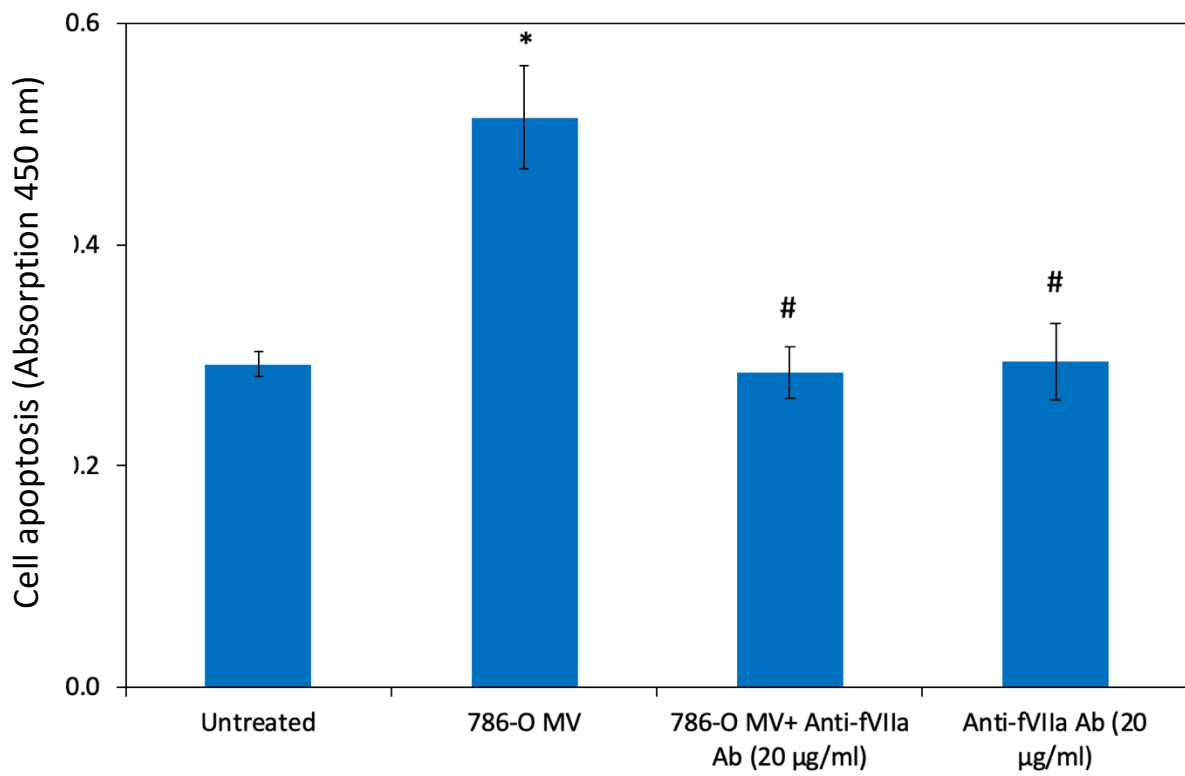
In addition, to examine the involvement of fVIIa in cellular apoptosis and proliferation, MV (0.05 nM) derived from 786-O or HepG2 cells were pre-incubated with an inhibitory anti-fVIIa antibody (20 µg/ml). HCAEC were incubated with the MV samples for 24 h and the rate of apoptosis and also the cell numbers were then determined. Neutralisation of fVIIa activity on MV prevented the induction of apoptosis in HCAEC by 786-O cell-derived MV (Figure 3.20). Similarly, blocking of fVIIa activity on HepG2 cell-derived MV in the same manner inhibited the resultant increase in cell numbers compared to untreated MV (Figure 3.21).

Figure 3. 19 MV-associated TF promotes endothelial cells apoptosis through pro-coagulant activity



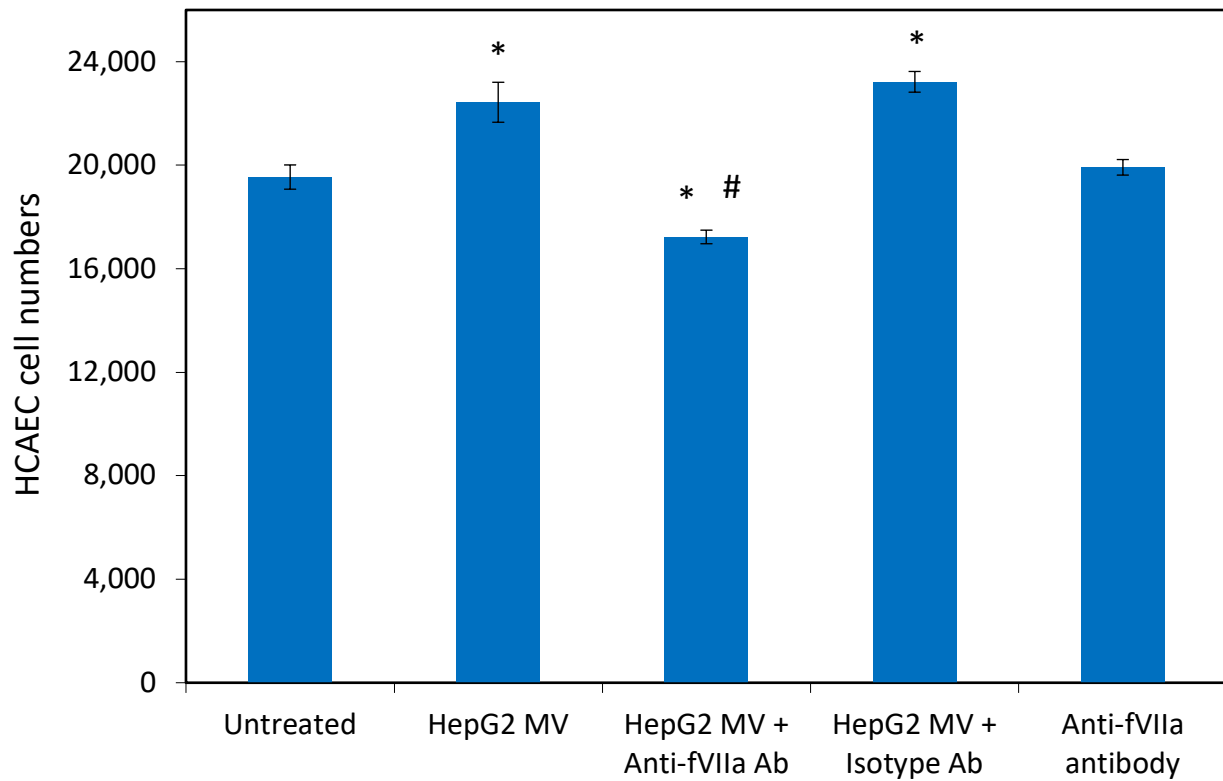
HCAEC (2×10^4) were seeded into 96-well plates and allowed to adhere. MV (0.05 nM) isolated from 786-O cells were pre-incubated with an HTF-1 anti-TF antibody to block fVIIa binding, a 10H10 anti-TF antibody to block TF signalling or an isotype mouse antibody (all antibodies at 20 µg/ml). The cells were then treated with the MV samples and incubated for 24 h. The rate of apoptosis was then determined using the TiterTACS chromogenic TUNEL assay (The results show the average of five separate experiments and expressed as the mean \pm SEM; * = $p < 0.05$ compared to the untreated sample).

Figure 3. 20 Neutralisation of fVIIa within 786-O-derived MV abolishes the promotion of apoptosis in endothelial cells



HCAEC (2×10^4) were seeded into 96-well plates and allowed to adhere. MV (0.05 nM) were isolated from 786-O cells and pre-incubated with an inhibitory anti-fVIIa antibody (20 µg/ml) prior to addition to the cells. The cells were incubated for 24 h and the rate of apoptosis was then determined using the TiterTACS chromogenic TUNEL assay (The results show the average of five separate experiments and expressed as the mean \pm SEM; * = $p < 0.05$ compared to the untreated sample, # = $p < 0.05$ compared to the MV sample without the antibody).

Figure 3. 21 Neutralisation of fVIIa within HepG2 cell-derived MV prevents the promotion of endothelial cells proliferation



HCAEC (2×10^4) were seeded into 96-well plates and allowed to adhere. MV (0.05 nM) purified from HepG2 cells were pre-incubated with an inhibitory anti-fVIIa antibody (20 $\mu\text{g}/\text{ml}$) prior to addition to the cells. The cells were incubated for 24 h and cell numbers were measured using the crystal violet staining assay (The results show the average of five separate experiments and expressed as the mean \pm SEM; * = $p < 0.05$ compared to the untreated sample, # = $p < 0.05$ compared to the MV sample without the antibody).

3.3.12 Measurement of the exposure of fVII on the surface of endothelial cells in response to TF and PAR2 activation

In the previous experiments, MV-associated TF were shown to induce apoptosis in endothelial cells through pro-coagulant activity which was also mediated via PAR2 receptor. However, incubation of HCAEC with TF alone prompted cell apoptosis (Figure 3.12). Therefore, this study was designed to examine if endothelial cells can themselves be a source of fVII through measuring the presence of the antigen on the cell surface. HCAEC were seeded in 96-well plates, allowed to adhere, and the cells were then incubated with recombinant TF (2 U/ml) for up to 60 min or activated using PAR2-AP (20 μ M) for up to 240 min. One set of the cells was permeabilised with 0.01% (v/v) Triton diluted in dH₂O in order to determine the total amount of fVII protein. The cells were then fixed and the cell-surface and total amount of fVII antigen were quantified, using an ELISA-based assay as described in section 2.2.10. Measurement of the fVII protein in intact and lysed HCAEC indicated that approximately 20% of the fVII antigens were present on the surface of the resting cells (Figure 3.22). Incubation of HCAEC with recombinant TF (2 U/ml) for 10 or 20 min resulted in significant increases in cell-surface fVII antigen (48%) and (45%), respectively (Figure 3.22). Similarly, activation of HCAEC using PAR2-AP (20 μ M) significantly increased cell-surface fVII antigen (33%) at 30 min (Figure 3.23).

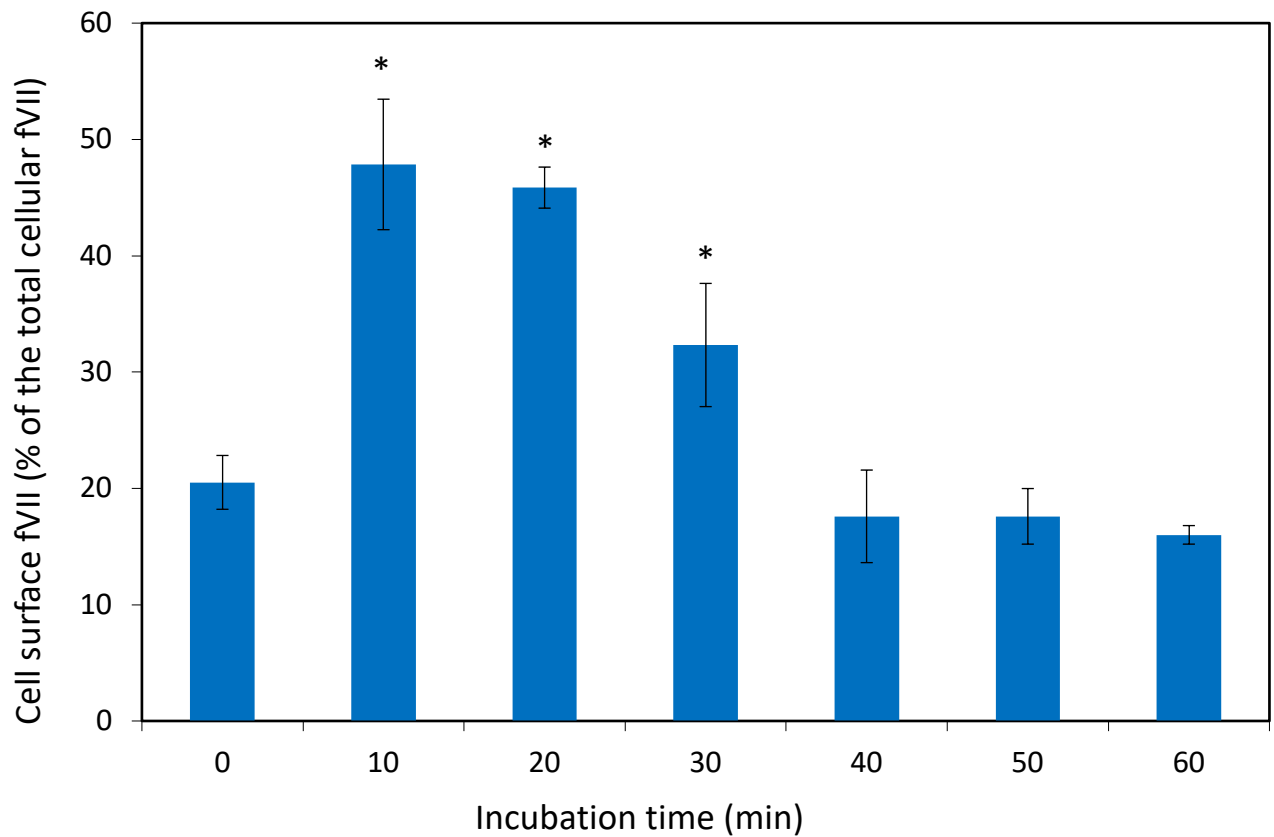
The next set of experiment aimed to examine if the exposure of endothelial cells to repeated treatment with TF can deplete the amount of cell-surface fVII antigen. HCAEC were seeded into 96-well plates and allowed to adhere. The cells were then treated with recombinant TF (2 U/ml) at 60 min intervals. In these experiments, both the remaining cell-surface fVII antigen and MV-associated fVII antigen were measured and calculated as the percentage of the amount of fVII present on the surface of the resting cells. Treatment of HCAEC with recombinant TF progressively decreased the amount of fVII exposed at the surface of the cells (Figure 3.24).

Furthermore, the magnitudes of these reductions were comparable to, and therefore most likely accounted for, by the amount of fVII that was associated with the released MV (Figure 3.25).

3.3.13 Examination of the ability of direct oral anticoagulants to prevent MV-induced apoptosis in endothelial cells

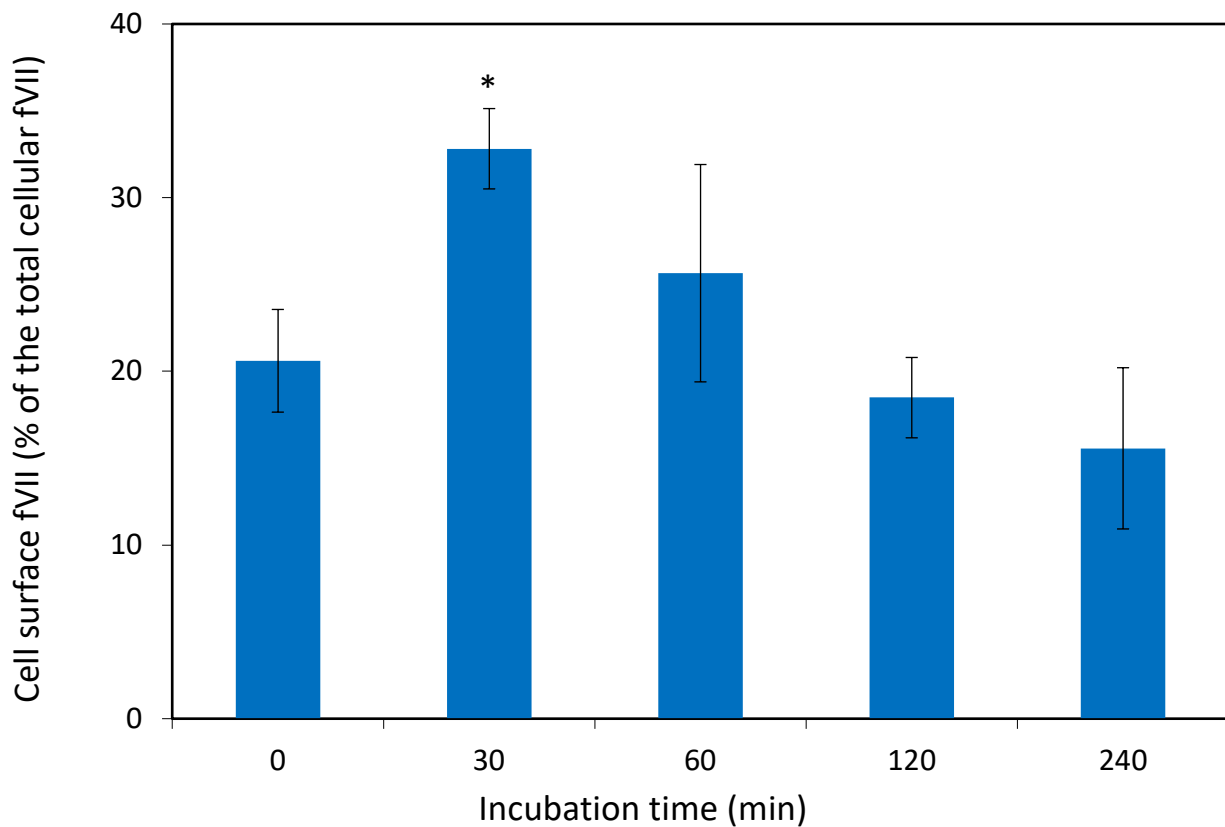
Since MV isolated from 786-O cell line were capable of causing apoptosis in endothelial cells, the next set of experiments aimed to examine the potential for DOAC to prevent the pro-apoptotic influence of these MV. The 786-O cell-derived MV (0.05 nM) were pre-incubated with rivaroxaban (1.8 μ M), apixaban (1.8 μ M) or an inhibitory polyclonal anti-fVIIa antibody (10 μ g/ml) prior to addition to HCAEC. The cells were incubated for 24 h and the rate of apoptosis was measured using the TiterTACS chromogenic TUNEL assay. Pre-incubation of 786-O cell-derived MV with apixaban but not rivaroxaban eliminated the pro-apoptotic effect of these MV (Figure 3.26). Furthermore, inhibition of MV-associated fVIIa from 786-O cells with an inhibitory anti-fVIIa antibody also prevented the induction of cell apoptosis. Therefore, it is possible that apixaban may be capable of acting as a protease inhibitor, blocking the proteolytic activity of fVIIa, in addition to fXa.

Figure 3. 22 Examination of the alteration in endothelial cell-surface fVII antigen levels in response to TF



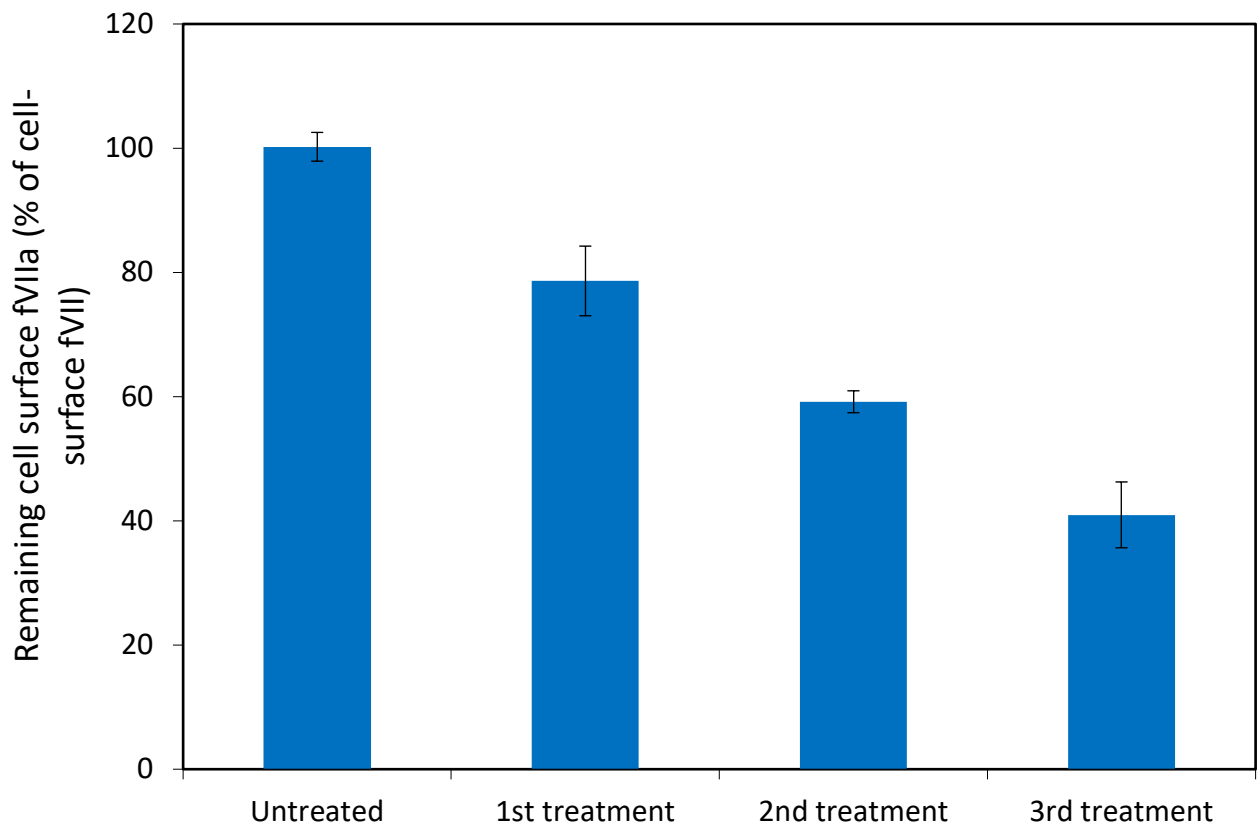
HCAEC (2×10^4) were seeded into 96-well plates and allowed to adhere. The cells were then treated with recombinant TF (2 U/ml) and incubated for up to 60 min. After the incubation, the cells were washed with PBS and fixed with 4% (v/v) formaldehyde. One set was permeabilised with 0.01% (v/v) Triton diluted in dH₂O. The surface and total amounts of fVII were determined using a modified procedure for fVII-ELISA. The ratio of surface fVII antigen was then calculated as a percentage of the total cellular fVII antigen (The results show the average of five separate experiments and expressed as the mean \pm SEM; * = $p < 0.05$ compared to the observed ratio at time zero).

Figure 3. 23 Examination of the alteration in endothelial cell-surface fVII antigen levels in response to PAR2-AP



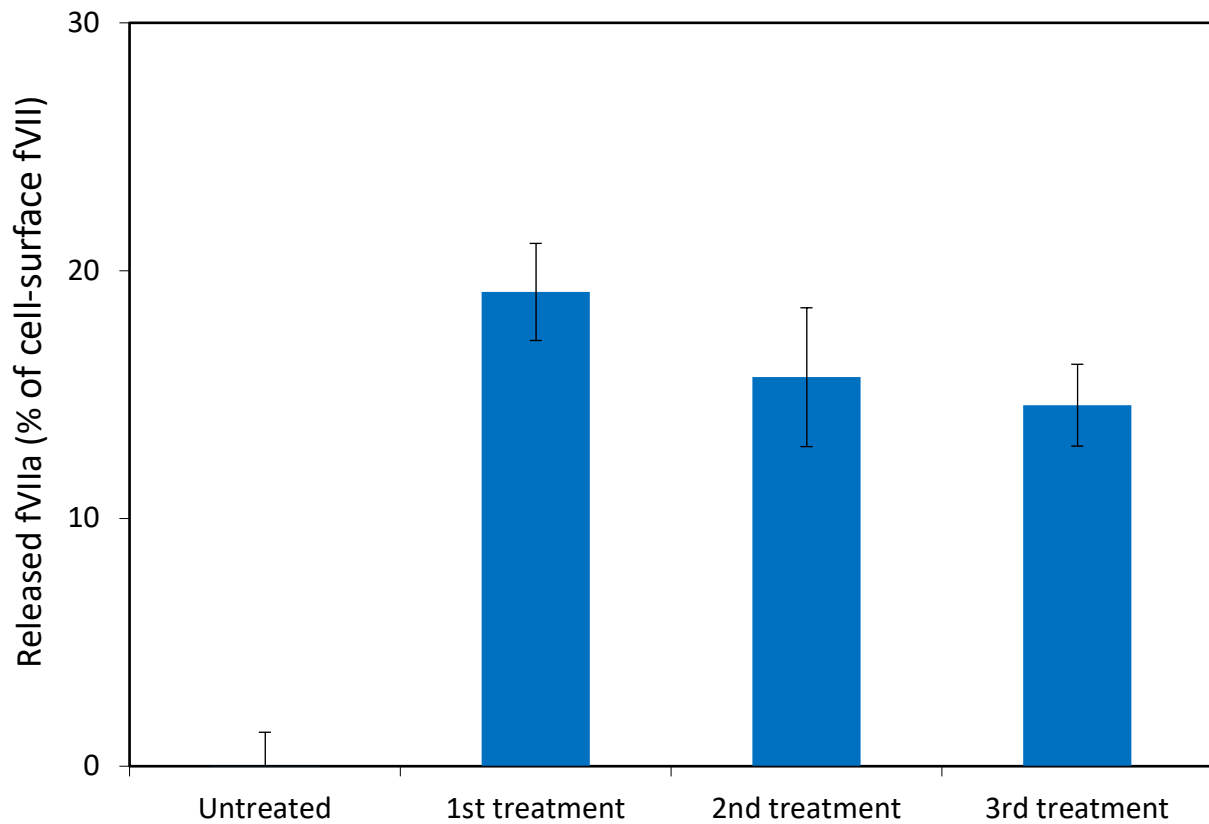
HCAEC (2×10^4) were seeded into 96-well plates and allowed to adhere. The cells were then treated with PAR2-AP (20 μ M) and incubated for up to 240 min. After the incubation, the cells were washed with PBS and fixed with 4% (v/v) formaldehyde. One set was permeabilised with 0.01 % (v/v) Triton diluted in dH₂O. The surface and total amounts of fVII were determined using a modified procedure for fVII-ELISA. The ratio of surface fVII antigen was then calculated as a percentage of the total cellular fVII antigen (The results show the average of five separate experiments and expressed as the mean \pm SEM; * = $p < 0.05$ compared to the observed ratio at time zero).

Figure 3. 24 Examination of the alteration in endothelial cell-surface fVII antigen in response to repeated treatment with recombinant TF



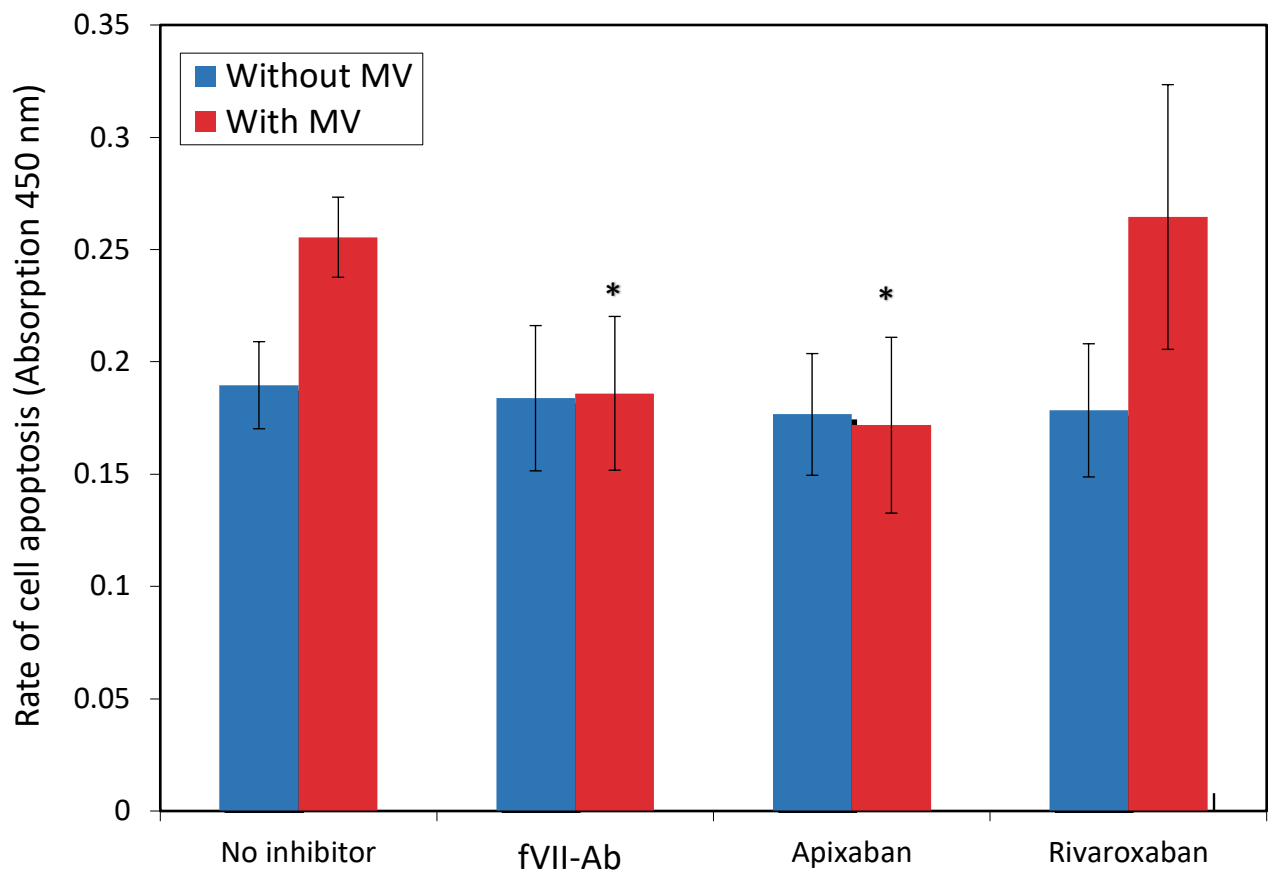
HCAEC (2×10^4) were seeded into 96-well plates and allowed to adhere. The cells were subjected to repeated treatment with recombinant TF (2 U/ml) at 60 min intervals. After each treatment, the cells were then washed and fixed with 4% (v/v) formaldehyde. The surface expression of fVII in each sample was measured by incubating the cells with a mouse anti-fVIIa antibody (20 μ g/ml). The samples were then probed with an HRP-conjugated goat anti-mouse antibody diluted 1:1000 (v/v) and developed using the TMB substrate. The ratio of remaining cell-surface fVII antigens of treated cells compared to cell-surface fVII antigens of resting cells was then calculated as a percentage (The results show the average of five separate experiments and expressed as the mean \pm SEM).

Figure 3. 25 Quantification of the release of MV-associated fVII antigen following multiple treatments with TF



HCAEC (2×10^4) were seeded into 96-well plates and allowed to adhere. The cells were subjected to repeated treatment with recombinant TF (2 U/ml) at 60 min intervals. The media was collected and the MV-associated fVII antigen was quantified using fVII-ELISA. The results were compared to the amounts of cell-surface fVII antigen in the untreated cells to provide the ratio as a percentage (The results show the average of five separate experiments and expressed as the mean \pm SEM).

Figure 3. 26 Examination of the ability of DOAC on blocking the pro-apoptotic effect of MV on endothelial cells



HCAEC (2×10^4) were seeded into 96-well plates and allowed to adhere. The optimal concentration of MV (0.05 nM) isolated from 786-O cells were pre-incubated with rivaroxaban (1.8 μ M), apixaban (1.8 μ M) or an inhibitory polyclonal anti-fVIIa antibody (10 μ g/ml) prior to addition to the cells and incubated for 24 h. The rate of apoptosis was then evaluated using the TiterTACS chromogenic TUNEL assay (The results show the average of five separate experiments and expressed as the mean \pm SEM; * = $p < 0.05$ compared to the untreated sample).

3.3.14 Examination of the ability of DOAC to block the proteolytic activity of fVIIa

To further examine the potential of apixaban to inhibit the proteolytic activity of fVIIa, the proteolytic activity of fVIIa was measured directly in the presence and absence of DOAC, using two chromogenic substrates. First, the activity of fVIIa (5 nM) and fXa (10 nM) were measured using the Pefachrom substrate (1.6 mM) or a synthetic chromogenic substrate (NH₂-Asn-Leu-Thr-Arg-pNA; 1.6 mM). Incubation of the Pefachrom substrate with fVIIa or fXa resulted in colour production, while the synthetic chromogenic substrate (NH₂-Asn-Leu-Thr-Arg-pNA; 0.4 mM) was only digested by purified fVIIa but not purified fXa (Figure 3.27).

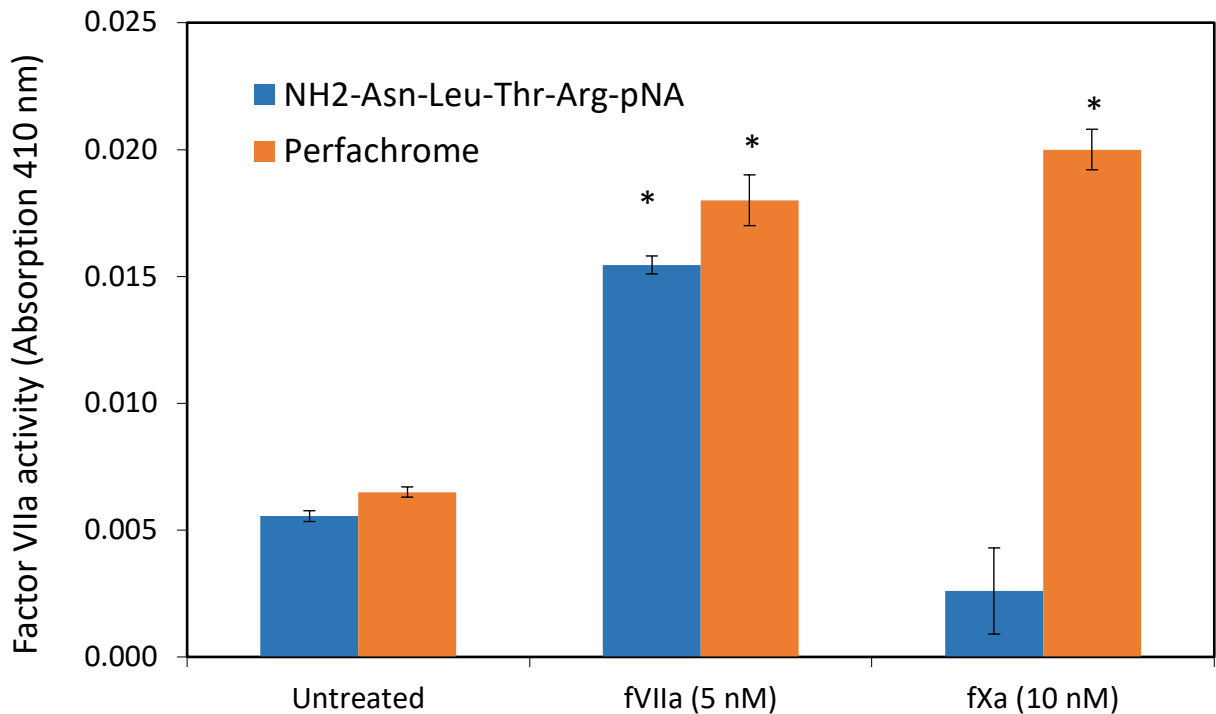
In addition, the proteolytic activity of fVIIa (5 nM) was measured using the Pefachrom substrate (1.6 mM) in the presence of rivaroxaban (1.8 μM), apixaban (1.8 μM) or a polyclonal anti-fVII antibody (10 μg/ml) and compared to an untreated sample as described in section 3.2.4. Interestingly, apixaban (1.8 μM) was capable of inhibiting fVIIa activity but not rivaroxaban (1.8 μM) and the level of inhibition was comparable to that attained by a polyclonal anti-fVII antibody (Figure 3.28).

3.3.15 Examination of the ability of apixaban to block fVIIa and MV-associated fVIIa activity in the presence of recombinant TF

In the previous experiments, apixaban was shown to suppress the pro-apoptotic influence of MV-associated TF-fVIIa complex by inhibiting the proteolytic activity of fVIIa. Therefore, the next set of experiments were carried out to examine the ability of apixaban to block proteolytic activity of fVIIa without interference from TF cofactor activity. The proteolytic activity of purified fVIIa (5 nM) was examined using Pefachrom substrate (1.6 mM) in the presence of TF (1 U/ml) and apixaban (1.8 μM). Analysis of the samples showed that the presence of TF did not alter the ability of apixaban to inhibit the proteolytic activity of fVIIa (Figure 3.29).

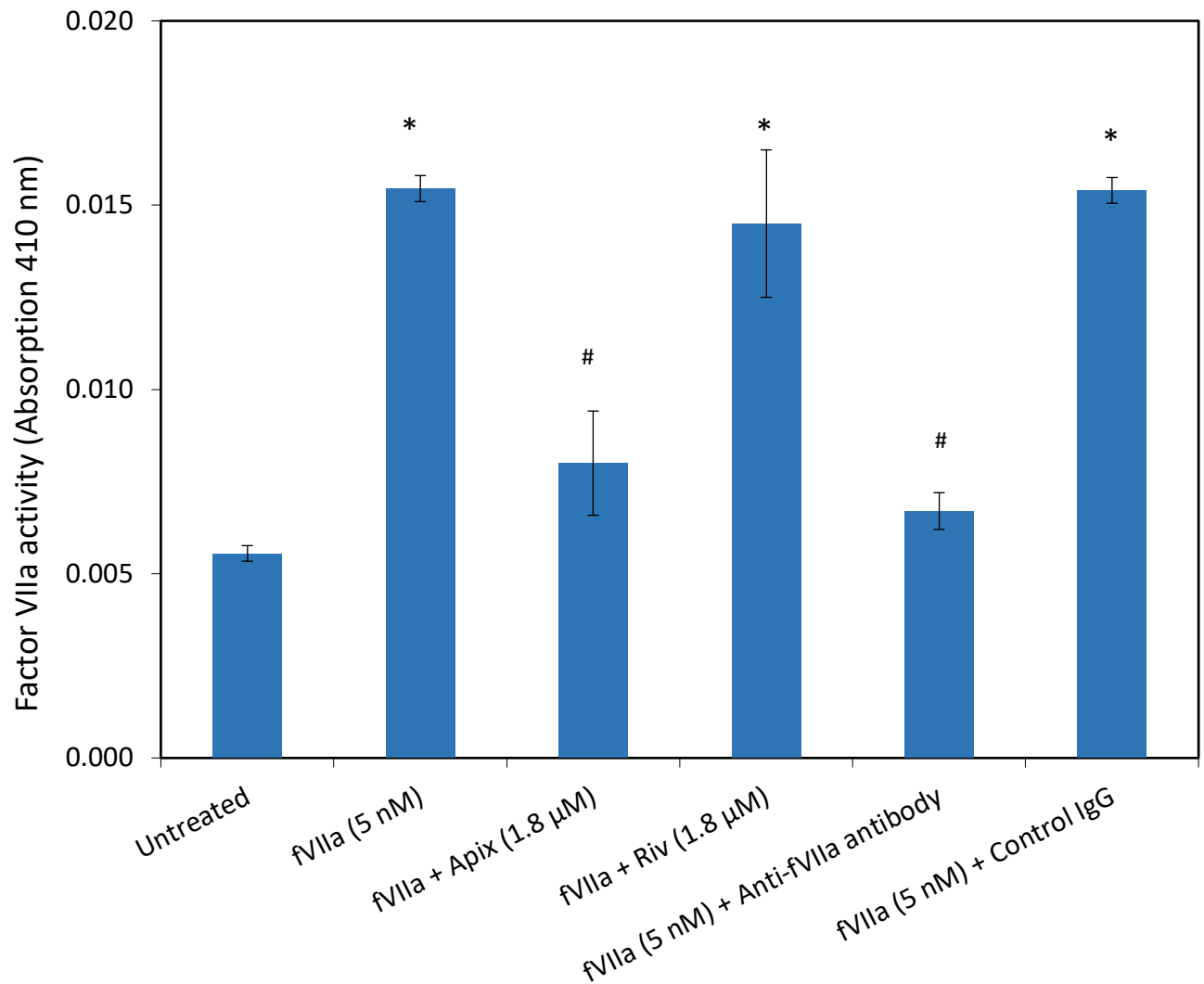
Finally, the proteolytic activity of MV-associated fVIIa derived from MDA-MB-231 cells (0.05 nM) was also measured in conjunction with apixaban (1.8 μ M), rivaroxaban (1.8 μ M) or dimethyl sulfoxide (DMSO) vehicle, using the synthetic fVIIa-chromogenic substrate (1.6 mM), as described in section 3.2.5. Incubation of MDA-MB-231 cell-derived MV with apixaban but not rivaroxaban eliminated the proteolytic activity of fVIIa in these MV compared to untreated samples (Figure 3.30).

Figure 3. 27 Measurement of the proteolytic activity of exogenous fXa and fVIIa using two chromogenic substrates



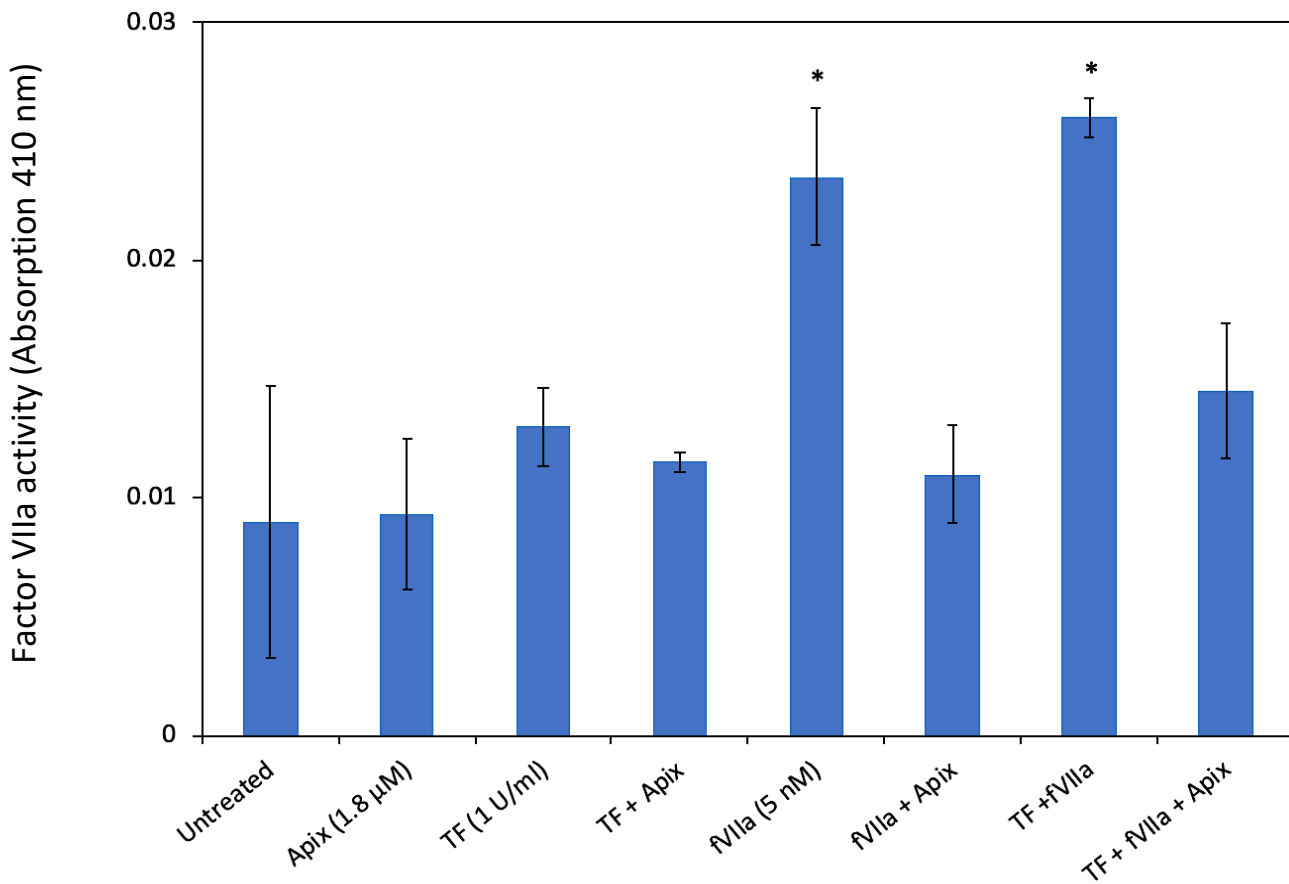
Perfachrome (1.6 mM) or a synthetic fVIIa-chromogenic substrate (NH₂-Asn-Leu-Thr-Arg-pNA; 1.6 mM) were separately incubated for 1 hour at 37°C, with either purified fVIIa (5 nM) or purified fXa (10 nM). The absorptions were then measured at 410 nm using a plate reader (The results show the average of four separate experiments and expressed as the mean ± SEM; * = p < 0.05 compared to the untreated sample).

Figure 3. 28 Examination of the influence of DOAC on the proteolytic activity of fVIIa



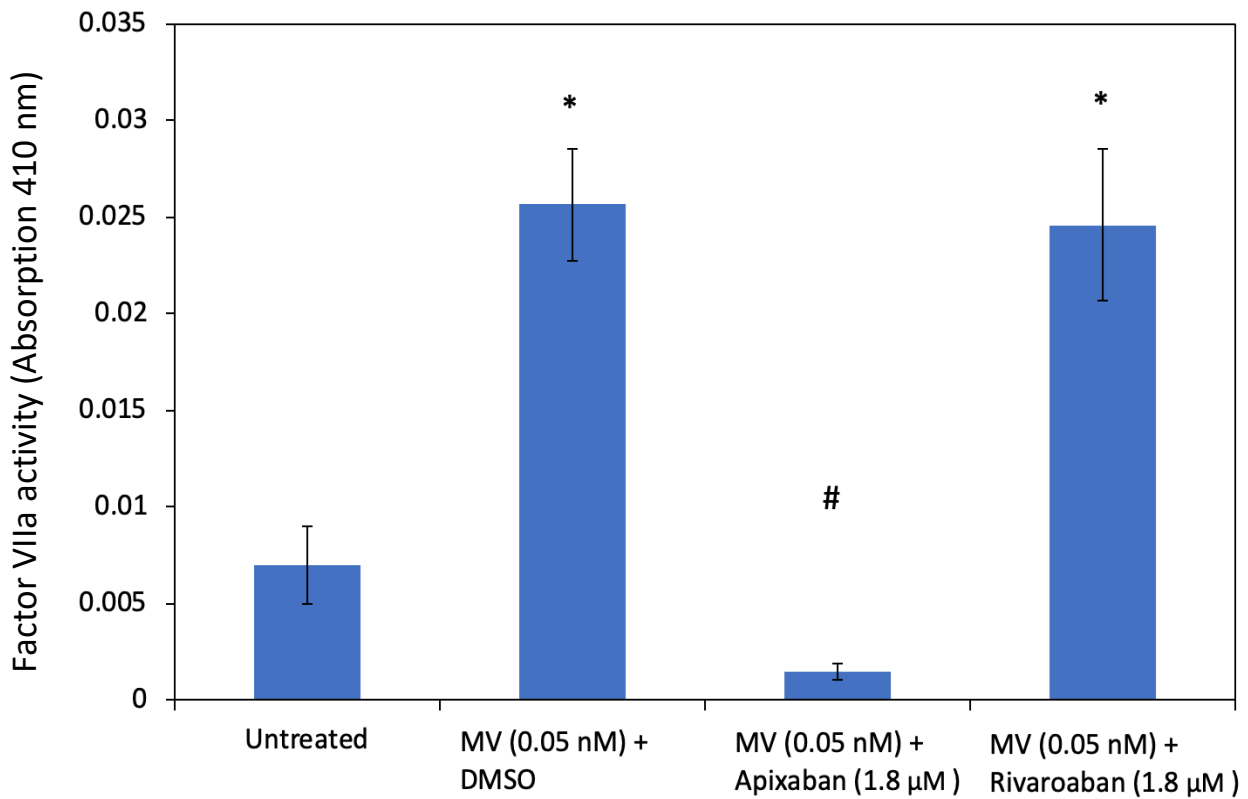
Samples of purified fVIIa (5 nM) were incubated with apixaban (1.8 μM), rivaroxaban (1.8 μM), an inhibitory polyclonal anti-fVIIa antibody (10 μg/ml) or a control isotype IgG (10 μg/ml). The synthetic fVIIa-chromogenic substrate (NH₂-Asn-Leu-Thr-Arg-pNA; 1.6 mM) was then added to the samples and incubated for 1 hour at 37°C. The absorptions were then measured at 410 nm using a plate reader (The results show the average of four separate experiments and expressed as the mean ± SEM; * = p < 0.05 compared to the untreated sample; # = p < 0.05 compared to fVIIa without DOAC).

Figure 3. 29 Examination of the influence of apixaban on the proteolytic activity of fVIIa in combination with recombinant TF



Samples of purified fVIIa (5 nM) or recombinant TF (1 U/ml) were incubated with the Perfachrome substrate for 1 hour at 37°C in the presence and absence of apixaban (1.8 μM). Set of samples of purified fVIIa (5 nM) in conjunction with recombinant TF (1 U/ml) and apixaban (1.8 μM) were also examined. The absorptions were measured at 410 nm using a plate reader (The results show the average of five separate experiments and expressed as the mean ± SEM; *= p < 0.05 compared to the untreated sample).

Figure 3. 30 Examination of the effectiveness of DOAC in blocking the proteolytic activity of fVIIa within MV



Samples of MDA-MB-231 cell-derived MV (0.05 nM) were pre-incubated with apixaban (1.8 μM), rivaroxaban (1.8 μM) or dimethyl sulfoxide (DMSO) vehicle. The samples were then incubated with the synthetic chromogenic substrate (NH₂-Asn-Leu-Thr-Arg-pNA; 1.6 mM) for 1 h at 37°C. The absorptions were then measured at 410 nm using a plate reader (The results show the average of four separate experiments and expressed as the mean ± SEM; * = p < 0.05 compared to the untreated sample; # = p < 0.05 compared to DMSO carrier).

3.4 Discussion

The distinction between the severely injured cells and those which remain intact is imperative in understanding the precise vascular function and homeostasis. The regulatory properties of TF appear to be also present in MV-associated TF that are released from into the bloodstream from various tissue sources. In addition to TF, these MV contain a complement of negatively charged phospholipids (Morel et al., 2006; Freyssinet and Toti, 2010; Gardiner et al., 2015; Date et al., 2013; Hron et al., 2007; Thaler et al., 2014; Auwerda et al., 2011) and functional fVIIa (Figures 3.4 and 3.7). It is known that MV from different sources exert dissimilar influence on endothelial cells which may provide crucial clues for the understanding of the destructive influence of MV in various diseases (Hjortoe et al., 2004; Boulanger et al., 2001; Morel et al., 2004; Morel et al., 2006). Therefore, in this study, it was hypothesised that the ratios of fVIIa:TF within MV may confer different outcomes on cultured primary endothelial cells. In agreement with this hypothesis, incubation of HCAEC with combinations of purified fVIIa and recombinant TF resulted in cellular apoptosis or proliferation depending on the fVIIa:TF ratio. The transition from pro-apoptotic to proliferative property appears to occur at an estimated fVIIa:TF molar ratio of 15:1. This was in agreement with the ratios observed in the MV purified from the cell lines. Particularly, the fVIIa:TF ratio in the 786-O renal carcinoma cell line was 10:1 and these MV induced cellular apoptosis in HCAEC (Figure 3.10). In contrast, this ratio was 17:1 in MV obtained from BxPC-3 pancreatic cell line which were largely ineffective. Moreover, the higher molar ratios of 54:1 and 38:1 observed in HepG2 hepatocellular line, MCF-7 breast cancer line (Figure 3.10) were concurrent with increased cell proliferation.

Interestingly, the change in cell numbers was significantly proportional (Pearson correlation = 0.956) to the observed fVIIa:TF ratio. However, it also appears that as well as the fVIIa:TF ratio, the concentration of TF with which the cell comes into contact with is an additional

critical factor in determining the outcome. Therefore, despite the similar fVIIa:TF molar ratios, TF-rich MV derived from MDA-MB-231 (34:1) were significantly less proliferative than those derived from MCF-7 cell lines (38:1). Therefore, the proliferative/pro-apoptotic property may also be regulated by the higher TF content of MV from MDA-MB-231 cells. However, in these studies, only the amounts of exogenous fVIIa and TF were used in calculating the fVIIa:TF molar ratios to which HCAEC were exposed to. The availability of endogenous cellular fVII will alter the true ratios obtained, thus the level for the transition from pro-apoptotic to proliferative form is likely to be higher than those reported here (15:1). Previous studies have also shown the proliferation response by a number of TF-expressing cells following supplementation with exogenous fVIIa (Åberg et al., 2020; Cirillo et al., 2004)

To elucidate the underlying signalling mechanism, SAM11 antibody was used to block the activation of PAR2 on HCAEC prior to addition of MV from 786-O cells. Inhibition of PAR2 prevented the pro-apoptotic function of these MV indicating the requirement for PAR2 activation. However, simultaneous activation of PAR2 using the activating peptide, at the time of addition of MV also inhibited the pro-apoptotic influence of 786-O cell-derived MV. It was also observed that maximal HCAEC apoptosis was detected at 0.05 nM of 786-O cell-derived MV, and higher concentrations were less effective. These observations were attributed to the endocytosis of PAR2 following rapid activation with fVIIa:TF or with PAR2-AP, leading to de-sensitisation of HCAEC to further stimuli. Therefore, the induction of apoptosis in endothelial cells appears to require the controlled activation of PAR2.

Prototypic activity of fVIIa was shown to be essential for both the proliferative and pro-apoptotic influence of MV and were blocked by preincubation of MV with an inhibitory polyclonal antibody against fVIIa. In addition, the presence of TF was obligatory since addition of purified fVIIa alone to HCAEC was ineffective in promoting either proliferation or

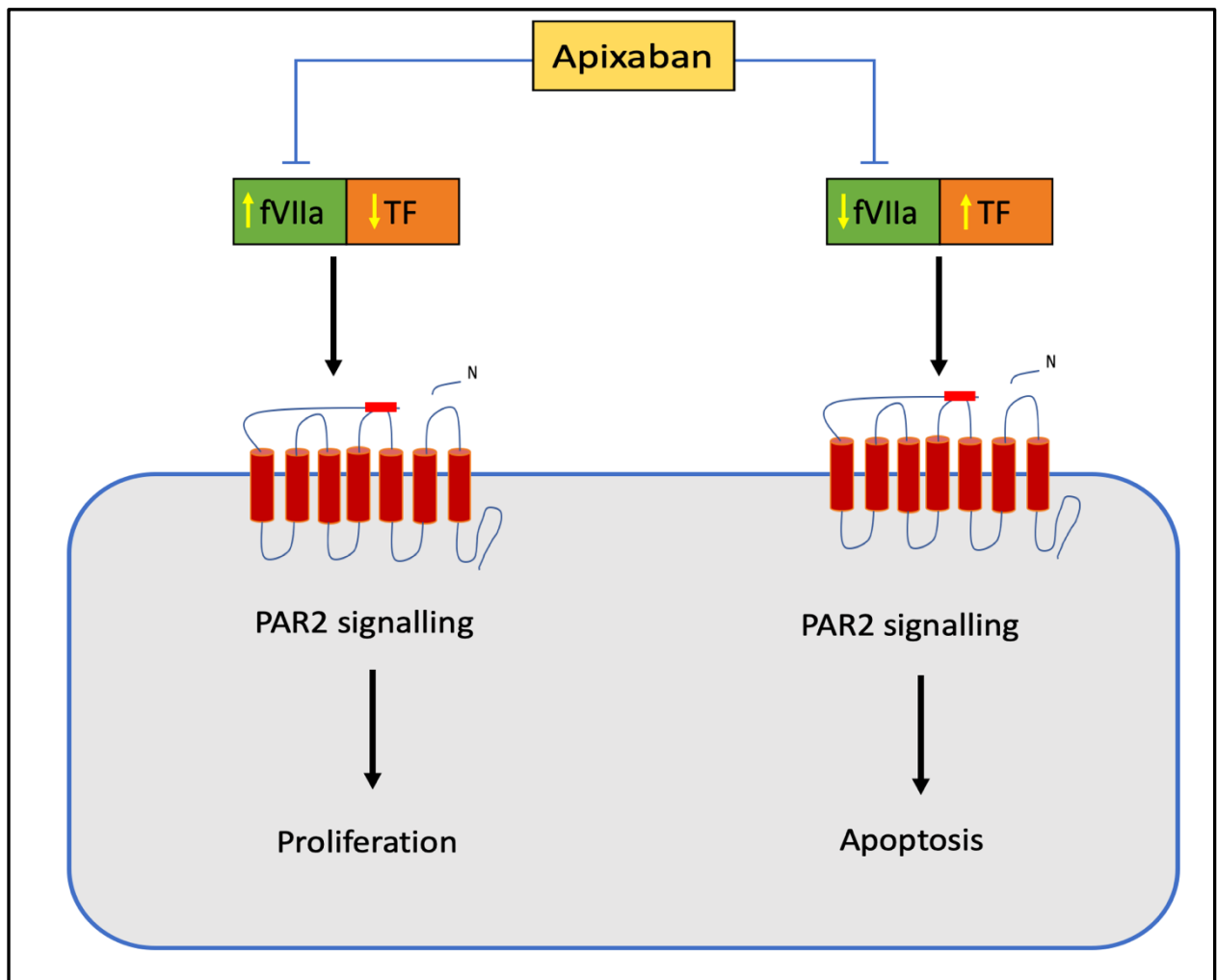
apoptosis. Moreover, pre-incubation of MV with the inhibitory antibody against TF (HTF1) but not an antibody that blocks TF signalling (10H10) prevented the pro-apoptotic influence of the 786-O cell-derived MV. This result indicates that TF induces cellular apoptosis through pro-coagulant signalling which requires the binding of fVIIa with TF. However, incubation of HCAEC with higher concentrations of TF alone (2-10 U/ml) also promoted cell apoptosis (Figure 3.12). Therefore, since fVII is needed to induce apoptosis, this fVII ought to be derived from another source. These results are in agreement with previous studies which showed that incubation of endothelial cells with high levels of recombinant TF or MV-associated TF led to cellular apoptosis (Pradier and Ettelaie, 2007; Frentzou et al., 2010; ElKeeb et al., 2015). In order to determine if endothelial cells can be a source for fVII, the amount of fVII on the surface of the cells was measured. Measurement of the fVII protein in intact and lysed endothelial cells indicated that approximately 20% of the fVII antigen were present on the surface of the resting cells (Figure 3.22). Furthermore, incubation of HCAEC with recombinant TF or activation of PAR2 increased the amount of the cell-surface fVII antigen (Figure 3.22 and 3.23). Therefore, it is possible that endothelial cells respond to the stimulatory signals arising from injury/trauma by altering the fVIIa:TF ratio to counter the proapoptotic influence that arises from the presence of excessive levels of TF. However again, since in these studies only the amounts of exogenous fVIIa and TF were used in calculating the fVIIa:TF molar ratios, the ratios for the transition from the pro-apoptotic to proliferative are likely to be higher than those determined here. In addition, repeated exposure of HCAEC to recombinant TF resulted in the depletion of cellular fVII reserves (Figures 3.24 and 3.25). Therefore, it was hypothesised that repeated exposure of cells to TF-positive MV, for example during chronic disease, may exhaust the ability of endothelial cells to counter the excess amount of TF. Such a compromise in endothelial cell function implies that the response by these cells may become insufficient in ensuring the survival of the cell.

As mentioned previously, cancer cell-derived MV can induce apoptosis in endothelial cells (Figure 3.10). Featherby et al. (2019) demonstrated that the incubation of MDA-MB-231 and AsPC1 cells with direct oral anticoagulants (DOAC) inhibited the release of MV as well as reducing the rate of cell proliferation. Rivaroxaban and apixaban were used in this study to examine the potential of DOAC in blocking the pro-apoptotic influence of cancer cell-derived MV on endothelial cells. Incubation of MV derived from 786-O cells with apixaban prior to addition to HCAEC suppressed the pro-apoptotic effect of these MV. This arose from the ability of apixaban to inhibit fVIIa activity and was comparable to that attained by an inhibitory polyclonal anti-fVII antibody (Figure 3.28). Collectively, this data has demonstrated the previously unknown ability of apixaban to block the proteolytic activity of fVIIa, in addition to that of fXa.

In conclusion, this study has for the first time shown that the ratio of fVIIa:TF determines the outcome in endothelial cells resulting in either proliferation or apoptosis. The induction of cell proliferation and apoptosis by MV appears to be mediated through the activation of PAR2 (Figure 3.31), but the cellular outcome is entirely dependent on the amounts of TF protein and the molar ratio of fVIIa:TF protease activity. Furthermore, the pro-coagulant activity of TF is a pre-requisite for both the proliferative and pro-apoptotic activities, and requires the interaction with fVII. This fVII may be present on surface of MV or be derived from endothelial cells. Finally, apixaban shows a potential in blocking fVIIa proteolytic activity and consequently deactivates TF-fVIIa complex signals.

The involvement of PAR2 in cell apoptosis and proliferation has been established in this section of the study. The activation of PAR2 on the surface of cancer cells releasing MV and the cells coming into contact with these MV is explored in the next chapter.

Figure 3. 31 Schematic representation of the outcomes of the ratio of fVIIa:TF on endothelial cells



The ratio of fVIIa:TF can determine the outcomes in endothelial cells. A high ratio of fVIIa:TF has the potential to activate PAR2 and induce proliferative signals. In contrast, low ratio of fVIIa:TF appears to induce an alternative signal, but also initiated via PAR2 activation, that promote cell apoptosis. In addition, apixaban has been shown to be capable of blocking fVIIa activity and consequently abolishes both the proliferative and apoptotic signals.

Chapter 4

Investigation of PAR2 activation in response to TF:fVIIa complex using a novel hybrid protein

4.1 Introduction

Protease-activated receptor 2 (PAR2), also known as thrombin receptor-like 1 (F2RL1) protein, is a seven-transmembrane receptor which is a member of the G-protein-coupled receptor (GPCR) family. The cleavage of the PAR2 protein at a specific site results in the unmasking of an N-terminal peptide which acts as a tethered ligand. Subsequently, the tethered ligand domain binds to the second extracellular loop of the receptor which causes a change in the receptor formation and initiates an internal signal (Coughlin, 1999; Zhao et al., 2014). It is known that PAR2 can be activated by proteases such as TF-fVIIa complex, factor Xa (fXa) and trypsin (Vergnolle et al., 1999; Rothmeier & Ruf, 2011; Zhao et al., 2014; Benelhaj et al., 2019). PAR2 can signal through two mechanisms involving G-protein signalling and through β -arrestin signalling. In the G-protein-mediated pathway, PAR2 activation can induce Ras, protein kinase C (PKC) and inositol trisphosphate (IP3)-mediated pathways. In contrast, the association of PAR2 with β -arrestin activates Raf and ERK1/2 cascades (Rothmeier and Ruf, 2011).

PAR2 plays a key role in many physiological events (Figure 4.1) (Feistritzer et al., 2005; Benelhaj et al., 2019; Darmoul et al., 2004) and over-expression of PAR2 can lead to a number of pathological conditions (Cicala, 2002; Antoniak et al., 2013). It has been reported that activation of PAR2 receptor in human breast and pancreatic cancer cells by using PAR2-AP, trypsin or fVIIa increased the expression of vascular endothelial growth factor (VEGF). This in turn resulted in increased rate of angiogenesis in the surrounding vascular cells which was mediated through the MAPK pathway (ERK1/2 and p38) (Liu and Mueller, 2006; Ikeda et al., 2003; Shibuya., 2011). PAR2 activation also has been found to induce cellular proliferation of cancer cells. A study has shown that the activation of PAR2 in colon cancer, using either trypsin or PAR2-AP, led to the phosphorylation of ERK1/2 by the epidermal growth factor receptor (EGFR) and prompted cell proliferation (Darmoul et al., 2004).

It has also been suggested that PAR2 is involved in a number of inflammatory responses. Studies have reported that the activation of PAR2 in human dermal microvascular endothelial cells (HDMEC), increased the expression of IL-6 and IL-8 through a mechanism involving nuclear factor kappa B (NF- κ B) pathway (Shpacovitch et al., 2002; Heuberger and Schuepbach, 2019). A different study showed that the injection of a monoclonal antibody (SAM11) to block the PAR2 in mice with collagen-induced arthritis, resulted in a significant reduction in cartilage damage and inflammatory cell infiltration compared to control animals (Crilly et al., 2012). Therefore, together these studies suggest that PAR2 signalling has a key role in initiating inflammatory responses.

As mentioned in chapter 1, a number of studies have reported the elevated expression of TF in patients with diabetes, infection or atherosclerosis (Williams & Mackman, 2012; Eisenreich et al., 2016; Witkowski et al., 2016). Similarly, the high expression of TF has been measured in a number of types of cancers, including breast, liver, prostate and brain (Chu, 2011). Raised levels of TF are also expressed on monocytes during inflammatory diseases such as sepsis (Bode & Mackman, 2014). In addition to the increased levels of TF in chronic diseases, the expression of fVII is also known to be elevated during pathological conditions including liver cirrhosis (Hollestelle et al., 2004) and heart disease (Suzuki et al., 1991). Moreover, although the liver cells are the main site of synthesis of the coagulation protein factor VII (fVII), cancer cells appear to express “ectopic fVII” protein. For example, expression of significant amounts of fVII has been demonstrated in ovarian cell lines (Yokota et al., 2009). Similarly, a study conducted by Koizume et al. (2006) reported that lung, ovarian, thyroid, prostate and stomach cell lines can all express significant amounts of ectopic fVII protein.

MV are known to be released following cellular activation, or apoptosis (Morel et al., 2011). One of the mechanisms that leads to increases in MV release is the activation of PAR2 on the cell surface (Ettelaie et al., 2012; Das et al. 2018). A recent study comparing the levels of

released MV by cancer cell lines showed that the activation of PAR2 using PAR2-AP (20 μ M) resulted in dissimilar increases in the release of TF-associated MV from these cell lines (Ettelaie et al., 2016). Furthermore, the study conducted by Das et al. (2018) using the MDA-MB-231 cell line, reported that PAR2 signalling enhanced MV release through Rab5a activation via the phosphorylation of Ser 473 within Akt (also known as Protein kinase B). In addition, as stated above, the level of PAR2 expression has been shown to become elevated in many malignant tumours including lung, breast and liver (Jiang et al., 2018; Chen et al., 2019; Sébert et al., 2019). Therefore collectively, these data suggest that PAR2 activation could be a major initiator of MV release from cells, in response to injury and trauma.

In the previous chapter, it was demonstrated that MCF-7, MDA-MB-231, 786-O, HepG2 and BxPC3 cell lines express various amounts of TF and also active fVIIa. The presence of endogenous or exogenous TF and fVIIa on the surface of cancer cells may be sufficient to enhance PAR2 activation by the TF-fVIIa complex. This in turn may lead to the auto-activation of the cells and MV release (Ungefroren et al., 2017). The MV released from the cells are known to carry cellular contents which are derived from the original cells. These include proteins and lipids (Hugel et al., 2005; Mizrak et al., 2013; Gaetani et al., 2018). Furthermore, MV have been shown to transfer genetic materials and various active proteins between cells (Jaiswal et al., 2013; Gaetani et al., 2018; Hugel et al., 2005). For instance, monocytes are activated by stimuli such as cell damage, shear stress or pro-apoptotic stimuli, releasing high levels of circulating TF-bearing MV (Burnouf et al., 2015; Grover and Mackman, 2018). The MV-associated TF released by the monocytes may be taken up by endothelial cells, platelets and neutrophils (del Conde et al., 2005; Osterud & Bjorklid, 2012). MV have also been shown to actively participate in inflammatory responses (Cognasse et al., 2015) as well as being a main contributor to thrombosis (Burnouf et al., 2015). High level of circulating MV have been reported in patients with diabetes, hypertension, cancers, sepsis and cardiovascular disease

(Enjeti et al., 2008; Vanwijk et al., 2003; Badimon et al., 2017; Ender et al., 2019). Furthermore, it has been suggested that MV may also induce endothelial cell deterioration through the induction of cellular apoptosis (Hugel et al., 2005; Nomura et al., 2008). In fact, increases in the levels of MV release have been associated with endothelial dysfunction by disrupting the synthesis of nitric oxide (Boulanger et al., 2001; Badimon et al., 2017) and this has been suggested to be involved in the development of atherosclerosis (Davignon and Ganz, 2004).

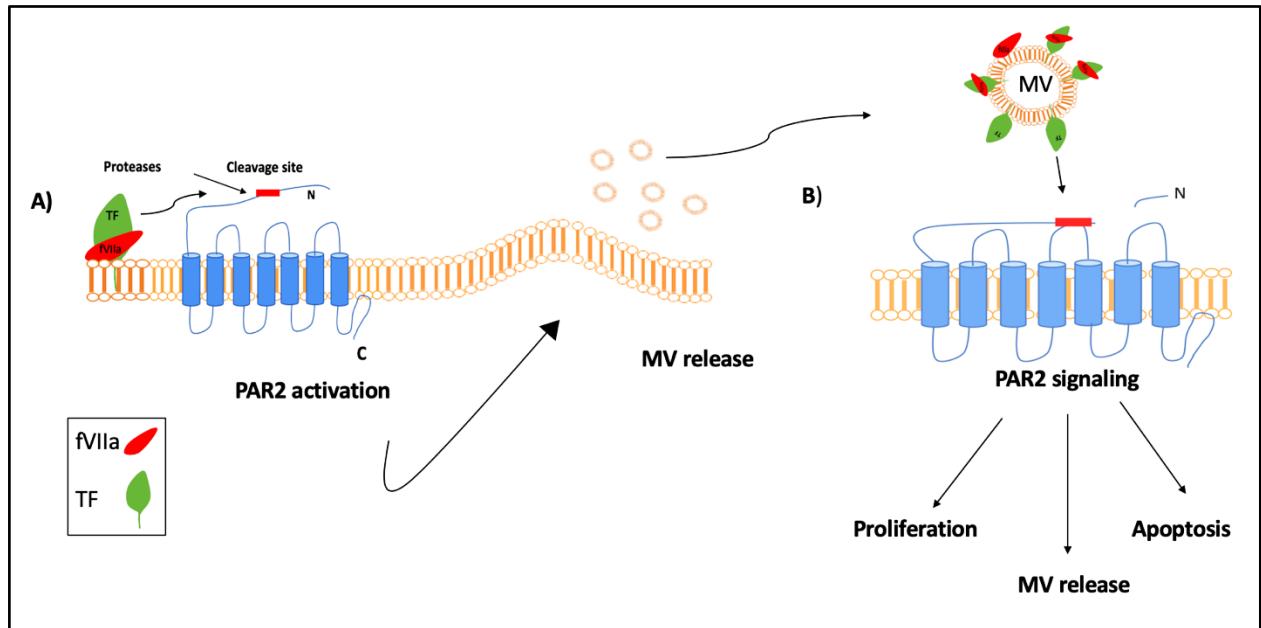
Previously, Frentzou et al. (2010) suggested that TF can promote cellular apoptosis through the extrinsic pathway of apoptosis, in a death receptor-like manner. Incubation of rat cardiomyocyte line H9c2 with high concentrations of recombinant TF was shown to induce apoptosis through increasing the activity of caspase-3 (Frentzou et al., 2010). In addition, treatment of endothelial cells with TF-positive MV has been shown to induce p38 MAPK signalling resulting in increased levels of p53 activity. This in turn led to the upregulation of Bax expression and cellular apoptosis (ElKeeb et al., 2014). Similarly, the accumulation of TF within endothelial cells has been shown to cause endothelial cell apoptosis via the activation of Src1 and involving β 1-integrin (Ethaeab et al., 2019). In support of these findings, a study by Aharon et al. (2008) showed that the accumulation of TF-associated MV derived from monocyte cells induced cellular apoptosis and increased thermogenicity in human umbilical vein endothelial cells (HUVEC). In chapter 3, it was demonstrated that MV-associated TF isolated from HepG2 and 786-O cells are capable of inducing cellular proliferation and apoptosis in endothelial cells, respectively. Both of these outcomes were shown to be mediated through PAR2 activation. Interestingly, the ratio of fVIIa:TF appeared to be a determining factor in the outcomes of incubation of these MV with endothelial cells. This finding suggests that PAR2 signalling may be moderated differentially, depending on the ratio of fVIIa:TF with which the cells come into contact with. In this chapter, it was envisaged that the amount of TF,

fVIIa and also the ratio of fVIIa:TF are capable of differentially activating any PAR2 present on the surface of cells. In addition, the study aimed to determine if the released MV, containing different amounts of TF and fVIIa, are capable of activating PAR2 on recipient endothelial cells to different magnitudes.

4.1.1 Aims

In this study, the auto-activation of PAR2 and its association with the release of MV from cancer cell lines was examined. The PAR2 cDNA was cloned into an expression plasmid at the C-terminus of a fluorescent tag; so that the activation of PAR2 resulted in the release of the fluorescent tag. Five cell lines (HepG2, 786-O, MCF-7, BxPC-3 and MDA-MB-231) were transfected with the construct and the activation of PAR2 examined by measuring the fluorescence intensity released into the media. In addition, HDBEC transfected with the PAR2 fluorescent reporter plasmid were incubated with MV from the cell lines, or with combinations of exogenous TF and fVIIa and the outcomes on PAR2 activation on endothelial cells were investigated. The data were used to determine the requirements of TF and fVIIa for PAR2 activation, to attempt to explain the reason for the differential outcomes on cellular function.

Figure 4. 1 The proposed study for by which PAR2 signalling induces MV release and the activation of recipient cells.



The digestion of PAR2 by endogenous or exogenous proteases such as TF-fVIIa complex results in the unmasking of the tethered ligand domain. The exposed tethered ligand binds to the second extracellular loops of the cleaved PAR2 and activates the receptor. The activation of PAR2 (A) induces MV release which contain TF and fVIIa. The released MV activate PAR2 on nearby or remote cells (B) and consequently induce signalling.

4.2 Methods

4.2.1 Measurement of PAR2 activation on the cell surfaces

This study aimed to measure the activation of PAR2 on the surface of cells that also express coagulation proteases. Also, to examine the influence of exogenous TF-fVIIa complex on the PAR2 activation in endothelial cells. In order to produce a measurable means of PAR2 activation, the PAR2 cDNA was sub-cloned into plasmids at the C-terminus of a mEmerald or mCherry fluorescent tag encoded by the plasmid. However, since it was not clear if the leader peptide of PAR2 is essential for its processing to the cell surface, the cDNA for complete protein and the mature PAR2 were cloned and tested to determine the most suitable model. Therefore, the mEmerald-C1 and mCherry2-C1 plasmids were used as vectors to deliver and distinguish between the two forms of PAR2: the mEmerald-C1 plasmid contained the full-length PAR2-green fluorescent tag and the mCherry2-C1 plasmid contained the shortened PAR2-red tag. Digestion of PAR2 by proteases results in the release of the fluorescent tag in the media (Figure 4.2). Subsequently, the concentration of the released tag is measured by determining the fluorescence intensity.

To measure PAR2 activation on the surface of cancer cells by endogenous proteases (auto-activation), the cells were transfected with constructs and PAR2 activation was determined by measuring the fluorescence intensity released into the media. In addition, the influence of exogenous TF-fVIIa complex as well as that present on MV derived from cancer cell lines on PAR2 activation were tested in HDBEC transfected with the construct plasmids.

4.2.2 Preparation of LB agar plates, LB broth and freeze medium

To prepare LB agar plates containing antibiotics for bacterial selection, LB agar powder (7 g) was dispersed in distilled water (200 ml) and the solution was autoclaved and allowed to cool down to approximately 50°C. Kanamycin (25 µg/ml) or penicillin (25 µg/ml) antibiotic was

then added to the solution and thoroughly mixed. The agar medium (25 ml) was then poured into sterile Petri dishes (75 mm) and allowed to solidify at room temperature in a sterile environment. The plates were sealed in sterile plastic bags and stored at 5°C until required. To prepare the LB broth, LB broth powder (12.5 g; 1% (w/v) tryptone, 1% (w/v) NaCl and 0.5% (w/v) yeast extract) was dissolved in distilled water (500 ml) and autoclaved. The broth was stored at room temperature until required. Freezing medium (20% (w/v) glycerol) was prepared by adding glycerol to LB broth. The solution was thoroughly mixed by vortexing, sterilised by filtration through a 0.22 µm filter and stored at -20°C until required.

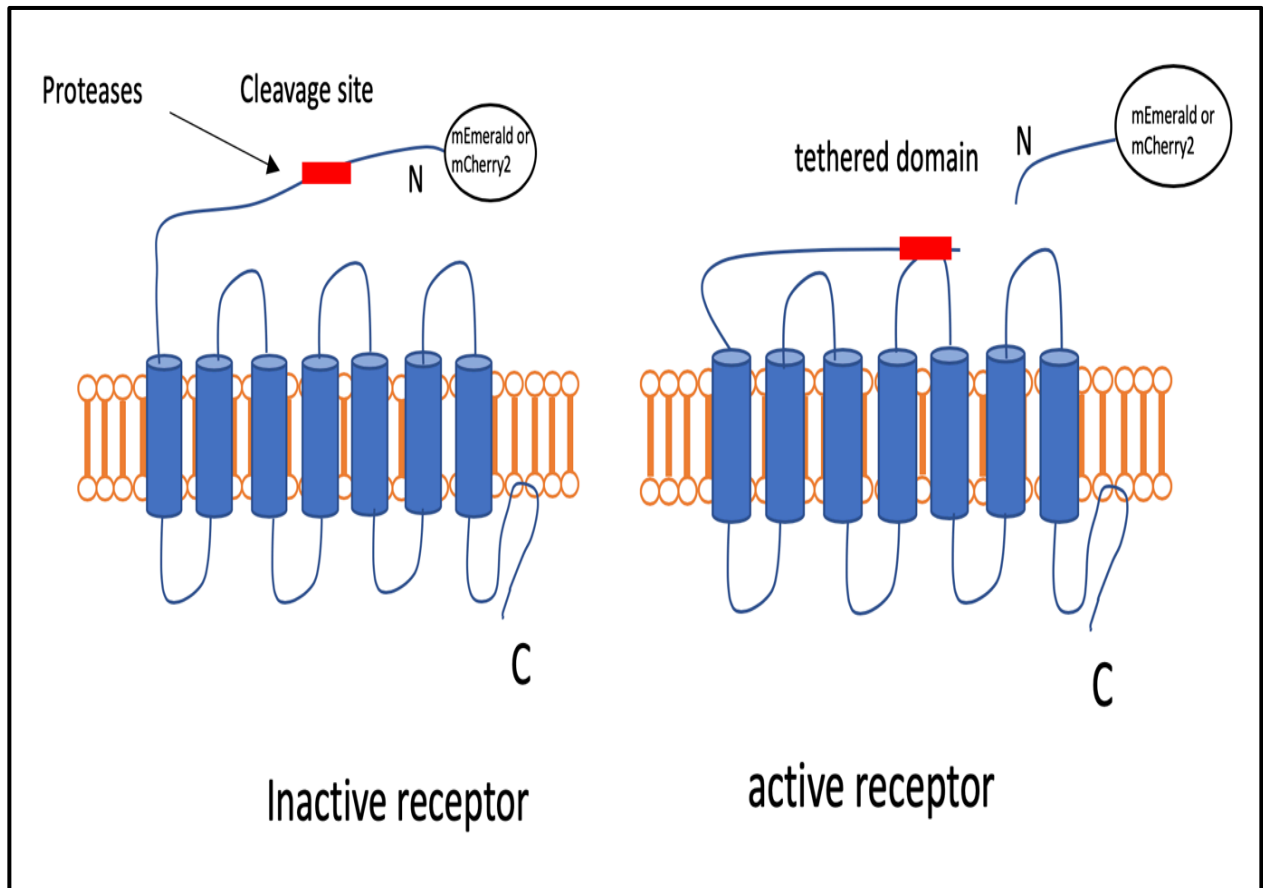
4.2.3 Bacterial transformation

In order to transform the plasmid DNA into *E. coli* TB1 cells, the DNA was added to competent *E. coli*, mixed gently and placed on ice for 30 min. The cells were then heat-shocked for 30 s at 42°C and cooled for 4 min at 4°C. 150 µl of SOC medium (2% (w/v) tryptone, 0.5% (w/v) yeast extract, 8.6 mM NaCl, 2.5 mM KCl, 20 mM MgSO₄, and 20 mM glucose) was then pipetted into each sample and incubated for 1 h at 37°C. Aliquots (50 µl) of bacterial cells were spread onto LB agar plate containing kanamycin (25 µg/ml) or penicillin (25 µg/ml) as appropriate. The plates were then incubated overnight at 37°C. Single colonies were picked from the plate and propagated in LB broth at 37°C overnight with shaking. On the following day, the cells were centrifuged at 200 g for 5 min and the supernatant was discarded. The cell pellet was re-suspended in freezing medium and stored at -20°C until required.

4.2.4 Purification of plasmid DNA using the Wizard® Plus Midipreps kit

TB1 *E. coli* containing with empty mEmerald-C1 or mCherry2-C1 plasmids (Figure 4.3 and 4.4) were plated on LB agar plates containing kanamycin (25 µg/ml) and incubated at 37°C overnight. Single colonies were picked from each plate and cultured in LB broth at 37°C overnight with shaking at 180 rpm. On the following day, the cultures were cooled down and

Figure 4. 2 Schematic of the strategy for measuring PAR2 activation



To determine PAR2 activation, cells are transfected to express mEmerald-C1 full-length PAR2 construct or mCherry2-C1 shortened PAR2 construct. Digestion of PAR2 results in the release of the fluorescent tag in the media which is collected and the fluorescence intensity measured using a plate reader.

transferred to 20 ml tubes. The cells were centrifuged at 2,500 g for 15 min, resuspended in 3 ml Midipreps buffer (50 mM Tris pH 7.5, 10 mM EDTA and 100 µg/ml RNase A) and transferred to a fresh 20 ml tube. The cells were lysed by addition of the lysis buffer provided with the kit (3 ml; 0.2 M NaOH and 1% (w/v) SDS) and gently inverting the tube 5 times. The solution was then neutralised by adding the neutralising buffer provided by the kit (4 ml; 1.32 M potassium acetate pH 4.8) and the tube inverted. The lysate was then centrifuged again at 3,000 g for 15 min. The supernatant was transferred to a fresh 20 ml tube and centrifuged at 3,000 g for 15 min. To isolate the plasmid DNA, the DNA-binding resin provided with the kit (10 ml) was added to midiprep columns and followed by lysate supernatant. The mixture was mixed thoroughly by pipetting and then cleared through the column under vacuum. The column was then washed using 20 ml wash solution (80 mM potassium acetate, 8.3 mM Tris-HCl pH 7.5, 40 µM EDTA and 55% (v/v) ethanol) and cleared under vacuum. The lower end of the midiprep column was broken off and placed in a 1.5 ml microcentrifuge tube. The column was then centrifuged at 12,000 g for 7 min to remove any residual wash buffer. The midiprep column was then placed in a fresh 1.5 ml tube and nuclease-free water (400 µl) was added to the top. The column was incubated at room temperature for 1 min and plasmid DNA eluted by centrifugation at 12000 g for 3 min. The eluted plasmid was stored at -20°C until required.

4.2.5 Isolation of plasmid DNA using the miniprep kit

To isolate the plasmid DNA using the miniprep kit, TB1 *E. coli* containing the plasmid DNA were plated on LB agar plates containing kanamycin (25 µg/ml) or penicillin (25 µg/ml) as appropriate and incubated at 37°C overnight. Single colonies were picked from each plate and cultured in LB medium (10 ml) at 37°C overnight with shaking at 180 rpm. On the following day, the cells were collected from 2 ml of the culture by centrifuging at 12,000 g for 1 min. According to manufacturer's protocol, the supernatant was discarded and the pellet was re-suspended in plasmid resuspension buffer provided with the kit (100 µl) and vortexed. Lysis

buffer (200 µl) was added to the tube and gently inverted 5 times and incubated at room temperature for 1 min. Neutralisation buffer (400 µl) was then added to the tube and gently inverted and incubated at room temperature for 2 min. The tube was then centrifuged at 12,000 g for 5 min. The supernatant was then carefully transferred to a spin column and centrifuged at 12,000 g for 1 min. The column was then washed with provided wash buffer 1 (200 µl) and the tube was centrifuged at 12,000 g for 1 min. The column was then washed with provided wash buffer 2 (400 µl) and centrifuged at 12,000 g for 4 min. Finally, the column was transferred to a fresh 1.5 ml tube and the plasmid DNA eluted with the elution buffer and collected by centrifugation at 12,000 g for 1 min. The sample was stored at -20°C until required.

4.2.6 Ethanol precipitation of plasmid DNA

To remove any traces of endotoxin and salts, the DNA was precipitated with ethanol. The plasmid DNA sample (200 µl) was mixed with absolute ethanol (800 µl) and 5 M sodium acetate pH 5.2 (200 µl) and incubated for 40 min at -20°C. The DNA was then pelleted out by centrifuging at 12,000 g for 15 min at 4°C in a microcentrifuge. The pellet was washed with 75% (v/v) ice-cold ethanol solution (400 µl) and then centrifuged for a further 15 min at 12,000 g at 4°C. The pellet was dried by evaporation in a sterile environment and then resuspended in nuclease-free water (200 µl) and stored at -20°C until required.

4.2.7 Analysis of plasmid DNA by agarose gel electrophoresis

1% (w/v) agarose gel was made by adding agarose powder (0.6 g) to TBE buffer (60 ml; 89 mM Tris-borate, 89 mM boric acid pH 8.3 and 2 mM EDTA). The powder was dissolved by boiling the mixture in a microwave oven. The agarose solution, once cooled to approximately 50°C, was poured into electrophoresis tray with sealed ends. An appropriately sized comb was placed in the tray and the agarose was allowed to solidify. The samples were prepared by mixing individual DNA samples (5 µl) with loading buffer (5 µl) and pre-stained with SYBR®

Figure 4. 3 The DNA map of the mEmerald-C1 mammalian plasmid

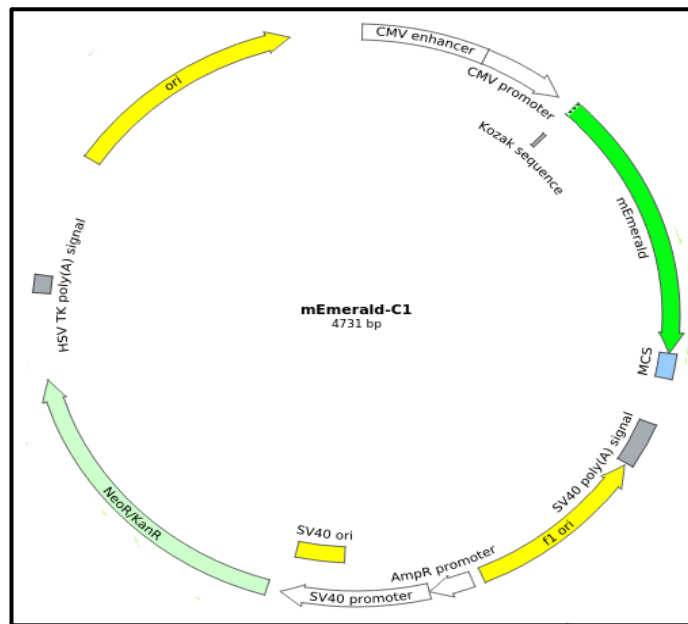
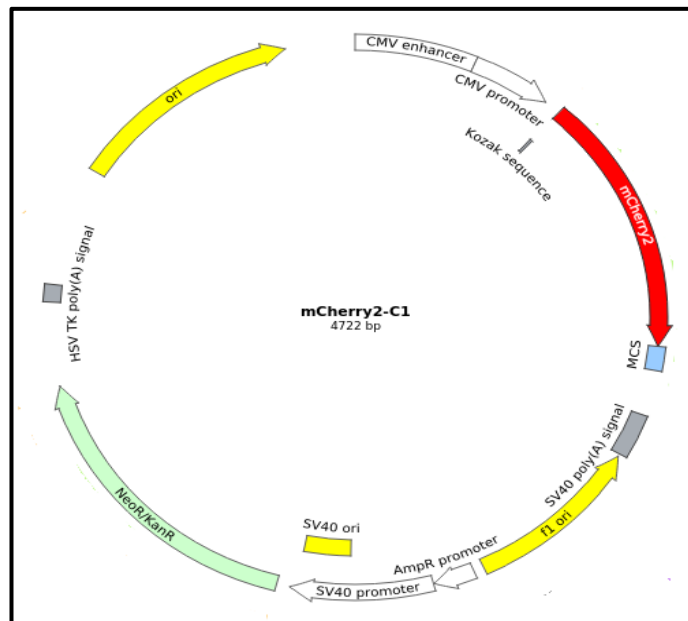


Figure 4. 4 The DNA map of mCherry2-C1 mammalian plasmid



The vectors express mEmerald (green) and mCherry (red) fluorescent tag respectively. The plasmids also contain a suitable multi-cloning site in order to insert the cDNA of interest in tandem with the tag. The size of the mEmerald-C1 plasmid is 4,731 bp while mCherry2-C1 is 4,722 bp. Finally, the vectors contain a constitutively-expressed neomycin/kanamycin resistance gene for selection of the transformed bacterial cells. Images taken from www.addgene.org.

Green I (1 μ l). In addition, a standard was prepared by mixing the DNA molecular weight marker (5 μ l) with loading buffer (5 μ l) and stained with SYBR Green I (1 μ l). The DNA samples and the standard were loaded into the agarose gel wells and electrophoresis carried out at 120 V for 1 h. The bands were then visualized on a UV transilluminator and photographed.

4.2.8 Design of DNA primers for PCR amplification of full- and short-length PAR2 DNA

The forward and reverse primers for full- and short-length PAR2 were designed to amplify the respective PAR2 cDNA fragments based on the target sequences, and were synthesized by Eurofins Genomics (Figure 4.5). To facilitate the ligation of the amplified sequences into the vectors, the primers were designed to contain restriction sites for *HindIII* and *BamHI*. The use of two different restriction sites ensured the correct orientation of the amplified DNA into the plasmids. The forward primer for the full-length PAR2 was designed to include 20 bp of coding sequence. This was preceded by the *HindIII* restriction site and a further 4 nucleotides to ensure optimal digestion by the restriction enzyme. The short-length primer was designed to start at the mature protein and included 23 bp of coding sequence. In addition, 4 bp were added before the restriction sites to ensure optimal digestion. The reverse primer was designed to include the stop codon and 20 bp complementary to the coding sequence. Moreover, 4 bp were also added before the restriction site to ensure efficient digestion (Figure 4.5).

4.2.9 PCR amplification of PAR2 cDNA

E. coli TB1 cells were transformed with (20 ng/ μ l) of VersaClone plasmid containing hPAR2 (Figure 4.6) as described in section 4.2.3 and propagated. The plasmid was then isolated using the miniprep kit (see section 4.2.5) and the PAR2 cDNA amplified using the Platinum™ *Taq* DNA high fidelity polymerase to ensure accuracy of the sequences. The PCR master mix was prepared as shown in Table 4.1 in a PCR tube. The DNA was denatured at

Figure 4. 5 The cDNA sequence of the human PAR2 and the designed cloning primers

```

AGCGCGGCCGCCACCATGCGAAGTCCTAGTGCTGCGTGGC
TGCTGGGGGCGCCATCCTGCTAGCAGCCTCTCTCTCCTGC
AGTGGCACCATCCAAGGAACCAATAGATCCTCTAAAGGA
AGAAGCCTTATTGGTAAGGTTGATGGCACATCCCACGTCA
CTGGAAAAGGAGTTACAGTTGAAACAGTCTTTTCTGTGGA
TGAGTTTTCTGCATCTGTCCTCACTGGAAAACCTGACCACTG
TCTTCCTTCCAATTGTCTACACAATTGTGTTTGTGGTGGGT
TTGCCAAGTAACGGCATGGCCCTGTGGGTCTTTCTTTTCCG
AACTAAGAAGAAGCACCCCTGCTGTGATTTACATGGCCAAT
CTGGCCTTGGCTGACCTCCTCTCTGTCATCTGGTTCCCCTT
GAAGATTGCCTATCACATACATGGCAACAACCTGGATTTAT
GGGGAAGCTCTTTGTAATGTGCTTATTGGCTTTTTCTATGG
CAACATGTACTGTTCCATTCTCTTCATGACCTGCCTCAGTG
TGCAGAGGTATTGGGTCATCGTGAACCCCATGGGGCACTC
CAGGAAGAAGGCAAACATTGCCATTGGCATCTCCCTGGCA
ATATGGCTGCTGATTCTGCTGGTCACCATCCCTTTGTATGT
CGTGAAGCAGACCATCTTCATTCCTGCCCTGAACATCACG
ACCTGTCATGATGTTTTGCCTGAGCAGCTCTTGGTGGGAG
ACATGTTCAATTACTTCCTCTCTCTGGCCATTGGGGTCTTT
CTGTTCCAGCCTTCCTCACAGCCTCTGCCTATGTGCTGAT
GATCAGAATGCTGCGATCTTCTGCCATGGATGAAAACCTCA
GAGAAGAAAAGGAAGAGGGCCATCAAACCTCATTGTCACT
GTCCTGGCCATGTACCTGATCTGCTTCACTCCTAGTAACCT
TCTGCTTGTGGTGCATTATTTTCTGATTAAGAGCCAGGGCC
AGAGCCATGTCTATGCCCTGTACATTGTAGCCCTCTGCCTC
TCTACCCTAACAGCTGCATCGACCCCTTTGTCTATTAATT
TGTTTCACATGATTTTCAGGGATCATGCAAAGAACGCTCTC
CTTTGCCGAAGTGTCCGCACTGTAAAGCAGATGCAAGTAT
CCCTCACCTCAAAGAAACACTCCAGGAAATCCAGCTCTTA
CTCTTCAAGTTCACCACTGTTAAGACCTCCTATTAAAGG
CGCGCCAGTA
    
```

Forward full-length PAR2 primer: 5'-GCTC**AAGCTT****AGTCGAAGTCCTAGTGCTGC**-3'

HindIII

PAR2 cDNA

Forward short-length PAR2 primer: 5'-GCTC**AAGCTT****ATCCAAGGAACCAATAGATCCTC**-3'

HindIII

PAR2 cDNA

Reverse PAR2 primer: 5'-CGGT**GGATCTCA****ATAGGAGGTCTTAACAGTGG**-3'

BamHI Stop
codon

PAR2 cDNA

95°C for 2 min and the amplification was carried out in 35 cycles (1 min at 95°C, 2 min at 62°C, and 1 min at 72°C). A final extension step was included at 72°C for 10 min. The sizes of the PCR products were analysed by 1% (w/v) agarose gel electrophoresis and the gels were viewed under UV light as described in section 4.2.7. The expected PCR products were 1,194 bp for full-length PAR2 and 1,119 bp for short-length PAR2 cDNA.

4.2.10 Restriction digestion of the empty expression plasmids and the amplified PAR2 cDNA

The plasmids (mEmerald-C1 and mCherry2-C1) and the amplified PAR2 cDNA (full- and short- length) incorporate the *HindIII* and *BamHI* restriction sites to allow the unidirectional ligation of the insert into the plasmid. The digestion reactions were carried out using enzymes from two manufactures in order to determine the optimal enzymes (Table 4.2 and 4.3). In addition, the samples were digested using different conditions by incubating with the restriction enzymes for intervals up to 3 h to optimise the ideal digestion conditions for each of the empty plasmids and also for the two amplified PAR2 cDNA.

4.2.11 Purification of DNA following the restriction reactions

Following the restriction digestion, the plasmid DNA and amplified DNA were purified using Monarch® DNA Cleanup Kit. According to manufacturer's protocol, the samples were diluted with DNA binding buffer provided with the kit (1:4 v/v) and transferred to individual columns. The columns were then placed into collection tubes and centrifuged at 12,000 g for 1 min. The columns were then washed with the provided DNA wash buffer (200 µl; 80% (v/v) ethanol) and centrifuged at 12,000 g for 4 min. The columns were placed in fresh 1.5 ml tubes and 30 µl of the elution buffer was added. The samples were then incubated for 1 min and collected

Figure 4. 6 The map of VersaClone plasmid containing hPAR2 cDNA

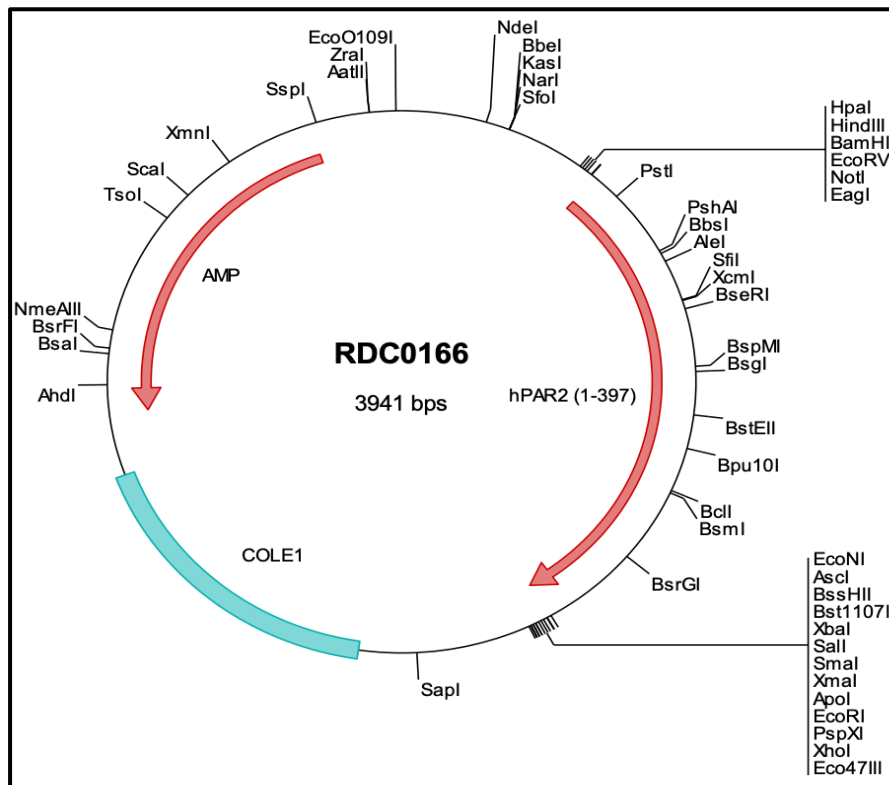


Table 4 1 PCR master mix

Reagent	Volume per reaction (μ l)	Final concentration
DNA template	Variable	200 ng
10 μ M forward primer	0.5	0.2 μ M
10 μ M reverse primer	0.5	0.2 μ M
10X High Fidelity Buffer	2.5	1X
10 mM dNTP mix	0.5	0.2 mM
Platinum <i>Taq</i> DNA polymerase	0.1	2 U
50 mM MgCl ₂	0.75	1.5 mM
Nuclease-free water	Variable	-
Total	25	-

Table 4 2 Master mix for DNA digestion with restriction enzymes from Promega

Reagent	Volume (μ l)	Final concentration
DNA	variable	1 μ g
10X Buffer	5	1X
100X BSA	0.5	1X
<i>Bam</i> HI (10 U/ml)	1	0.2 U/ml
<i>Hind</i> III (10 U/ml)	1	0.2 U/ml
RNase-free water	variable	-
Total	50	-

Table 4 3 Master mix for DNA digestion with high-fidelity restriction enzymes

Reagent	Volume (μ l)	Final concentration
DNA	variable	1 μ g
10X NEBuffer	5	1X
<i>Bam</i> HI-HF (20 U/ml)	1	0.4 U/ml
<i>Hind</i> III-HF (20 U/ml)	1	0.4 U/ml
RNase-free water	variable	-
Total	50	-

All enzymes from New England Biolabs

by centrifugation at 12,000 *g* for 1 min. The samples were examined and confirmed by agarose gel electrophoresis as described in section 4.2.7 and stored at -20°C until required.

4.2.12 Ligation of the PAR2 DNA inserts into the mCherry2-C1 and mEmerald-C1 plasmids

The full-length of PAR2 DNA was inserted into mEmerald-C1 plasmid while the short version was ligated into mCherry2-C1 plasmid. The concentrations of the DNA plasmids and also the inserts were determined as described in section 2.2.14. A range of insert:plasmid molar ratios (1:1, 3:1, 5:1, 10:1 and 20:1) were used to attain the optimal ligation reaction condition. Appropriate volumes of the inserts and plasmids were placed in PCR tubes and adjusted to 5 µl with RNase-free water. Instant Sticky-end Ligase Master Mix (5 µl), containing T4 DNA Ligase was added to the tubes, and the reactions were mixed by pipetting and then placed on ice for 20 min. After incubation, competent *E. coli* were transformed with each ligation mix (4 µl) as described in section 4.2.3. A negative control containing *E. coli* without any DNA was also included. The cells (50 µl) were plated out on LB agar plates containing kanamycin (25 µg/ml) and incubated overnight at 37°C. Colonies were picked from the agar plates and cultured in LB medium (10 ml) overnight at 37°C with shaking at 180 rpm. On the following day, plasmid DNA was isolated from each colony using miniprep plasmid isolation kit as described in section 4.2.5. The samples were stored at -20°C until required.

4.2.13 Examination and identification of sub-cloned inserts into the plasmids

To validate the successful sub-cloning of the insert into the vector, the plasmid samples isolated from the colonies in section 4.2.12 were examined by three methods. First, the plasmid samples were digested by restriction enzymes and assessed by agarose gel electrophoresis to ensure the presence of the insert and the plasmid. The samples were prepared as described in section 4.2.7 and an empty plasmid was used as a negative control. The size of the plasmid was expected to be approximately 4,700 bp and the insert around 1,100 bp.

In addition, the presence of the full- and short-length PAR2 DNA into the vectors were also examined by PCR amplification of the insert. Samples (100 ng) of the construct plasmid isolated from the colonies in section 4.2.12 were placed individually in the Ready-To-Go RT-PCR bead tubes. Depending on the length of the PAR2 DNA cloned, respective PAR2 forward and reverse primers (0.2 μ M) were then added to the tube and the volumes were adjusted to 50 μ l with RNase-free water. The PCR was performed as described in section 4.2.9 and the products examined by agarose gel electrophoresis as described in section 4.2.7. Finally, the plasmids from the previous two confirmatory steps were submitted for sequencing by Eurofins MWG. The sequences of the clones were aligned with the published PAR2 cDNA sequence using the Clustal Omega software (available at <https://www.ebi.ac.uk>). The sequences of the primers used for sequencing the samples were:

Primer name	Primer sequence
-mEmerald-C1	5'-CATGGTCCTGCTGGAGTTCGT-3' (Full-length construct)
-mCherry2-C1	5'-CAACGAGGACTACACCATCG-3' (Short-length construct)

4.2.14 Transfection of primary cells and cancer cell lines with plasmid DNA

Endothelial cells (HDBEC), (HCAEC) and cancer cell lines (HepG2, BxPC-3, 786-O, MDA-MB-231 and MCF7) were transfected with construct mEmerald to express full-length PAR2 or with the mCherry2 construct to express shortened PAR2. To optimise the transfection procedure, two transfection reagents were used in endothelial cells as described below. Once optimised, the procedure was applied to all cells.

4.2.14.1 Transfection of HDBEC and HCAEC using Viromer® RED reagent

Cells (8×10^4) were seeded into 12-well plates and incubated overnight. On the following day, the media was removed from each well and replaced with fresh medium (400 μ l). For each transfection, the relevant plasmid construct (1 μ g) was diluted in transfection buffer provided by the kit (90 μ l). Viromer RED reagent (0.4 μ l) together with the provided transfection buffer (9.6 μ l) were pipetted into separate eppendorf tubes. The mixtures were then vortexed for few seconds and the diluted plasmid DNA samples were transferred into the tubes containing the Viromer solution. The transfection mixture was mixed gently and incubated at room temperature for 15 min. The mixtures were then added dropwise to the cells, gently shaken and incubated for up to 48 h at 37°C. The cells were harvested and the transfection efficiency was assessed by flow cytometry.

4.2.14.2 Transfection of HDBEC and HCAEC using TransIT®-2020 reagent

Cells (8×10^4) were seeded into 12-well plates and incubated overnight. On the next day, the media was removed and fresh medium (450 μ l) was added to the wells. For each transfection, plasmid DNA (1 μ g) was diluted in Opti-MEM™ I Reduced Serum Medium (48 μ l). TransIT®-2020 reagent (2 μ l) was then added to each DNA sample. The mixture was mixed gently and incubated for 30 min at room temperature. After the incubation, the mixture was added dropwise to the cells and incubated for up to 48 h at 37°C. The transfected cells were harvested and the transfection efficiency was then examined by flow cytometry.

4.2.15 Determination of transfection efficiency by flow cytometry

In order to examine the transfection efficiency, the transfected cells were examined by flow cytometry. The instrument detector was set on FL2 channel to detect the mCherry2 which emits red light (Ext. 580 nm, Em. 610 nm), whereas FL1 channel was used to detect mEmerald which produces green fluorescence (Ext. 480 nm, Em. 510 nm). The transfected cells were harvested by washing the plates twice with PBS and then incubated with enzyme-free cell dissociation

buffer (300 μ l) for 5 min at 37°C. The cells were placed in 1.5 ml tubes and centrifuged at 800 g for 5 min. The cells were then suspended in PBS (500 μ l) and transferred to polypropylene FACS tubes and analysed using a Becton Dickinson FACSCalibur™. For each sample, 10,000 events were analysed. Untransfected control cells were used to determine the background emission produced and a gate was drawn to include 4% of events. The percentage of transfected cells and the mean fluorescence was then calculated for each set of cells.

4.2.16 Determination of plasmid DNA transfection by fluorescence microscopy

The transfection of the cells was also monitored visually as follows. Transfected cells were washed twice with PBS, fixed with 4% (v/v) formaldehyde (200 μ l) and incubated for 15 min. The plates were then washed twice with PBS and imaged using a Zeiss Axio Vert.A1 fluorescence microscope with an Axiocam ICm 1 camera attachment.

4.2.17 Measurement of PAR2 auto-activation on cancer cell surfaces

The aim of this experiment was to measure the PAR2 auto-activation on the surface of cancer cells which is mediated by endogenous proteases. Cancer cell lines (10^4) were seeded into 96-well plates and incubated overnight. On the following day, the cells were transfected with construct mCherry2 short-length PAR2 plasmid (see section 4.2.14.2) and incubated for 24 h at 37°C. After the incubation, the media was removed and fresh serum-free medium (200 μ l) was added to the wells. The plates were then incubated for 1 h at 37°C. Since higher PAR2 activation results in greater release of mCherry2 into the medium, the medium was then collected and fluorescence intensities of mCherry was measured (Ext. 580 nm, Em. 610 nm) using a plate reader. For comparison, similar sets of cells were permeabilised with 0.01% (v/v) of Triton X100 diluted in serum-free medium to release the entire mCherry2 short-length PAR2 total protein. The percentage of PAR2 activation on the cell surface was calculated as follows:

$$= \frac{\text{Fluorescence of non-permeabilised cells medium}}{\text{Fluorescence of permeabilised cells medium}} \times 100$$

4.2.18 Measurement of MV release by PAR2 auto-activation in the transfected cancer cells

The media from section 4.2.17 collected from intact cells was also used to quantify the density of release MV by the cells. This was used to associate the release of MV by cancer cells to PAR2 auto-activation. To assess MV release from the transfected cell lines, the medium (50 μ l) was collected from the cells and quantified using the Zymuphen MP assay as described in 2.2.8.

4.2.19 Measurement of PAR2 activation in HDBEC in response to TF-fVIIa complex

HDBEC (10^4) were seeded into 96-well plates and incubated overnight. On the following day, the cells were transfected with mCherry2 construct short-length PAR2 as described in section 4.2.14.2 and incubated for 24 h at 37°C. The transfected cells were then treated with combinations of recombinant TF (4 U/ml) and purified fVIIa (0-10 nM) and incubated for 1 h at 37°C. The media from the transfected cells was collected and the fluorescence intensities measured using a plate reader (Ext. 580 nm, Em. 610 nm).

4.2.20 Assessment of the influence of cell line-derived MV on PAR2 activation in HDBEC

HDBEC (10^4) were seeded into 96-well plates and incubated at 37°C overnight. On the following day, the cells were transfected with the mCherry2-PAR2 construct as described in section 4.2.14.2 and incubated for 24 h at 37°C. The transfected cells were then incubated for 1 h at 37°C with MV (0.05 nM) prepared from various untransfected cancer cell lines. After the incubation, the media from the transfected cells was collected and the fluorescence intensities were measured using a plate reader (Ext. 580 nm, Em. 610 nm).

4.3 RESULTS

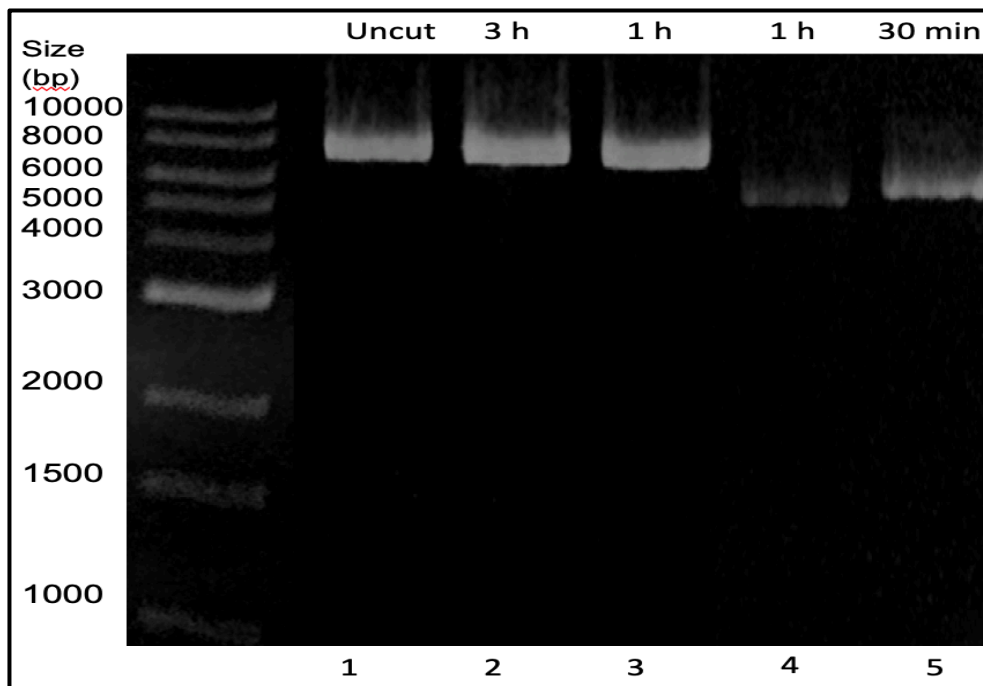
4.3.1 Optimisation of digestion of the plasmids and the amplified PAR2 cDNA with *HindIII* and *BamHI* restriction enzymes

The mCherry2-C1 plasmid was digested with the restriction enzymes *HindIII* and *BamHI* to produce 5' overhangs which would facilitate the cloning of the PAR2 cDNA into the vector. To optimise the reagents and conditions, the plasmid was incubated with the restriction enzymes (*HindIII* and *BamHI*) from two different manufacturers (Promega and New England Biolabs) in the same tubes for up to 3 h at 37°C. The samples were then examined by agarose gel electrophoresis against an undigested construct (see section 4.2.7). Incubation of the plasmid with restriction enzymes from New England Biolabs but not Promega resulted in a change in the apparent DNA mobility compared to the control (Figure 4.7). Consequently, this procedure was used for digestion of both mEmerald-C1 and mCherry2-C1 plasmids as well as the DNA inserts.

4.3.2 Sub-cloning of the PAR2 cDNA into the vector

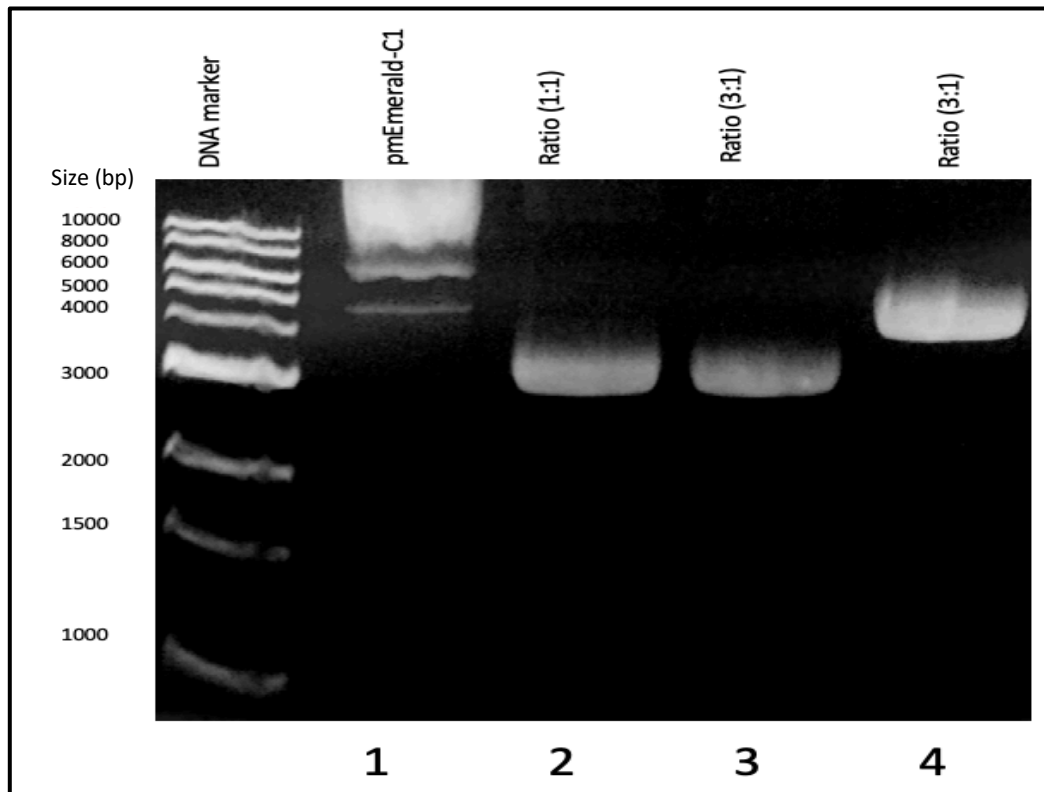
The full-length PAR2 cDNA was digested and sub-cloned into the mEmerald-C1 plasmid while the shortened PAR2 was sub-cloned into the mCherry2-C1 plasmid. The concentration of the inserts and the plasmids were determined as described in 2.2.14. The ligation and transformation procedures were then carried out using various molar ratios of insert:plasmid ranging between (20:1 to 1:1) as described in section 4.2.3. Clones were obtained on transferring the bacteria following ligation of insert:plasmid at ratios of 1:1, 3:1 and 5:1 but not at higher ratios. Single colonies were then picked from the petri dishes, propagated in LB broth and the plasmids were purified as described in section 4.2.5. The DNA samples were then examined by agarose gel electrophoresis to confirm the presence of the plasmids (Figures 4.8 and 4.9). Samples that contained the plasmid were further examined as below to validate the insertion (see section 4.3.3).

Figure 4. 7 Optimisation of digestion mCherry2-C1 plasmid with *HindIII* and *BamHI* restriction enzymes



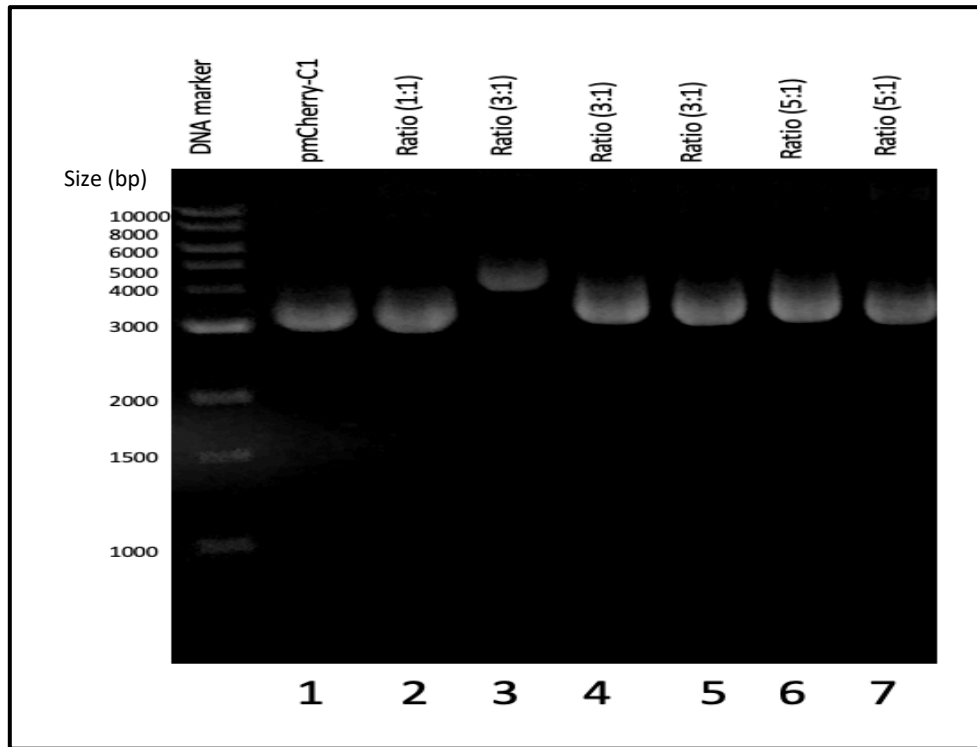
mCherry2-C1 plasmid (1 μ g) was digested with *HindIII* and *BamHI* restriction enzymes. The plasmid was incubated with the restriction enzymes from Promega for 1 h at 37°C (lane 3) up to 3 h (lane 2). For optimal results, the plasmid was also incubated with high-fidelity *HindIII* and *BamHI* restriction enzymes from New England Biolabs where the samples were incubated for 30 min (lane 5) or 1 h (lane 4). Set of the sample was examined and used as control (lane 1). The samples were analysed by 1%(w/v) agarose gel electrophoresis.

Figure 4. 8 Optimisation of the ligation of the full-length PAR2 cDNA into the mEmerald-C1 plasmid



The full-length PAR2 cDNA was ligated into the mEmerald-C1 plasmid. A range of insert:plasmid ratios were used (20:1 to 1:1) in order to optimise the ligation. The mixture was incubated with the ligation enzyme and then transformed into competent *E.coli*. The transfected bacteria were plated out on kanamycin-agar plates and incubated at 37°C overnight. Single colonies were picked from the plates and propagated in LB broth. The plasmids were then isolated and examined by 1% (w/v) agarose gel electrophoresis. The transfection with the ligated DNA at 3:1 ratio (lane 4) which showed a change in the apparent DNA mobility compared to the other samples (lanes 2 and 3) was further examined by PCR and DNA sequencing. The empty plasmid without the insert (lane 1) was used as a negative control.

Figure 4. 9 Optimisation of the ligation of the short-length PAR2 cDNA into the mCherry2-C1 plasmid

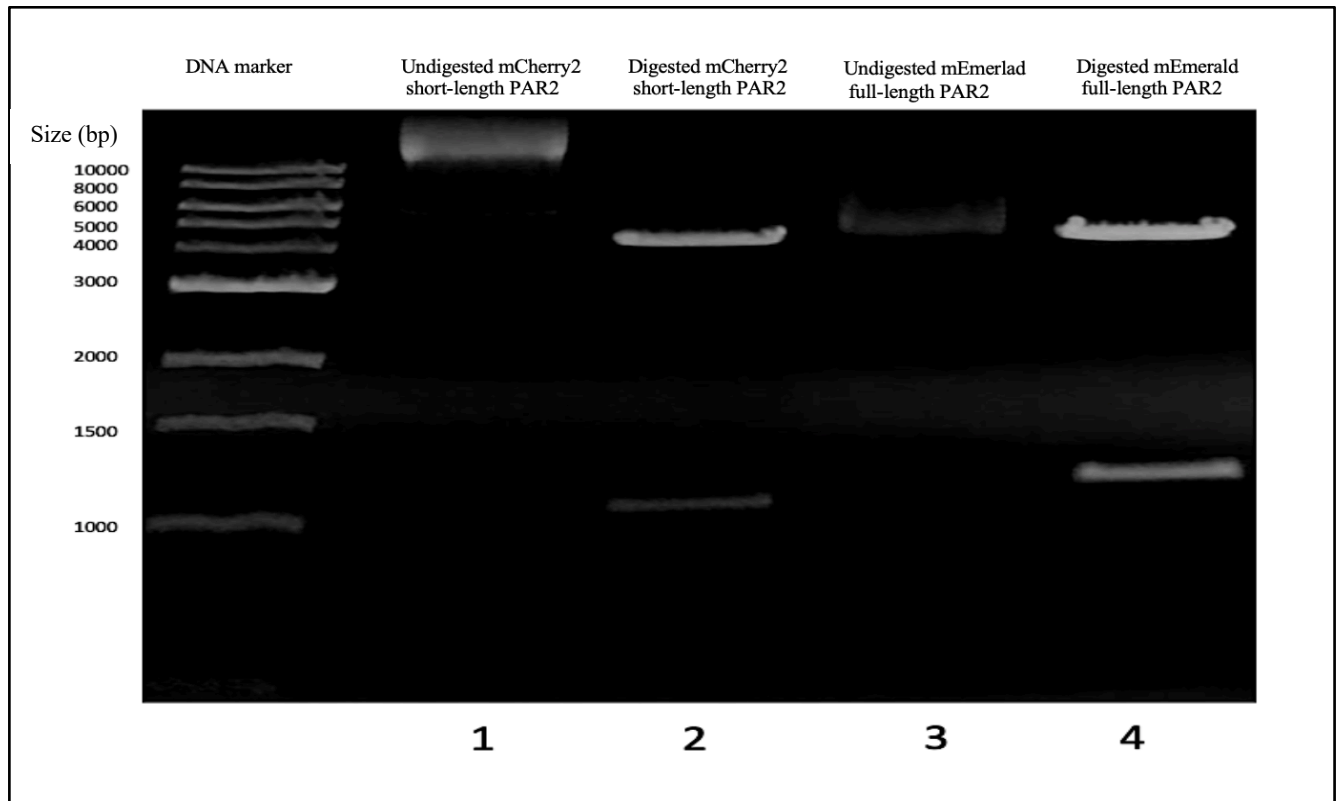


The short-length PAR2 cDNA was ligated into the mCherry2-C1 plasmid. A range of insert:plasmid ratios were used (20:1 to 1:1) in order to optimise the ligation. The mixture was incubated with the ligation enzyme and then transformed into competent *E.coli*. The transfected bacteria were plated out on kanamycin-agar plates and incubated at 37°C overnight. Single colonies were picked from the plates and propagated in LB broth. The plasmids were then isolated and examined by 1% (w/v) agarose gel electrophoresis. The transfection with the ligation DNA at 3:1 ratio (lane 3) which showed a change in the apparent DNA mobility compared to the other samples (lanes 2, 4, 5, 6 and 7) was further examined by PCR and DNA sequencing. The empty plasmid without insert (lane 1) was used as a negative control.

4.3.3 Validation of the sub-cloning of the insert into the plasmid

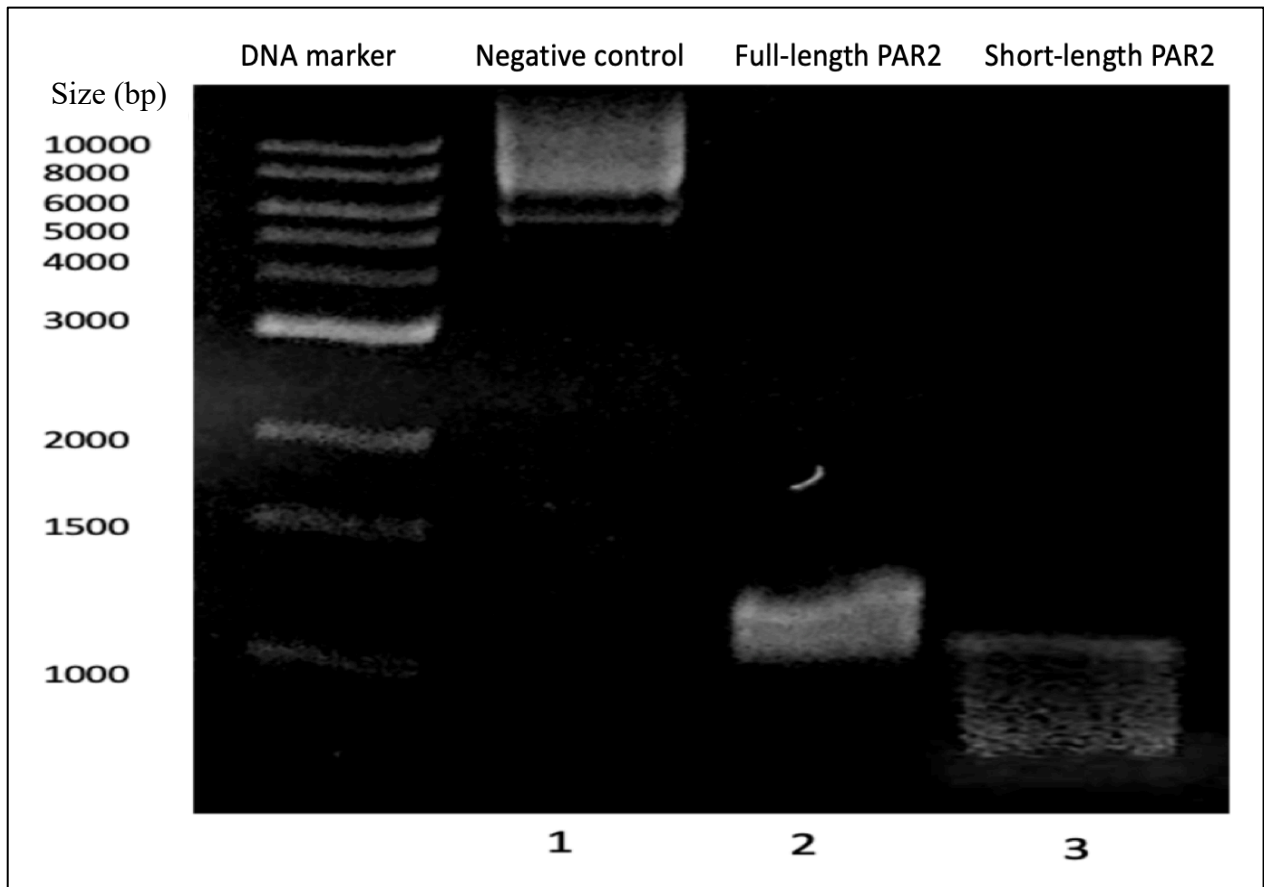
Initially, the successful ligation of the inserts into the plasmids was examined by digestion of the constructed plasmids with *HindIII* and *BamHI* as described in section 4.3.1 and analysed by agarose gel electrophoresis. The digested DNA in the positive samples showed two bands at 4,700 bp and 1,200 bp respectively which can be attributed to the size of the mEmerald-2 plasmid and the full-length PAR2 DNA (Figure 4.10). Another set of digested DNA sample exhibited a band approximately at 1,100 bp which corresponds to the size of the short-length PAR2 DNA together with another band at 4,700 bp which corresponds to the mCherry-C1 plasmid (Figure 4.10). To further validate the insertion of the DNA into the vectors, the cloned inserts were amplified using Ready-To-Go RT-PCR bead as described in 4.2.13 and examined by agarose gel electrophoresis. The amplified samples exhibited bands at approximately 1,200 bp and 1,100 bp which correspond to the full- and short-length PAR2 DNA (Figure 4.11). To finally confirm the correct insertion of the PAR2 cDNA into the plasmids, positive samples from the previous amplification method were further examined by sequencing. These were carried out alongside the amplified PAR2 cDNA from VersaClone plasmid (containing PAR2 cDNA) and was sequenced for comparison, and used together with the published sequence. All DNA sequences were analysed and aligned using the Clustal Omega software. The results confirmed that the full-length PAR2 was successfully ligated into the mEmerald-C1 plasmid in the correct direction whilst the shortened version of PAR2 was inserted into the mCherry2-C1 plasmid. Also, the amplified PAR2 cDNA from the VersaClone plasmid matches with the published sequence of the PAR2 protein (Figures 4.12-4.14).

Figure 4. 10 Analysis of the constructed plasmids by *HindIII* and *BamHI* restriction digestion



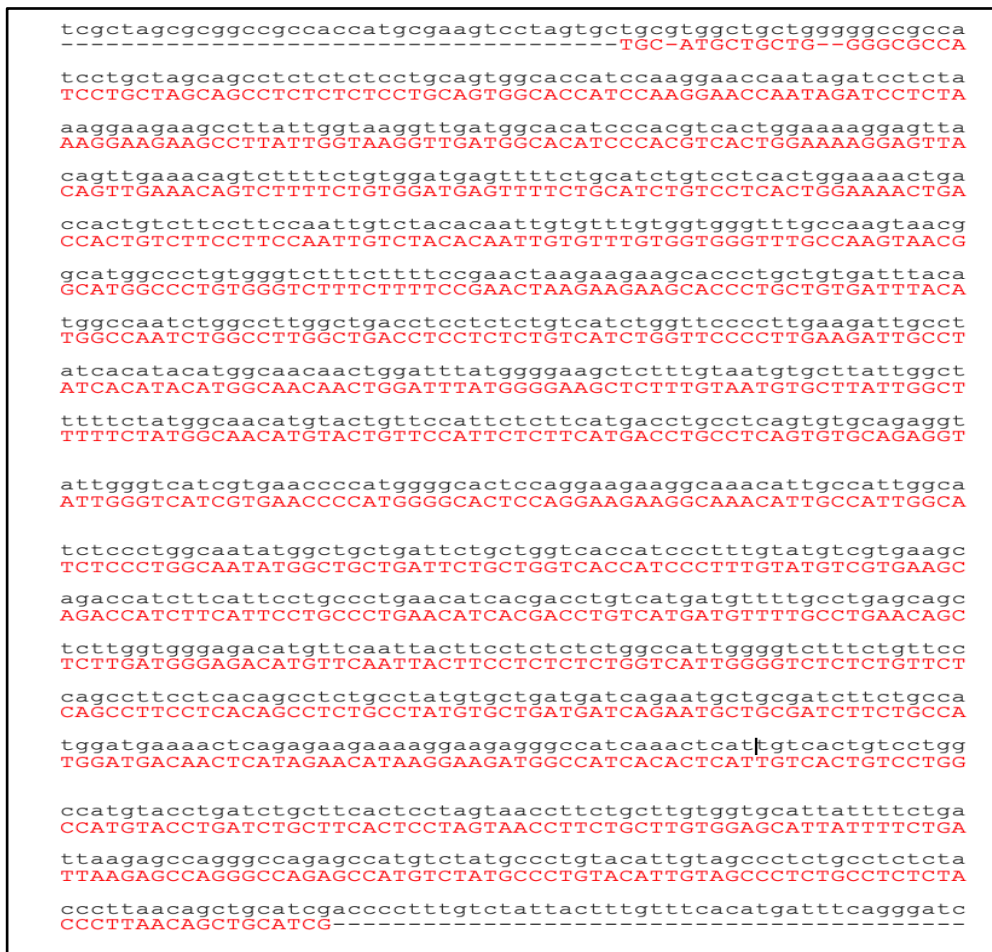
The constructed plasmids were digested with high-fidelity *HindIII* and *BamHI* restriction enzymes and the digested DNA were analysed by agarose gel electrophoresis. The digestion of the DNA samples produced two fragments of approximately 4,700 bp and 1,100 bp, correspondingly to the mCherry2-C1 plasmid and the short-length PAR2 cDNA respectively (lane 2). Another digested DNA sample showed bands at 4,700 bp and 1,200 bp which corresponds to the mEmerald-C1 plasmid and the full-length PAR2 cDNA respectively (lane 4). The undigested DNA samples were used as control (lanes 1 and 3).

Figure 4. 11 Confirmation of cloning of PAR2 inserts by PCR amplification



The cloned inserts were amplified by PCR using the appropriate primers. The PCR products were analysed using agarose gel electrophoresis. The amplified DNA samples contained fragments at approximate sizes of 1,200 bp (lane 2) and 1,100 bp (lane 3) respectively which correspond to the full- and short-length PAR2 cDNA respectively. The empty plasmid without insert (lane 1) was used as control.

Figure 4. 12 Alignment of the amplified PAR2 cDNA PCR product with the published PAR2 sequence



A sample of the PAR2 amplified from the VersaClone plasmid (containing PAR2 cDNA) was submitted for sequencing to ensure that its sequence matches that of the published PAR2 protein. The alignment of the sequences showed that the sequence of the amplified PAR2 (red) matched with the published PAR2 sequence (black). The sequences were aligned using Clustal Omega software (EMBL-EBI).

Figure 4. 13 Confirmation of the sub-cloning of the full-length PAR2 cDNA into the mEmerald-C1 plasmid

```

-----cgaagtcct
GCATGGACGAGCTGTACAAGTCCGGACTCAGATCTCGAGCTCAAGCTTATGCGAAGTCCT
agtgctgcgctggctgctgggggcccgcacatcctgctagcagcctctctctcctgcagtggc
AGTGCTGCGTGGCTGCTGGGGGCCGCCATCCTGCTAGCAGCCTCTCTCTCCTGCAGTGGC
accatccaaggaaccaatagatcctctaaaggaagaagccttattggttaagggttgatggc
ACCATCCAAGGAACCAATAGATCCTCTAAAGGAAGAAGCCTTATTGGTAAGGTTGATGGC
acatcccacgtcactggaaaaggagttacagttgaaacagtccttttctgtggatgagttt
ACATCCCACGTCCTGGAAAAGGAGTTACAGTTGAAACAGTCTTTTCTGTGGATGAGTTT
tctgcatctgtcctcactggaaaactgaccactgtcttccttccaattgtctacacaatt
TCTGCATCTGTCTCCTCACTGGAAAACGACCACTGTCTTCCTTCCAATTGTCTACACAATT
gtgtttgtggtgggtttgccaagtaacggcatggccctgtgggtctttcttttccgaact
GTGTTTGTGGTGGGTTTGCCAAGTAACGGCATGGCCCTGTGGGTCTTTCTTTTCCGAAC
aagaagaagcaccctgctgtgatttacatggccaatctggccttggtgacccctcctctct
AGAAGAAGCACCCCTGCTGTGATTTACATGGCCAATCTGGCCTGGCTGACCTCCTCTCT
gtcatctggttccccttgaagattgcctatcacatacatggcaacaactggatttatggg
GTCACTGGTTCCCCTTGAAGATTGCCATCACATACATGGCAACAACCTGGATTTATGGG
gaagctctttgtaatgtgcttattggctttttctatggcaacatgtactgttccattctc
GAAGCTCTTTGTAATGTGCTTATTGGCTTTTTCTATGGCAACATGTACTIONTCCATTCTC
ttcatgacctgcctcagtgctgagaggtattgggtcatcgtgaacccatggggcactcc
TTCATGACCTGCCTCAGTGTGCAGAGGTATTGGGTCACTCGTGAACCCCATGGGGCCTCC
aggaagaaggcaaacattggcattggcatctccctggcaatatggctgctgattctgctg
AGGAAGAAGGCAACATTGCCATTGGCATCTCCCTGGCAATATGGCTGCTGATTCTGCTG
gtcaccatccctttgtatgtcgtgaagcagaccatcttcattcctgcctgaacatcacg
GTCACCATCCCTTTGTATGTCGTGAAGCAGACCATCTTCATTCTGCCCTGAACATCACG
acctgtcatgatgttttgctgagcagctcttggtgggagacatgttcaattacttctc
ACCTGTCAATGATGTTTTGCCTGAGCAGCTCTTGGTGGGAGACATGTTCAATTACTTCTC
tctctggccattggggcttttctgttcccagccttccctcacagcctctgcctatgtgctg
TCTCTGGCCATTGGGGTCTTTCTGTCCCAGCCTTCTCACAGCCTCTGCCTATGTGCTG
atgatcagaatgctgcatcttctgcatggatgaaaactcagagaagaaaaggaagagg
ATGATCAGAAATGCTGCGATCTTCTGCCATGGATGAAAACCTCAGAGAAGAAAAGGAAGAG
gccatcaaacctattgtcactgtcctggccatgtacctgatctgcttactcctagtaac
GCCATCAAACCTATTGTCACTGTCTGGCCATGTACCTGATCTGCTTCACTCCTAGT---

```

The full-length PAR2 cDNA was ligated into the mEmerald-C1 plasmid. A sample of the construct was isolated and sequenced to ensure the right sequence of the insert. The sequenced sample of the mEmerald-full-length PAR2 construct (red) was aligned against the published PAR2 sequence (black) using Clustal Omega software (EMBL-EBI) and both sequences appeared to match.

Figure 4. 14 Confirmation of the sub-cloning of the short-length PAR2 cDNA into the mCherry2-C1 plasmid

```

-----caaggaaccaatagatcctcctctaaaggaagaagccttattggtaagggttgatggca
TTATCCAAGGAACCAATAGATCCTCTAAAGGAAGAAGCCTTATTGGTAAGGTTGATGGCA

catcccacgtcactggaaaaggagttacagttgaaacagtcttttctgtggatgagtttt
CATCCCACGTCACTGGAAAAGGAGTTACAGTTGAAACAGTCTTTTCTGTGGATGAGTTTT

ctgcatctgtcctcactggaaaactgaccactgtcttcccttccaattgtctacacaattg
CTGCATCTGTCCCTCACTGGAAAAC TGACCAC TGTCTTCCCTTCCAATTGTCTACACAATTG

tgtttgggtgggtttgccaagtaacggcatggccctgtgggtctttcttttccgaacta
TGTTTGTGGTGGGTTTGCCAAGTAACGGCATGGCCCTGTGGGTCTTCTTTTCCGAACTA

agaagaagcaccctgctgtgatttacatggccaatctggccttggtgacctcctctctg
AGAAGAAGCACCCCTGCTGTGATTTACATGGCCAATCTGGCCCTGGCTGACCTCCTCTCTG

tcactctggttccccttgaagattgcctatcacatacatggcaacaactggatttatgggg
TCATCTGGTTCCCTTGAAGATTGCCATACACATACATGGCAACAACCTGGATTTATGGGG

aagctctttgtaatgtgcttattggcttttctatggcaacatgtactgttccattctct
AAGCTCTTTGTAATGTGCTTATTGGCTTTTCTATGGCAACATGTACTGTTCCATTCTCT

tcatgacctgcctcagtgctgagaggtattgggtcatcgtgaaccccatggggcactcca
TCATGACCTGCCTCAGTGTGCAGAGGTATTGGGT CATCGTGAACCCCATGGGGC ACTCCA

ggaagaaggcaaacattgccattggcatctcccctggcaatatggctgctgattctgctgg
GGAAGAAGGCAAACATTGCCATTGGCATCTCCCTGGCAATATGGCTGCTGATTCTGCTGG

tcaccatccccttggatgtcgtgaagcagaccatcttcattcctgcccgaacatcacga
TCACCATCCCCTTGTATGTCGTGAAGCAGACCATCTTCATTCTGCCCCTGAACATCACGA

cctgtcatgatgttttgcctgagcagctcttgggtgggagacatgttcaattacttctct
CCTGT CATGATGTTTTGCCTGAGCAGCTCTGGTGGGAGACATGTTCAATTACTTCTCT

ctctggccattggggcttttctgttcccagccttccctcacagcctctgcctatgtgctga
CTCTGGCCATTGGGGTCTTTCTGTTCCCAGCCTTCCCTCACAGCCTCTGCCTATGTGCTGA

tgatcagaatgctgcatcttctgcatggatgaaaactcagagaagaaaaggaagaggg
TGATCAGAATGCTGCGATCTTCTGCCATGGATGAAAAC T CAGAGAAGAAAAGGAAGAGGG

ccatcaaacctcattgtcactgtcctggccatgtacctgatctgcttcaactcctagtaacc
CCATCAAACCTCATTGTCACTGTCTGACCATGTACCTGATCTGCTTCACTCCTAGTAACC

ttctgcttgggtgcattatcttctgattaagagccagggccagagccatgtctatgccc
TTCTGCTTGTGGTGCATTATTTTCTGATTAAGAA-----

```

The short-length PAR2 cDNA was ligated into Cherry2-C1 plasmid. A sample of the construct was isolated and sequenced to ensure the right sequence of the insert. The sequenced sample of the mCherry2-short-length PAR2 construct (red) was aligned against the published PAR2 sequence (black) using Clustal Omega software (EMBL-EBI) and the sequences appeared to match.

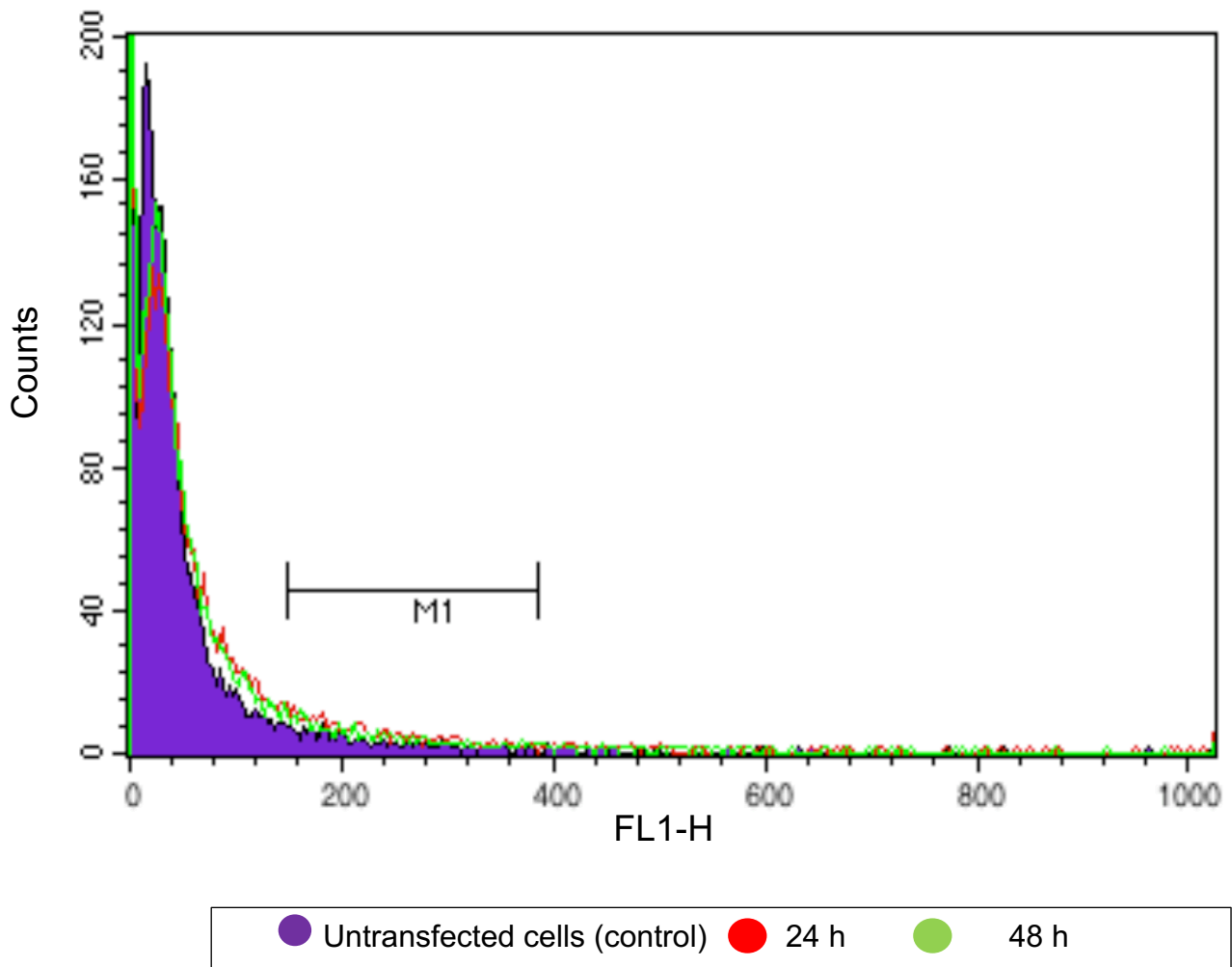
4.3.4 Assessment of DNA transfection efficiency into HCAEC and HDBEC

Viromer RED and TransIT-2020 transfection reagents were used to transfect endothelial cells (HCAEC or HDBEC) with the mEmerald-full-length PAR2 construct or mCherry2-short-length PAR2 construct as described in section 4.2.14. The cells were then incubated for 24 h and examined for viability by light microscope. The transfection of HDBEC with the construct (1 µg) had no obvious effect on the cell viability. In contrast, the transfection of HCAEC with the construct (1-2 µg) was shown to reduce cell viability. Therefore, only HDBEC were used for subsequent studies.

4.3.4.1 Examination of Viromer RED transfection efficiency in HDBEC

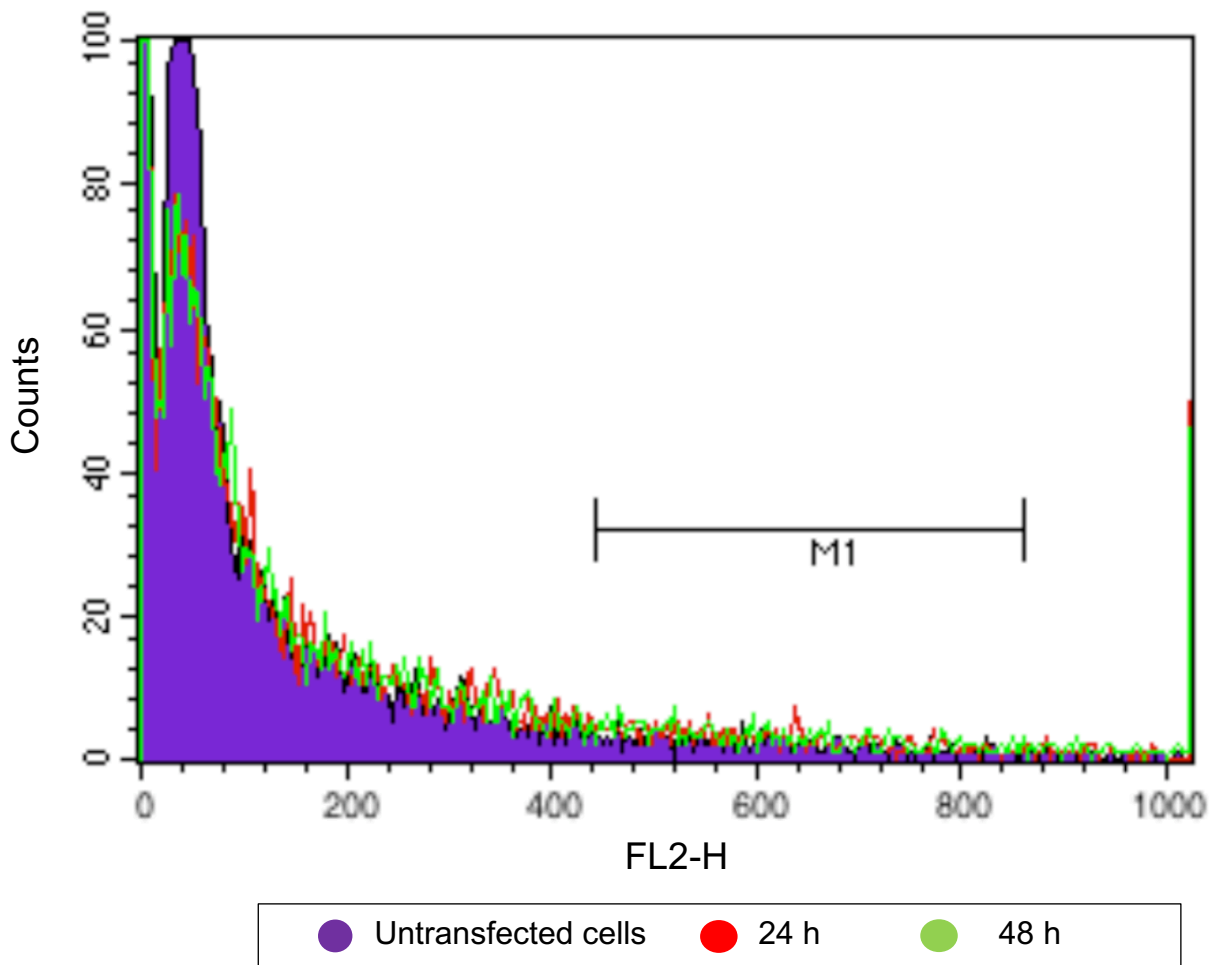
HDBEC (8×10^4) were seeded into 12-well plates and incubated in complete MV medium overnight. On the following day, the cells were transfected as described in section 4.2.14.1 and incubated up to 48 h at 37°C. The cells were then harvested and the transfection efficiency was assessed by flow cytometry as described in 4.2.15. Transfection of HDBEC with the mEmerald-full-length PAR2 construct did not result in efficient expression of the protein as measured by flow cytometry after 24 h (8.79%; mean fluorescence = 26) and 48 h incubation (7.20%; mean fluorescence = 55) (Figure 4.15). Furthermore, the mCherry2-short-length PAR2 construct was not expressed efficiently by HDBEC which showed 6.15% (mean fluorescence = 135) after 48 h incubation and 5.76% (mean fluorescence = 138) after 24 h (Figure 4.16). Therefore, the Viromer RED reagent was not used in further studies.

Figure 4. 15 Analysis of transfection efficiency using the Viromer RED-mediated



HDBEC (8×10^4) were transfected with the mEmerald-full-length PAR2 construct (1 μ g) using the Viromer RED transfection reagent (4 μ l) and incubated up to 48 h. Sets of the transfected cells were analysed by flow cytometry after 24 h (red) and after 48 h (green). For each sample, 10,000 events were analysed. A set of untransfected cells were used as a control to determine the background fluorescence produced by untransfected cells. A gate was set (M1) to include 4% of untransfected cells (purple) and used to compare the fluorescence of the transfected cells. The data is representative of two separate experiments.

Figure 4. 16 Analysis of transfection efficiency using the Viromer RED-mediated



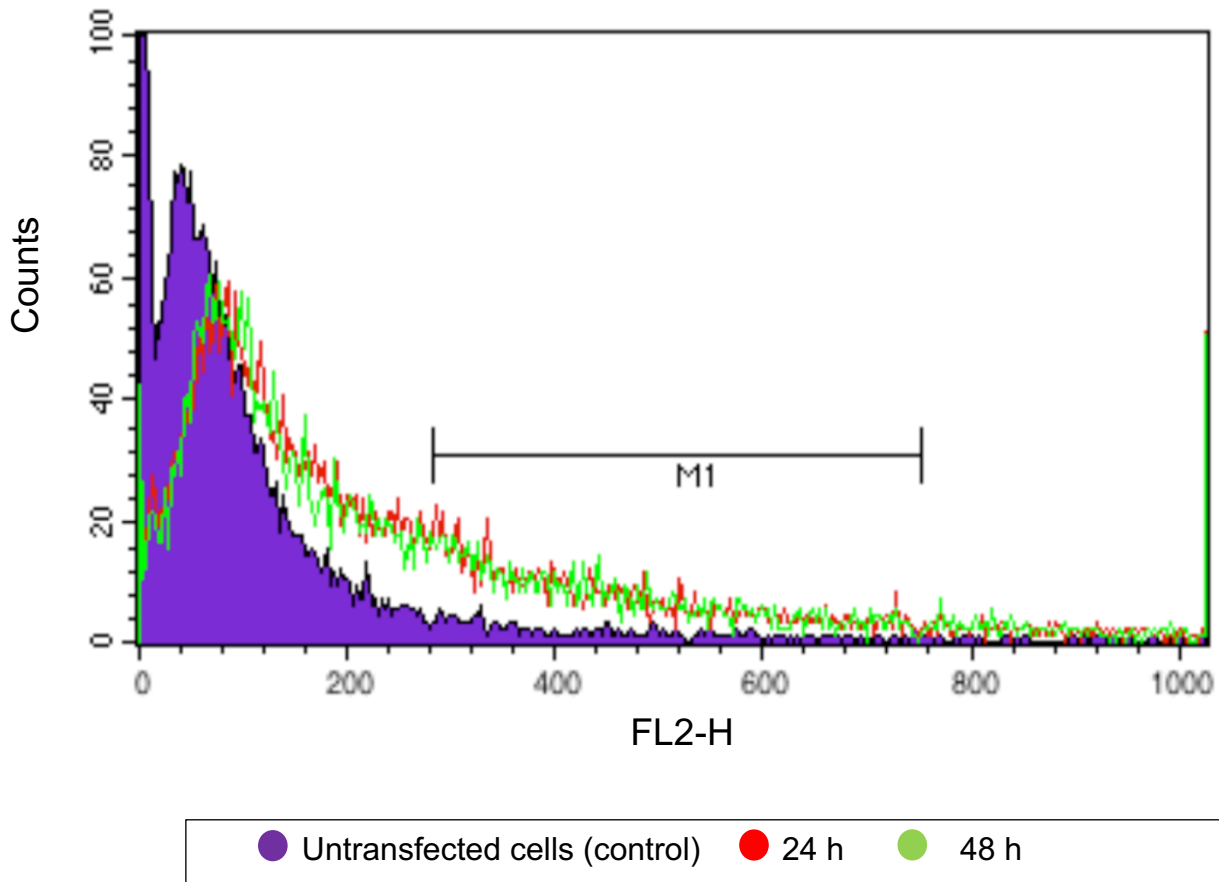
HDBEC (8×10^4) were transfected with the mCherry2-short-length PAR2 construct ($1 \mu\text{g}$) using the Viromer RED transfection reagent ($4 \mu\text{l}$) and incubated up to 48 h. Sets of the transfected cells were analysed by flow cytometry after 24 h (red) and after 48 h (green). For each sample, 10,000 events were analysed. A set of untransfected cells were used as a control to determine the background fluorescence produced by untransfected cells. A gate was set (M1) to include 4% of untransfected cells (purple) and used to compare the fluorescence of the transfected cells. The data is representative of two separate experiments.

4.3.4.2 Examination of TransIT-2020-mediated transfection efficiency in HDBEC

Due to the low transfection efficiency obtained using the Viromer RED transfection reagent, TransIT-2020 reagent was used in attempt to increase it. HDBEC (8×10^4) were seeded into 12-well plates and incubated overnight. On the next day, the cells were transfected separately with the constructs mCherry2-short-length PAR2 or mEmerald-full-length PAR2 as described in section 4.2.14.2 and incubated for up to 48 h at 37°C. The transfected cells were then collected and analysed by flow cytometry as described in section 4.2.15. Transfection of HDBEC with the mCherry2-short-length PAR2 construct showed the highest rate of the protein expression as measured by flow cytometry after 24 h (23.1%; mean fluorescence = 277) and 48 h incubation (23%; mean fluorescence = 231) respectively (Figure 4.17). The mEmerald-full-length PAR2 construct was not expressed efficiently by HDBEC as measured by flowcytometry after 24 h (12.25%; mean fluorescence = 451) and 48 h incubation (11.47%; mean fluorescence = 439) (Figure 4.18).

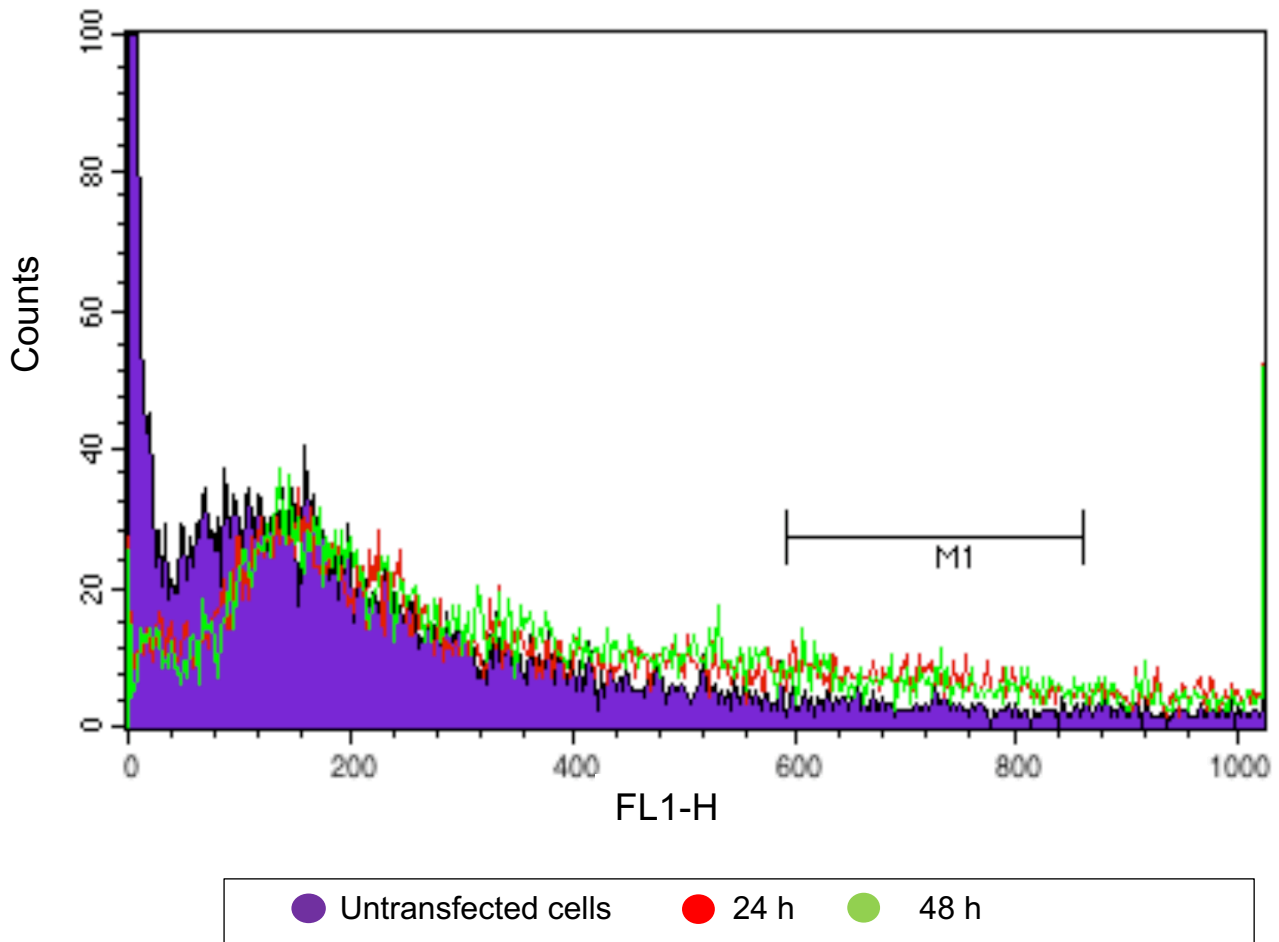
To further assess the expression of the mCherry2-short-length PAR2 in HDBEC, the cells were transfected with the construct, incubated for 24 h and visualised by fluorescence microscopy. Some of these cells were labelled with FITC-conjugated anti-PAR2 (SAM11; 20 µg/ml) for comparison. Both the transfected and labelled cells showed same distribution of PAR2 protein (Figure 4.19). Therefore, the optimised procedure using the mCherry2-short-length PAR2 construct and TransIT-2020 transfection reagent was used to transfect HDBEC and cell lines in subsequent studies.

Figure 4. 17 Analysis of transfection efficiency using the TransIT-2020-mediated



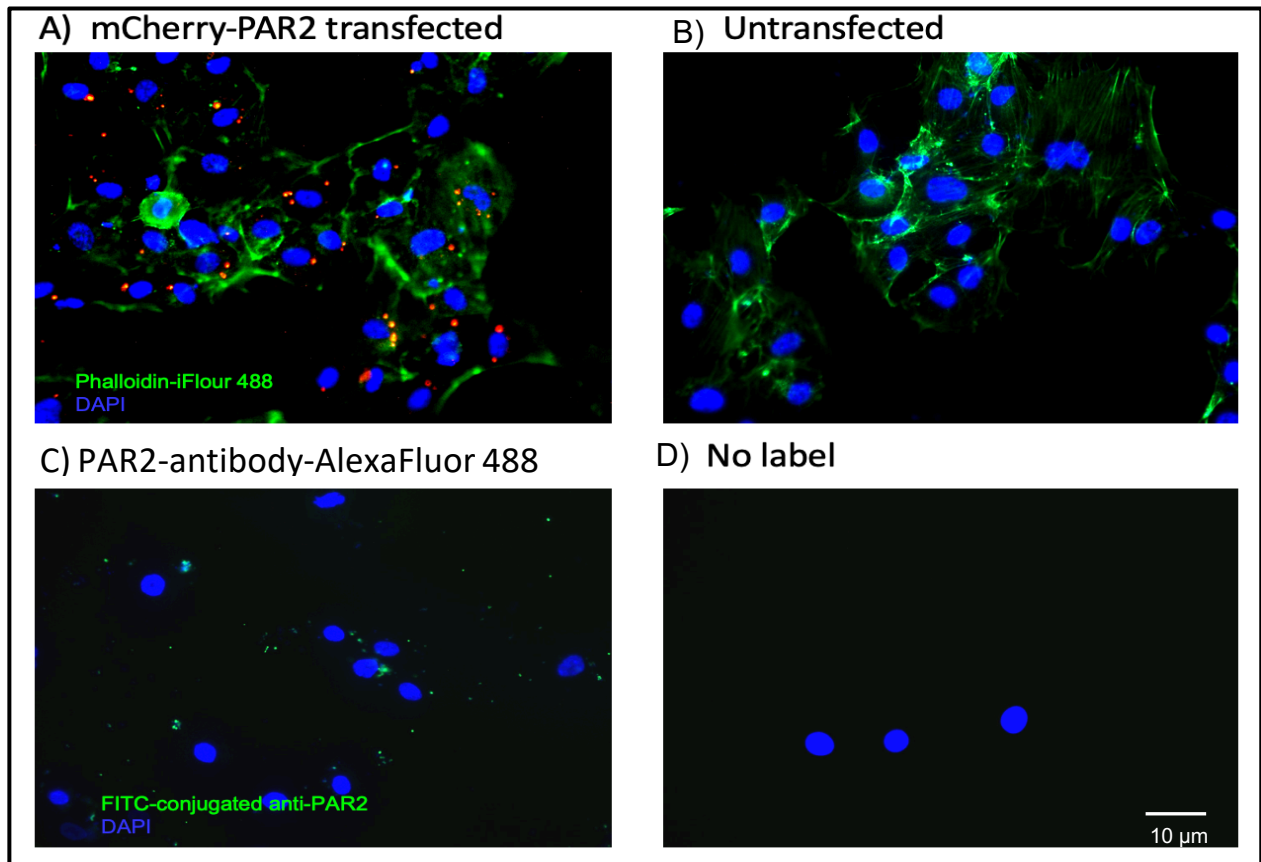
HDBEC (8×10^4) were transfected with the mCherry2-short-length PAR2 construct ($1 \mu\text{g}$) using the TransIT-2020 transfection reagent ($2 \mu\text{l}$) and incubated up to 48 h. Sets of the transfected cells were analysed by flow cytometry after 24 h (red) and after 48 h (green). For each sample, 10,000 events were analysed. A set of untransfected cells were used as a control to determine the background fluorescence produced by untransfected cells. A gate was set (M1) to include 4% of untransfected cells (purple) and used to compare the fluorescence of the transfected cells. The data is representative of two separate experiments.

Figure 4. 18 Analysis of transfection efficiency using the TransIT-2020-mediated



HDBEC (8×10^4) were transfected with the mEmerald-full-length PAR2 construct ($1 \mu\text{g}$) using the TransIT-2020 transfection reagent ($2 \mu\text{l}$) and incubated up to 48 h. Set of the transfected cells were analysed by flow cytometry after 24 h (red) and after 48 h. For each sample, 10,000 events were analysed. A set of untransfected cells were used as a control to determine the background fluorescence produced by untransfected cells. A gate was set (M1) to include 4% of untransfected cells (purple) and used to compare the fluorescence of the transfected cells. The data is representative of two separate experiments.

Figure 4. 19 Analysis of the expression of the mCherry2-short-length PAR2 construct by fluorescence microscopy



HDBEC (5×10^3) were seeded into glass bottom dishes (35 mm) and transfected with the mCherry2-short-length PAR2 construct (1 μ g) using the TransIT-2020 transfection reagent. The transfected (A) and untransfected (B) cells were then fixed, stained with phalloidin-iFluor 488 (2 μ g/ml) and DAPI (2 μ g/ml). The samples were then examined by fluorescence microscopy with a X40 magnification for mCherry2 short-length PAR2 (red), phalloidin-iFluor 488 (green) and DAPI (blue). For comparison, sets of cells were labelled (C) with FITC-conjugated anti-PAR2 (SAM11; 20 μ g/ml) or (D) without a label and examined for PAR2 (green) and DAPI (blue). The data is representative of one experiment.

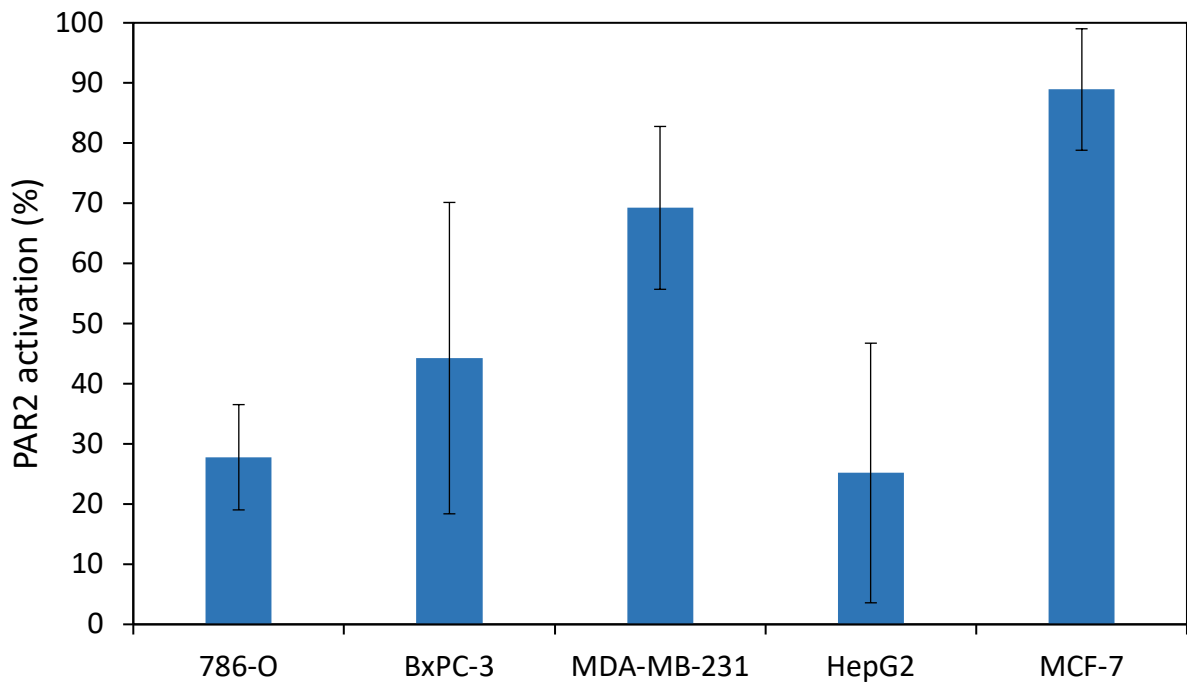
4.3.5 Measurement of PAR2 activation on the surface of cells and MV release using cell lines expressing the mCherry2-short-length PAR2 construct

The aim of this study was to measure the activation of PAR2 on the surface of cancer cell lines (HepG2, 786-O, BxPC-3, MDA-MB-231 and MCF7) which may be induced by endogenous cellular proteases (auto-activation). All of the cell lines were transfected with the mCherry2-short-length PAR2 construct as described in section 4.2.14.2. The digestion of PAR2 by proteases results in the release of the fluorescent tag into the media. Therefore, by measuring the fluorescence intensity of mCherry2 in the media, the level of the PAR2 activation can be quantified. To determine the percentage of PAR2 activation, the fluorescence in both non-permeabilised (released mCherry) and the permeabilised (total mCherry) cells was measured (Ext. 580 nm, Em. 610 nm). The percentage of PAR2 activation on the cell surface was then calculated as described in section 4.2.17. MCF7 cell line was found to exhibit the highest level of PAR2 activation 89% followed by MDA-MB-231 69%. In contrast, HepG2 and 786-O cell lines showed the lowest levels of PAR2 activation 25% and 27%, respectively (Figure 4.20). Furthermore, the release of MV by the transfected cell lines was quantified using the Zymuphen MP assay kit. Interestingly, the potential to release MV appeared to be proportional to the percentage of PAR2 activation (Figure 4.21). This result agrees with the study conducted by Collier and Ettelaie (2011) which suggests that the magnitude of the release of MV is related to the level of activation of PAR2.

4.3.6 Examination of the influence of TF-fVII complex on the activation of PAR2 in HDBEC

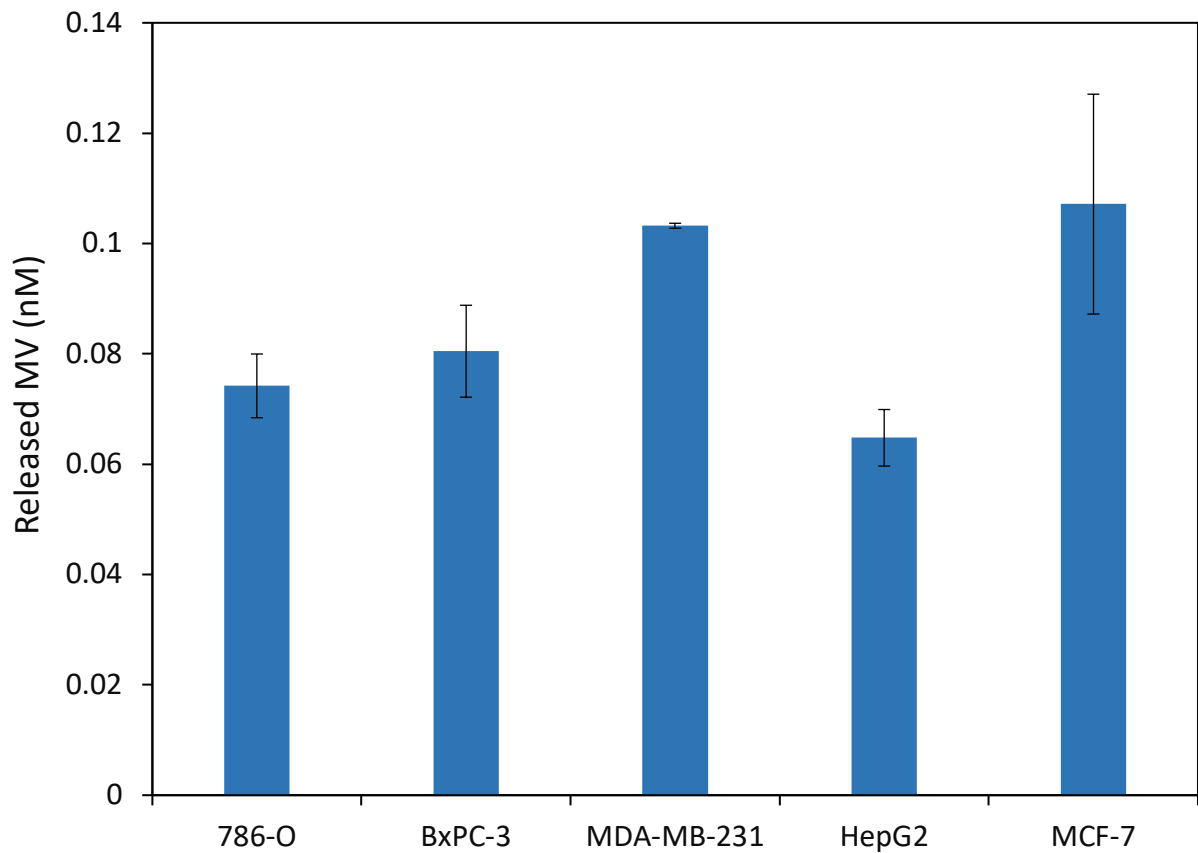
The aim of this study was to examine the influence of exogenous TF-fVIIa complex on PAR2 activation on the surface of HDBEC. The cells (10^4) were transfected with the mCherry2-short-length PAR2 construct (1 μ g) using TransIT-2020 transfection reagent. On the following day, the

Figure 4. 20 Auto-activation of PAR2 on the surface of the transfected cancer cell lines



Cell lines (10^4) were seeded into 96-well plates and permitted to adhere. The cells were then transfected with the mCherry2-short-length PAR2 construct (1 μ g) using the TransIT-2020 transfection reagent and incubated for 24 h at 37°C. On the following day, the media were replaced with serum-free medium and the cells incubated for 1 h. Parallel sets of cells were permeabilised with 0.01% (v/v) triton diluted in serum-free medium to facilitate the measurement of total mCherry2-short-length PAR2 hybrid protein expressed within the cells. The media was collected from all samples and the of mCherry2 fluorescence intensities in the supernatants of permeabilised and non-permeabilised samples were measured at (Ext. 580 nm, Em. 610 nm) with a plate reader. The percentage of PAR2 activation on the cells surface was then calculated by dividing the fluorescence of non-permeabilised cells medium by fluorescence of permeabilised cells medium multiplied by 100 (The results show the average of five independent experiments and expressed as the mean \pm SEM).

Figure 4. 21 Measurement of the MV release from the transfected cell lines



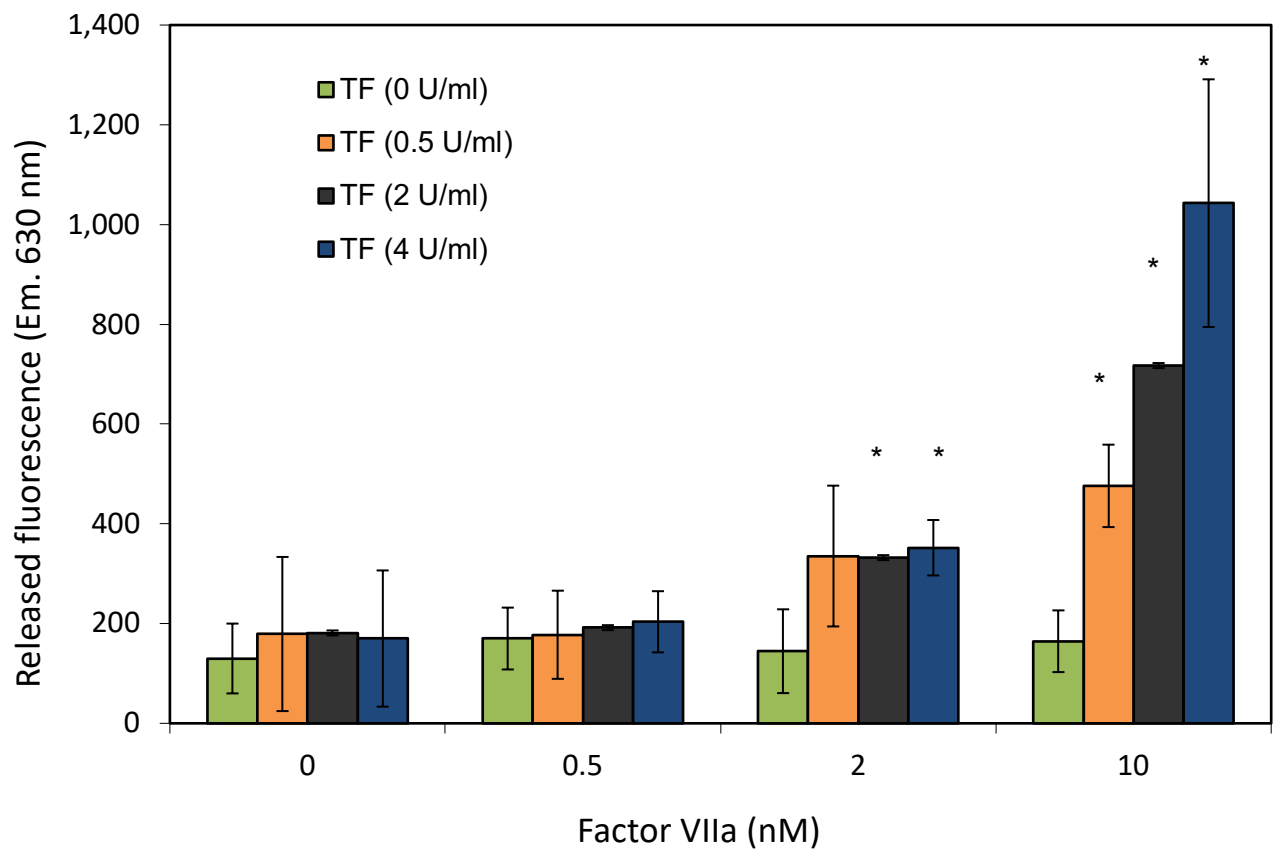
Cell lines (10^4) were seeded into 96-well plates and permitted to adhere. The cells were then transfected with the mCherry2-short-length PAR2 construct (1 μ g) using the TransIT-2020 transfection reagent and incubated for 24 h at 37°C. On the following day, the cells were adapted to serum-free medium for 1 h. Aliquots of media (50 μ l) were collected from the intact cells and analysed using the Zymuphen MP assay to determine the concentrations of released MV (The data is the average of three independent experiments and expressed as the mean \pm SEM).

cells were treated with a combination of recombinant TF (0-4 U/ml) and purified fVIIa (0-10 nM) and incubated for 1 h. The media was collected and the mCherry2 fluorescence intensities were measured (Ext. 580 nm, Em. 610 nm) with a plate reader. In the absence of TF, fVIIa (0-10 nM) had no detectable effect on PAR2 activation in HDBEC. Moreover, treatment of the transfected cells with TF alone or in combination with a low concentration of purified fVIIa (0.5 nM) did not result in significant release of mCherry2 fluorescence into the media. However, higher concentrations of fVIIa (2 nM), together with TF (0.5-4 U/ml) resulted in the activation of PAR2 which was significantly elevated in the presence of 10 nM fVIIa (Figure 4.22).

4.3.7 Examination of the influence of MV isolated from cell lines on PAR2 activation in HDBEC

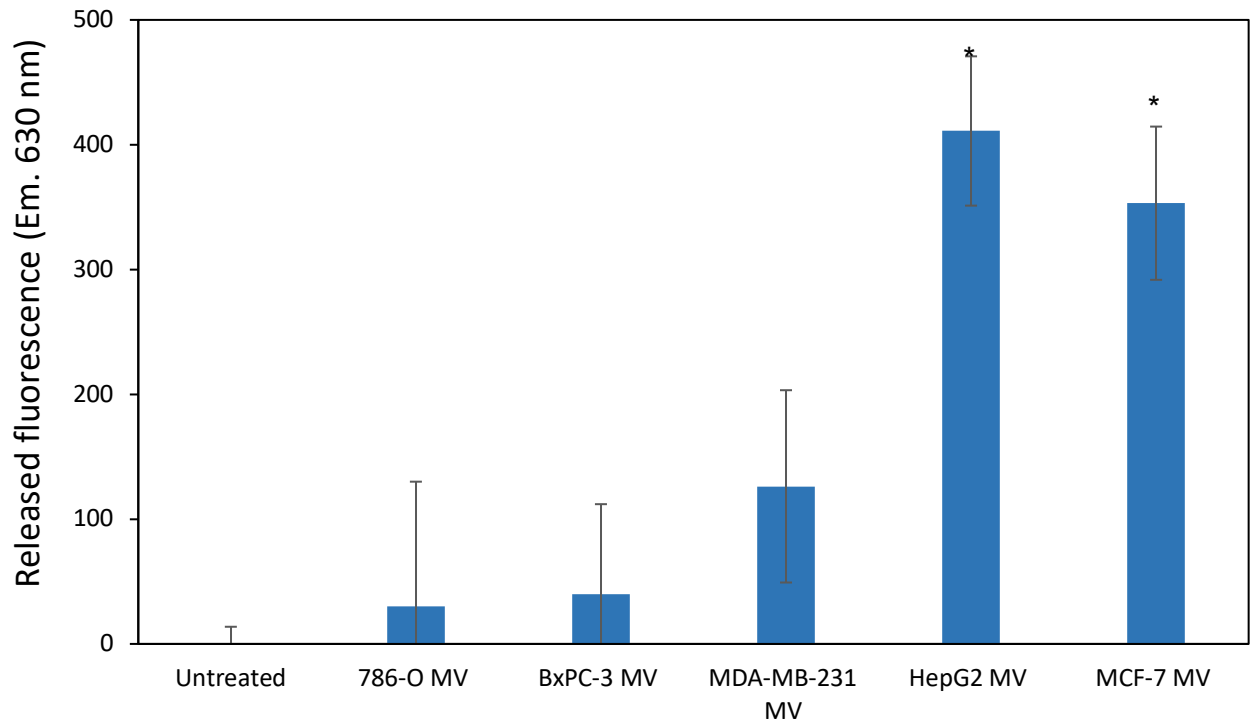
In the previous chapter, the amount of TF and fVII proteins were within MV isolated from different cell lines was quantified. One aim of the current study was to evaluate if the differences in the amount of these proteins in MV can influence PAR2 activation on the surface of HDBEC. The cells (10^4) were transfected with the mCherry2-short-length PAR2 construct (1 μ g) using the TransIT-2020 transfection reagent as before. On the following day, the cells were incubated for 1 h with MV (0.05 nM) derived from each different of the five cell lines (786-O, BxPC-3, MDA-MB-231, HepG2 and MCF7). The supernatants were collected and the mCherry2 fluorescence intensities were measured using a plate reader (Ext. 580 nm, Em. 610 nm). Treatment of the transfected HDBEC with MV isolated from HepG2 and MCF7 cell lines resulted in high levels of PAR2 activation while MV isolated from MDA-MB-231 cell line had a lower, but still significant influence on PAR2 activation. MV isolated from BxPC3 and 786-O cells were found to exert lower influence on PAR2 activation (Figure 4.23).

Figure 4. 22 Measurement of the activation of PAR2 in HDBEC by combinations of exogenous TF and fVIIa



HDBEC (10^4) were transfected with the mCherry2-short-length PAR2 construct (1 μ g) using the TransIT-2020 transfection reagent and incubated for 24 h at 37°C. The cells were then incubated for 1 h with a combination of recombinant TF (0-4 U/ml) and purified fVIIa (0-10 nM). The intensities of mCherry2 fluorescence in the media were then measured using a plate reader (Ext. 580 nm, Em. 610 nm) (The results show the average of five independent experiments and expressed as the mean \pm SEM; * = $p < 0.05$ versus the untreated sample).

Figure 4. 23 The influence of isolated MV from cell lines on PAR2 activation on the surface of HDBEC



HDBEC (10^4) were transfected with the mCherry2-short-length PAR2 construct ($1 \mu\text{g}$) using the TransIT-2020 transfection reagent and incubated for 24 h at 37°C . The cells were then incubated with MV (0.05 nM) isolated from cell lines (786-O, BxPC-3, MDA-MB-231, HepG2 and MCF7) for 1 h. The intensities of mCherry2 fluorescence in the media were then measured using a plate reader (Ext. 580 nm , Em. 610 nm) (The data is the average of five independent experiments and expressed as the mean \pm SEM; * = $p < 0.05$ versus the untreated sample).

4.4 Discussion

PAR2 has been reported to initiate many cellular functions involved in pathological and physiological processes including MV release, cell proliferation and cancer metastasis (Indrakusuma et al., 2017; Vergnolle et al., 1999; Rothmeier and Ruf, 2011; Yang et al., 2015; Collier and Ettelaie, 2011). PAR2 is expressed by various cells and can be activated by many proteases including the TF-fVIIa complex. It has been reported that as well as expressing TF, cancer cells can also express ectopic fVIIa (Yang et al., 2015; Ungefroren et al., 2017; Featherby et al., 2019). The expression of TF and fVIIa by cancer cells can result in the formation of TF-fVIIa complex on the cell surface which in turn promotes PAR2 auto-activation and enhances PAR2-initiated signalling (Ungefroren et al., 2017). One aim of this study was to measure the PAR2 activation on the surface of cancer cell lines by endogenous TF-fVIIa complex (auto-activation). For this purpose, the cDNA corresponding to the complete and the mature forms of PAR2 were sub-cloned into plasmids in tandem at the C-terminus of mEmerald or mCherry fluorescent tags encoded within the two plasmids used, respectively. The aim of using these two clones was to ensure the optimal surface expression of PAR2 cloned when transfected into HDBEC. While the cells showed a high level of surface expression of mCherry2-short-length PAR2 protein after 24 h, the mEmerald-full-length PAR2 construct was not expressed efficiently in the cells possibly due to incorrect transport to the cell surface.

On analysis, both MCF7 and MDA-MB-231 exhibited strong endogenous potential for PAR2 auto-activation while BxPC3 cell was less effective. In contrast, HepG2 and 786-O cells showed the lowest percentage of PAR2 activation although some level of activation was detectable (Figure 4.20). Studies conducted by ElKeeb et al. (2015) and Ethaeb et al. (2019) have shown that the accumulation of TF in endothelial cells can induce apoptosis whereas lower levels of TF promote cellular proliferation (Collier et al., 2008). Collier and Ettelaie

(2011) showed that the activation of PAR2 can induce the release of procoagulant MV containing TF. Therefore, the release of TF within MV has been proposed as a mechanism by which the cells can manage the excessive amounts of TF (Collier and Ettelaie, 2011, Date et al 2017). Furthermore, in the previous chapter it was shown that MCF7 and MDA-MB-231 cell lines expressed higher levels of TF than the other cells (Figures 3.6). Therefore, MCF7 and MDA-MB-231 cells displayed higher percentage of PAR2 activation in order to release the excessive amount of TF within MV and regulate the cellular TF. In contrast, 786-O cells were found to express a lower level of TF compared to other cell lines as well as a lower level of PAR2 activation. Further examination of cancer cells from various tissues may produce evidence for the different potential of different cancers for PAR2 activation. Even though the exact processes involved in MV release are not understood, it has been suggested that cellular activation or apoptosis can trigger the release of MV (Burnouf et al. 2015). In keeping with the above hypothesis, cell lines with the highest level of PAR2 activation (MCF7 and MDA-MB-231) also released the greatest amounts of MV compared to HepG2 and 786-O (Figure 4.21). The release of MV with different contents from cancer cells can in turn have various influences on the surrounding tissue as well as the whole body. Among the more exposed cells to circulating MV are the vascular endothelial cells. Therefore, to examine these influences further the outcome on endothelial cells were examined next.

It has been suggested that MV which originate from different cell types have different effects on endothelial cells (Lovren and Verma, 2013). Furthermore, in the previous chapter it was shown that the incubation of HCAEC with MV isolated from HepG2 or MCF-7 enhanced cell proliferation. In contrast, treating HCAEC with MV purified from 786-O cells induced cellular apoptosis. In this section of the study, MV were isolated from different cell lines and were then incubated with HDBEC expressing the mCherry2-short-length PAR2 protein and the level

PAR2 activation on the endothelial cells was examined. The results indicate that MV isolated from HepG2, MCF-7 and MDA-MB-231 were more efficient in activating PAR2 on the recipient endothelial cells respectively compared to those purified from 786-O cells. It is hypothesised that the amount of fVIIa and TF carried by the MV can determine the rate of PAR2 activation. In addition, although some level of TF was detected in MV isolated from HepG2, MCF-7 and MDA-MB-231, the MV from these cells was found to contain high levels of fVIIa (Figure 3.4). Therefore, while low amounts of TF may be sufficient for PAR2 activation, a minimum concentration of fVIIa associated with the MV is a prerequisite to PAR2 activation on the recipient cells. In support of this, MV purified from 786-O cell which possess low concentrations of fVIIa but high amounts of TF showed a low potential for PAR2 activation on endothelial cells. Therefore, these results strongly suggest that the amounts of both fVIIa and TF within MV are important criteria for the potential of cancer cell-derived MV to activate PAR2 on the recipient cells (Figure 4.24).

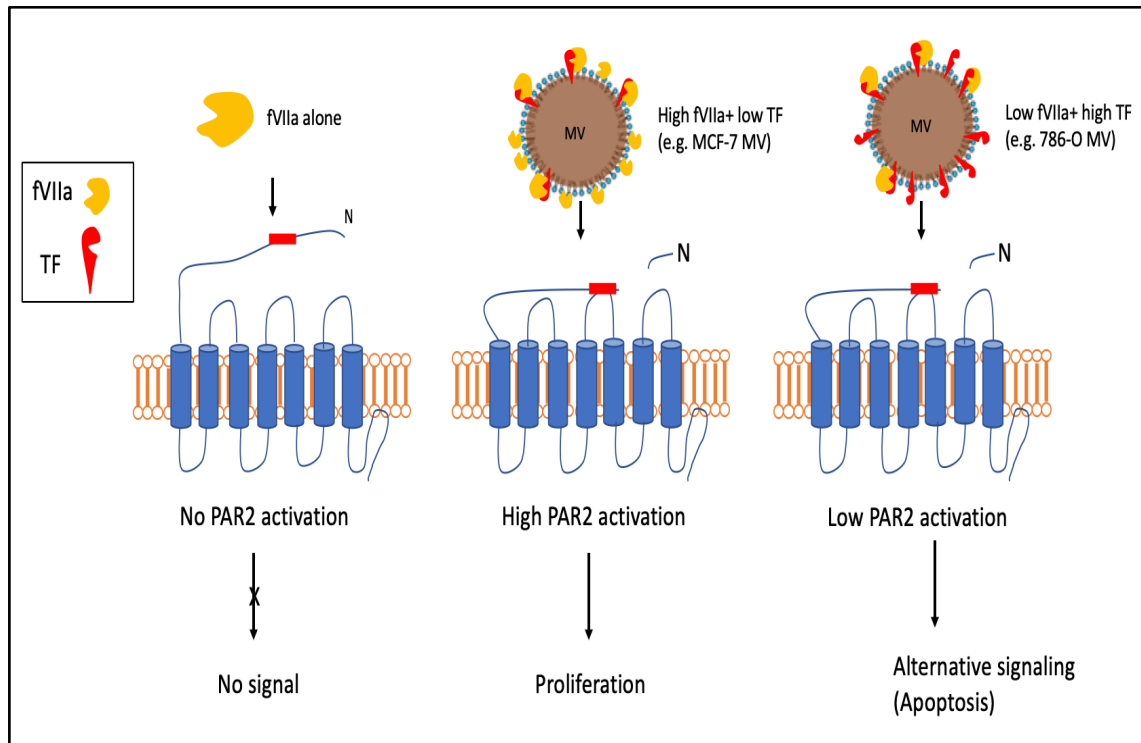
As well as the quantities, the ratio of fVIIa:TF within MV appears to be a determinant of the outcome on the endothelial cells. In the previous chapter, it was shown that MV isolated from HepG2, MCF7 and MDA-MB-231 exhibited high ratios of fVIIa:TF and were also found to enhance endothelial cell proliferation. In contrast, MV purified from 786-O displayed a lower ratio of fVIIa:TF and was capable of inducing cellular apoptosis (Figure 3.10). However, inhibition of PAR2 activation by antibody (SAM11; 20 µg/ml) abolished both MV-induced mechanisms involved in proliferation and apoptosis (Figure 3.15). An explanation for the different behavior of the MV isolated from these cell lines may also involve the dissimilar potential of these cells to activate PAR2.

Furthermore, in the previous chapter it was demonstrated that incubation of HCAEC with either MV isolated from 786-O or PAR2-AP promoted the internalization of PAR2, causing less accessibility of this receptor protein on the cell surface. This may also be an explanation for the lower influence of MV isolated from 786-O cells on PAR2 activation, although the mechanism needs clarification. A separate study was thus undertaken to further investigate the influence of the ratio of fVIIa:TF on activation of PAR2, using exogenous TF and fVIIa and measuring the release of mCherry from HDBEC transfected to express the mCherry2-short-length PAR2 protein. In agreement with above results, incubation of the transfected cells with fVIIa alone or with a low concentration (0.5 nM) in combination with TF (0.5 U/ml) did not induce PAR2 activation. This observation is in agreement with the result obtained in the previous chapter which showed that incubation HCAEC with fVIIa alone (2-10 nM) had no effect on cell proliferation (Figure 3.12). Additionally, it would be expected that some of the exogenous fVIIa will be lost in the media and therefore the threshold concentrations could not be achieved in order to activate PAR2. In contrast, treatment of cells with higher concentrations of exogenous fVIIa (2 nM) together with either concentration of recombinant TF (0.5-4 U/ml) resulted in significant release of mCherry. This release was significantly enhanced when using a higher concentration of fVIIa (10 nM) and further supports the dependence on fVIIa activity (Figure 4.22). Finally, while it was originally aimed to examine the activation of PAR2 by both fVIIa and fXa, because fXa is capable of multiple digestion of the mCherry2 protein, it was not possible to repeat the study using fXa.

In conclusion, cancer cells can auto-activate by expressing endogenous fVIIa and TF through a mechanism involving PAR2 activation. The amounts of TF and fVIIa influence the rate of PAR2 activation in cancer cells and consequently determine the amount of MV released. In addition, cancer cells appear to regulate the presence of excessive amounts of TF through

release within MV. This *in vitro* study highlights some of the properties of MV released with different types of cancers that express TF (Kleinjan et al., 2012). In addition, analysis of the differences in MV-associated TF and fVIIa in circulating MV from patients with diabetes, hypertension, myocardial infraction or cancers (Badimon et al., 2017) may have ramifications for understanding the disease progress and the nature of the affected organs. In particular, the increase in the amount of MV release can cause endothelial dysfunction (Boulanger et al., 2001; Badimon et al., 2017) which subsequently result in endothelial denudation and disease (Davignon and Ganz, 2004). Therefore, in order to examine the mechanism by which endothelial cells cope with the excessive amounts of TF, the association of TF, fVIIa, and PAR2 proteins on cells was investigated in the next chapter.

Figure 4. 24 The proposed role of TF-fVIIa complex on PAR2 activation



The activation of PAR2 can be regulated by the amounts of TF and fVIIa proteins. fVIIa alone is not capable of activating PAR2. However, high concentration of fVIIa in combination with TF, associated with MV possess a potential for PAR2 activation and induce cell proliferation signal. In contrast, low concentrations of fVIIa, particularly in conjunction with high concentration of TF, results in lower PAR2 activation but produces an alternative signal promoting cell apoptosis.

Chapter 5

Excess tissue factor is preferentially cleared from the surface of endothelial cells through microvesicle release and caveolae-mediated internalisation

5.1 Introduction

The presence of cancer increases the risk of VTE which is considered one of the main causes of mortality and morbidity in cancer patients. It is estimated that up to 20% of cancer patients will develop VTE at some point during disease condition (Khorana et al., 2007). The most commonly encountered venous thrombotic complications are deep vein thrombosis (DVT) and pulmonary embolism (PE) (Heit et al., 2000). It has been shown that patients who suffer from chronic disease such as atherosclerosis, cancer and other inflammatory conditions express higher levels of TF compared with healthy individuals (Tatsumi and Mackman, 2015; Eisenreich et al., 2016; Witkowski et al., 2016). TF-fVIIa complex is known as a main initiator of the coagulation system. In addition, TF-fVIIa complex on cell surfaces is capable of regulating a number of cellular functions including MV release, cell proliferation, angiogenesis, and tumour metastasis (Rao and Pendurthi, 2005; Belting et al., 2005; Collier and Ettelaie, 2010). However, recent studies conducted by ElKeeb et al. (2015) and Ethaeb et al. (2019) have shown that the accumulation of TF in endothelial cells can induce apoptosis. Apoptosis can give rise to impairment of cellular functions leading to vascular endothelial cell denudation associated with a number of chronic diseases. It has been also demonstrated that the formation of TF-fVIIa complex is required for PAR2 activation (Camerer et al., 2000; Riewald and Ruf, 2001; Rao and Pendurthi, 2005). Collier and Ettelaie (2011) showed that the activation of PAR2 can induce the release of procoagulant MV containing TF. This has been proposed as a mechanism by which the cells can manage the excessive amounts of TF associated with inflammatory condition (Collier and Ettelaie, 2011). However, the role of fVIIa is largely unexplored. Although, liver cells are known to be the main producer of the fVII protein, cancer cells such as ovarian have been shown to express ectopic fVII as well as TF expression (Koizume et al., 2006; Yokota et al., 2009; Koizume and Miyagi, 2015). It was demonstrated in chapter 3 that repeated treatment of endothelial cells with recombinant TF

reduced the amount of fVII stores available within cells (Figure 3.24). In addition, the magnitude of these reductions was dependent on amount of fVII that was released within MV (Figure 3.25). The repetitive treatment of cells with TF resulted in the depletion of cellular fVII reserves in endothelial cells. As a result, the process of activation of PAR2 and TF release within MV became impaired. A study conducted by Kawamoto et al. (2012) showed that MV isolated from cancer cells were taken up by endothelial cells through endocytic processes. A similar study conducted by Collier et al. (2013) demonstrated that TF associated MV can be internalised and recycled by endothelial cells.

Endocytic mechanisms are cellular processes by which receptor proteins or their ligands are engulfed within the cells. Once the cargo is endocytosed by the cell, it can be either degraded, stored within Golgi apparatus or recycled to the cell surface (Grant and Donaldson, 2009). There are a number of mechanisms by which endocytosis process can occur including the clathrin-dependent, clathrin-independent, and the caveolae-dependent mechanisms. However, it has been suggested that the prominent mechanism by which cells regulate cargo uptake is the clathrin-dependent process (Aguilar and Wendland, 2005). The internalisation of TF-fVIIa-TFPI complex has also been demonstrated to be mediated through the clathrin-dependent mechanism (Hamik et al., 1999). However, a study conducted by Hansen et al. (2001) showed that TF-fVIIa complex alone is internalised through the clathrin-independent processes. This suggests an alternative mechanism by which these proteins are endocytosed. It has been shown that TF can localise within cholesterol rich membrane microdomains, including the caveolae and the lipid rafts (Mandal et al., 2005). Caveolae are small (50-100 nm), flask-shaped, invaginations within the plasma membrane and differ from lipid rafts in that caveolae contain caveolin proteins as well as being rich in cholesterol within the membrane (Mandal et al., 2005). Caveolae dynamically harbour receptor proteins which may include TF protein (Sevinsky et al., 1996). In fact, a number of studies have suggested that TF protein alone, or in

complex with fVIIa can associate with caveolae (Liu et al., 1997; Sevinsky et al., 1996; Mulder et al., 1996; Mandal et al., 2006; Awasthi et al., 2007). Furthermore, the depletion of cholesterol from the cell membrane significantly reduced the amount of TF associated with lipid rafts (Mandal et al., 2006). Dietzen et al. (2004) suggested that the TF present within caveolae remains in an encrypted form. This caveolae-associated TF may act as a latent pool which becomes activated once the caveolae release their content (Mulder et al., 1996). In support of this hypothesis, depletion of cholesterol from the cell membrane was shown to increase TF procoagulant activity on the cell surface (Dietzen et al., 2004).

5.1.1 Aims

The results obtained in chapter 3 showed that cancer cells have the ability to express fVII. It was also demonstrated that TF-fVIIa complex can induce cellular apoptosis in HCAEC which was shown to be mediated through PAR2. Therefore, the first aim of this study was to examine the association of TF and fVII with PAR2 in MDA-MB-231 cell line using PLA. It was also demonstrated that the repeated treatment of HCAEC with recombinant TF resulted in the depletion of cellular reserves of fVII and the exhaustion of MV release. However, some TF appeared to remain on the cells even after the release of MV by the cells. Since the mechanism of releasing TF within MV might not be enough to manage the excess amounts of TF, it was hypothesised that cells may also manage the excess TF through caveolae uptake where it can be stored in a non-functional form. Therefore, the second aim of this study was to investigate the association of TF and fVII with caveolin-1 in HCAEC by PLA. In addition, the co-localisation of labelled TF with caveolae on the surface of HCAEC was examined by confocal microscopy. Finally, the influence of cholesterol-depletion of cell-membrane on TF-mediated cell apoptosis was assessed.

5.2 Methods

5.2.1 Optimization of the knockdown of fVII expression using siRNA

Small interfering RNA (siRNA) is a synthetic version of a small double-stranded RNA (consisting of 21-25 nucleotides) which can interfere with mRNA translation by enhancing the degradation of messenger RNA coding for specific proteins. The prevention of the synthesis of specific protein using this procedure is known as knockdown or siRNA silencing (Agrawal et al, 2003). A set of siRNA (Ambion® Silencer® Select Pre-designed siRNA) specific for the coagulation factor VII was used to silence the expression of fVII protein in MDA-MB-231 cell line. In order to optimize the silencing, a range of fVII siRNA concentration (0-200 nM) was initially used to determine the optimal concentration for suppressing the expression of fVII protein. MDA-MB-231 cells (8×10^4) were seeded into 6-well plates and incubated overnight. On the following day, the media was replaced with 0.9 ml of complete fresh medium and incubated for 30 min at 37°C. The cells were subsequently transfected with the different concentrations of fVII siRNA using Trans IT-2020 transfection reagent, as described in section 4.2.14.2. The cells were incubated for 48 h at 37°C and lysed in Laemmli buffer. To test the efficiency of gene silencing, the samples were subjected to western blot analysis, as described in section 2.2.8. The nitrocellulose membranes were incubated with a mouse polyclonal anti-fVII antibody 1:2000 (v/v) and developed with a goat anti-mouse antibody 1:4000 (v/v). The membranes were analysed by the ImageJ program to determine the level of expression of fVII protein. The expression levels were normalised against the respective GAPDH.

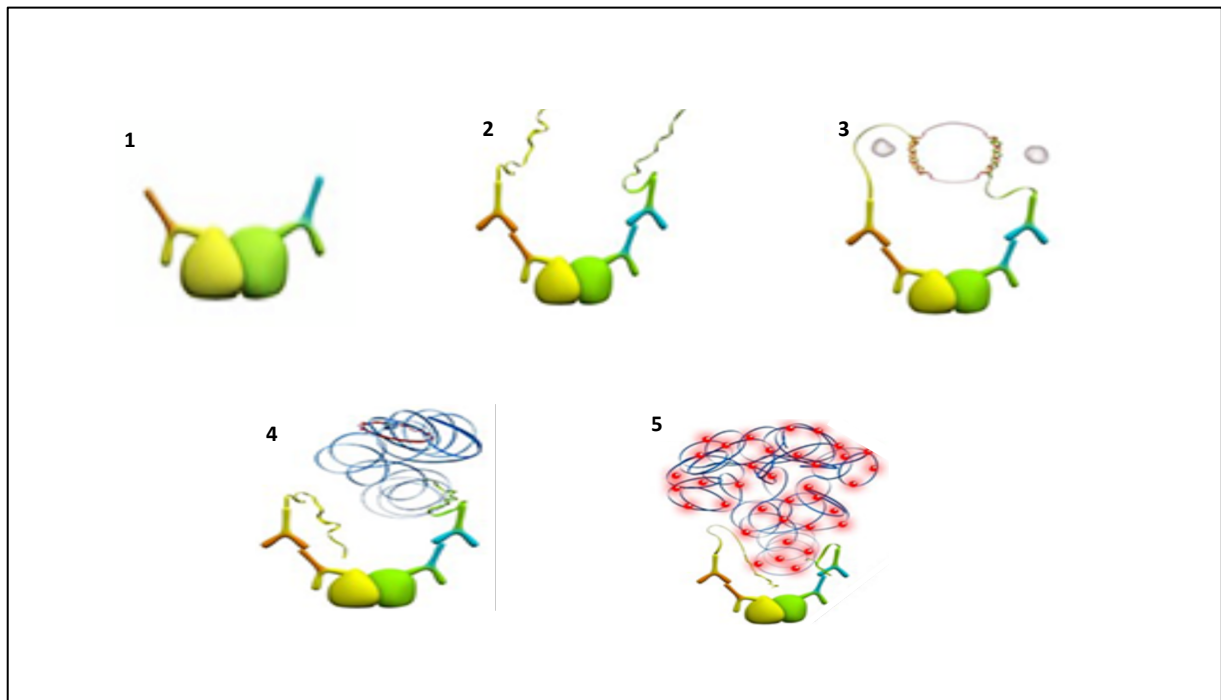
5.2.2 *In situ* Proximity ligation assay (PLA) using the Duolink® kit

Duolink® *in situ* proximity ligation assay is a sensitive technique that detects protein-protein interactions in cells. PLA is sensitive to the proximity of proteins if within 40 nm of each other. During the procedure, proteins of interest are probed with primary antibodies raised in two

different species. These are then labelled using complementary oligonucleotide-labelled secondary antibodies (plus and minus probes, respectively) specific to IgG from the two species. The proximity of the PLA probes produces a closed circular DNA template, which can be amplified using a polymerase enzyme. Consequently, a signal is generated only when the two PLA probes interact in close proximity. The amplified DNA is then detected by hybridizing a fluorescence-labelled oligo-nucleotides and counting the number of fluorescent labels using an appropriate microscope (Figure 5.1).

Cells (10^4) were seeded into glass bottom dishes (35 mm) and allowed to attach. The media was then removed. The cells were washed twice with PBS buffer and fixed with 4% (v/v) formaldehyde for 15 min at room temperature. The cells were then washed again with PBS and blocked with Duolink[®] blocking solution provided with kit (100 μ l/well) for 75 min at room temperature with shaking. After the incubation, the blocking solution was discarded and the samples were incubated with the two primary antibodies (dilute 1:100 v/v with Duolink[®] Antibody Diluent) overnight at 4°C. On the following day, the samples were washed twice with the provided wash buffer A (0.01 M Tris, 0.15 M NaCl and 0.05% (v/v) Tween 20; pH 7.4) each time for 10 min and then incubated with plus and minus PLA probes (dilute 1:5 v/v with Duolink[®] Antibody Diluent) for 1 h at 37°C. The samples were washed twice with buffer A and the ligation mixture (8 μ l ligation + 1.25 μ l ligation enzyme + 32 μ l dH₂O) was added into each dish and incubated for 30 min at 37°C. The cells were then washed twice with wash buffer A and the amplification mixture (8 μ l amplification stock + 40 μ l dH₂O + 0.625 μ l polymerase) was added into each sample and incubated at 37°C for 2 h in the dark. The cells were then washed with the wash buffer B (0.2 M Tris and 0.1 M NaCl; pH 7.5) for 10 min. The samples were then washed twice with wash buffer B (1:100 diluted) for 2 min and then stained with DAPI (2 μ g/ml) and phalloidin-iFluor 488 (2 μ g/ml) for 10 min. Finally, the cells were

Figure 5. 1 The principle of Duolink[®] *in situ* proximity ligation assay reaction



Duolink[®] *in situ* proximity ligation assay is a sensitive technique that detects protein-protein interactions in cells. **(1)** Proteins of interest are probed with primary antibodies raised in two different species. **(2)** The primary antibodies then labelled using complementary oligonucleotide-labelled secondary antibodies (plus and minus probes, respectively) specific to IgG from the two species. **(3)** The proximity of the PLA probes produces a closed circular DNA template. **(4)** The DNA template can be amplified using a polymerase enzyme. **(5)** The amplified DNA is then detected by hybridizing a fluorescence-labelled oligo-nucleotides and counting the number of fluorescent labels using an appropriate microscope (Adapted from www.sigmaaldrich.com).

washed twice with wash buffer B (1:100 diluted) for 2 min and analysed using a fluorescence microscope with a X40 magnification.

5.2.3 Examination the association of TF, fVII and PAR2 proteins

This experiment was aimed to assess the interaction between the TF, fVII and PAR2 proteins. The proximity of each of the proteins TF, fVII and PAR2 was examined using the Duolink[®] PLA. MDA-MB-231 cells (10^4) were seeded into glass bottom dishes (35 mm) and allowed to adhere. The cells were fixed and probed with a mouse anti-fVII antibody (10 $\mu\text{g/ml}$) and a rabbit anti-TF antibody (5 $\mu\text{g/ml}$) to examine the interaction between fVII and TF. when testing the proximity between fVII and PAR2, the cells were probed with a rabbit anti-fVII antibody (10 $\mu\text{g/ml}$) and mouse anti-PAR2 antibody (SAM11; 20 $\mu\text{g/ml}$). Also, sets of cells were probed with a rabbit anti-TF antibody (5 $\mu\text{g/ml}$) and a mouse anti-PAR2 antibody (SAM11; 20 $\mu\text{g/ml}$) to examine the association of TF and PAR2 proteins. The procedure was carried out as described in section 5.2.2.

In addition, the influence of fVIIa on the association of TF and PAR2 was evaluated. The expression of fVII in MDA-MB-321 cells was suppressed using fVII siRNA. MDA-MB-321 cells (10^4) were seeded into glass bottom dishes (35 mm) and allowed to adhere. The cells were subsequently transfected with the optimal concentration fVII siRNA (150 nM) as determined in section 5.3.2. Additionally, a set of transfected cells devoid fVII were supplemented with exogenous fVIIa (10 nM). The cells were then fixed with 4% (v/v) formaldehyde and probed with a rabbit anti-TF antibody (5 $\mu\text{g/ml}$) and mouse anti-PAR2 antibody (SAM11; 20 $\mu\text{g/ml}$). A set of cells were also examined without any antibodies and used as a control. The proximity between TF and PAR2 protein was then assessed in all samples using PLA.

The association of fVII and PAR2 protein was examined in the absence of TF. The interaction between fVII and PAR in MDA-MB-231 TF knockout cells (Rondon et al., 2018) was assessed

to examine if TF is required for fVIIa and PAR2 association. To ensure the MDA-MB-231 TF knockout cells lacked TF protein, the cells were first examined by flow cytometry. In addition, MDA-MB-231 TF knock out cells were supplemented with a range of concentration of recombinant TF (0-4 U/ml) for 24 h and cell numbers assessed using crystal violet assay prior to the PLA experiment. MDA-MB-231 TF knockout cells were seeded into glass bottom dishes (35 mm) and allowed to adhere. The cells were then fixed with 4% (v/v) formaldehyde and probed with a rabbit anti-fVII antibody (10 µg/ml) and a mouse anti-PAR2 antibody (SAM11; 20 µg/ml). A set of wild type MDA-MB-231 cells were used as control. The interaction between fVII and PAR2 was examined using PLA, as described in 5.2.2.

5.2.4 Examination of the association of fVII and TF within caveolin-1 in HCAEC

In chapter 3, it was demonstrated that the stimulation of HCAEC with recombinant TF results in a significant increase in cell surface fVII antigen (Figure 3.22). It was speculated that the additional fVII antigen might be released from the caveolae on the cell surface following cell stimulation. Therefore, this study was designed to investigate the association of fVII and TF within caveolin-1 in HCAEC. To assess the interaction between fVII and caveolin-1, HCAEC (10^4) were seeded into glass bottom dishes (35 mm) and permitted to adhere. The cells were then treated with a range of human recombinant TF (0-4 U/ml) for up to 40 min. A set of untreated cells were used as a control. The cells were fixed and permeabilised with 0.01 % (v/v) Triton. The cells were then probed with a mouse anti-fVII antibody (10 µg/ml) and a rabbit anti-caveolin-1 antibody (10 µg/ml). The association of fVII and caveolin-1 was then assessed using PLA.

In addition, the proximity between TF and caveolin-1 in HCAEC was evaluated. HCAEC (10^4) were seeded into glass bottom dishes (35 mm) and permitted to adhere. The cells were then treated with a range of recombinant TF (0 -4 U/ml) for up to 40 min. The cells were then fixed,

permeabilised with 0.01 % (v/v) Triton and probed with a mouse anti-TF antibody (5 µg/ml) and a rabbit anti-caveolin-1 antibody (10 µg/ml). The association of TF and caveolin-1 was examined using PLA as described in section 5.2.2.

5.2.5 Optimisation of the depletion of cell-membrane cholesterol in HCAEC

One of the most common chemical methods used in cholesterol removal is methyl- β -cyclodextrin (M β CD). In this study, a protocol described by Christian et al. (1997), using M β CD was adapted for the removal of cholesterol from cell membranes. HCAEC (2×10^4) were seeded in 96-well plates containing complete medium and incubated overnight. On the following day, the media was removed and the cells were treated with a range of concentrations of M β CD (0-5 mM) diluted in serum-free MV medium (w/v) for 1 h at 37°C. After the incubation, the cells were washed twice with PBS and incubated with complete MV medium for 24 h at 37°C. Cell numbers were then measured using crystal violet assay as described in 2.2.11 to determine the optimal concentration of M β CD in order to maintain cell viability.

5.2.6 Optimization the M β CD:cholesterol molar ratios for labelling lipid rafts in HCAEC

This study was aimed to further investigate the association of TF and cavolin-1 initially examined using PLA in section 5.2.4. The experiment was designed to label lipid rafts (including caveolae) and recombinant TF with fluorescent tags and examine the localisation of TF. The cellular cholesterol in HCAEC was depleted using M β CD as described in section 5.2.5 and replaced with 3-dodecanoyl-NBD cholesterol which is fluorescently-tagged (Ext. 465 nm, Em. 535 nm). The experiment was optimized using a range of M β CD (0- 2 mM) in conjunction with NBD cholesterol at molar ratios 6:1, 8:1 and 12:1. HCAEC (10^4) were seeded into glass bottom dishes (35 mm) and permitted to adhere. Subsequently, the cells were treated with the various M β CD:NDB cholesterol complexes and then incubated for 1 h at 37°C. The media was discarded, and the cells were fixed with 4% (v/v) formaldehyde for 15 min. The cells were then

washed with PBS and stained with DAPI (2 µg/ml) for 10 min. The cells were finally washed twice with PBS and visualized using a fluorescence microscope with a X40 magnification.

5.2.7 Labelling human recombinant TF using the Lightning-Link® Rapid Texas Red® conjugation kit

Human recombinant TF (1 µg/ml) was labelled with a Texas Red® tag using the Lightning-Link® conjugation kit. TF (1 µg/ml) was diluted with the LL-Modifier reagent provided with the kit at a ratio 10:1 (v/v). The mixture was then added into the lyophilized Lightning-Link® vial, gently shaken, and then incubated overnight at room temperature in the dark. The LL-quencher reagent provided with the kit was then added to the vial at a ratio 1:4 and incubated at room temperature for 30 min in the dark which acts to remove any unlabelled Texas Red. To examine the success of the labelling procedure, HCAEC were seeded into glass bottom dishes (35 mm) and allowed to adhere. The cells were then incubated with the labelled Texas-Red -TF (5.2 ng/ml) for 30 min. The cells were then fixed with 4% (v/v) formaldehyde and stained with DAPI (2 µg/ml) for 10 min. The cells were then washed twice with PBS and visualized using a fluorescent microscope with a X40 magnification.

5.2.8 Analysis of the co-localisation of TF on the surface of HCAEC by confocal microscopy

To examine the co-localisation of the recombinant TF on the surface of cells, HCAEC (10^4) were seeded out into glass bottom dishes (35 mm) and permitted to adhere. The cells were subsequently enriched in NBD cholesterol at a ratio 8:1 as above and incubated for 1 h at 37°C. After the incubation, the cells were washed and incubated with the Texas Red-conjugated TF (5.2 ng/ml) for up to 40 min at 37°C. After the incubation, the cells were fixed with 4% (v/v) formaldehyde for 15 min, washed with PBS and stained with DAPI (2 µg/ml) for 10 min. Subsequently, the cells were washed again two times with PBS. The cells were then analysed

for TF cell surface using a Zeiss LSM 710 confocal microscope with a X60 magnification and the images were acquired by the ZEN software.

5.2.9 Evaluating the influence of cell-membrane cholesterol on preventing TF inducing apoptosis in HCAEC

This study was designed to investigate the influence of cell-membrane cholesterol on induction of cell apoptosis by TF. Initially, the cell-membrane cholesterol in HCAEC was depleted using a range of M β CD (0-5 mM). The cholesterol depleted cells and the normal cells were then stimulated with recombinant TF (4 U/ml) to induce apoptosis. The cells were subsequently incubated for 24 h at 37°C and the cell numbers were determined using crystal violet assay, as described in 2.2.11.

5.3 Results

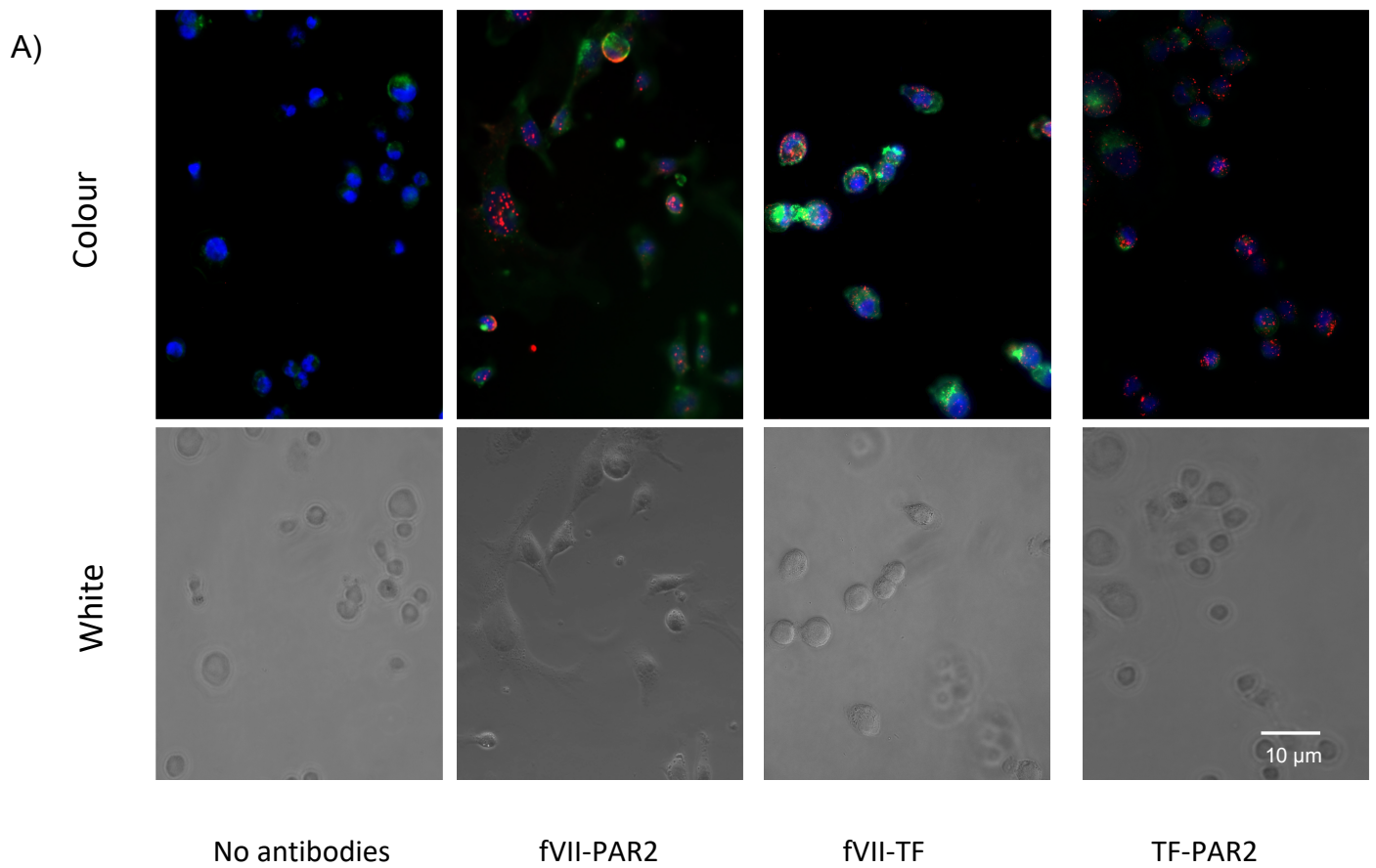
5.3.1 Examination of the interactions of fVII, TF and PAR2 in cancer cells using PLA

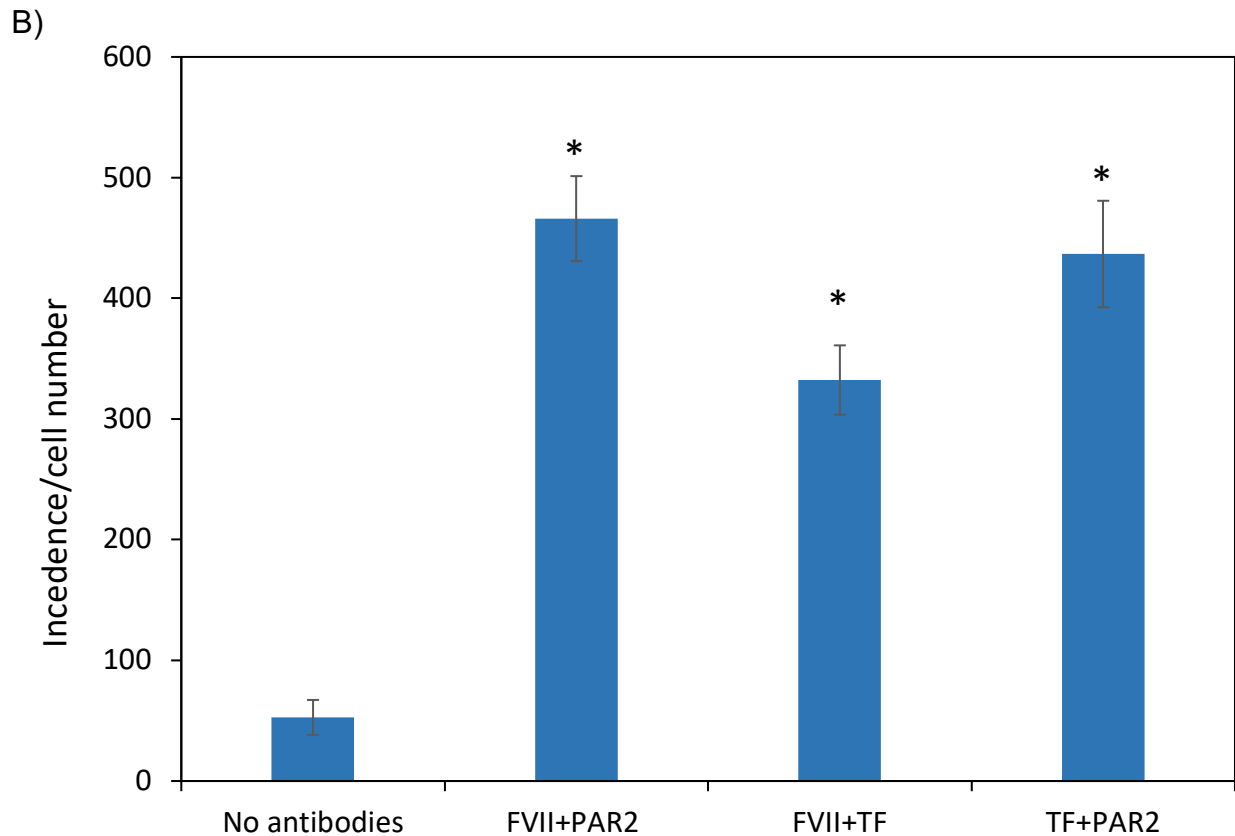
This experiment aimed to assess the interaction between TF, fVIIa and PAR2 proteins. The proximity of each of the proteins with the other two was examined in turn using the Duolink[®] PLA. MDA-MB-231 cells (10^4) were seeded into glass bottom dishes (35 mm) and allowed to adhere. The cells were fixed and probed with a mouse anti-fVII antibody (10 $\mu\text{g/ml}$) and a rabbit anti-TF antibody (5 $\mu\text{g/ml}$) to confirm the interaction between fVIIa and TF. When examining the proximity between fVIIa and PAR2, the cells were probed with a rabbit anti-fVII antibody (10 $\mu\text{g/ml}$) and a mouse anti-PAR2 antibody (20 $\mu\text{g/ml}$). Finally, sets of cells were probed with a rabbit anti-TF antibody (5 $\mu\text{g/ml}$) and a mouse anti-PAR2 antibody (20 $\mu\text{g/ml}$) to examine the proximity between TF and PAR2 proteins. Analysis of cells using PLA showed close proximity between all of these proteins (Figure 5.2 A and B). The results also suggest that the association between fVIIa, TF and PAR2 proteins may be initiated by the formation of TF-fVIIa complex which may then form a ternary complex with PAR2.

5.3.2 Optimization of the silencing of fVII expression in MDA-MB-231 cell line

To examine whether fVIIa is required for the interaction between TF and PAR2, the silencing of fVII expression in MDA-MB-321 cells was optimised using a specific fVII-siRNA. MDA-MB-231 cells (8×10^4) were seeded into 6-well plates and incubated overnight. The cells were transfected on the following day with a range of fVII siRNA (0-200 nM) and incubated for a further 48 h. The expression of fVII protein was then analysed by western blot and the membranes were analysed by the ImageJ program. The amount of fVII protein was normalised against GAPDH, as described in 5.2.1. Assessment of fVII knockdown using fVII-siRNA showed a reduction in the protein expression content as follows. Maximal gene silencing was 82% obtained using 200 nM fVII-siRNA, while transfection with 150 nM resulted in

Figure 5. 2 Interactions between fVII, TF and PAR2 as detected by PLA





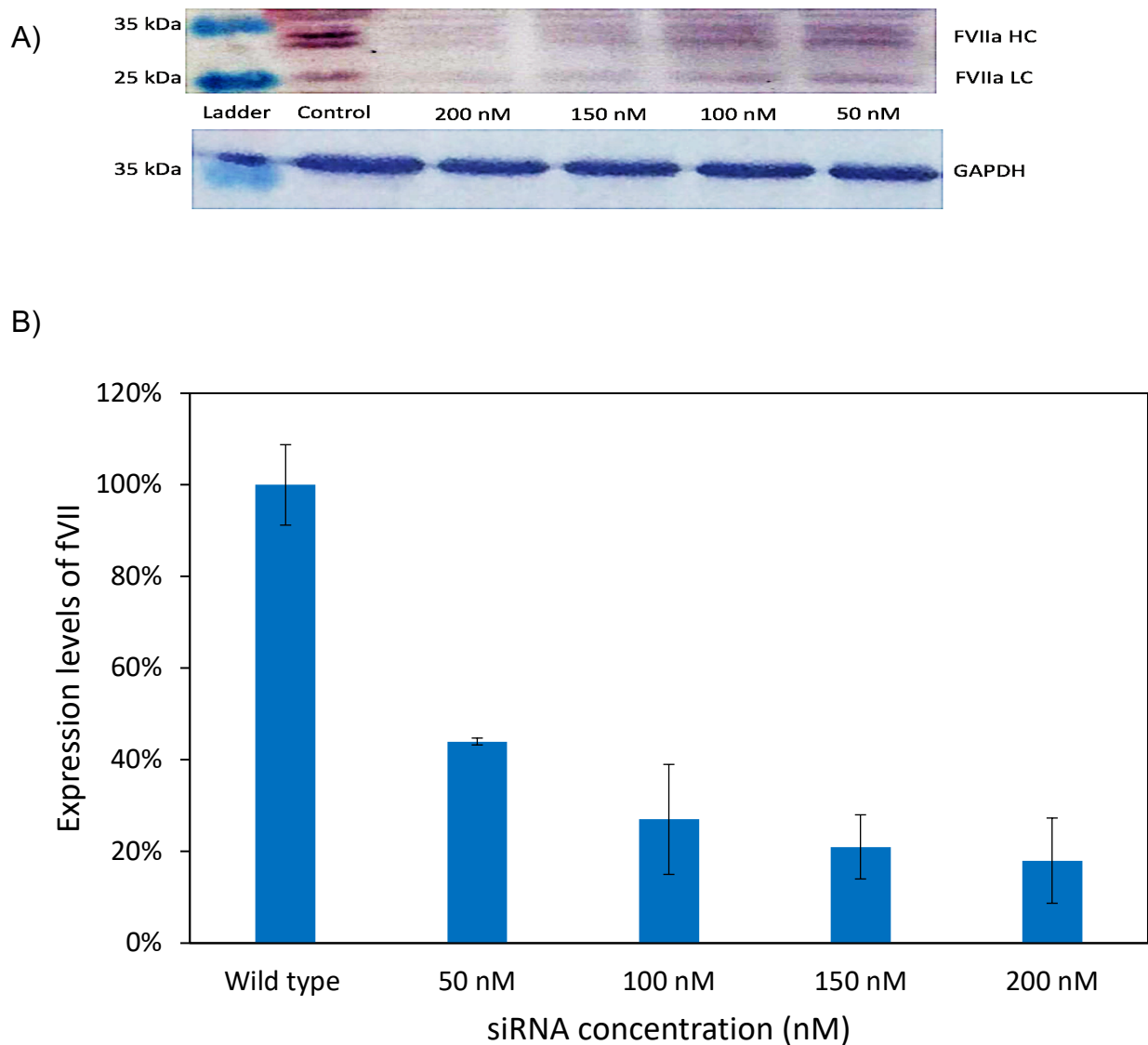
MDA-MB-231 cells (10^4) were seeded into glass bottom dishes (35 mm) and allowed to adhere. The cells were fixed with 4% (v/v) formaldehyde. The cells then probed with a mouse anti-fVII antibody (10 $\mu\text{g/ml}$) and a rabbit anti-TF antibody (5 $\mu\text{g/ml}$) to assess the interaction between fVIIa and TF. To examine the association of fVIIa and PAR2, another set of cells were probed with a rabbit anti-fVII antibody (10 $\mu\text{g/ml}$) and a mouse anti-PAR2 antibody (20 $\mu\text{g/ml}$). Sets of cells were probed with a rabbit anti-TF antibody (5 $\mu\text{g/ml}$) and a mouse anti-PAR2 antibody (20 $\mu\text{g/ml}$) to examine the interaction between TF and PAR2. Another set of cells were examined without antibodies and used as a control. **(A)** Proximity ligation assay was performed and the cells were then stained with phalloidin-iFluor 488 (green; 2 $\mu\text{g/ml}$) and DAPI (blue; 2 $\mu\text{g/ml}$) and visualized by fluorescence microscopy with a X40 magnification. **(B)** Ten images were captured for each sample and the number of incidences were determined using the ImageJ software (The results show the average of three independent experiments and expressed as the mean \pm SEM; * = $p < 0.05$ vs devoid of antibodies).

approximately 79% reduction of fVII protein expression. However, cell viability was preserved when using 150 nM of fVII-siRNA but was reduced when using 200 nM siRNA. Therefore, 150 nM of fVII-siRNA was considered the optimal concentration for further studies to silence fVII expression (Figure 5.3 A and B).

5.3.3 Examination of the influence of fVII on the association of TF and PAR2 protein

To examine whether fVIIa is essential for the interaction between TF and PAR2, the expression of fVII was suppressed in MDA-MB-321 cells using a fVII siRNA. The interaction between TF and PAR2 was then assessed by PLA. MDA-MB-321 cells (10^4) were seeded into glass bottom dishes (35 mm) and allowed to adhere. The cells were subsequently transfected with fVII-siRNA (150 nM) according to the optimized procedure described in section 5.3.2. Additionally, a set of siRNA-transfected cells was supplemented with exogenous fVIIa protein (10 nM). The proximity between TF and PAR2 was then assessed in all cell samples and controls using PLA. The data indicates that the reduction in fVIIa expression significantly disrupted the association between TF and PAR2 in MDA-MB-231 cells (Figure 5.4 A and B). Furthermore, supplementation of the siRNA-transfected cells with exogenous fVIIa marginally restored the interaction between TF and PAR2. Therefore, these results suggest that fVIIa is an essential component which facilitates the interaction of TF with PAR2.

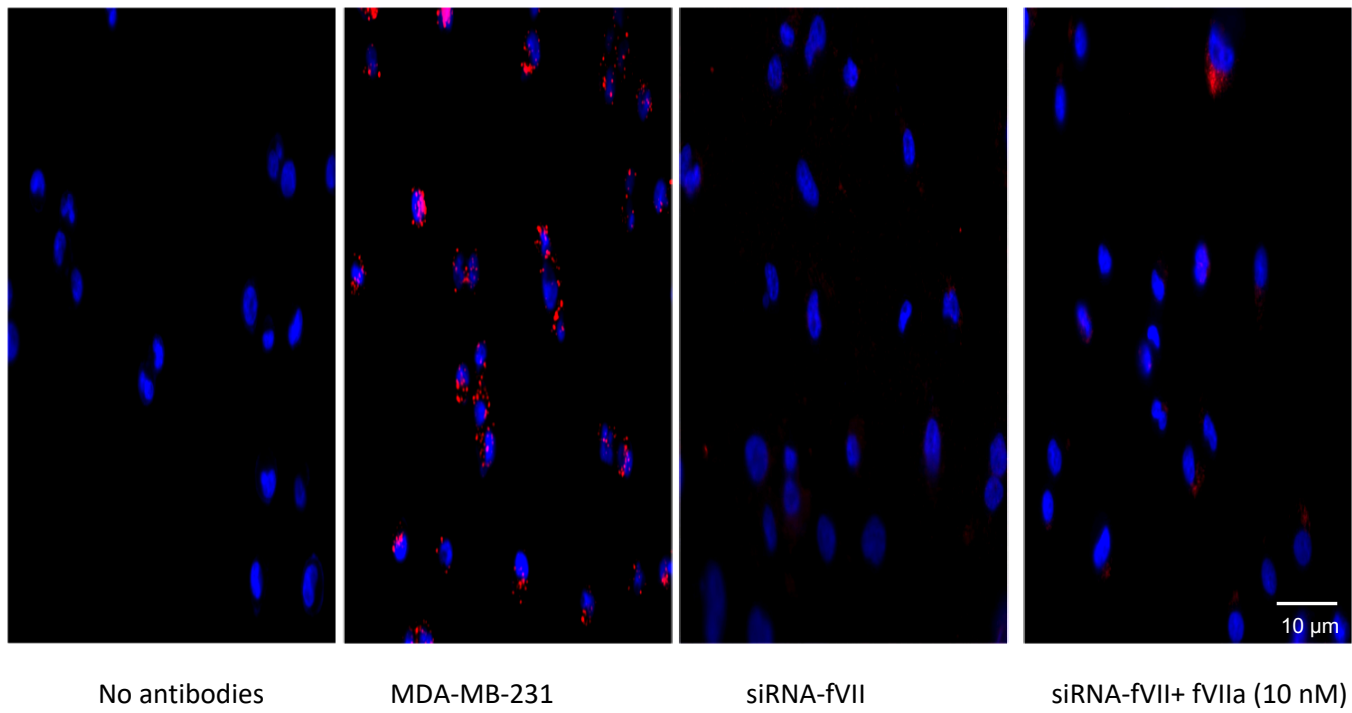
Figure 5. 3 Optimization of the suppression of fVII expression



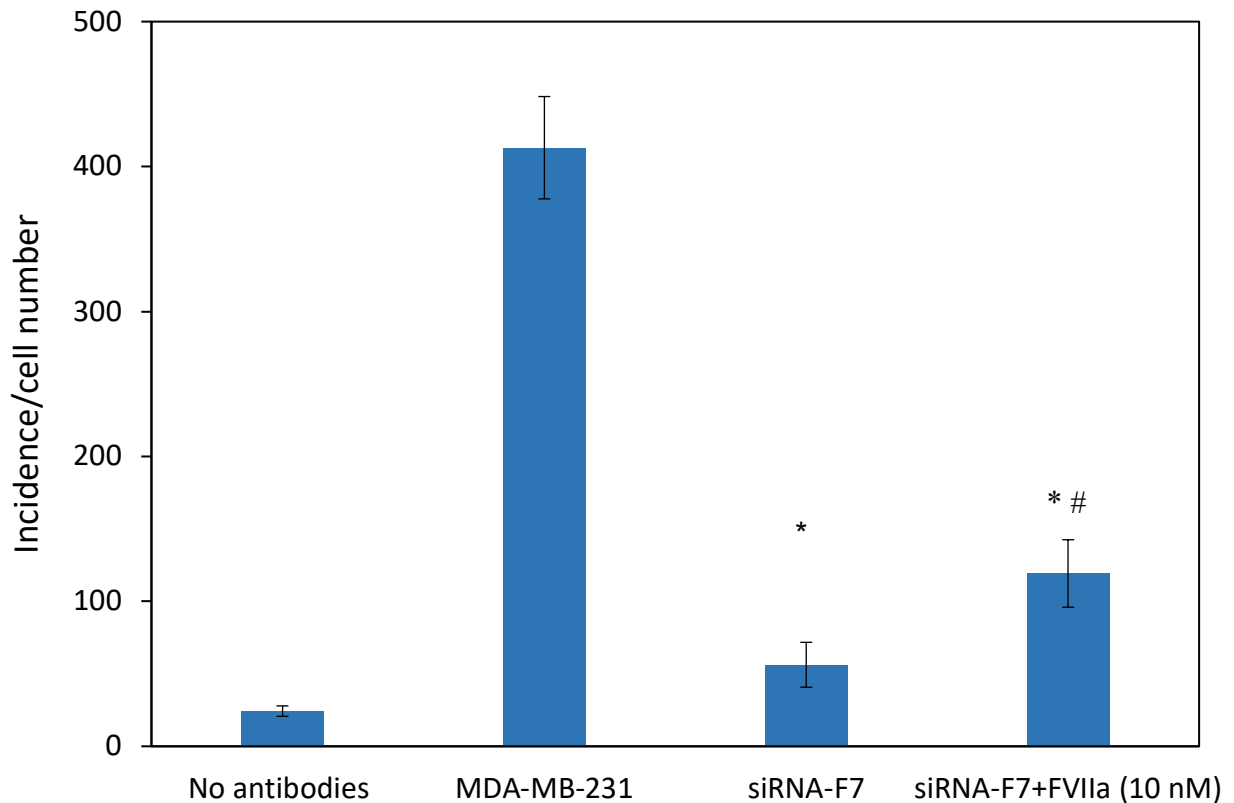
MDA-MB-231 cells (8×10^4) were seeded into 6-well plates and allowed to adhere overnight. The cells were transfected with a range of fVII-siRNA (0-200 nM) using Trans IT-2020 transfection reagent and incubated for 48 h at 37°C. **(A)** The cells were harvested, and fVIIa protein was examined by western blot by incubating the nitrocellulose membrane with a mouse anti-fVII antibody 1:2000 (v/v) and developed with a goat anti-mouse alkaline phosphatase-conjugated antibody 1:4000 (v/v). The bands were visualised using western blue stabilised substrate for alkaline phosphatase. **(B)** The bands were analysed using the ImagJ program and the protein expression quantified against GPADH bands (The results show the average of two separate experiments and expressed as the mean \pm SD).

Figure 5. 4 The influence of fVIIa on the association of TF with PAR2

A)



B)



MDA-MB-231 cells (10^4) were seeded into glass bottom dishes (35 mm) and allowed to adhere. The cells were subsequently transfected with the optimal concentration of fVII-siRNA (150 nM) and then incubated for 48 h at 37°C. A set of siRNA-transfected cells was also supplemented with exogenous fVIIa (10 nM). The cells were fixed with 4% (v/v) formaldehyde and probed with a rabbit anti-TF antibody (5 μ g/ml) and a mouse anti-PAR2 antibody (20 μ g/ml). **(A)** PLA was carried out and the cells were then stained with DAPI (blue; 2 μ g/ml) and visualized by fluorescence microscopy with a X40 magnification. **(B)** Ten images were captured for each sample and the data were analysed using the ImageJ software (The results show the average of three independent experiments and expressed as the mean \pm SEM; * = $p < 0.05$ vs no antibodies; # = $p < 0.05$ vs siRNA-transfected cells without fVIIa).

5.3.4 Confirmation of the lack of TF expression in MDA-MB-231 TF knock out cell line

The aim of this study was to confirm the lack of TF in MDA-MB-231 TF KO cells. MDA-MB-231 TF KO cells along with the wild type cells were incubated with a FITC-conjugated mouse anti-TF antibody (0.5 µg/ml) and analysed by flow cytometry. A set of wild type MDA-MB-231 cells were also tested and used as a control. The flow cytometric analysis confirmed the lack of TF in MDA-MB-231 TF KO cells compared to the wild type MDA-MB-231 cells. A gate was set to contain 4% of unlabelled cells. From a total of 10,000 events, 41% of MDA-MB-231 wild type cells (mean fluorescence = 115) and 0.8% of MDA-MB-231 TF KO cells (mean fluorescence = 22) were within this region (Figure 5.5). To further examine the influence of the lack of TF on the MDA-MB-231 TF KO cell, sets of cells were incubated with a range of concentrations of recombinant TF (0-4 U/ml) for 24 h and cell numbers were determined by crystal violet assay. The addition of any amount of recombinant TF to the MDA-MB-231 KO cells enhanced the rate of cell proliferation in comparison to the untreated cells but the highest rate was achieved on incubation with 4 U/ml of recombinant TF (Figure 5.6).

5.3.5 Examination of the association of fVIIa and PAR2 protein in the absence of TF

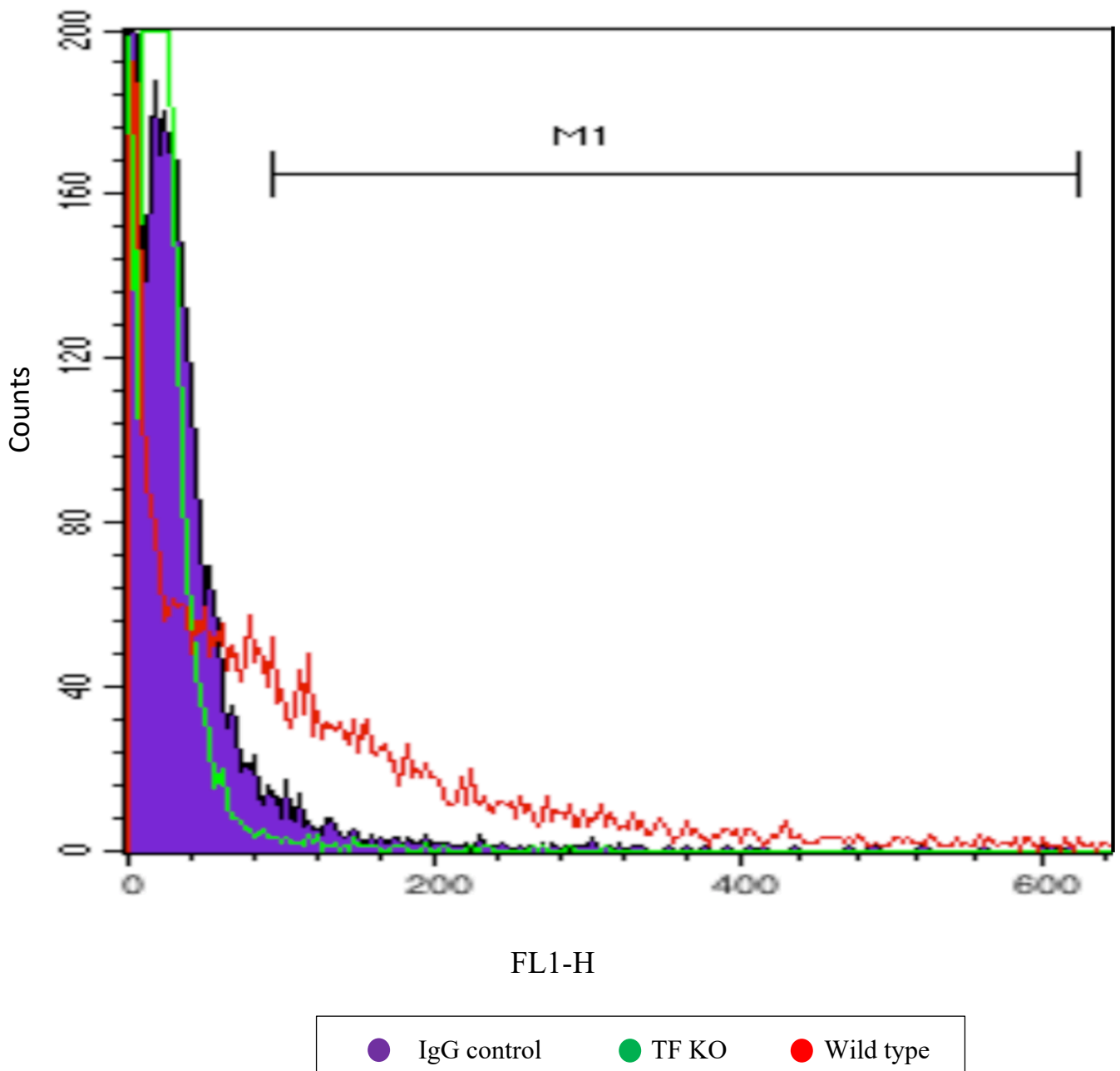
The aim of this study was to examine whether TF is required for the interaction between fVIIa with PAR2. To examine the association between fVIIa and PAR2, MDA-MB-231 TF KO cells were seeded into glass bottom dishes (35 mm) and allowed to adhere. The cells were then fixed and probed with a rabbit anti-fVII antibody (10 µg/ml) and a mouse anti-PAR2 antibody (20 µg/ml). A set of wild type MDA-MB-231 cells were used as a control. The interaction between fVIIa and PAR2 was examined using PLA, as described in 5.2.2. The data obtained from PLA indicates that the absence of TF expression significantly reduced the association of fVIIa and PAR2 protein (Figure 5.7 A and B). This finding agrees with the data from the previous chapter (Figure 4.22) which showed that the addition of exogenous fVIIa to HCAEC which do not

normally express TF, does not induce PAR2 activation. Therefore, it is suggested that TF may act as a molecular scaffold for fVII and promote the interaction of fVIIa with PAR2.

5.3.6 Examination of the association of fVII and caveolae in HCAEC

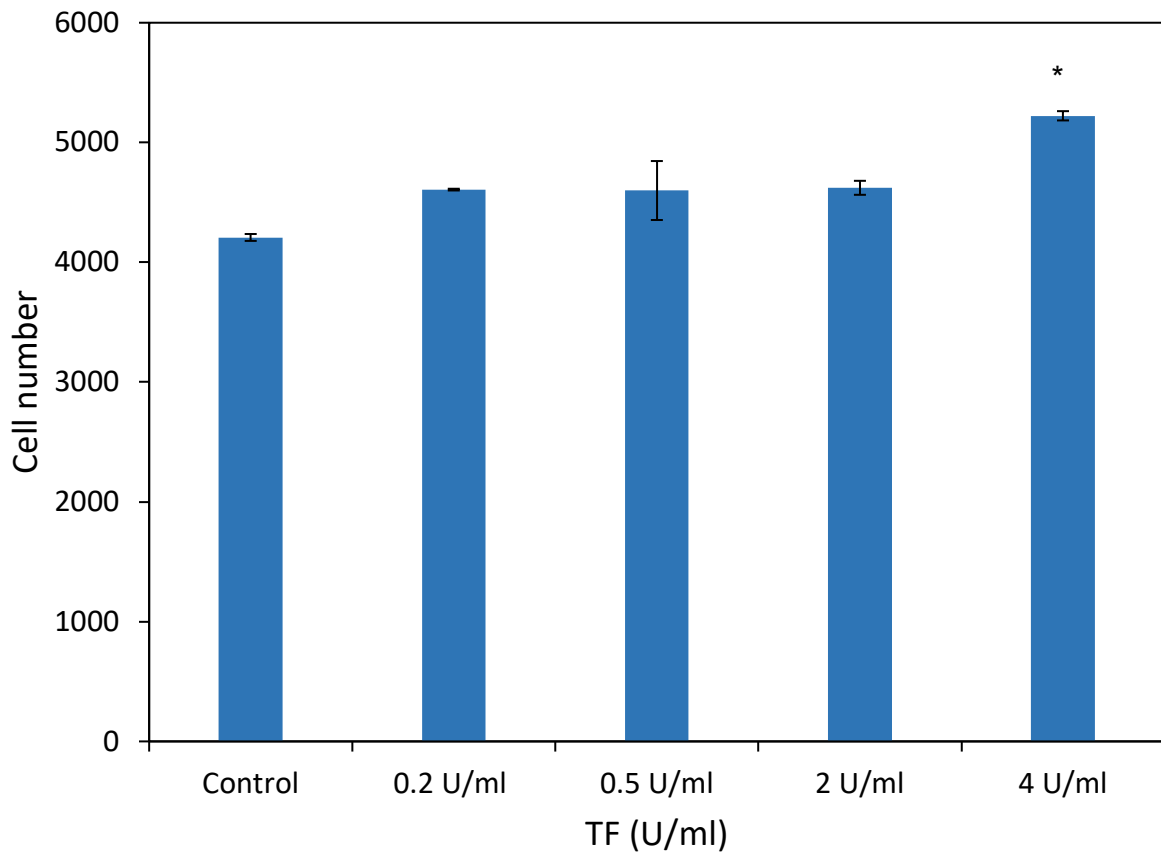
In the previous chapter, it was demonstrated that stimulation of HCAEC with recombinant TF resulted in a significant increase in the cell-surface fVII antigen. One possible explanation for this may be due to the disruption of caveolae resulting in the release of fVII reserves onto the cell surface. Also, it has been suggested that caveolae may harbour proteins such as TF-fVIIa complex (Liu et al., 1997). Therefore, this study was designed to examine the proximity between fVII and caveolin-1 before and after the addition of TF. HCAEC were seeded into glass bottom dishes (35 mm) and allowed to adhere. The cells were subsequently treated with a range of human recombinant TF (0-4 U/ml) for up to 40 min. The cells were then fixed, permeabilised and probed with a mouse anti-fVII antibody (10 µg/ml) and a rabbit anti-caveolin-1 antibody (10 µg/ml). The samples were then examined using PLA, as described in 5.2.2. The analysis of the data showed a high level of proximity between fVII and caveolin-1 in resting cells (Figure 5.8 A and B). However, the association of fVII and caveolin-1 was significantly reduced at 10 min following the supplement with either concentration of TF. Interestingly, a recovery in the association between fVIIa and caveolin-1 was observed on incubation with 2 U/ml TF which was absent on addition of 0.5 U/ml. Furthermore, an enhancement in the association between fVIIa and caveolin-1 was observed following 40 min on incubation with 4 U/ml TF. This finding agrees with the previous result (Figure 3.22) which shows an increase in the fVII antigen on the cell surface of HCAEC in response to TF treatment at 10 min.

Figure 5. 5 Confirmation of the lack of TF expression in MDA-MB-231 TF KO cells by flow cytometry



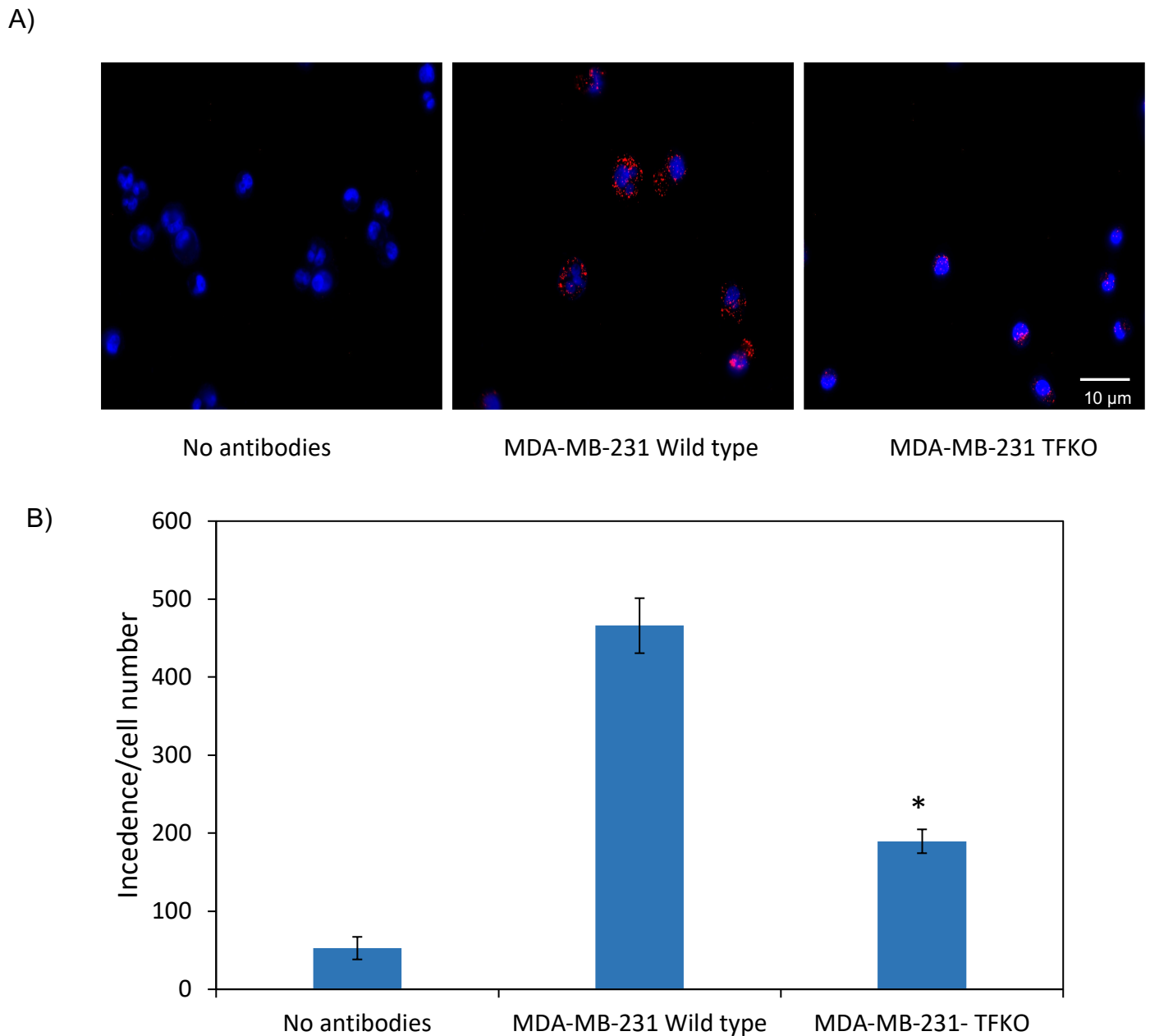
Cells (3×10^5) were collected in eppendorf tube and washed twice with PBS. The cells were suspended in PBS containing 3% (w/v) BSA and a FITC-conjugated mouse anti-TF antibody (0.5 $\mu\text{g}/\text{ml}$) and incubated for 1 h in the dark. A set of cells was incubated with an IgG isotype control antibody. After the incubation, the cells were washed with PBS, resuspended in 500 μl PBS and analysed by flow cytometry. 10,000 events were examined for each sample and a gate (M1) was set to include 4% of unlabelled cells. The data represents one experiment.

Figure 5. 6 The influence of recombinant TF on MDA-MB-231 TF KO proliferation



MDA-MB-231 TF knock out cells (2×10^3) were seeded into 96-well plates and incubated for overnight. The cells were then treated with a range of recombinant TF (0-4 U/ml) and incubated for 24 h. Cell numbers were then determined using crystal violet assay (The results show the average of four independent experiments and expressed as the mean \pm SEM, * = $p < 0.05$ vs untreated cells).

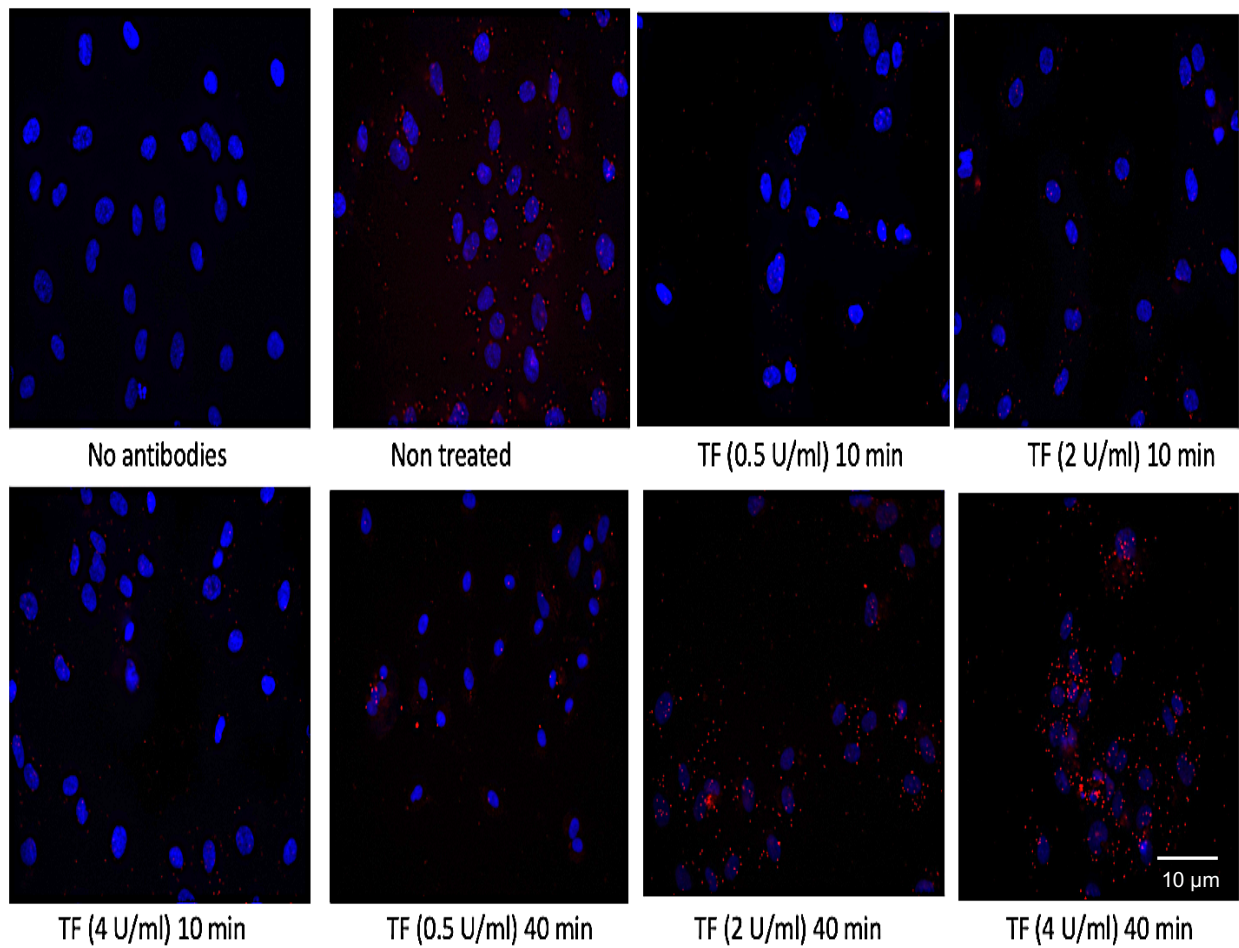
Figure 5. 7 Analysis of the association of fVIIa and PAR2 in TF knock out cells



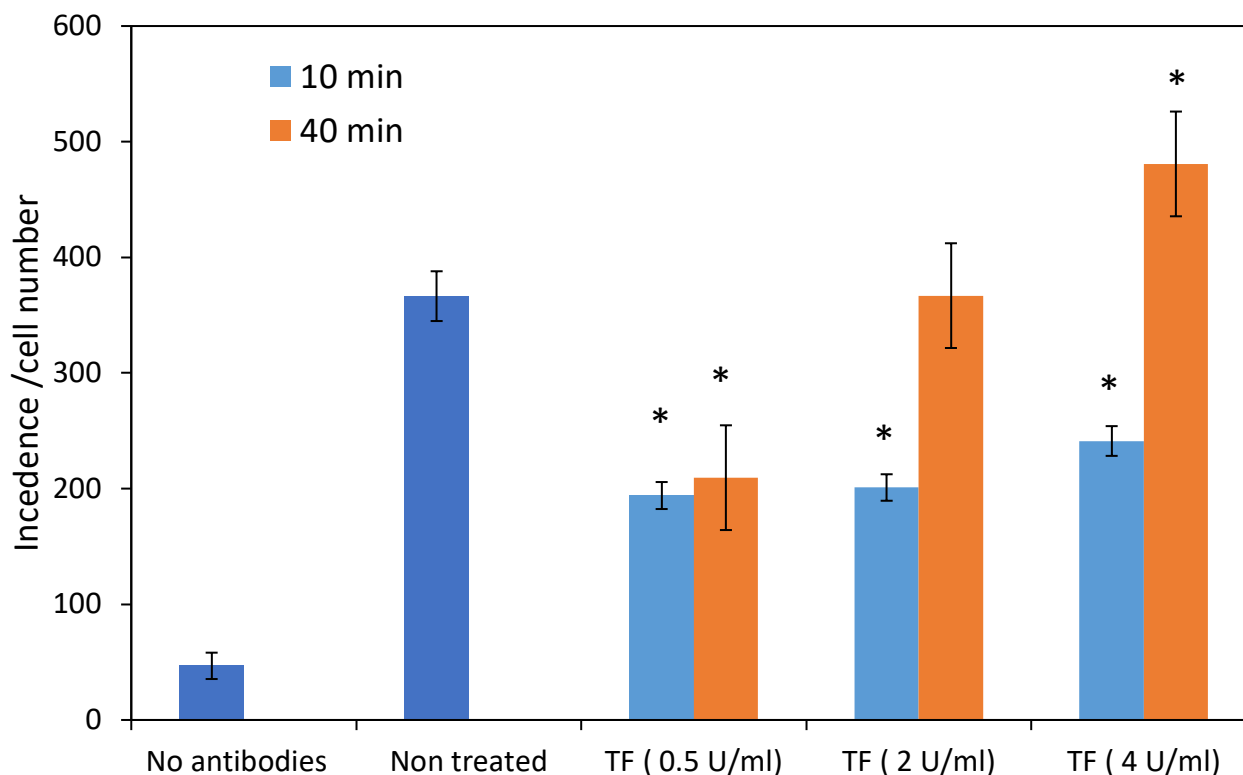
Cells (10^4) were seeded into glass bottom dishes (35 mm) and allowed to adhere. The cells were then fixed and probed with a rabbit anti-fVII antibody (1 $\mu\text{g/ml}$) and a mouse anti-PAR2 antibody (1 $\mu\text{g/ml}$). **(A)** PLA was used to examine the association between fVIIa and PAR2 and the cells were then stained with DAPI (2 $\mu\text{g/ml}$) and visualized by fluorescence microscopy with a X40 magnification. **(B)** Ten images were captured for each sample and the data were analysed using the ImageJ software (The results show the average of three independent experiments and expressed as the mean \pm SEM; * = $p < 0.05$ vs wild type cell).

Figure 5. 8 Analysis of the proximity between fVII and caveolin-1 in HCAEC

A)



B)



HCAEC cells (10^4) were seeded into glass bottom dishes (35 mm) and allowed to adhere. The cells were subsequently incubated with a range of recombinant TF (0-4 U/ml) for up to 40 min at 37°C. A set of untreated cells was used as a control. The cells were then fixed with 4% (v/v) formaldehyde, permeabilised with 0.01 % (v/v) Triton and probed with a mouse anti-fVII antibody (10 μ g/ml) and a rabbit anti-caveolin-1 antibody (10 μ g/ml). (A) PLA was performed to examine the association between fVII and caveolin-1 and the cells were then stained with DAPI (2 μ g/ml) and visualized by fluorescence microscopy with a X40 magnification. (B) Ten images were captured for each sample and the data were analysed using the ImageJ software (The results show the average of three independent experiments and expressed as the mean \pm SEM; * = $p < 0.05$ vs the non-treated sample).

5.3.7 Examination of the association of TF and caveolin-1 in HCAEC

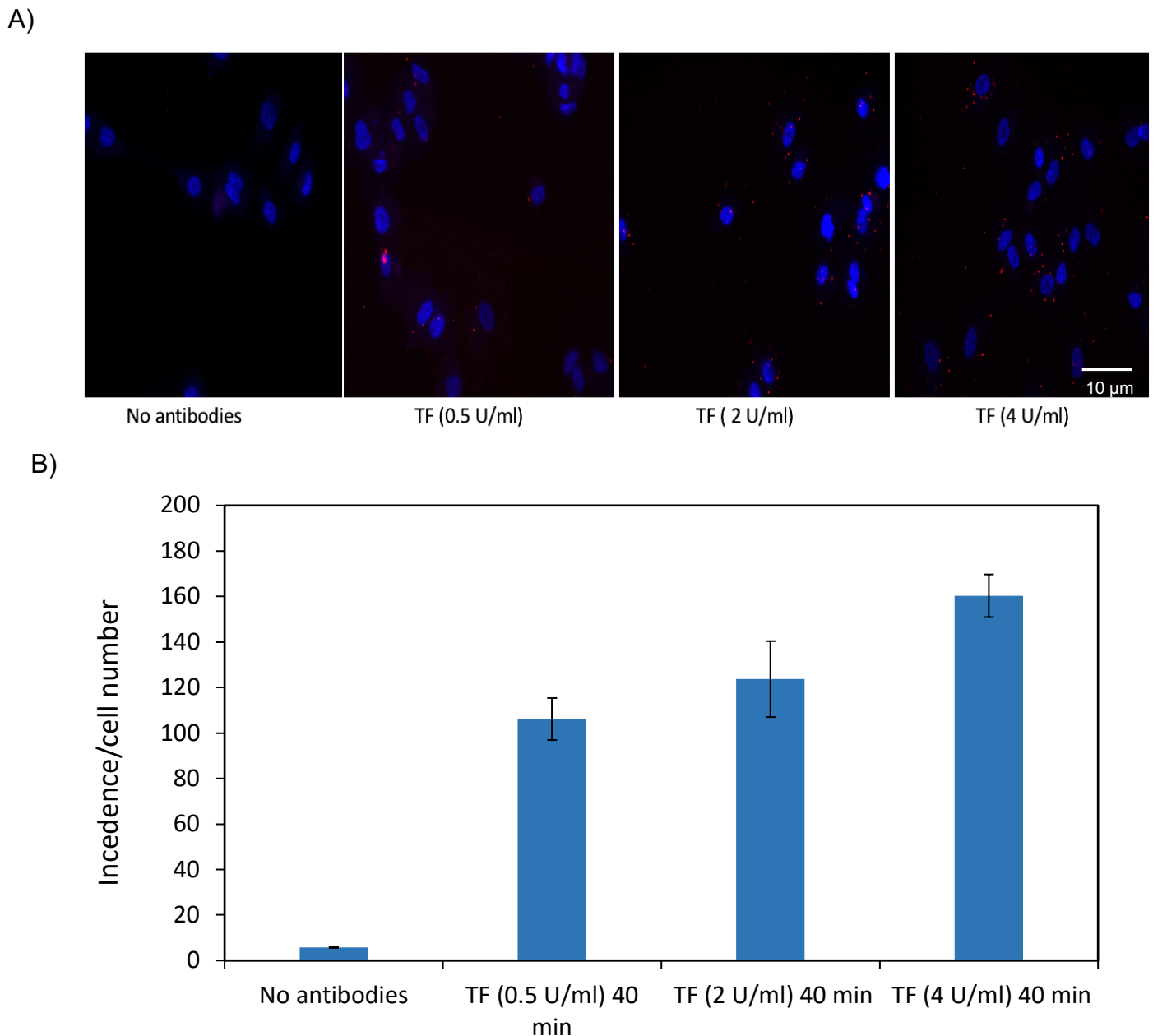
In the above section, a high degree of association between fVII and caveolin-1 was detected. It was suggested that TF can be taken up by caveolae in the presence of fVIIa (Mandal et al., 2006). Therefore, the aim of this study was to examine the association between TF and caveolin-1 in HCAEC. The cells were seeded into glass bottom dishes (35 mm) and permitted to adhere. The cells were then incubated with a range of recombinant TF (0-4 U/ml) for 40 min. after the incubation, the cells were fixed, permeabilised and probed with a mouse anti-TF antibody (5 µg/ml) and a rabbit anti- caveolin-1 antibody (1 µg/ml). The proximities between TF and caveolin-1 was then assessed by PLA. Analysis of the samples showed a concentration dependent association between the supplemented TF and caveolin-1 following 40 min incubation with recombinant TF (Figure 5.9).

5.3.8 Optimization of the depletion and exchange of cell-membrane cholesterol in HCAEC

This study was designed to determine the optimal concentration of M β CD which can be used in order to deplete cell-membrane cholesterol without any detrimental effect on cell viability. HCAEC were seeded into 96-well plates and allowed to adhere. The cells were subsequently treated with a range of M β CD (0-5 mM) for 1 h at 37°C. After the incubation, the cells were washed twice with PBS and incubated with fresh complete MV medium for 24 h. Cell numbers were determined using crystal violet assay. Incubation of HCAEC with 1 mM of M β CD did not have any effect on cell viability. However, higher concentrations of M β CD (2-5 mM) caused a notable reduction in the cell numbers (Figure 5.10).

A second aim of this study was to replace the cholesterol in lipid rafts (including caveolae) in HCAEC with NBD-cholesterol by exchange. To optimise the procedure, HCAEC (10^4) were seeded and incubated for 1 h with a range of M β CD (0-2 mM) combined with NBD-cholesterol

Figure 5. 9 Analysis of the proximity between TF and caveolin-1 in HCAEC



HCAEC (10^4) were seeded into glass bottom dishes (35 mm) and allowed to adhere. The cells were subsequently incubated with a range of recombinant TF (0-4 U/ml) for 40 min. The cells were then fixed with 4% (v/v) formaldehyde, permeabilised with 0.01 % (v/v) Triton and probed with a mouse anti-TF antibody (5 $\mu\text{g/ml}$) and a rabbit anti-caveolin-1 antibody (10 $\mu\text{g/ml}$). **(A)** PLA was used to examine the proximity between TF and caveolin-1 and the cells were then stained with DAPI (2 $\mu\text{g/ml}$) and visualized by fluorescence microscopy with a X40 magnification. **(B)** Ten images were captured for each sample and the data were analysed using the ImageJ software (The results show the average of three independent experiments and expressed as the mean \pm SEM).

at different molar ratios 6:1, 8:1 and 12:1. The cells were subsequently fixed and examined by fluorescent microscopy. Analysis of the data showed that using a combination of 1 mM of M β CD together with the NBD-cholesterol complex at a ratio 8:1 was optimal to enrich the lipid rafts with NBD-cholesterol without affecting cell viability (Figure 5.11).

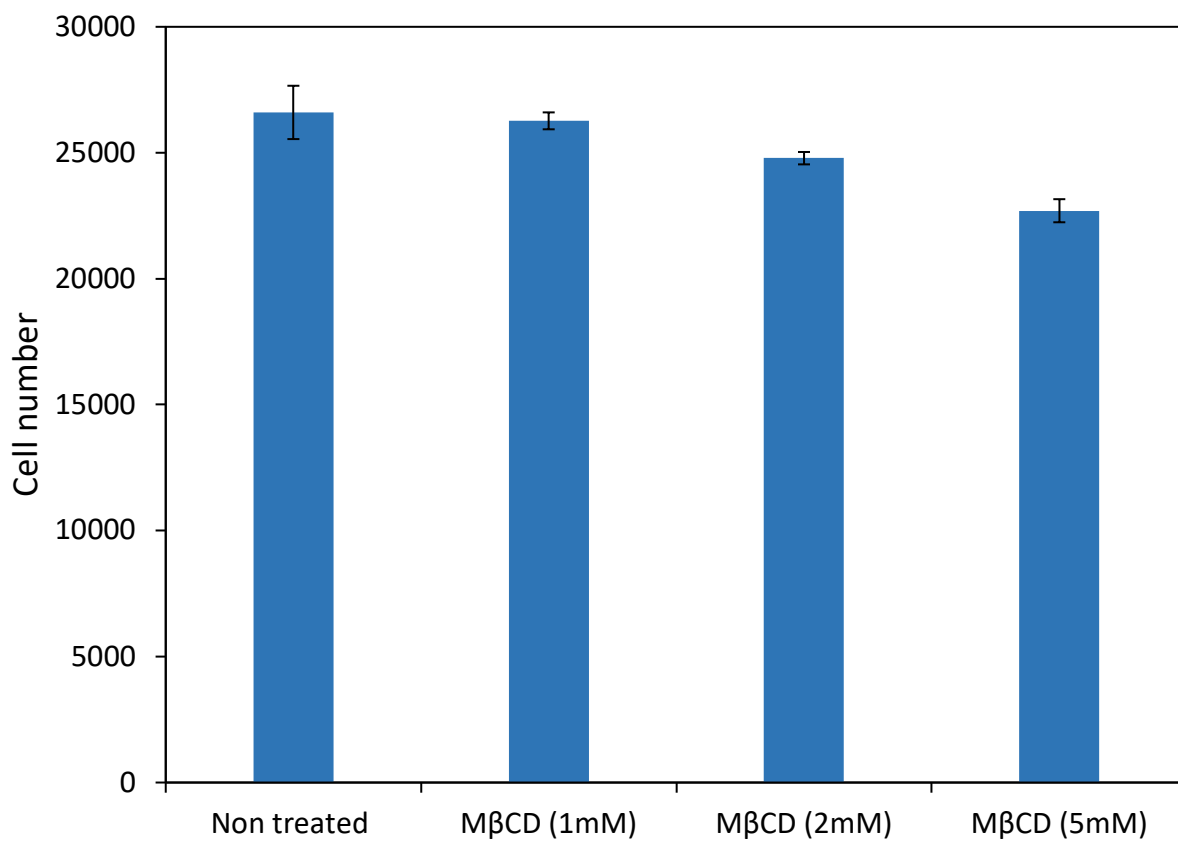
5.3.9 Analysis of the incorporation of Texas-Red labelled TF into cell membrane

This study was designed to label TF with Texas-Red tag before examining the co-localisation of TF on the cell membrane. Human recombinant TF (1 μ g/ml) was labelled with a Texas Red[®] tag using the Lightning-Link[®] kit, as described in section 5.2.7. To confirm the successful labelling of recombinant TF with Texas-Red, HCAEC (10^4) were seeded into glass bottom dishes (35 mm) and allowed to adhere. The cells were subsequently incubated for 30 min at 37°C with labelled Texas Red-conjugated TF (5.2 ng/ml). The cells were then fixed and stained with DAPI (2 μ g/ml) and examined by fluorescence microscopy. Analysis of the cell treated with labelled TF in comparison to the untreated cells confirmed the successful conjunction of the fluorescent label and the incorporation of the TF into the cell membrane (Figure 5.12).

5.3.10 Examination of the co-localisation of TF with the lipid rafts within HCAEC membrane by confocal microscopy

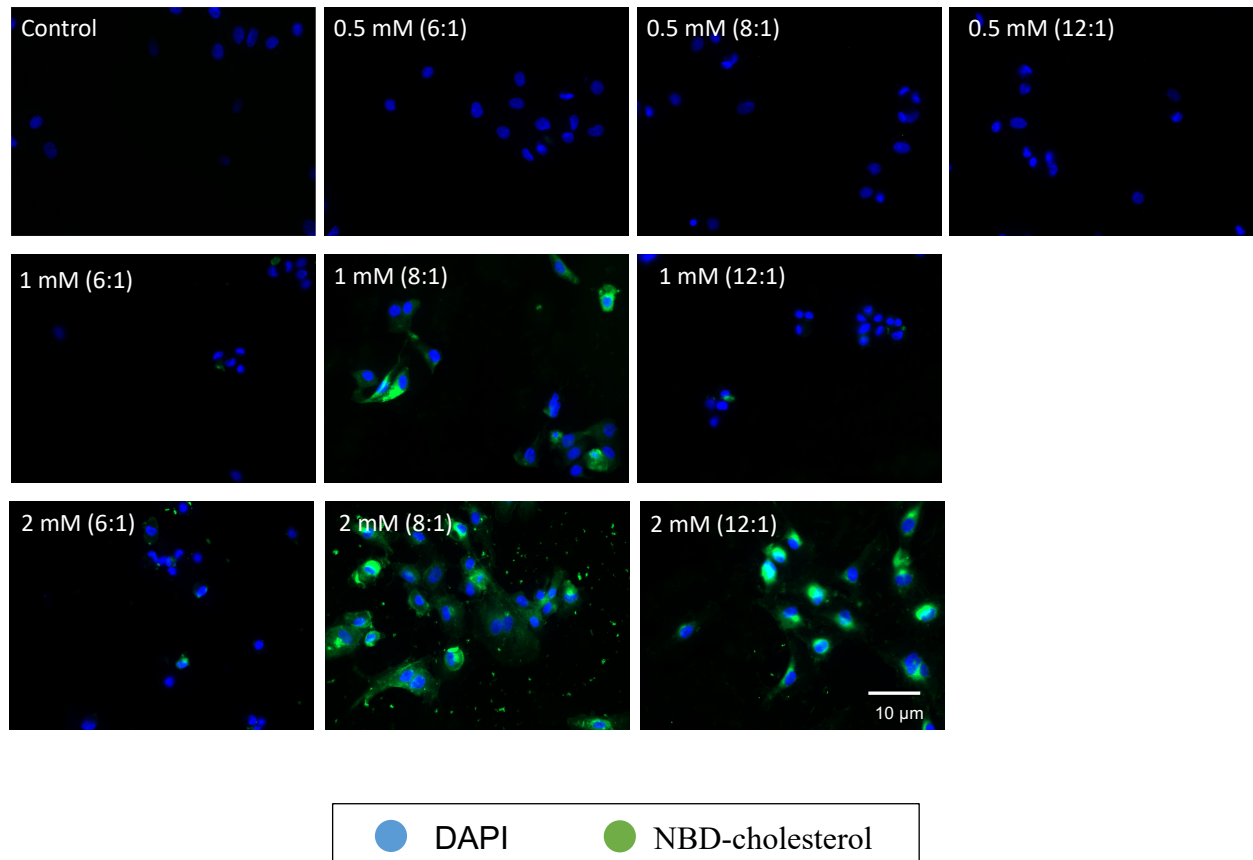
The results from section 5.3.7 show an association between supplemented TF and caveolin-1 in HCAEC. The aim of this study was to investigate the co-localisation of the TF within the plasma membrane of HCAEC. The cells were enriched with NBD cholesterol and incubated with Texas Red-conjugated TF. The cells (10^4) were seeded into glass bottom dishes (35 mm) and allowed to adhere. The cells were subsequently treated with M β CD (1 mM) in combination with NBD-cholesterol complex at a molar ratio of 8:1 and incubated for 1 h according to optimized procedure described in section 5.2.9. The mixture was removed from the dishes and

Figure 5. 10 Analysis of cell viability for the optimisation of cholesterol depletion



HCAEC (2×10^4) were seeded into 96-well plates and permitted to adhere. The media were removed and the cells were incubated for 1 h at 37°C with a range of concentration of MβCD (0-5 mM) diluted in serum free MV. After the incubation, the cells were washed twice with PBS and incubated with fresh complete MV medium for 24 h at 37°C. Cell numbers were determined using crystal violet assay (The results show the average of four independent experiments and expressed as the mean \pm SEM).

Figure 5. 11 Optimisation of the ratio of M β CD:cholesterol complex for labelling lipid rafts on HCAEC



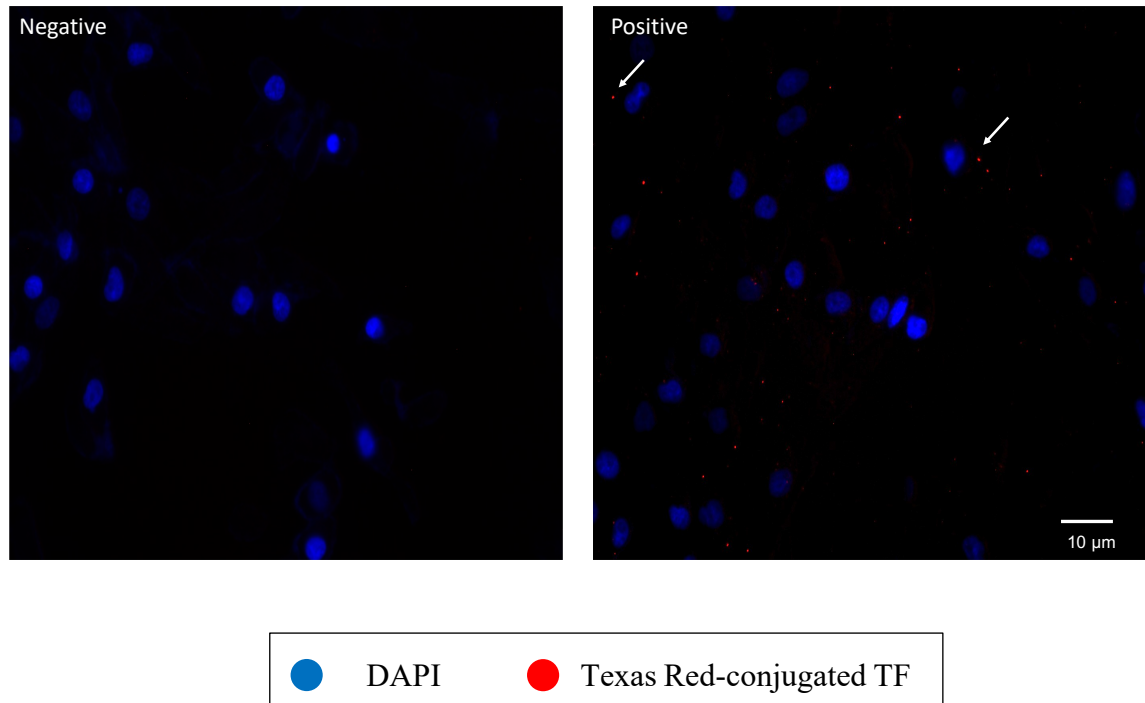
HCAEC (10^4) were seeded into glass bottom dishes (35 mm) and allowed to adhere. The cells were subsequently incubated for 1 h at 37°C with a range of M β CD (0-2 mM) in conjunction with NBD-cholesterol at molar ratios of 6:1, 8:1 and 12:1. The cells were then fixed with 4% (v/v) formaldehyde and stained with DAPI (2 μ g/ml). The samples were visualized by fluorescence microscopy with a X40 magnification and images were captured. The data represents one experiment.

the cells were incubated with Texas Red-conjugated TF (5.2 ng/ml) for up to 40 min. The cells were then fixed and examined by confocal microscopy. Incubation of the cells with Texas Red-conjugated TF resulted in the progressive increases in the incorporation of red fluorescent label (Figure 5.13). In addition, the labelled TF was mainly incorporated within the cholesterol-rich domain/rafts at 40 min post incubation which were identified by NBD-cholesterol.

5.3.11 Examination of the influence of cell-membrane cholesterol on TF- mediated cell apoptosis

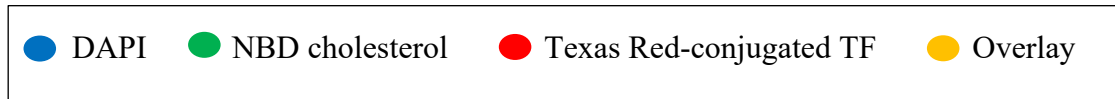
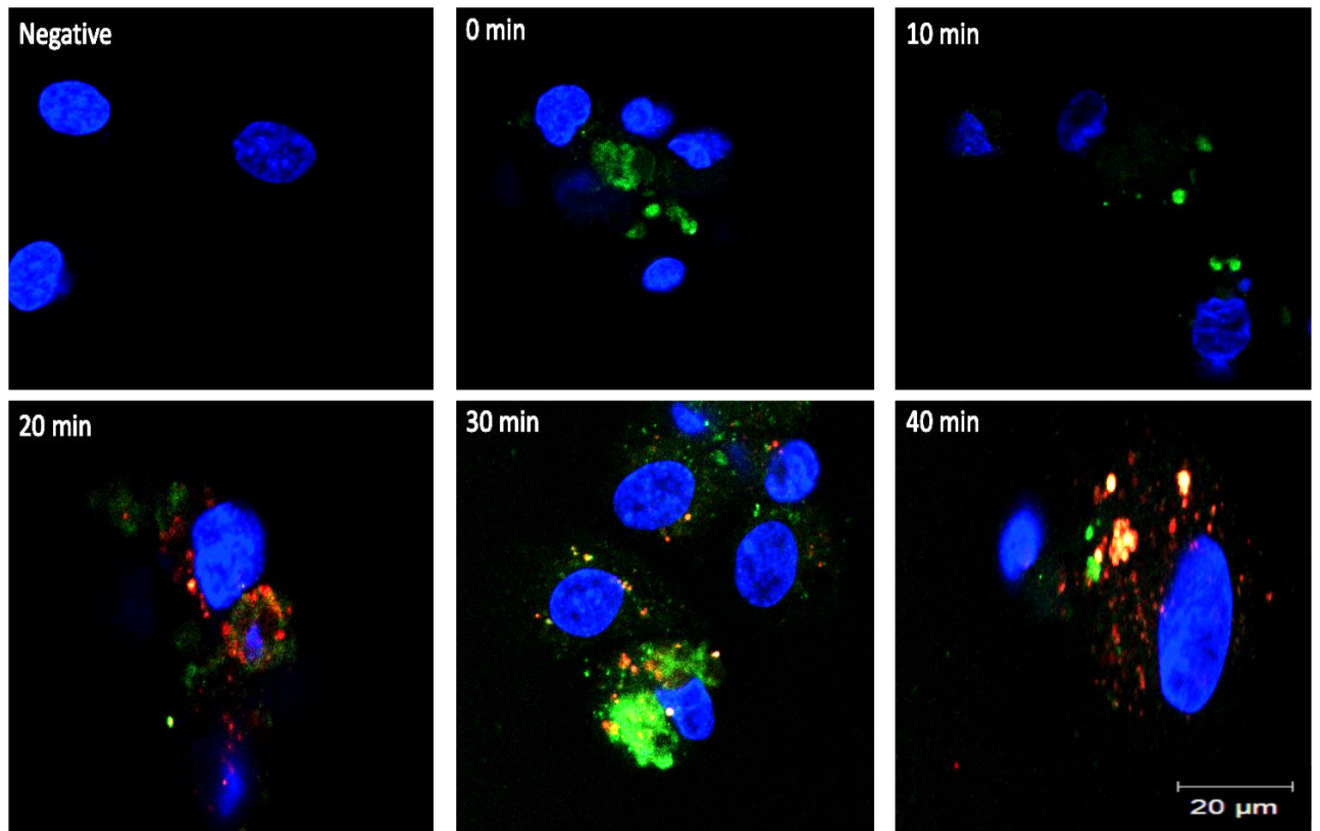
It was demonstrated in chapter 3 that TF has the capability to induce cell apoptosis in HCAEC. It is also hypothesized that TF can be stored at lipid rafts (including caveolae) in a non-functional form (Dietzen et al., 2004). Therefore, in this study an attempt was made to disrupt the lipid rafts prior to treatment of the cells with recombinant TF and measuring the outcome on cell number. HCAEC were seeded into 96-well plates and allowed to adhere. The cells were subsequently treated with M β CD (0-5 mM) for 1 h at 37°C. After the incubation, the M β CD was replaced with complete MV medium containing recombinant TF (4 U/ml) and incubated for 24 h at 37°C. Cell numbers were then determined using crystal violet assay. Pre-treatment of cells with M β CD prior to the addition of recombinant TF resulted in a concentration-dependent reduction in cell numbers compared to recombinant TF alone reaching a maximum of 16% on pre-incubation with 5 mM M β CD (Figure 5.14).

Figure 5. 12 Examination the incorporation of Texas-Red labelled TF into cell membrane by fluorescent microscopy



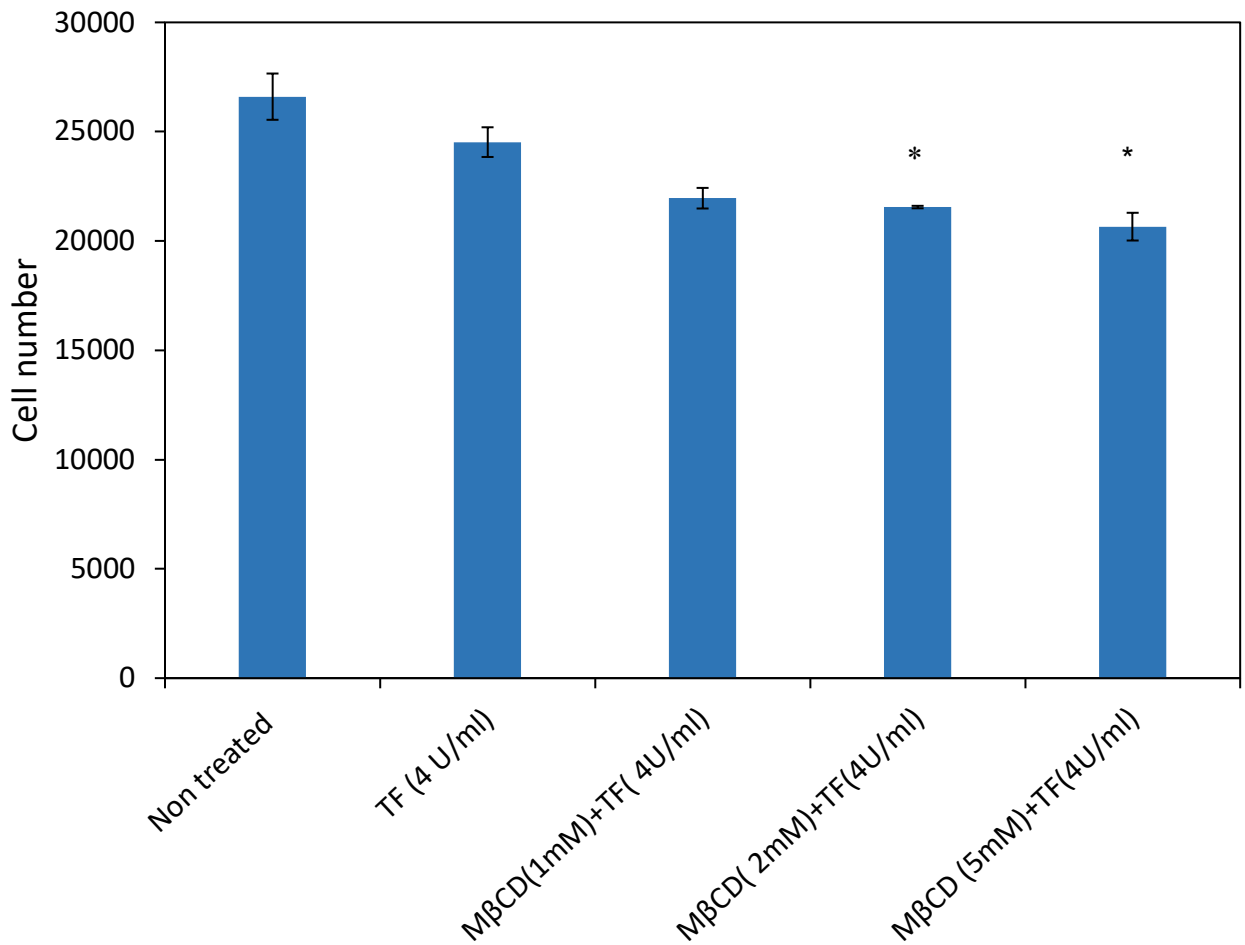
HCAEC (10^4) were seeded into glass bottom dishes (35 mm) and allowed to adhere. The cells were then incubated with the Texas Red-conjugated TF (5.2 ng/ml) for 30 min at 37°C. After the incubation, the cells were fixed with 4% (v/v) formaldehyde and stained with DAPI (blue; 2 μ g/ml). The samples were visualized by fluorescent microscopy with a X40 magnification and images were captured. The data represents one experiment.

Figure 5. 13 Examination of the co-localisation of TF within lipid rafts in HCAEC



HCAEC (10^4) were seeded into glass bottom dishes (35 mm) and allowed to adhere. The cells were incubated for 1 h with M β CD (1 mM) in conjunction with NBD-cholesterol at molar ratio 8:1. The mixture was then removed from the dishes and the cells were incubated with Texas Red-conjugated TF (5.2 ng/ml) for up to 40 min at 37°C. The samples were fixed with 4% (v/v) formaldehyde and stained with DAPI (2 μ g/ml). The samples were visualized by confocal microscopy with a X60 magnification. The data represents one experiment.

Figure 5. 14 The influence of cholesterol on the influence of TF on cell numbers



HCAEC (2×10^4) were seeded into 96-well plates and allowed to adhere. The media was removed and the cells were incubated with a range of MβCD (0-5mM) for 1 h. After the incubation, the cells were washed twice with PBS and then incubated with fresh complete MV medium containing recombinant TF (4 U/ml) for 24 h at 37°C. A set of untreated cells were also incubated with TF (4 U/ml) and used as a control. Cell numbers were determined using crystal violet assay (The results show the average of four independent experiments and expressed as the mean \pm SEM; * = $p < 0.05$ vs 4 U/ml TF sample).

5.4 Discussion

Previous studies have suggested that the TF-fVIIa complex can promote tumour growth and metastasis mediated through the activation of PAR2 (Shi X et al., 2004; Rao and Pendurthi, 2005; Belting et al., 2005). It has been shown that the expression of TF is elevated in many diseases such as atherosclerosis (Tatsumi and Mackman, 2015), cancer (Eisenreich et al., 2016) and other inflammatory conditions (Witkowski et al., 2016). Moreover, the accumulation of TF in endothelial cells has been demonstrated to induce cellular apoptosis mediated through overactivation of Src and P38 (ElKeeb et al., 2015; Ethaeb et al., 2019). A proposed mechanism by which the cells manage the excessive amounts of TF associated with inflammatory condition is to incorporate and release this TF within MV (Collier and Ettelaie, 2011). Studies conducted by Koizume et al. (2006, 2015) demonstrated that cancer cells are capable of expressing ectopic fVII protein. It has been demonstrated that the activation of PAR2 can induce MV release (Collier and Ettelaie, 2011). In this model, the TF-fVIIa complex interacts with the PAR2 protein on the cell surface in order to activate the later receptor. In this study, PLA was used to demonstrate the association between TF, fVIIa and PAR2 proteins on the surface of MDA-MB-231 cell line. The data showed associations between TF and PAR2, fVIIa and PAR2, as well as between TF and fVIIa suggesting the formation of a ternary complex (Figure 5.2). These data also confirmed the ability of MDA-MB-231 cells to express fVII. PAR2 is activated by the proteolytic action of fVIIa which needs to bind to TF forming the TF-fVIIa complex (Camerer et al., 2000; Larsen et al., 2010; Rao and Pendurthi, 2005). Since these cells express both fVII and PAR2, the ability of fVII alone to bind to PAR2 in the absence of TF was examined. Therefore, MDA-MB-231 TF knockout cells were used to examine the association between fVII and PAR2 proteins in the absence of TF (Figure 5.5). PLA analysis of the association of fVII with PAR2 in MDA-MB-231 TF KO cells showed a 60% reduction compared to that in the wild-type cell (Figure 5.7). This finding agrees with the data from

previous chapter (Figure 4.22) which showed that the addition of exogenous fVIIa to HCAEC, which do not normally express TF, did not result in PAR2 activation. Therefore, in the absence of TF, fVII does not appear to be effective in binding or activating PAR2 protein. This suggests a mechanism by which the cells gauge the amount of the TF they come into contact with, or that is expressed by the cells, and by which regulate how much TF is released without the excessive production of MV.

In addition to TF, fVIIa is also an essential component of the complex responsible for the activation of PAR2. In the previous chapter, it was shown that repeated treatment of HCAEC with recombinant TF decreased the amount of fVII available to the cells (Figure 3.24). Furthermore, the magnitude of these reductions was accounted for by the amount of fVII that was released in MV (Figure 3.25). The repetitive treatment with TF caused a depletion of cellular fVII reserves in HCAEC. Consequently, the activation of PAR2 resulting in TF release within MV became impaired. To examine the hypothesis that TF is required as part of complex with fVII to activate PAR2, the expression of fVII was suppressed in MDA-MB-231 cells using siRNA and the outcome on association of TF and PAR2 examined by PLA. The suppression of fVII expression in MDA-MB-231 using siRNA resulted in a significant reduction in the association of PAR2 and TF indicating the importance of TF-fVIIa complex formation for the interaction with PAR2. This was further supported by the supplementing the fVII-knock down cells with exogenous fVIIa which partially restored the interaction of TF and PAR2 (Figure 5.4). These data indicate that the source of fVII is derived from the treated cells which agrees with the result from previous chapter which showed that HCAEC can also express fVII protein (Figure 3.23 and 3.24). In addition, it was shown in the previous chapter that the stimulation of HCAEC with TF resulted in exposure of fVII protein on the cell surface. However, the cellular location of the source of fVII is undetermined. It has been suggested by Mandal et al. (2005) and Awasthi et al. (2006) that fVII can associate with the caveolae. This accounts for

the rapid exposure of fVII following the cell activation which also rules out the *de novo* expression of fVII, or the endvesicular transport of the fVII from the golgi apparatus. Therefore, the association of fVII and caveolin-1 in HCAEC, which lack TF, was examined before and after the addition of recombinant TF. Analysis of the cells using PLA indicated the presence of fVII in caveolae in resting HCAEC. This association between fVII caveolin-1 was significantly reduced at 10 min following the incubation of the cells with TF. Interestingly, a recovery in the association between fVIIa and caveolin-1 was observed on incubation with 2 U/ml TF but was absent at lower concentration of 0.5 U/ml. This agrees with the hypothesis that fVII is released from its source in caveolae following cellular contact with TF to allow the activation of PAR2 and release of MV. At lower TF concentration, the release of MV is sufficient to dispose of the cell surface TF while at the higher concentrations a secondary mechanism of TF clearance through the caveolae endocytosis is initiated. Furthermore, an enhancement in the association between fVIIa and caveolin-1 was observed following 40 min incubation with 4 U/ml TF (Figure 5.8). This further suggests that the release of TF within MV is limited and exhaustible and therefore any excess TF have to be cleared by another mechanism.

Following the prolonged exposure of cells to TF such as during chronic inflammatory diseases, the depletion of reserves of fVII results in excessive amounts of TF which cannot be cleared through the release of MV. Therefore, an alternative cellular mechanism involving endocytosis through the caveolae manage the excessive amounts of TF. As stated before, caveolae are cable of harbouring proteins such as TF (Mandal et al., 2005; Awasthi et al., 2006). To examine the hypothesis that this mechanism allows further clearance of TF, the association of TF with caveolin-1 in HCAEC was examined. PLA analysis of the samples showed an association between the supplemented TF and caveolin-1 following 40 min incubation (Figure 5.9) which was also TF concentration dependent. To further consolidate these finding, the

association/localisation of the exogenous TF with cholesterol-rich lipid rafts was examined. Data obtained using confocal microscopy revealed that increasing amounts of Texas Red-conjugated TF co-localised within cholesterol rich domain/lipid rafts within 40 min of supplementation (Figure 5.13). These findings are also in agreement with a study conducted by Awasthi et al. (2006) who used specific antibodies to TF and caveolin-1 to demonstrate the co-localisation of cellular TF with caveolae. In addition, it was hypothesised that the regulation of TF on the cell surface is essential to prevent the pro-apoptotic influence of TF on cells. To explore the consequence of preventing the clearance of TF from the cell surface, the formation of caveolae in HCAEC was disrupted by cholesterol depletion using M β CD prior to the addition of recombinant TF. It was envisaged that by removing the cholesterol, TF would remain active and capable of signalling through PAR2. Pre-treatment of cells with M β CD prior to the addition of recombinant TF resulted in a M β CD-concentration dependent reduction in cell numbers compared to the recombinant TF alone reaching a maximum of 16% on pre-incubation with 5 mM M β CD (Figure 5.14). This result agrees with the study conducted by Dietzen et al., (2004) which suggested that removing cholesterol from the cell membrane could also enhance the procoagulant activity of TF. Therefore, the association of TF with caveolae may also result in the storage of TF in an encrypted form devoid of any procoagulant or signalling activities.

In conclusion, the regulation of the amount of active TF on the cell surface is mediated through two separate mechanisms. The incorporation and release of TF within MV constitutes the primary means of disposing excess TF and is dependent on complex formation with fVIIa and PAR2 activation. Consequently, this mechanism is dependent on the amounts of fVIIa and MV available to the cell. The alternative mechanism clears any unreleased TF through caveolae-mediated endocytosis and this mechanism is also dependent on TF-fVIIa complex formation. Therefore, although the cells respond to acute exposures to varying amounts of TF through

these mechanisms, the long-term exposure of cells to TF during chronic inflammatory condition results in the exhaustion of the cellular potential to manage TF activity. This in turn can give rise to impairment of cellular functions such as the vascular endothelial cell denudation associated with chronic diseases.

Chapter 6

Discussion

6.1 General discussion

In the course of this study, the ability of cells to cope with excess TF and avoid the associated detrimental effects were investigated. The exposure of TF at the site of injury initiates the coagulation mechanism which prevents excessive bleeding (Lasne et al., 2006; Owens and Mackman, 2010). However, the ability of TF is not limited to initiating the coagulation system and growing evidence demonstrates that TF can induce multiple cellular signalling mechanisms (Rao and Pendurthi, 2005; Ruf et al., 2011; Zelaya et al., 2018). It is postulated that TF possesses the dual functions of instructing cells to divide (Cirillo et al., 2004; Pradier and Ettelaie, 2007) or become apoptotic (Pradier and Ettelaie, 2007; Frentzou et al., 2010; ElKeeb et al., 2015; Ethaeb et al., 2019). Having these two, contrasting, activities may be crucial in distinguishing between viable and irreparably injured cells essential for precise vascular homeostasis.

In addition, the functional properties of TF appear to be replicated in TF-bearing MV, which may be released into the bloodstream from various sources. These MV may also contain a complement of negatively charged phospholipids (Morel et al., 2006; Freyssinet and Toti, 2010; Gardiner et al., 2015; Date et al., 2013; Hron et al., 2007; Thaler et al., 2014; Auwerda et al., 2011) and functional fVIIa (Yokota et al., 2009; Koizume et al., 2006; Featherby et al., 2019). Furthermore, MV-associated TF can be acquired and internalised by vascular and blood cells (Lösche et al., 2004; Escolar et al., 2008; Collier et al., 2013; Osterud and Bjorklid, 2012) and may in turn be beneficial, or detrimental to cells (Widlansky et al., 2003).

The current study aimed to examine the processes involved in gauging the level of injury and determining the fate of the cells. One important factor is the amount of TF that cells come in contact with, but this this study has also investigated the hypothesis that different ratios of fVII/fVIIa and TF within MV mediate different functional outcomes in cultured primary

endothelial cells. For the first time, this study showed that the ratio of fVIIa:TF in MV is a determining factor driving endothelial cell proliferation or apoptosis. This was demonstrated by incubation of HCAEC with a combination of purified fVIIa and recombinant TF which resulted in different cellular outcomes, depending on the fVIIa:TF ratio. This was also reflected in the outcome of incubation of endothelial cells: whilst MV derived from HepG2 (54:1) and MCF-7 (38:1) cells, which contained high ratios of fVIIa:TF, had proliferative effect, MV derived from 786-O cells (10:1) were pro-apoptotic. However, no significant influence on proliferation or apoptosis were observed with MV derived from MDA-MB-231 (34:1) and BxPC-3 (16:1) cells, which had relatively low levels of TF which demonstrated both the fVII:TF ratio and the concentration of TF are critical factors. These observations are in agreement with previous studies showing that incubating cardiomyocytes with low concentrations of TF induced proliferation, while high TF concentrations caused apoptosis, but the fVII:TF ratio were not measured (Pradier and Ettelaie, 2007; Frentzou et al., 2010; ElKeeb et al., 2015; Ethaeb et al., 2019).

To investigate the mechanism by which the ratio of fVIIa:TF is a determinate of the fate of the cells, the role of fVIIa was examined further. The effects of MV on cell proliferation and apoptosis appear to require the proteolytic activity of fVIIa, since blocking of fVIIa by an inhibitory polyclonal antibody prevented both these outcomes. Similarly, Cirillo et al. (2004) reported that blocking of the active site of fVIIa prevented the proliferative stimulatory function of fVIIa when added to smooth muscle cells. Moreover, in order to induce cell signalling, fVIIa is required to form a complex with TF (Sørensen et al., 1999; Cirillo et al., 2004; Rao and Pendurthi, 2005). TF-fVIIa complex is then capable of approaching and activating of PAR2 on the cell surface. In fact, adding purified fVIIa alone did not significantly promote proliferation or apoptosis in HCAEC (Figure 3.12). Furthermore, the proximity between PAR2 and fVIIa observed in wild-type cells was not detectable in MDA-MB-231-TF KO cells that were

deficient in TF (Figure 5.7). The pro-apoptotic influence of cancer cell-derived MV was prevented by pre-incubating the MV with an inhibitory antibody against TF that blocks fVIIa binding (HTF1) (Tripisciano et al., 2017), but not with an antibody that blocks TF signalling (10H10) (Versteeg et al., 2008). Therefore, TF appears to induce apoptosis and proliferation in endothelial cells through procoagulant signalling, which requires an association with fVIIa.

As mentioned above, PAR2 is a target for TF-fVIIa complex on cell surface. PAR2 signalling can induce either cellular proliferation (Hu et al., 2013) or apoptosis (Ethaeab et al., 2019). PAR2 can be activated by fVIIa alone as well as the TF-fVIIa complex (Vergnolle et al., 1999; Rothmeier and Ruf, 2011; Zhao et al., 2014; Benelhaj et al., 2019). Therefore, it was envisaged that the mechanism for inducing apoptosis or proliferation in endothelial cells via MV-associated TF-fVII complex could be mediated by PAR2. To demonstrate this association, the blocking of PAR2 in endothelial cells with the SAM11 antibody was shown to abolish both the proliferative and the pro-apoptotic effects of MV, indicating that PAR2 activation is required for both. However, activation of PAR2 by incubating with an activating peptide, concurrent with the addition of the MV also did not result in the pro-apoptotic outcome of cancer cell-derived MV on the endothelial cells. This observation is consistent with a previous study suggesting that the activation of PAR2 using PAR2-AP can prevent cellular apoptosis in colonic epithelial cells (Iablokov et al., 2014). However, rapid activation of PAR2 due to high fVIIa:TF activity appears to lead to HCAEC de-sensitisation and suggests that inducing apoptosis in endothelial cells requires controlled PAR2 activation (Ettelaie et al., 2012; Ethaeab et al., 2019). This was further evident by the maximal activation levels of cells apoptosis being achieved at 0.05 nM using 786-O cell-derived MV, whereas higher concentrations were less effective. Further analysis of cell-surface PAR2 indicated the possible endocytosis of the receptor as an explanation for the desensitisation, following rapid activation by TF-fVIIa complex or by PAR2-AP.

However, incubation of endothelial cells with recombinant TF alone caused significant levels of cellular apoptosis (Figure 3.12) and since fVIIa is pre-requisite to the induction of apoptosis, this suggests that cells have an alternative source of fVII. Examination of fVII expression by endothelial cells revealed that only approximately 20% of the antigen is presented on the surface of resting cells (Figure 3.22). High levels of fVII/fVIIa were associated with caveolin-1 as detected using PLA. Interestingly, these cells responded to stimulation with recombinant TF, or PAR2 activation by exposing significantly increased levels of fVII on the cell surface (Figures 3.22 and 3.23). Therefore, endothelial cells may respond to the stimulatory signals arising from injuries or trauma by altering the fVIIa:TF ratio to counter the pro-apoptotic influence of excess TF. It suggests that endothelial cells may express fVII/fVIIa as a defence mechanism against the apoptotic effects of TF, since fVIIa binds to TF and promotes the release of excess TF within MV (Figures 3.24 and 3.25). In fact, the addition of exogenous fVIIa rescued endothelial cells from any MV-induced apoptosis and promoted proliferation instead (Figure 3.14). Moreover, repeated exposure of endothelial cells to TF resulted in depletion of cellular fVII reserves (Figures 3.24 and 3.25). This compromise in endothelial cell function implies that eventually the cellular response becomes insufficient to maintain cell survival. Therefore, repeated exposure to TF-positive MV, for example during chronic diseases, may potentially exhaust the ability of endothelial cells to counter the pro-apoptotic function of TF resulting in cell death.

As stated above, in addition to its signalling function in proliferation and apoptosis (Darmoul et al., 2004; Hu et al., 2013; Ethaeb et al., 2019), PAR2 is also capable of inducing MV release which contain TF (Collier and Ettelaie, 2011; Ettelaie et al., 2012; Das et al., 2018). Therefore, the second part of this study focused on the relationship between MV release and PAR2 activation. TF and fVIIa expression by cancer cells can result in the formation of the TF-fVIIa complex on the cell surface, which in turn promotes PAR2 auto-activation, and enhances

PAR2-initiated signalling (Ungefroren et al., 2017). The cDNA for PAR2 was cloned and expressed as a hybrid protein, in tandem with either mCherry or mEmerald tags. Proteolytic digestion of PAR2 resulted in the release of the fluorescent group into the media, which was measured using a fluorescence plate reader. Cell lines that expressed relatively high levels of TF, such as BxPC-3 and MDA-MB-231, showed a high percentage of PAR2 activation and high levels of MV release. In contrast, cell lines with low TF expression levels demonstrated low PAR2 activation and released fewer MV, in agreement with previous studies (Ettelaie et al. 2016). Therefore, these findings support the hypothesis that cells attempt to dispose of excess cellular TF by releasing it within MV, which may otherwise become detrimental (Figure 6.1). Accumulation of TF by endothelial cells has been shown previously to promote cell apoptosis (Ethaeab et al. 2019; Elkeeb et al. 2015).

Earlier studies by the group have on the whole concentrated on the examination of MV release as a result of PAR2 activation by an exogenous stimulus, such as PAR2-AP or trypsin (Ettelaie et al., 2012; Collier and Ettelaie, 2011; Das et al., 2018; Featherby et al., 2019). The released MV carry content that is derived from source cells and therefore mediates a range of outcomes on the surrounding tissue. Vascular endothelial cells are amongst the cells with the greatest exposure to any circulating MV (Lovren and Verma, 2013), therefore this study examined the influence of cancer cell-derived MV on the activation of PAR2, present on the surface of HCAEC. MV carrying high ratios of fVIIa:TF were more efficient in activating PAR2 in recipient endothelial cells as expected. Therefore, it is proposed that the amount of fVIIa and TF carried by MV also determines the rate of PAR2 activation. Furthermore, consistent with this hypothesis, MV purified from the 786-O cell line, which carry low concentrations of fVIIa but high TF levels, demonstrated low potential for PAR2 activation in endothelial cells. These results further demonstrate that both fVIIa and TF levels contribute to the potential of cancer cell-derived MV to activate PAR2 in recipient cells.

In turn, the amount of fVIIa and TF present on the surface of the cells determines the ability of the cells to regulate the TF with which the cells come into contact. Consequently, given the significant differences in MV from various sources the analysis of circulating MV in patients with diabetes, hypertension, myocardial infarction, or cancers may potentially provide new disease biomarkers (Badimon et al., 2017; Silambanan et al., 2019; Atehortúa et al., 2019). For example, high levels of circulating procoagulant MV are thought to cause endothelial dysfunction (Boulangier et al., 2001; Badimon et al., 2017; Silambanan et al., 2019) leading to endothelial denudation and atherosclerotic disease conditions (Davignon and Ganz, 2004; Atehortúa et al., 2019).

A second possible mechanism of coping with excess TF appears to involve endocytosis by the cells. Although MV release is sufficient to dispose of lower concentrations of cell-surface TF, it appears that a secondary TF clearance mechanism involving caveolar endocytosis is utilised in response to higher TF concentrations. Following prolonged exposure of cells to TF, as during chronic inflammatory diseases, the depletion of fVII reserves may result in excess TF that cannot be cleared by releasing MV, thereby initiating the alternative cellular mechanism involving endocytosis through caveolae. Several studies have shown that MV-associated TF can be endocytosed by recipient cells such as endothelium (Collier et al., 2013; del Conde et al., 2005; Osterud and Bjorklid, 2012). As well as being a source of fVII, caveolae can harbour proteins, including TF (Mandal et al., 2005; Awasthi et al., 2006). Furthermore, Mandal et al. (2005) reported that the internalised TF in fibroblasts was functionally inactive, suggesting that the association of TF with caveolin-1 may result in storage of TF in an encrypted form that is devoid of either procoagulant or signalling activities. To examine the hypothesis that the caveolar endocytosis mechanism facilitates further TF clearance, the association of TF with caveolin-1 in HCAEC was examined. PLA and other microscopy co-localisation studies showed the concentration-dependent association between exogenous TF and caveolin-1, as

well as with cholesterol rich membranous lipid rafts which occurred within 40 min of addition. This is in agreement with the data reported by Awasthi et al. (2006) who showed the co-localisation of cellular TF with cholesterol rich domain. Moreover, Mandal et al. (2005) earlier reported that the internalisation of TF by fibroblasts requires the complex formation between TF and fVIIa.

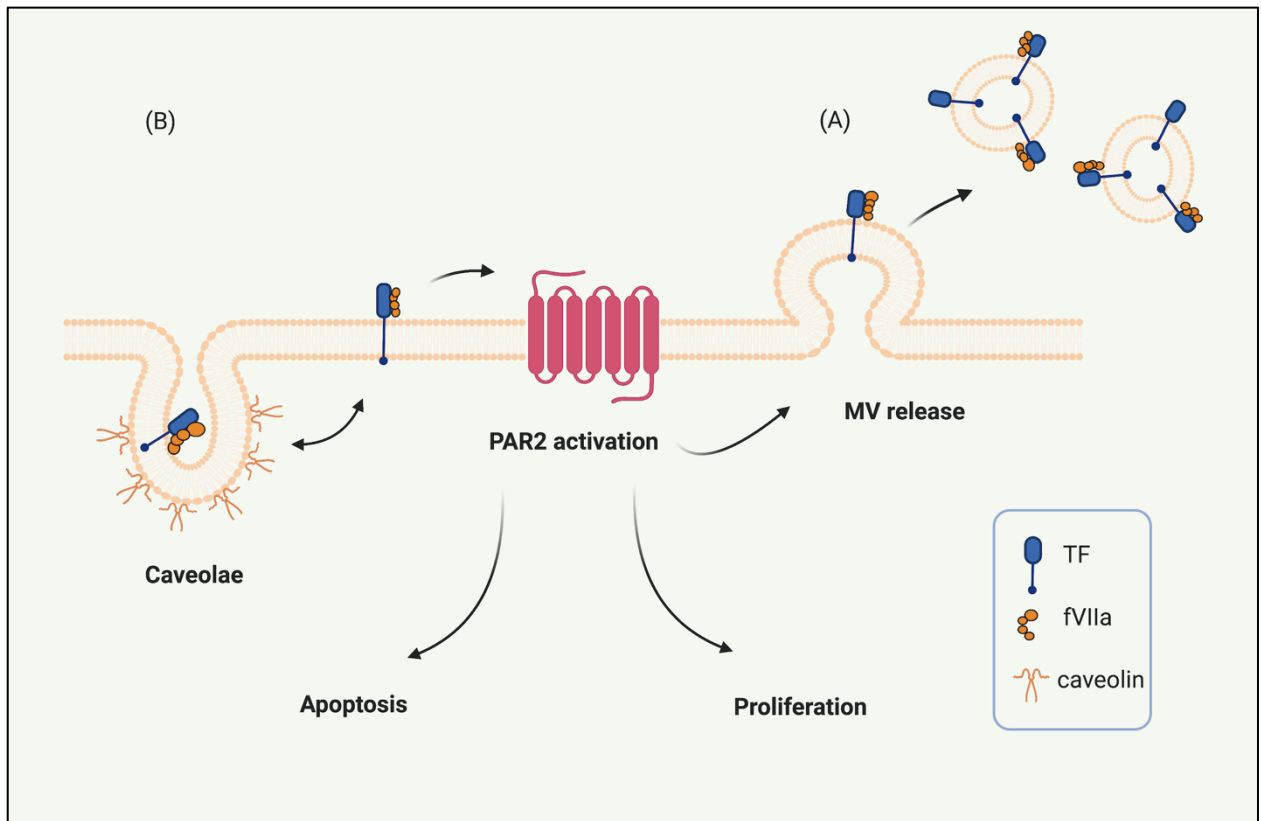
As stated above, fVII may associate with caveolae (Mandal et al., 2005; Awasthi et al., 2006), which could explain the rapid exposure of fVII following stimulation of cells with exogenous TF (Figure 3.22). Analysis of resting HCAEC by PLA further indicated the association of fVII with the caveolae. This association was significantly reduced after incubation of the cells with recombinant TF for 10 min. Interestingly, the association of fVII with caveolae recovered following addition of 2 or 4 U/ml TF, but not 0.5 U/ml TF (Figure 5.8). Therefore, these findings suggest that fVII is released from caveolae on the cells upon contact with TF activating PAR2 and the releasing the fVIIa-TF complex within MV. However, at higher concentrations of TF, the second mechanism is initiated and the excess TF which cannot be released within the MV is returned as the fVIIa-TF complex to the caveolae to be retained in a latent form. To explore the consequences of preventing the clearance of TF from the cell surface, caveolae were disrupted in HCAEC using M β CD before the addition of recombinant TF. Previously, Dietzen et al. (2004) demonstrated that the removal of cholesterol from the cell membrane enhanced the procoagulant activity of TF. Pre-treatment of cells with M β CD before the addition of recombinant TF resulted in a concentration-dependent reduction in cell numbers compared to treatment with recombinant TF alone (Figure 5.14). Therefore, upon disruption of caveolae, high concentrations of cell surface TF remaining active on the cell surface, together with enhanced PAR2 signalling, are likely to promote cellular apoptosis. Therefore, the caveolae mediated internalisation of TF acts as alternative mechanism to counter both the procoagulant and the pro-apoptotic effects of TF on cells (Figure 6.1).

During normal physiological conditions, the body responds to injury by releasing TF in order to initiate clotting and preventing blood loss, which is crucial for homeostasis and cell repair. In addition, cells regulate the excess amount of cell-surface TF through either MV release, or by endocytosis. However, in disease conditions, repeated exposure to MV-associated TF (Boulangier et al., 2001; Badimon et al., 2017) overwhelms the ability of cells to regulate TF by depleting the fVII from the cells which then, results in the retention of TF on the cell surface. This in turn promotes both cell death and thrombosis. The outcomes of the exaggerated TF activities are clearly manifested in cardiovascular diseases as the enhanced denudation of endothelium and promotion of myocardial infraction (Steffel et al., 2006), and also in the promotion of VTE in cancer patients (Manly et al., 2011). Although this study clearly demonstrated two separate mechanisms by which cells deal with excess amount of TF, the effectiveness and relative contribution of each was not determined. The maximal levels of MV release by a panel of cancer cell lines was determined to be approximately 30 min following PAR2 activation (Ettelaie et al., 2016). In addition, the co-localisation of TF within caveolae/lipid rafts appeared to occur at 40 min post-stimulation. Similarly, Collier et al. (2013) demonstrated a reduction in TF activity on the surface of endothelial cells at 30 min as a result of TF being endocytosed. Collectively, it may be speculated that the mechanism of MV release may precede those of endocytosis. However, the similarity in timeframes of these mechanisms suggests a concurrent initiation of the regulation of cell-surface TF. Additional experiments based on blocking each mechanism separately would be needed to clarify the effectiveness, inter-dependence and importance of each mechanism. Furthermore, a study of the alterations in the resultant signalling mechanisms arising from the release, or endocytosis of TF may be discerning in the understanding of differences that lead to the promotion of cell apoptosis or proliferation. Finally, since the mechanisms of proliferation and apoptosis both involve the activation of PAR2 and the activities of TF and fVIIa on cell surface, it will be of interest to

investigate the difference in cell signalling arising from excess TF, that promote either progress through cell cycle or alternatively its arrest. Such studies can be carried out by examining the activities of various cell cycle regulators and pro-apoptotic proteins, as before (Pradier and Ettelaie, 2007; Frentzou et al, 2010).

In conclusion, the results from this study propose the existence of two distinct mechanisms of regulation of active TF levels on the cell surface (Figure 6.1). The incorporation and release of TF within MV appears to be the primary means of disposing of excess TF. This process is dependent on activation of PAR2 which itself requires the formation of a complex between fVIIa and TF. This process is affected by the amounts of fVIIa and MV available to the cell. The alternative mechanism clears unreleased TF through caveolae-mediated endocytosis in a manner that is also dependent on TF-fVIIa complex formation. Although cells respond to acute exposure to TF through these mechanisms, cells exposed to TF over prolonged periods in chronic inflammatory conditions exhaust their ability to manage TF activity. This can impair cellular function, as is the case for vascular endothelial cell denudation in chronic disease.

Figure 6. 1 Postulated cellular mechanisms for the management of excess TF



Cells can use either of two mechanisms to manage cell-intrinsic excess TF or TF endocytosed from the extracellular environment. The first mechanism is the release of TF within MV, which requires PAR2 activation (A). The second mechanism is the localisation and encryption of TF within caveolae/lipid rafts (B). The fVIIa:TF ratio influences the degree of PAR2 activation and determines the induction of cell proliferation or apoptosis. The figure was created using BioRender.com

Chapter 7

References

References

- Abdulkadir, S., Carvalhal, G., Kaleem, Z., Kisiel, W., Humphrey, P., Catalona, W. and Milbrandt, J. (2000) Tissue factor expression and angiogenesis in human prostate carcinoma. *Human Pathology*, 31(4), 443-447.
- Abid Hussein, M., Nieuwland, R., Hau, C., Evers, L., Meesters, E. and Sturk, A. (2005) Cell-derived microparticles contain caspase 3 in vitro and in vivo. *Journal of Thrombosis and Haemostasis*, 3(5), 888-896.
- Åberg, M., Edén, D. and Siegbahn, A. (2020) Activation of β 1 integrins and caveolin-1 by TF/FVIIa promotes IGF-1R signaling and cell survival. *Apoptosis*, 25(7-8), 519-534.
- Agrawal, N., Dasaradhi, P. V., Mohammed, A., Malhotra, P., Bhatnagar, R. K. and Mukherjee, S. K. (2003) RNA interference: biology, mechanism, and applications. *Microbiol Mol Biol Rev*, 67(4), 657-85.
- Aguilar, R. and Wendland, B. (2005) Endocytosis of membrane receptors: two pathways are better than one. *Proceedings of the National Academy of Sciences*, 102(8), 2679-2680.
- Aharon, A., Tamari, T. and Brenner, B. (2008) Monocyte-derived microparticles and exosomes induce procoagulant and apoptotic effects on endothelial cells. *Thrombosis and Haemostasis*, 100(05), 878-885.
- Akinmolayan, A., Goodall, A. and Collier, M. (2016) Comparison of tissue factor expression in adult and foetal endothelial cells in response to inflammatory cytokines. *Atherosclerosis*, 244, e4.
- Alberts, B., Wilson, J. and Lewis, J. (2002) *Molecular Biology of the Cell*. 4th ed. New York: Garland Science.
- Albrecht, S., Kotzsch, M., Siegert, G., Luther, T., Grossmann, H., Grosser, M. and Müller, M. (1996) Detection of circulating tissue factor and factor VII in a normal population. *Thrombosis and haemostasis*, 75 (5), 772-777.
- Anderson, R. G., Kamen, B. A., Rothberg, K. G. and Lacey, S. W. (1992) Potocytosis: sequestration and transport of small molecules by caveolae. *Science*, 255(5043), 410-411.
- Antoniak, S., Sparkenbaugh, E., Tencati, M., Rojas, M., Mackman, N. and Pawlinski, R. (2013) protease activated receptor-2 contributes to heart failure. *PLoS ONE*, 8(11), e81733.
- Arora, P., Ricks, T. and Trejo, J. (2007) Protease-activated receptor signalling, endocytic sorting and dysregulation in cancer. *Journal of Cell Science*, 120(6), 921-928.
- Atehortúa, L., Rojas, M., Vásquez, G., Muñoz-Vahos, C., Vanegas-García, A., Posada-Duque, R. and Castaño, D. (2019) Endothelial activation and injury by microparticles in patients with systemic lupus erythematosus and rheumatoid arthritis. *Arthritis Research & Therapy*, 21(1).

- Auwerda, J., Yuana, Y., Osanto, S., de Maat, M., Sonneveld, P., Bertina, R. and Leebeek, F. (2011) Microparticle-associated tissue factor activity and venous thrombosis in multiple myeloma. *Thrombosis and Haemostasis*, 105(01), 14-20.
- Awasthi, V., Mandal, S., Papanna, V., Rao, L. and Pendurthi, U. (2006) Modulation of Tissue Factor-Factor VIIa Signaling by Lipid Rafts and Caveolae. *Blood*, 108(11), 1744-1744.
- Awasthi, V., Rao, L. and Pendurthi, U. (2004) Modulation of tissue Factor-Factor VIIa coagulant and signaling functions by membrane cholesterol and caveolae. *Blood*, 104(11), 2627-2627.
- Badimon, L., Suades, R., Arderiu, G., Peña, E., Chiva-Blanch, G. and Padró, T. (2017) Microvesicles in Atherosclerosis and Angiogenesis: from bench to bedside and reverse. *Frontiers in Cardiovascular Medicine*, 4.
- Baran, J., Baj-Krzyworzeka, M., Weglarczyk, K., Szatanek, R., Zembala, M., Barbasz, J., Czupryna, A., Szczepanik, A. and Zembala, M. (2009) Circulating tumour-derived microvesicles in plasma of gastric cancer patients. *Cancer Immunology, Immunotherapy*, 59(6), 841-850.
- Batool, S., Abbasian, N., Burton, J. and Stover, C. (2013) Microparticles and their roles in inflammation: A Review. *The Open Immunology Journal*, 6(1), 1-14.
- Bastiani, M. and Parton, R. (2010) Caveolae at a glance. *Journal of Cell Science*, 123(22), 3831-3836.
- Baugh, R. and Krishnaswamy, S. (1996) Role of the activation peptide domain in human factor X activation by the extrinsic xase complex. *Journal of Biological Chemistry*, 271(27), 16126-16134.
- Belting, M., Ahamed, J. and Ruf, W. (2005) Signaling of the Tissue Factor Coagulation Pathway in Angiogenesis and Cancer. *Arteriosclerosis, Thrombosis, and Vascular Biology*, 25(8), 1545-1550.
- Benelhaj, N., Maraveyas, A., Featherby, S., Collier, M., Johnson, M. and Ettelaie, C. (2019) Alteration in endothelial permeability occurs in response to the activation of PAR2 by factor Xa but not directly by the TF-factor VIIa complex. *Thrombosis Research*, 175, 13-20.
- Bode, M. and Mackman, N. (2014) Regulation of tissue factor gene expression in monocytes and endothelial cells: Thromboxane A2 as a new player. *Vascular Pharmacology*, 62(2), 57-62.
- Bona, R., Lee, E. and Rickles, F. (1987) Tissue factor apoprotein: Intracellular transport and expression in shed membrane vesicles. *Thrombosis Research*, 48(4), 487-500.
- Boulanger, C., Scoazec, A., Ebrahimian, T., Henry, P., Mathieu, E., Tedgui, A. and Mallat, Z. (2001) Circulating microparticles from patients with myocardial infarction cause endothelial dysfunction. *Circulation*, 104(22), 2649-2652.

- Branza-Nichita, N., Macovei, A. and Lazar, C. (2012) Caveolae-dependent endocytosis in viral infection. In *Cereza B (ed)*, Molecular regulation of endo cytosis. IntechOpen.
- Broze, G. J., Jr, and Majerus, P. W. (1980) Purification and properties of human coagulation factor VII. *The Journal of biological chemistry*, 255(4), 1242–1247.
- Burger, D., Schock, S., Thompson, C., Montezano, A., Hakim, A. and Touyz, R. (2013) Microparticles: biomarkers and beyond. *Clinical Science*, 124(7), 423-441.
- Burnier, L., Fontana, P., Kwak, B. and Angelillo-Scherrer, A. (2009) Cell-derived micro-particles in haemostasis and vascular medicine. *Thrombosis and Haemostasis*, 101(03), 439-451.
- Burnouf, T., Chou, M., Goubran, H., Cognasse, F., Garraud, O. and Seghatchian, J. (2015) An overview of the role of micro particles/micro vesicles in blood components: Are they clinically beneficial or harmful?. *Transfusion and Apheresis Science*, 53(2), 137-145.
- Butenas, S. (2012) Tissue Factor Structure and Function. *Scientifica*, 2012, 1-15.
- Butenas, S., Orfeo, T. and Mann, K. (2009) Tissue factor in coagulation. *Arteriosclerosis, Thrombosis, and Vascular Biology*, 29(12), 1989-1996.
- Callander, N., Varki, N. and Vijaya Rao, L. (1992) Immunohistochemical identification of tissue factor in solid tumors. *Cancer*, 70(5), 1194-1201.
- Camerer, E., Gjernes, E., Wiiger, M., Pringle, S. and Prydz, H. (2000) Binding of factor VIIa to tissue factor on keratinocytes induces gene expression. *The Journal of biological chemistry*, 275(9), 6580–6585.
- Camerer, E., Huang, W. and Coughlin, S. (2000) Tissue factor- and factor X-dependent activation of protease-activated receptor 2 by factor VIIa. *Proceedings of the National Academy of Sciences*, 97(10), 5255-5260.
- Campbell, S. M., Crowe, S. M. and Mak, J. (2001) Lipid rafts and HIV-1: from viral entry to assembly of progeny virions. *Journal of clinical virology: the official publication of the Pan American Society for Clinical Virology*, 22(3), 217-227.
- Capozza, F., Williams, T., Schubert, W., McClain, S., Bouzahzah, B., Sotgia, F. and Lisanti, M. (2003) Absence of Caveolin-1 sensitizes mouse skin to carcinogen-induced epidermal hyperplasia and tumor formation. *The American Journal of Pathology*, 162(6), 2029-2039.
- Caruso, R., Pallone, F., Fina, D., Gioia, V., Peluso, I., Caprioli, F., Stolfi, C., Perfetti, A., Spagnoli, L., Palmieri, G., MacDonald, T. and Monteleone, G. (2006) Protease-Activated Receptor-2 Activation in Gastric Cancer Cells Promotes Epidermal Growth Factor Receptor Trans-Activation and Proliferation. *The American Journal of Pathology*, 169(1), 268-278.
- Chao, D. and Korsmeyer, S. (1998) BCL-2 Family: regulators of cell death. *Annual Review of Immunology*, 16(1), 395-419.

- Chapman, H., Allen, C., Stone, O. and Fair, D. (1985) Human alveolar macrophages synthesize factor VII in vitro: Possible role in interstitial lung disease. *Journal of Clinical Investigation*, 75(6), 2030-2037.
- Chen, Y., Huang, L., Qi, X. and Chen, C. (2019) Insulin Receptor Trafficking: Consequences for Insulin Sensitivity and Diabetes. *International Journal of Molecular Sciences*, 20(20), 5007.
- Chen, P., Yang, N., Xu, L., Zhao, F. and Zhang, M. (2019) Increased expression of protease-activated receptors 2 indicates poor prognosis in HBV related hepatocellular carcinoma. *Infectious Agents and Cancer*, 14(1).
- Chen, Y., Li, G. and Liu, M. L. (2018) Microvesicles as Emerging Biomarkers and Therapeutic Targets in Cardiometabolic Diseases. *Genomics Proteomics Bioinformatics*, 16(1), 50-62.
- Cheng, T., Mathews, K. A., Abrams-Ogg, A. C. G. and Wood, R. D. (2009) Relationship between assays of inflammation and coagulation: A novel interpretation of the canine activated clotting time. *Canadian Journal of Veterinary Research*, 73(2), 97-102.
- Cheng, J. and Nichols, B. (2016) Caveolae: One Function or Many?. *Trends in Cell Biology*, 26(3), 177-189.
- Chiba, K., Kawakami, K. and Tohyama, K. (1998) Simultaneous evaluation of cell viability by neutral red, MTT and crystal violet staining assays of the same cells. *Toxicology in Vitro*, 12(3), 251-258.
- Chidlow, J. and Sessa, W. (2010) Caveolae, caveolins, and cavins: complex control of cellular signalling and inflammation. *Cardiovascular Research*, 86(2), 219-225.
- Chinnaiyan, A., O' Rourke, K., Tewari, M. and Dixit, V. (1995) FADD, a novel death domain-containing protein, interacts with the death domain of fas and initiates apoptosis. *Cell*, 81(4), 505-512.
- Christian, A. E., Haynes, M. P., Phillips, M. C. and Rothblat, G. H. (1997) Use of cyclodextrins for manipulating cellular cholesterol content. *Journal of lipid research*, 38(11), 2264-2272.
- Chu, A. (2011) Tissue factor, blood coagulation, and beyond: an overview. *International Journal of Inflammation*, 1-30.
- Cicala, C. (2002) Protease activated receptor 2 and the cardiovascular system. *British Journal of Pharmacology*, 135(1), 14-20.
- Cimmino, G. and Cirillo, P. (2018) Tissue factor: newer concepts in thrombosis and its role beyond thrombosis and hemostasis. *Cardiovascular Diagnosis and Therapy*, 8(5), 581-593.
- Cirillo, P., Cali, G., Golino, P., Calabrò, P., Forte, L., Rosa, S., Pacileo, M., Ragni, M., Scopacasa, F., Nitsch, L. and Chiariello, M. (2004) Tissue factor binding of activated factor VII triggers smooth muscle cell proliferation via extracellular Signal-Regulated kinase activation. *Circulation*, 109(23), 2911-2916.

- Collier, M., Xiao, Y., Maraveyas, A., Mah, P. and Ettelaie, C. (2013) Microparticle-associated tissue factor is recycled by endothelial cells resulting in enhanced surface tissue factor activity. *Thrombosis and Haemostasis*, 110(11), 966-976.
- Collier, M. and Ettelaie, C. (2011) Regulation of the Incorporation of Tissue Factor into Microparticles by Serine Phosphorylation of the Cytoplasmic Domain of Tissue Factor. *Journal of Biological Chemistry*, 286(14), 11977-11984.
- Collier, M. and Ettelaie, C. (2010) Induction of endothelial cell proliferation by recombinant and microparticle-tissue factor involves β 1-Integrin and extracellular signal regulated kinase activation. *Arteriosclerosis, Thrombosis, and Vascular Biology*, 30(9), 1810-1817.
- Collier, M., Ettelaie, C., Goult, B., Maraveyas, A. and Goodall, A. (2017) Investigation of the Filamin A-Dependent mechanisms of tissue factor incorporation into Microvesicles. *Thrombosis and Haemostasis*, 117(11), 2034-2044.
- Collier, M. E., Li, C. and Ettelaie, C. (2008). Influence of exogenous tissue factor on estrogen receptor alpha expression in breast cancer cells: involvement of beta1-integrin, PAR2, and mitogen-activated protein kinase activation. *Molecular Cancer Research*, 6(12), 1807-1818.
- Collier, M., Mah, P., Xiao, Y., Maraveyas, A. and Ettelaie, C. (2013) Microparticle-associated tissue factor is recycled by endothelial cells resulting in enhanced surface tissue factor activity. *Thrombosis and Haemostasis*, 110(11), 966-976.
- Cooper, G. M. (2000) Endocytosis. In Cooper, G. M. (ed). *The Cell: A Molecular Approach* (2nd ed). Sunderland: Boston University. Available online: <https://www.ncbi.nlm.nih.gov/books/NBK9831/> [Accessed 24 April 2020].
- Corrotte, M., Almeida, P., Tam, C., Castro-Gomes, T., Fernandes, M., Millis, B., Cortez, M., Miller, H., Song, W., Mangel, T. and Andrews, N. (2013) Caveolae internalization repairs wounded cells and muscle fibers. *eLife*, 2.
- Coughlin, S. (1999) How the protease thrombin talks to cells. *Proceedings of the National Academy of Sciences*, 96(20), 11023-11027.
- Crilly, A., Palmer, H., Nickdel, M., Dunning, L., Lockhart, J., Plevin, R., McInnes, I. and Ferrell, W. (2012) Immunomodulatory role of proteinase-activated receptor-2. *Annals of the Rheumatic Diseases*, 71(9), 1559-1566.
- Cunningham, M., Romas, P., Hutchinson, P., Holdsworth, S. and Tipping, P. (1999) Tissue factor and factor VIIa receptor/ligand interactions induce pro-inflammatory effects in macrophages. *Blood*, 94(10), 3413-3420.
- Danial, N. N. and Korsmeyer, S. J. (2004) Cell death: critical control points. *Cell*, 116, 205-19.
- Darmoul, D., Gratio, V., Devaud, H. and Laburthe, M. (2004) Protease-activated Receptor 2 in Colon Cancer. *Journal of Biological Chemistry*, 279(20), 20927-20934.

- Das, K., Prasad, R., Roy, S., Mukherjee, A. and Sen, P. (2018) The Protease Activated Receptor2 Promotes Rab5a Mediated Generation of Pro-metastatic Microvesicles. *Scientific Reports*, 8(1).
- Date, K., Hall, J., Greenman, J., Maraveyas, A. and Madden, L. (2013) Tumour and microparticle tissue factor expression and cancer thrombosis. *Thrombosis Research*, 131(2), 109-115.
- Davignon, J. and Ganz, P. (2004) Role of endothelial dysfunction in atherosclerosis. *Circulation*, 109, III27-III32.
- Date, K., Ettelaie, C. and Maraveyas, A. (2017) Tissue factor-bearing microparticles and inflammation: a potential mechanism for the development of venous thromboembolism in cancer. *Journal of Thrombosis and Haemostasis*, 15(12), 2289-2299.
- De Almeida, C. (2017) Caveolin-1 and Caveolin-2 can be antagonistic partners in inflammation and beyond. *Frontiers in Immunology*, 8.
- Del Conde, I., Shrimpton, C., Thiagarajan, P. and López, J. (2005) Tissue-factor-bearing microvesicles arise from lipid rafts and fuse with activated platelets to initiate coagulation. *Blood*, 106(5), 1604-1611.
- Denis, C. (2002) Molecular and Cellular Biology of von Willebrand Factor. *International Journal of Hematology*, 75(1), 3-8.
- Deurs, B., Roepstorff, K., Hommelgaard, A. and Sandvig, K. (2003) Caveolae: anchored, multifunctional platforms in the lipid ocean. *Trends in Cell Biology*, 13(2), 92-100.
- Deveraux, Q. L., Roy, N., Stennicke, H. R., Van Arsdale, T., Zhou, Q., Srinivasula, S. M., Alnemri, E. S., Salvesen, G. S. and Reed, J. C. (1998) IAPs block apoptotic events induced by caspase-8 and cytochrome c by direct inhibition of distinct caspases. *The EMBO Journal*, 17(8), 2215-2223.
- Dietzen, D. J., Page, K. L., and Tetzloff, T. A. (2004) Lipid rafts are necessary for tonic inhibition of cellular tissue factor procoagulant activity. *Blood*, 103(8), 3038-3044.
- Distler, J., Huber, L., Hueber, A., Reich, C., Gay, S., Distler, O. and Pisetsky, D. (2005) The release of Microvesicles by apoptotic cells and their effects on macrophages. *Apoptosis*, 10(4), 731-741.
- Drake, T. A., Morrissey, J. H. and Edgington, T. S. (1989) Selective cellular expression of tissue factor in human tissues. Implications for disorders of hemostasis and thrombosis. *Am J Pathol*, 134(5), 1087-97.
- Echarri, A. and Del Pozo, M. (2015) Caveolae - mechanosensitive membrane invaginations linked to actin filaments. *Journal of Cell Science*, 128(15), 2747-2758.
- Edgington, T., Dickinson, C. and Ruf, W. (1997) The structural basis of function of the TF-VIIa complex in the cellular initiation of coagulation. *Thrombosis and Haemostasis*, 78(01), 401-405.

- Eisenreich, A., Bolbrinker, J. and Leppert, U. (2016) Tissue Factor: A Conventional or Alternative Target in Cancer Therapy. *Clinical Chemistry*, 62(4), 563-570.
- ElKeeb, A., Collier, M., Ettelaie, C. and Maraveyas, A. (2015) Accumulation of tissue factor in endothelial cells induces cell apoptosis, mediated through p38 and p53 activation. *Thrombosis and Haemostasis*, 114(08), 364-378.
- Ellinger, I. and Pietschmann, P. (2016) Endocytosis in health and disease- a thematic issue dedicated to Renate Fuchs. *Wiener Medizinische Wochenschrift*, 166(7-8), 193-195.
- Elmore, S. (2007) Apoptosis: A Review of Programmed Cell Death. *Toxicologic Pathology*, 35(4), 495-516.
- Ender, F., Freund, A., Quecke, T., Steidel, C., Zamzow, P., von Bubnoff, N. and Gieseler, F. (2019) Tissue factor activity on microvesicles from cancer patients. *Journal of Cancer Research and Clinical Oncology*, 146(2), 467-475.
- Enjeti, A., Lincz, L. and Seldon, M. (2008) Microparticles in Health and Disease. *Seminars in Thrombosis and Hemostasis*, 34(07), 683-691.
- Erlich, J., Fearn, C., Mathison, J., Ulevitch, R. J. and Mackman, N. (1999) Lipopolysaccharide induction of tissue factor expression in rabbits. *Infect Immun*, 67(5), 2540-6.
- Escolar, G., Lopez-Vilchez, I., Diaz-Ricart, M., White, J. and Galan, A. (2008) Internalization of tissue factor by platelets. *Thrombosis Research*, 122, S37-S41.
- Ethaeb, A., Mohammad, M., Madkhali, Y., Featherby, S., Maraveyas, A., Greenman, J. and Ettelaie, C. (2019) Accumulation of tissue factor in endothelial cells promotes cellular apoptosis through over-activation of Src1 and involves β 1-integrin signalling. *Apoptosis*, 25(1-2), 29-41.
- Ettelaie, C., Collier, M., Featherby, S., Benelhaj, N., Greenman, J. and Maraveyas, A. (2016) Analysis of the potential of cancer cell lines to release tissue factor-containing microvesicles: correlation with tissue factor and PAR2 expression. *Thrombosis Journal*, 14(1).
- Ettelaie, C., Collier, M., Mei, M., Xiao, Y. and Maraveyas, A. (2012) Enhanced binding of tissue factor-microparticles to collagen-IV and fibronectin leads to increased tissue factor activity in vitro. *Thrombosis and Haemostasis*, 109(01), 61-71.
- Fan, L., Yotov, W., Zhu, T., Esmailzadeh, L., Joyal, J., Sennlaub, F., Heveker, N., Chemtob, S. and Rivard, G. (2005) Tissue factor enhances protease-activated receptor-2-mediated factor VIIa cell proliferative properties. *Journal of Thrombosis and Haemostasis*, 3(5), 1056-1063.
- Featherby, S., Madkhali, Y., Maraveyas, A. and Ettelaie, C. (2019) Apixaban suppresses the release of TF-Positive microvesicles and restrains cancer cell proliferation through directly inhibiting TF-fVIIa activity. *Thrombosis and Haemostasis*, 119(09), 1419-1432.
- Feistritzer, C., Lenta, R. and Riewald, M. (2005) Protease-activated receptors-1 and -2 can mediate endothelial barrier protection: role in factor Xa signaling. *Journal of Thrombosis and Haemostasis*, 3(12), 2798-2805.

Fernandes, C., Morinaga, L., Alves, J., Castro, M., Calderaro, D., Jardim, C. and Souza, R. (2019) Cancer-associated thrombosis: the when, how and why. *European Respiratory Review*, 28(151), 180119.

Fernandez, P. M. and Rickles, F. R. (2002). Tissue factor and angiogenesis in cancer. *Current opinion in hematology*, 9(5), 401-406.

Fong, A., Garcia, E., Gwynn, L., Lisanti, M., Fazzari, M. and Li, M. (2003) Expression of Caveolin-1 and Caveolin-2 in Urothelial Carcinoma of the Urinary Bladder Correlates With Tumor Grade and Squamous Differentiation. *American Journal of Clinical Pathology*, 120(1), 93-100.

Fortin, J., Rivard, G., Adam, A., and Marceau, F. (2005) Studies on rabbit natural and recombinant tissue factors: intracellular retention and regulation of surface expression in cultured cells. *American Journal of Physiology-Heart and Circulatory Physiology*, 288(5), H2192-2202.

Frank, P. (2010) Endothelial Caveolae and Caveolin-1 as Key Regulators of Atherosclerosis. *The American Journal of Pathology*, 177(2), 544-546.

Frentzou, G., Collier, M., Seymour, A. and Ettelaie, C. (2010) Differential induction of cellular proliferation, hypertrophy and apoptosis in H9c2 cardiomyocytes by exogenous tissue factor. *Molecular and Cellular Biochemistry*, 345(1-2), 119-130.

Freyssinet, J. and Toti, F. (2010) Formation of procoagulant microparticles and properties. *Thrombosis Research*, 125, S46-48.

Fulda, S. and Debatin, K. (2006) Extrinsic versus intrinsic apoptosis pathways in anticancer chemotherapy. *Oncogene*, 25(34), 4798-4811.

Gaetani, E., Del Zompo, F., Marcantoni, M., Gatto, I., Giarretta, I., Porfidia, A., Scaldaferrri, F., Laterza, L., Lopetuso, L., Gasbarrini, A. and Pola, R. (2018) Microparticles produced by activated platelets carry a potent and functionally active angiogenic signal in subjects with crohn's disease. *International Journal of Molecular Sciences*, 19(10), 2921.

Gardiner, C., Harrison, P., Belting, M., Böing, A., Campello, E., Carter, B., Collier, M., Coumans, F., Ettelaie, C., van Es, N., Hochberg, F., Mackman, N., Rennert, R., Thaler, J., Rak, J. and Nieuwland, R. (2015) Extracellular vesicles, tissue factor, cancer and thrombosis – discussion themes of the ISEV 2014 Educational Day. *Journal of Extracellular Vesicles*, 4(1), 26901.

Garnier, D., Milsom, C., Magnus, N., Meehan, B., Weitz, J., Yu, J. and Rak, J. (2010) Role of the tissue factor pathway in the biology of tumor initiating cells. *Thrombosis Research*, 125, S44-50.

Ge, L., Shenoy, S., Lefkowitz, R. and DeFea, K. (2004) Constitutive Protease-activated Receptor-2-mediated Migration of MDA MB-231 Breast Cancer Cells Requires Both β -Arrestin-1 and -2. *Journal of Biological Chemistry*, 279(53), 55419-55424.

- Geddings, J. and Mackman, N. (2013) Tumor-derived tissue factor–positive micro-particles and venous thrombosis in cancer patients. *Blood*, 122(11), 1873-1880.
- Gessler, F., Voss, V., Dützmann, S., Seifert, V., Gerlach, R. and Kögel, D. (2009) Inhibition of tissue factor/protease-activated receptor-2 signaling limits proliferation, migration and invasion of malignant glioma cells. *Neuroscience*, 165(4), 1312-1322.
- Göbel, K., Eichler, S., Wiendl, H., Chavakis, T., Kleinschnitz, C. and Meuth, S. (2018) The coagulation factors fibrinogen, thrombin, and factor xii in inflammatory disorders—a systematic review. *Frontiers in Immunology*, 9.
- Grant, B. and Donaldson, J. (2009) Pathways and mechanisms of endocytic recycling. *Nature Reviews Molecular Cell Biology*, 10(9), 597-608.
- Grover, S. and Mackman, N. (2018) Tissue Factor. *Arteriosclerosis, Thrombosis, and Vascular Biology*, 38(4), 709-725.
- Grover, S. and Mackman, N. (2019) Intrinsic pathway of coagulation and thrombosis. *Arteriosclerosis, Thrombosis, and Vascular Biology*, 39(3), 331-338.
- Hadi, H. A., Carr, C. S. and Al Suwaidi, J. (2005) Endothelial dysfunction: cardiovascular risk factors, therapy, and outcome. *Vascular health and risk management*, 1(3), 183-198.
- Hamik, A., Setiadi, H., Bu, G., McEver, R. and Morrissey, J. (1999) Down-regulation of Monocyte Tissue Factor Mediated by Tissue Factor Pathway Inhibitor and the Low Density Lipoprotein Receptor-related Protein. *Journal of Biological Chemistry*, 274(8), 4962-4969.
- Hankins, H., Baldrige, R., Xu, P. and Graham, T. (2014) Role of Flippases, Scramblases and Transfer Proteins in Phosphatidylserine Subcellular Distribution. *Traffic*, 16(1), 35-47.
- Hansen, C. and Nichols, B. (2009) Molecular mechanisms of clathrin-independent endocytosis. *Journal of Cell Science*, 122(11), 1713-1721.
- Hansen, C. G., Howard, G. and Nichols, B. J. (2011) Pacsin 2 is recruited to caveolae and functions in caveolar biogenesis. *Journal of cell science*, 124(Pt 16), 2777-2785.
- Hansen, C. B., Pyke, C., Petersen, L. C. and Rao, L. V. (2001) Tissue factor–mediated endocytosis, recycling, and degradation of factor VIIa by a clathrin-independent mechanism not requiring the cytoplasmic domain of tissue factor. *Blood*, 97(6), 1712-1720.
- Hara, T., Phuong, P., Fukuda, D., Yamaguchi, K., Murata, C., Nishimoto, S., Yagi, S., Kusunose, K., Yamada, H., Soeki, T., Wakatsuki, T., Imoto, I., Shimabukuro, M. and Sata, M. (2018) Protease-Activated receptor-2 plays a critical role in vascular inflammation and atherosclerosis in apolipoprotein E–Deficient mice. *Circulation*, 138(16), 1706-1719.
- Hargett, L. and Bauer, N. (2013) On the origin of micro-particles: from “Platelet Dust” to mediators of intercellular communication. *Pulmonary Circulation*, 3(2), 329-340.
- Hayon, Y., Dashevsky, O., Shai, E., Varon, D. and Leker, R. (2012) Platelet Microparticles Promote Neural Stem Cell Proliferation, Survival and Differentiation. *Journal of Molecular Neuroscience*, 47(3), 659-665.

- Heit, J. A., Silverstein, M. D., Mohr, D. N., Petterson, T. M., O'Fallon, W. M. and Melton, L. J. (2000) Risk factors for deep vein thrombosis and pulmonary embolism: a population-based case-control study. *Arch Intern Med*, 160(6), 809-815.
- Hembrough, T. A., Swartz, G. M., Papathanassiou, A., Vlasuk, G. P., Rote W. E., Green, S. J. and Pribluda, V. S. (2003) Tissue Factor/Factor VIIa Inhibitors Block Angiogenesis and tumor growth through a nonhemostatic mechanism. *Cancer Res*, 63(11), 2997-3000.
- Henley, J., Krueger, E., Oswald, B. and McNiven, M. (1998) Dynamin-mediated Internalization of Caveolae. *Journal of Cell Biology*, 141(1), 85-99.
- Herring, J., McMichael, M. and Smith, S. (2013) Microparticles in Health and Disease. *Journal of Veterinary Internal Medicine*, 27(5), 1020-1033.
- Heuberger, D. and Schuepbach, R. (2019) Protease-activated receptors (PARs): mechanisms of action and potential therapeutic modulators in PAR-driven inflammatory diseases. *Thrombosis Journal*, 17(1).
- Heuberger, D. and Schuepbach, R. (2019) Protease-activated receptors (PARs): mechanisms of action and potential therapeutic modulators in PAR-driven inflammatory diseases. *Thrombosis Journal*, 17(1).
- Hjortoe, G., Petersen, L., Albrektsen, T., Sorensen, B., Norby, P., Mandal, S., Pendurthi, U. and Rao, L. (2004) Tissue factor-factor VIIa-specific up-regulation of IL-8 expression in MDA-MB-231 cells is mediated by PAR-2 and results in increased cell migration. *Blood*, 103(8), 3029-3037.
- Hoffman, M., Goldstein, J. and Levy, J. (2018) The impact of prothrombin complex concentrates when treating DOAC-associated bleeding: a review. *International Journal of Emergency Medicine*, 11(1).
- Hollestelle, M., Geertzen, H., Straatsburg, I., van Gulik, T. and van Mourik, J. (2004) Factor VIII expression in liver disease. *Thrombosis and Haemostasis*, 91(02), 267-275.
- Hoyer, F., Nickenig, G. and Werner, N. (2010) Microparticles-messengers of biological information. *Journal of Cellular and Molecular Medicine*, 14(9), 2250-2256.
- Hron, G., Kollars, M., Weber, H., Sagaster, V., Quehenberger, P., Eichinger, S., Kyrle, P. and Weltermann, A. (2007) Tissue factor-positive microparticles: Cellular origin and association with coagulation activation in patients with colorectal cancer. *Thrombosis and Haemostasis*, 97(01), 119-123.
- Hu, L., Xia, L., Zhou, H., Wu, B., Mu, Y., Wu, Y. and Yan, J. (2013) TF/FVIIa/PAR2 promotes cell proliferation and migration via PKC α and ERK-dependent c-Jun/AP-1 pathway in colon cancer cell line SW620. *Tumor Biology*, 34(5), 2573-2581.
- Hugel, B., Martínez, M. C., Kunzelmann, C. and Freyssinet, J. M. (2005) Membrane microparticles: two sides of the coin. *Physiology*, 20, 22-27.

- Huotari, J. and Helenius, A. (2011) Endosome maturation. *The EMBO Journal*, 30(17), 3481-3500.
- Iablokov, V., Hirota, C., Peplowski, M., Ramachandran, R., Mihara, K., Hollenberg, M. and MacNaughton, W. (2014) Proteinase-activated Receptor 2 (PAR2) decreases apoptosis in colonic epithelial cells. *Journal of Biological Chemistry*, 289(49), 34366-34377.
- Ikeda, O., Egami, H., Ishiko, T., Ishikawa, S., Kamohara, H., Hidaka, H., Mita, S. and Ogawa, M. (2003) Expression of proteinase-activated receptor-2 in human pancreatic cancer: A possible relation to cancer invasion and induction of fibrosis. *International Journal of Oncology*, 22(2), 295-300.
- Indrakusuma, I., Romacho, T. and Eckel, J. (2017) Protease-Activated Receptor 2 Promotes Pro-Atherogenic Effects through Transactivation of the VEGF Receptor 2 in Human Vascular Smooth Muscle Cells. *Frontiers in Pharmacology*, 7.
- Jacobson, M., Weil, M. and Raff, M. (1997) Programmed cell death in animal development. *Cell*, 88(3), 347-354.
- Jaiswal, R., Luk, F., Dalla, P., Grau, G. and Bebawy, M. (2013) Breast cancer-derived microparticles display tissue selectivity in the transfer of resistance proteins to cells. *PLoS ONE*, 8(4), e61515.
- Jiang, P., De Li, S., Li, Z., Zhu, Y., Yi, X. and Li, S. (2018) The expression of protease-activated receptors in esophageal carcinoma cells: the relationship between changes in gene expression and cell proliferation, apoptosis in vitro and growing ability in vivo. *Cancer Cell International*, 18(1).
- Jy, W., Jimenez, J., Mauro, L., Horstman, L., Cheng, P., Ahn, E., Bidot, C. and Ahn, Y. (2005) Endothelial microparticles induce formation of platelet aggregates via a von Willebrand factor/ristocetin dependent pathway, rendering them resistant to dissociation. *Journal of Thrombosis and Haemostasis*, 3(6), 1301-1308.
- Kaksonen, M. and Roux, A. (2018) Mechanisms of clathrin-mediated endocytosis. *Nature Reviews Molecular Cell Biology*, 19(5), 313-326.
- Kask, L., Jorsback, A., Winkvist, M., Alfredsson, J., Ek, B., Bergquist, J. and Siegbahn, A. (2014) Identification of novel downstream molecules of tissue factor activation by comparative proteomic analysis. *Journal of Proteome Research*, 13(2), 477-488.
- Kato, H. (2002) Regulation of functions of vascular wall cells by tissue factor pathway inhibitor. *Arteriosclerosis, Thrombosis, and Vascular Biology*, 22(4), 539-548.
- Kawamoto, T., Ohga, N., Akiyama, K., Hirata, N., Kitahara, S., Maishi, N., Osawa, T., Yamamoto, K., Kondoh, M., Shindoh, M., Hida, Y. and Hida, K. (2012) Tumor-Derived Microvesicles Induce Proangiogenic Phenotype in Endothelial Cells via Endocytosis. *PLoS ONE*, 7(3), e34045.

- Kemball-Cook, G., Johnson, D., Tuddenham, E. and Harlos, K. (1999) Crystal structure of active site-inhibited human coagulation factor VIIa (des-Gla). *Journal of Structural Biology*, 127(3), 213-223.
- Key, N. and Mackman, N. (2010) Tissue Factor and Its Measurement in Whole Blood, Plasma, and Microparticles. *Seminars in Thrombosis and Hemostasis*, 36(08), 865-875.
- Khorana, A., Francis, C., Culakova, E., Kuderer, N. And Lyman, G. (2007) Thromboembolism is a leading cause of death in cancer patients receiving outpatient chemotherapy. *Journal of Thrombosis and Haemostasis*, 5(3), 632-634.
- Kim, J., Shah, P., Tantry, U. and Gurbel, P. (2016) Coagulation Abnormalities in Heart Failure: Pathophysiology and Therapeutic Implications. *Current Heart Failure Reports*, 13(6), 319-328.
- Kirchhofer, D. and Nemerson, Y. (1996) Initiation of blood coagulation: the tissue factor/factor VIIa complex. *Current Opinion in Biotechnology*, 7(4), 386-391.
- Kitazumi, I. and Tsukahara, M. (2010) Regulation of DNA fragmentation: the role of caspases and phosphorylation. *FEBS Journal*, 278(3), 427-441.
- Kleinjan, A., Böing, A., Sturk, A. and Nieuwland, R. (2012) Microparticles in vascular disorders: How tissue factor-exposing vesicles contribute to pathology and physiology. *Thrombosis Research*, 130, S71-S73.
- Kocaturk, B., Van den Berg, Y., Tieken, C., Mieog, J., de Kruijf, E., Engels, C., van der Ent, M., Kuppen, P., Van de Velde, C., Ruf, W., Reitsma, P., Osanto, S., Liefers, G., Bogdanov, V. and Versteeg, H. (2013) Alternatively spliced tissue factor promotes breast cancer growth in a $\beta 1$ integrin-dependent manner. *Proceedings of the National Academy of Sciences*, 110(28), 11517-11522.
- Koizume, S. and Miyagi, Y. (2015) Tissue Factor–Factor VII complex as a key regulator of ovarian cancer phenotypes. *Biomarkers in Cancer*, 7(suppl 2), 1-13.
- Koizume, S., Jin, M., Miyagi, E., Hirahara, F., Nakamura, Y., Piao, J., Asai, A., Yoshida, A., Tsuchiya, E., Ruf, W. and Miyagi, Y. (2006) Activation of cancer cell migration and invasion by ectopic synthesis of coagulation factor VII. *Cancer Research*, 66(19), 9453-9460.
- Kuge, Y., Kume, N., Ishino, S., Takai, N., Ogawa, Y., Mukai, T., Minami, M., Shiomi, M. and Saji, H. (2008) Prominent Lectin-Like Oxidized Low Density Lipoprotein (LDL) Receptor-1 (LOX-1) Expression in Atherosclerotic Lesions Is Associated with Tissue Factor Expression and Apoptosis in Hypercholesterolemic Rabbits. *Biological and Pharmaceutical Bulletin*, 31(8), 1475-1482.
- Kumar, R., Herbert, P. and Warrens, A. (2005) An introduction to death receptors in apoptosis. *International Journal of Surgery*, 3(4), 268-277.
- Kumar, V., Abbas, A., Fausto, N., Robbins, S. and Cotran, R. (2010). *Robbins and Cotran pathologic basis of disease*. 8th ed. Philadelphia: Elsevier Saunders, 118-20.

- Kumari, S., MG, S. and Mayor, S. (2010) Endocytosis unplugged: multiple ways to enter the cell. *Cell Research*, 20(3), 256-275.
- Laemmli, U. (1970) Cleavage of Structural Proteins during the assembly of the head of bacteriophage T4. *Nature*, 227(5259), 680-685.
- Larsen, K., Østergaard, H., Olsen, O., Bjelke, J., Ruf, W. and Petersen, L. (2010) Engineering of Substrate Selectivity for Tissue Factor·Factor VIIa Complex Signaling through Protease-activated Receptor 2. *Journal of Biological Chemistry*, 285(26), 19959-19966.
- Lasne, D., Jude, B. and Susen, S. (2006) From normal to pathological haemostasis. *Can J Anaesth*, 53, S2-11.
- Laude, A. and Prior, I. (2004) Plasma membrane microdomains: Organization, function and trafficking (Review). *Molecular Membrane Biology*, 21(3), 193-205.
- Lee, B. J., Kim, J. H., Woo, S. H., Kim, J. H., Kim, D. H. and Yu, Y.S. (2011) Tissue factor is involved in retinoblastoma cell proliferation via both the Akt and extracellular signal-regulated kinase pathways. *Oncol Rep*, 26(3), 665-670.
- Li, A., Varney M. and Singh, R. K. (2001) Expression of interleukin 8 and its receptors in human colon carcinoma cells with different metastatic potentials. *Clin Cancer Res*, 7(10), 3298-304.
- Liao, W., Feng, L., Zhang, H., Zheng, J., Moore, T. and Chen, D. (2009) Compartmentalizing VEGF-Induced ERK2/1 Signalling in placental artery endothelial cell caveolae: a paradoxical role of caveolin-1 in placental angiogenesis in vitro. *Molecular Endocrinology*, 23(9), 1428-1444.
- Liu, J., Oh, P., Horner, T., Rogers, R. and Schnitzer, J. (1997) Organized endothelial cell surface signal transduction in caveolae distinct from glycosylphosphatidylinositol-anchored protein microdomains. *Journal of Biological Chemistry*, 272(11), 7211-7222.
- Liu, Y. and Mueller, B. (2006) Protease-activated receptor-2 regulates vascular endothelial growth factor expression in MDA-MB-231 cells via MAPK pathways. *Biochemical and Biophysical Research Communications*, 344(4), 1263-1270.
- Livak, K. J. and Schmittgen T. D. (2001) Analysis of relative gene expression data using real-time quantitative PCR and the 2(T) (-Delta Delta C) method. *Methods*, 25 (4), 402-408.
- López-Pedreira, C., Barbarroja, N., Dorado, G., Siendones, E. and Velasco, F. (2006) Tissue factor as an effector of angiogenesis and tumor progression in hematological malignancies. *Leukemia*, 20(8), 1331-1340.
- Loreto, C., La Rocca, G., Anzalone, R., Caltabiano, R., Vespasiani, G., Castorina, S., Ralph, D., Celler, S., Musumeci, G., Giunta, S., Djinic, R., Basic, D. and Sansalone, S. (2014) The role of intrinsic pathway in apoptosis activation and progression in peyronie's disease. *BioMed Research International*, 2014, 1-10.

- Lösche, W., Scholz, T., Temmler, U., Oberle, V. and Claus, R., (2004) Platelet-derived microvesicles transfer tissue factor to monocytes but not to neutrophils. *Platelets*, 15(2), 109-115.
- Lovren, F. and Verma, S. (2013) Evolving Role of Microparticles in the Pathophysiology of Endothelial Dysfunction. *Clinical Chemistry*, 59(8), 1166-1174.
- Luyendyk, J., Sullivan, B., Guo, G. and Wang, R. (2010) Tissue Factor-Deficiency and Protease Activated Receptor-1-Deficiency Reduce Inflammation Elicited by Diet-Induced Steatohepatitis in Mice. *The American Journal of Pathology*, 176(1), 177-186.
- Ma, G., Wang, C., Lv, B., Jiang, Y. and Wang, L. (2019) Proteinase-activated receptor-2 enhances Bcl2-like protein-12 expression in lung cancer cells to suppress p53 expression. *Archives of Medical Science*, 15(5), 1147-1153.
- Macfarlane, S. R., Seatter, M. J., Kane, T., Hunter, G. D. and Plevin, R. (2001) Proteinase-activated receptors. *Pharmacol Rev*, 53, 245-82.
- Mackman, N., Tilley, R. and Key, N. (2007) Role of the Extrinsic Pathway of Blood Coagulation in Hemostasis and Thrombosis. *Arteriosclerosis, Thrombosis, and Vascular Biology*, 27(8), 1687-1693.
- Mandal, S. K., Pendurthi, U. R., and Rao, L. V. (2006) Cellular localization and trafficking of tissue factor. *Blood*, 107(12), 4746-4753.
- Mandal, S. K., Iakhiaev, A., Pendurthi, U. R., and Rao, L. V. (2005) Acute cholesterol depletion impairs functional expression of tissue factor in fibroblasts: modulation of tissue factor activity by membrane cholesterol. *Blood*, 105(1), 153-160
- Mandal, S., Pendurthi, U. and Pendurthi, U. (2006) Cellular localization and trafficking of tissue factor. *Blood*, 107(12), 4746-4753.
- Manly, D., Wang, J., Glover, S., Kasthuri, R., Liebman, H., Key, N. and Mackman, N. (2010) Increased microparticle tissue factor activity in cancer patients with Venous Thromboembolism. *Thrombosis Research*, 125(6), 511-512.
- Manly, D. A., Boles, J., and Mackman, N. (2011) Role of tissue factor in venous thrombosis. *Annual review of physiology*, 73, 515–525.
- Manukyan, D., Von Bruehl, M., Massberg, S. and Engelmann, B. (2008) Protein disulfide isomerase as a trigger for tissue factor-dependent fibrin generation. *Thromb. Res.*, 122(1), 19-22.
- Mettlen, M., Chen, P. H., Srinivasan, S., Danuser, G. and Schmid, S. L. (2018) Regulation of Clathrin-Mediated Endocytosis. *Annual review of biochemistry*, 87, 871-896.
- Martinez, M., Tual-Chalot, S., Leonetti, D. and Andriantsitohaina, R. (2011) Microparticles: targets and tools in cardiovascular disease. *Trends in Pharmacological Sciences*, 32(11), 659-665.

- Martin, S., Tesse, A., Hugel, B., Martínez, M. C., Morel, O., Freyssinet, J. M. and Andriantsitohaina, R. (2004) Shed membrane particles from T lymphocytes impair endothelial function and regulate endothelial protein expression. *Circulation*, 109(13), 1653-1659.
- Maurer-Spurej, E., Larsen, R., Labrie, A., Heaton, A. and Chipperfield, K. (2016) Microparticle content of platelet concentrates is predicted by donor microparticles and is altered by production methods and stress. *Transfusion and Apheresis Science*, 55(1), 35-43.
- Mayor, S., Parton, R. and Donaldson, J. (2014) Clathrin-Independent pathways of endocytosis. *Cold Spring Harbor Perspectives in Biology*, 6(6), a016758-016758.
- McIlwain, D., Berger, T. and Mak, T.W. (2015). Caspase functions in cell death and disease. *Cold Spring Harbor perspectives in biology*, 7 (4).
- McVey, J. (2016) The role of the tissue factor pathway in haemostasis and beyond. *Current Opinion in Hematology*, 23(5), 453-461.
- Meijers, W. and de Boer, R. (2019) Common risk factors for heart failure and cancer. *Cardiovascular Research*, 115(5), 844-853.
- Mellman, I. (1996) Endocytosis and molecular sorting. *Annual Review of Cell and Developmental Biology*, 12(1), 575-625.
- Menzies, K., Mackman, N. and Taubman, M. (2009) Role of Tissue Factor in Cancer. *Cancer Investigation*, 27(sup1), 53-62.
- Michiels, C. (2003) Endothelial cell functions. *J Cell Physiol*, 196(3), 430-43.
- Mirzaahmadi, S., Asaadi-Tehrani, G., Bandehpour, M., Davoudi, N., Tahmasbi, L., Hosseinzadeh, N., Mirzahoseini, H., Parivar, K. and Kazemi, B. (2011) Expression of Recombinant Human Coagulation Factor VII by the Lizard Leishmania Expression System. *Journal of Biomedicine and Biotechnology*, 2011, 1-8.
- Mizrak, A., Bolukbasi, M., Ozdener, G., Brenner, G., Madlener, S., Erkan, E., Ströbel, T., Breakefield, X. and Saydam, O. (2013) Genetically engineered microvesicles carrying suicide mRNA/protein inhibit schwannoma tumor growth. *Molecular Therapy*, 21(1), 101-108.
- Morel, O., Jesel, L., Freyssinet, J. M. and Toti, F. (2011) Cellular mechanisms underlying the formation of circulating microparticles. *Arteriosclerosis, Thrombosis, and Vascular Biology*, 31(1), 15-26.
- Morel, O., Jesel, L., Freyssinet, J. and Toti, F. (2011) Cellular Mechanisms Underlying the Formation of Circulating Microparticles. *Arteriosclerosis, Thrombosis, and Vascular Biology*, 31(1), 15-26.
- Morel, O., Morel, N., Freyssinet, J. and Toti, F. (2008) Platelet microparticles and vascular cells interactions: A checkpoint between the haemostatic and thrombotic responses. *Platelets*, 19(1), 9-23.

- Morel, O., Toti, F., Bakouboula, B., Grunebaum, L. and Freyssinet, J. (2006) Procoagulant Microparticles: ‘Criminal Partners’ in Atherothrombosis and Deleterious Cellular Exchanges. *Pathophysiology of Haemostasis and Thrombosis*, 35(1-2), 15-22.
- Morel, O., Toti, F., Hugel, B. and Freyssinet, J. (2004) Cellular microparticles: a disseminated storage pool of bioactive vascular effectors. *Current Opinion in Hematology*, 11(3), 156-164.
- Morel, O., Toti, F., Hugel, B., Bakouboula, B., Camoin-Jau, L., Dignat-George, F. and Freyssinet, J. (2006) Procoagulant Microparticles. *Arteriosclerosis, Thrombosis, and Vascular Biology*, 26(12), 2594-2604.
- Morrissey, J. H., Fakhrai, H. and Edgington, T. S. (1987) Molecular cloning of the cDNA for tissue factor, the cellular receptor for the initiation of the coagulation protease cascade. *Cell*, 50 (1), 129-135.
- Morris, D., Ding, Y., Ricks, T., Gullapalli, A., Wolfe, B. and Trejo, J. (2006) Protease-Activated Receptor-2 Is Essential for Factor VIIa and Xa-Induced Signaling, Migration, and Invasion of Breast Cancer Cells. *Cancer Research*, 66(1), 307-314.
- Mulder, A., Smit, J., Bom, V., Blom, N., Ruiters, M., Halie, M., and Van der Meer, J. (1996) Association of smooth muscle cell tissue factor with caveolae. *Blood*, 88(4), 1306-1313.
- Nabi, I. and Le, P. (2003) Caveolae/raft-dependent endocytosis. *Journal of Cell Biology*, 161(4), 673-677.
- Naslavsky, N. and Caplan, S. (2018) The enigmatic endosome – sorting the ins and outs of endocytic trafficking. *Journal of Cell Science*, 131(13), jcs216499.
- Nishida, N., Yano, H., Nishida, T., Kamura, T. and Kojiro, M. (2006) Angiogenesis in cancer. *Vascular health and risk management*, 2(3), 213-219.
- Nixon, S., Carter, A., Wegner, J., Ferguson, C., Floetenmeyer, M., Riches, J., Key, B., Westerfield, M. and Parton, R. (2007) Caveolin-1 is required for lateral line neuromast and notochord development. *Journal of Cell Science*, 120(13), 2151-2161.
- Nomura, S., Ozaki, Y. and Ikeda, Y. (2008) Function and role of Microvesicles in various clinical settings. *Thrombosis Research*, 123(1), 8-23.
- Nunes-Correia, I., Eulálio, A., Nir, S. and Pedroso de Lima, M. C. (2004) Caveolae as an additional route for influenza virus endocytosis in MDCK cells. *Cell Mol Biol Lett*, 9, 47-60.
- Oh, P., McIntosh, D. and Schnitzer, J. (1998) Dynamin at the Neck of Caveolae Mediates Their Budding to Form Transport Vesicles by GTP-driven Fission from the Plasma Membrane of Endothelium. *Journal of Cell Biology*, 141(1), 101-114.
- Omoto, S., Nomura, S., Shouzu, A., Nishikawa, M., Fukuhara, S. and Iwasaka, T. (2002) Detection of monocyte-derived microparticles in patients with Type II diabetes mellitus. *Diabetologia*, 45(4), 550-555.

- Østerud, B. and Bjørklid, E. (2006) Sources of Tissue Factor. *Seminars in Thrombosis and Hemostasis*, 32(01), 011-023.
- Osterud, B. and Bjorklid, E. (2012) Tissue factor in blood cells and endothelial cells. *Front Biosci (Elite Ed)*, 4, 289-99.
- Owens, A. and Mackman, N. (2010) Tissue factor and thrombosis: The clot starts here. *Thrombosis and Haemostasis*, 104(3), 432-439.
- Owens, A. and Mackman, N. (2011) Microvesicles in Hemostasis and Thrombosis. *Circulation Research*, 108(10), 1284-1297.
- Pallister CJ and Watson MS (2010). *Haematology. Scion Publishing*, 336-347.
- Palta, S., Saroa, R. and Palta, A. (2014) Overview of the coagulation system. *Indian Journal of Anaesthesia*, 58(5), 515.
- Parton, R. (2018) Caveolae: Structure, Function, and Relationship to Disease. *Annual Review of Cell and Developmental Biology*, 34(1), 111-136.
- Parton, R. and Howes, M. (2010) Revisiting caveolin trafficking: the end of the caveosome. *The Journal of Cell Biology*, 191(3), 439-441.
- Parton, R. and Simons, K. (2007) The multiple faces of caveolae. *Nature Reviews Molecular Cell Biology*, 8(3), 185-194.
- Pearson, J. (1999) Endothelial cell function and thrombosis. *Best Practice & Research Clinical Haematology*, 12(3), 329-341.
- Pelkmans, L. and Zerial, M. (2005) Kinase-regulated quantal assemblies and kiss-and-run recycling of caveolae. *Nature*, 436, 128-133.
- Pelkmans, L., Bürli, T., Zerial, M. and Helenius, A. (2004) Caveolin-Stabilized Membrane Domains as Multifunctional Transport and Sorting Devices in Endocytic Membrane Traffic. *Cell*, 118(6), 767-780.
- Pepper, M. and Skobe, M. (2003) Lymphatic endothelium. *Journal of Cell Biology*, 163(2), 209-213.
- Perera, L., Darden, T. and Pedersen, L. (1999) Probing the Structural Changes in the Light Chain of Human Coagulation Factor VIIa Due to Tissue Factor Association. *Biophysical Journal*, 77(1), 99-113.
- Piccin, A., Murphy, W. and Smith, O. (2007) Circulating microparticles: pathophysiology and clinical implications. *Blood Reviews*, 21(3), 157-171.
- Pike, A., Brzozowski, A., Roberts, S., Olsen, O. and Persson, E. (1999) Structure of human factor VIIa and its implications for the triggering of blood coagulation. *Proceedings of the National Academy of Sciences*, 96(16), 8925-8930.
- Pongjantarasatian, S., Kadegasem, P., Sasanakul, W., Sa-ngiamsuntorn, K., Borwornpinyo, S., Sirachainan, N., Chuansumrit, A., Tanratana, P. and Hongeng, S. (2019) Coagulant activity of

recombinant human factor VII produced by lentiviral human F7 gene transfer in immortalized hepatocyte-like cell line. *PLOS ONE*, 14(8), e0220825.

Pradier, A. and Ettelaie, C. (2007) The Influence of exogenous tissue factor on the regulators of proliferation and apoptosis in endothelial cells. *Journal of Vascular Research*, 45(1), 19-32.

Pucci, B., Kasten, M., and Giordano, A. (2000) Cell cycle and apoptosis. *Neoplasia*, 2(4), 291-299.

Prandoni, P., Bilora, F., Marchiori, A., Bernardi, E., Petrobelli, F., Lensing, A. W., Prins, M. H. and Girolami, A. (2003) An association between atherosclerosis and venous thrombosis. *The New England journal of medicine*, 348(15), 1435-1441.

Rackov, G., Garcia-Romero, N., Esteban-Rubio, S., Carrión-Navarro, J., Belda-Iniesta, C. and Ayuso-Sacido, A. (2018) Vesicle-Mediated Control of Cell Function: The Role of Extracellular Matrix and Microenvironment. *Frontiers in Physiology*, 9, 651.

Rajendran, P., Rengarajan, T., Thangavel, J., Nishigaki, Y., Sakthisekaran, D., Sethi, G. and Nishigaki, I. (2013) The Vascular Endothelium and Human Diseases. *International Journal of Biological Sciences*, 9(10), 1057-1069.

Ramchandani, D., Unruh, D., Lewis, C., Bogdanov, V. and Weber, G. (2016) Activation of carbonic anhydrase IX by alternatively spliced tissue factor under late-stage tumor conditions. *Laboratory Investigation*, 96(12), 1234-1245.

Rao, L. and Pendurthi, U. (2005) Tissue Factor–Factor VIIa signaling. *Arteriosclerosis, Thrombosis, and Vascular Biology*, 25(1), 47-56.

Rao, L. and Pendurthi, U. (2012). Regulation of tissue factor coagulant activity on cell surfaces. *Journal of Thrombosis and Haemostasis*, 10(11), 2242-2253.

Reed J. C. (2000) Mechanisms of apoptosis. *The American journal of pathology*, 157(5), 1415-1430.

Riewald, M. and Ruf, W. (2001) Mechanistic coupling of protease signaling and initiation of coagulation by tissue factor. *Proceedings of the National Academy of Sciences*, 98(14), 7742-7747.

Rondon, A., de Almeida, V., Gomes, T., Verçoza, B., Carvalho, R., König, S., Rodrigues, J., Mermelstein, C., Versteeg, H. and Monteiro, R. (2018) Tissue factor mediates microvesicles shedding from MDA-MB-231 breast cancer cells. *Biochemical and Biophysical Research Communications*, 502(1), 137-144.

Rothmeier, A. and Ruf, W. (2012) Protease-activated receptor 2 signaling in inflammation. *Seminars in Immunopathology*, 34(1), 133-149.

Rothmeier, A., Liu, E., Chakrabarty, S., Disse, J., Mueller, B., Østergaard, H. and Ruf, W. (2018) Identification of the integrin-binding site on coagulation factor VIIa required for proangiogenic PAR2 signaling. *Blood*, 131(6), 674-685.

- Rubin, O., Delobel, J., Prudent, M., Lion, N., Kohl, K., Tucker, E., Tissot, J. and Angelillo-Scherrer, A. (2013) Red blood cell-derived microvesicles isolated from blood units initiate and propagate thrombin generation. *Transfusion*, 53(8), 1744-1754.
- Ruf, W., Disse, J., Carneiro-Lobo, T., Yokota, N. and Schaffner, F. (2011) Tissue factor and cell signalling in cancer progression and thrombosis. *Journal of Thrombosis and Haemostasis*, 9, 306-315.
- Samad, F. and Ruf, W. (2013) Inflammation, obesity, and thrombosis. *Blood*, 122(20), 3415-3422.
- Savitskaya, M. A. and Onishchenko, G. E. (2015) Mechanisms of apoptosis. *Biochemistry Moscow*, 80, 1393-1405
- Schaffner, F. and Ruf, W. (2008) Tissue factor and protease-activated receptor signaling in cancer. *Seminars in Thrombosis and Hemostasis*, 34(02), 147-153.
- Schaffner, F. and Ruf, W. (2009) Tissue factor and PAR2 signaling in the tumor microenvironment. *Arteriosclerosis, Thrombosis, and Vascular Biology*, 29(12), 1999-2004.
- Schaffner, F., Versteeg, H., Schillert, A., Yokota, N., Petersen, L., Mueller, B. and Ruf, W. (2010) Cooperation of tissue factor cytoplasmic domain and PAR2 signaling in breast cancer development. *Blood*, 116(26), 6106-6113.
- Schaffner, F., Yokota, N. and Ruf, W. (2012) Tissue factor proangiogenic signaling in cancer progression. *Thrombosis Research*, 129, S127-S131.
- Schnitzer, J. E., Oh, P., Pinney, E. and Allard, J. (1994) Filipin-sensitive caveolae-mediated transport in endothelium: reduced transcytosis, scavenger endocytosis, and capillary permeability of select macromolecules. *The Journal of cell biology*, 127(5), 1217-1232.
- Schneider, J., Chromik, A., Uhl, W., Mügge, A. and Bulut, D. (2012) Apoptosis in esophagus and pancreas carcinoma cells induced by circulating microparticles is related to phosphatidyl serine and microparticle-associated caspases. *Medical Oncology*, 29(2), 962-969.
- Sébert, M., Sola-Tapias, N., Mas, E., Barreau, F. and Ferrand, A. (2019) Protease-Activated Receptors in the Intestine: Focus on Inflammation and Cancer. *Frontiers in Endocrinology*, 10.
- Sendoel, A. and Hengartner, M. O. (2014) Apoptotic cell death under hypoxia. *Physiology (Bethesda)*, 29(3), 168-76.
- Sevinsky, J. R., Rao, L. V. M. and Ruf, W. (1996) Ligand-induced protease receptor translocation into caveolae: a mechanism regulating cell surface proteolysis of the tissue factor dependent coagulation pathway. *J Cell Biol*, 293-304.
- Shahbazi, S. and Mahdian, R. (2019) Factor VII Gene Defects: Review of Functional Studies and Their Clinical Implications. *Iranian Biomedical Journal*, 23(3), 165-174.
- Shi, X., Gangadharan, B., Brass, L. F., Ruf, W. and Mueller, B. M. (2004). Protease-activated receptors (PAR1 and PAR2) contribute to tumor cell motility and metastasis. *Molecular cancer research*, 2(7), 395-402.

- Shibata, Y., Hu, J., Kozlov, M. and Rapoport, T. (2009) Mechanisms Shaping the Membranes of Cellular Organelles. *Annual Review of Cell and Developmental Biology*, 25(1), 329-354.
- Shibuya, M. (2011) Vascular Endothelial Growth Factor (VEGF) and Its Receptor (VEGFR) Signaling in Angiogenesis: A Crucial Target for Anti- and Pro-Angiogenic Therapies. *Genes & Cancer*, 2(12), 1097-1105.
- Shinagawa, K., Ploplis, V. and Castellino, F. (2009) A severe deficiency of coagulation factor VIIa results in attenuation of the asthmatic response in mice. *American Journal of Physiology-Lung Cellular and Molecular Physiology*, 296(5), L763-770.
- Shpacovitch, V., Brzoska, T., Buddenkotte, J., Luger, T., Steinhoff, M., Stroh, C., Sommerhoff, C., Ansel, J., Schulze-Osthoff, K. and Bunnett, N. (2002) Agonists of Proteinase-Activated receptor 2 induce cytokine release and activation of nuclear transcription factor κ B in human dermal microvascular endothelial cells. *Journal of Investigative Dermatology*, 118(2), 380-385.
- Shvets, E., Bitsikas, V., Howard, G., Hansen, C. and Nichols, B. (2015) Dynamic caveolae exclude bulk membrane proteins and are required for sorting of excess glycosphingolipids. *Nature Communications*, 6(1).
- Sigmaaldrich. (n.d.). [online] Available at: <https://www.sigmaaldrich.com/technical-documents/protocols/biology/how-pla-works.html> [Accessed 15 Jan. 2020].
- Silambanan, S., Hermes, R., Bhaskar, E. and Gayathri, S. (2019) Endothelial microparticle as an early marker of endothelial dysfunction in patients with essential hypertension: A pilot study. *Indian Journal of Clinical Biochemistry*, 35(2), 245-250.
- Singh, R. K. and Varney, M. (2000) IL-8 expression in malignant melanoma: implications in growth and metastasis. *Histol Histopathol*, 15, 843-849.
- Singh, R., Letai, A. and Sarosiek, K. (2019) Regulation of apoptosis in health and disease: the balancing act of BCL-2 family proteins. *Nature Reviews Molecular Cell Biology*, 20(3), 175-193.
- Sørensen, B., Freskgård, P., Nielsen, L., Rao, L., Ezban, M. and Petersen, L. (1999) Factor VIIa-induced p44/42 Mitogen-activated Protein Kinase Activation Requires the Proteolytic Activity of Factor VIIa and Is Independent of the Tissue Factor Cytoplasmic Domain. *Journal of Biological Chemistry*, 274(30), 21349-21354.
- Sprague, A. and Khalil, R. (2009) Inflammatory cytokines in vascular dysfunction and vascular disease. *Biochemical Pharmacology*, 78(6), 539-552.
- Steffel, J., Lüscher, T. and Tanner, F. (2006) Tissue Factor in Cardiovascular Diseases. *Circulation*, 113(5), 722-731.
- Stenflo, J. (1999) Contributions of Gla and EGF-Like domains to the function of vitamin K-dependent coagulation factors. *Critical Reviews in Eukaryotic Gene Expression*, 9(1), 59-88.

- Su, S., Li, Y., Luo, Y., Sheng, Y., Su, Y., Padia, R., Pan, Z., Dong, Z. and Huang, S. (2009) Proteinase-activated receptor 2 expression in breast cancer and its role in breast cancer cell migration. *Oncogene*, 28(34), 3047-3057.
- Sumpio, B., Timothy Riley, J. and Dardik, A. (2002) Cells in focus: endothelial cell. *The International Journal of Biochemistry & Cell Biology*, 34(12), 1508-1512.
- Suzuki, T., Yamauchi, K., Matsushita, T., Furumichi, T., Furui, H., Tsuzuki, J. and Saito, H. (1991) Elevation of factor VII activity and mass in coronary artery disease of varying severity. *Clinical Cardiology*, 14(9), 731-736.
- Tahir, S. A., Yang, G., Ebara, S., Timme, T. L., Satoh, T., Li, L., Goltsov, A., Ittmann, M., Morrisett, J. D. and Thompson, T. C. (2001) Secreted caveolin-1 stimulates cell survival/clonal growth and contributes to metastasis in androgen-insensitive prostate cancer. *Cancer research*, 61(10), 3882–3885.
- Tamari, T., Brenner, B. and Aharon, A. (2008) Monocyte-derived microparticles and exosomes induce procoagulant and apoptotic effects on endothelial cells. *Thrombosis and Haemostasis*, 100(05), 878-885.
- Tatsumi, K. and Mackman, N. (2015) Tissue Factor and Atherothrombosis. *Journal of Atherosclerosis and Thrombosis*, 22(6), 543-549.
- Thaler, J., Koder, S., Kornek, G., Pabinger, I. and Ay, C. (2014) Microparticle-associated tissue factor activity in patients with metastatic pancreatic cancer and its effect on fibrin clot formation. *Translational Research*, 163(2), 145-150.
- The European Bioinformatics Institute (2019) EMBL-EBI. Available online: <https://www.ebi.ac.uk/> [Accessed 31 Jul. 2019].
- Thiec, F., Cherel, G. and Christophe, O. (2003) Role of the Gla and First Epidermal Growth Factor-like Domains of Factor X in the Prothrombinase and Tissue Factor-Factor VIIa Complexes. *Journal of Biological Chemistry*, 278(12), 10393-10399.
- Thomas, C. and Smart, E. (2008) Caveolae structure and function. *Journal of Cellular and Molecular Medicine*, 12(3), 796-809.
- Thomson, B. J. (2001) Viruses and apoptosis. *International Journal of Experimental Pathology*, 82(2), 65-76.
- Thompson, T., Tahir, S., Li, L., Watanabe, M., Naruishi, K., Yang, G., Kadmon, D., Logothetis, C., Troncoso, P., Ren, C., Goltsov, A. and Park, S. (2009) The role of caveolin-1 in prostate cancer: clinical implications. *Prostate Cancer and Prostatic Diseases*, 13(1), 6-11.
- Tripisciano, C., Weiss, R., Eichhorn, T., Spittler, A., Heuser, T., Fischer, M. and Weber, V. (2017) Different potential of extracellular vesicles to support thrombin generation: contributions of phosphatidylserine, tissue factor, and cellular origin. *Scientific Reports*, 7(1).

- Tsao, B., Fair, D., Curtiss, L. and Edgington, T. (1984) Monocytes can be induced by lipopolysaccharide-triggered T lymphocytes to express functional factor VII/VIIa protease activity. *The Journal of Experimental Medicine*, 159(4), 1042-1057.
- Turner, N. and Moake, J. (2015) Factor VIII Is Synthesized in Human Endothelial Cells, Packaged in Weibel-Palade Bodies and Secreted Bound to ULVWF Strings. *PLOS ONE*, 10(10), p.e0140740.
- Ungefroren, H., Witte, D., Rauch, B., Settmacher, U., Lehnert, H., Gieseler, F. and Kaufmann, R. (2017) Proteinase-Activated receptor 2 may drive cancer progression by facilitating TGF- β signaling. *International Journal of Molecular Sciences*, 18(11), 2494.
- Vadivel, K. and Bajaj, S. P. (2012) Structural biology of factor VIIa/tissue factor initiated coagulation. *Frontiers in bioscience (Landmark edition)*, 17, 2476-2494.
- Van Beers, E., Schaap, M., Berckmans, R., Nieuwland, R., Sturk, A., van Doormaal, F., Meijers, J. and Biemond, B. (2009) Circulating erythrocyte-derived microvesicles are associated with coagulation activation in sickle cell disease. *Haematologica*, 94(11), 1513-1519.
- Van Der Meijden, P., Van Schilfgaarde, M., Van Oerle, R., Renné, T., Ten Cate, H. and Spronk, H. (2012) Platelet- and erythrocyte-derived microvesicles trigger thrombin generation via factor XIIa. *Journal of Thrombosis and Haemostasis*, 10(7), 1355-1362.
- Vanwijk, M., Vanbavel, E., Sturk, A. and Nieuwland, R. (2003) Microparticles in cardiovascular diseases. *Cardiovascular Research*, 59(2), 277-287.
- Vergnolle, N., Hollenberg, M., Sharkey, K. and Wallace, J. (1999) Characterization of the inflammatory response to proteinase-activated receptor-2 (PAR2)-activating peptides in the rat paw. *British Journal of Pharmacology*, 127(5), 1083-1090.
- Verheij, M. and Bartelink, H. (2000) Radiation-induced apoptosis. *Cell Tissue Res*, 301(1), 133-42.
- Versteeg, H. and Ruf, W. (2006) Emerging insights in tissue factor-dependent signaling events. *Seminars in Thrombosis and Hemostasis*, 32(01), 024-032.
- Versteeg, H., Schaffner, F., Kerver, M., Petersen, H., Ahamed, J., Felding-Habermann, B., Takada, Y., Mueller, B. and Ruf, W. (2008) Inhibition of tissue factor signalling suppresses tumor growth. *Blood*, 111(1), 190-199.
- Wali, J., Masters, S. and Thomas, H. (2013) Linking metabolic abnormalities to apoptotic pathways in Beta cells in type 2 Diabetes. *Cells*, 2(2), 266-283.
- Widlansky, M. E., Gokce, N., Keaney, J. F., Jr. and Vita, J. A. (2003) The clinical implications of endothelial dysfunction. *J Am Coll Cardiol*, 42(7), 1149-60.
- Wattanakit, K., Lutsey, P. L., Bell, E. J., Gornik, H., Cushman, M., Heckbert, S. R., Rosamond, W. D., and Folsom, A. R. (2012) Association between cardiovascular disease risk factors and

occurrence of venous thromboembolism. A time-dependent analysis. *Thrombosis and haemostasis*, 108(3), 508-515.

Wilcox, J., Noguchi, S. and Casanova, J. (2003) Extrahepatic Synthesis of Factor VII in Human Atherosclerotic Vessels. *Arteriosclerosis, Thrombosis, and Vascular Biology*, 23(1), 136-141.

Williams, T., Hassan, G., Li, J., Cohen, A., Medina, F., Frank, P., Pestell, R., Di Vizio, D., Loda, M. and Lisanti, M. (2005) Caveolin-1 Promotes Tumor Progression in an Autochthonous Mouse Model of Prostate Cancer. *Journal of Biological Chemistry*, 280(26), 25134-25145.

Williams, J. and Mackman, N., (2012) Tissue factor in health and disease. *Frontiers in Bioscience*, E4(1), 358-372.

Witkowski, M., Landmesser, U. and Rauch, U. (2016) Tissue factor as a link between inflammation and coagulation. *Trends in Cardiovascular Medicine*, 26(4), 297-303.

Wolf, P. (1967) The nature and significance of platelet products in human plasma. *British Journal of Haematology*, 13(3), 269-288.

Wu, Y. (2015) Contact pathway of coagulation and inflammation. *Thrombosis Journal*, 13(1).

Yao, Q., Chen, J., Cao, H., Orth, J., Michael McCaffery, J., Stan, R. and McNiven, M. (2005) Caveolin-1 Interacts Directly with Dynamin-2. *Journal of Molecular Biology*, 348(2), 491-501.

Yang, L., Ma, Y., Han, W., Li, W., Cui, L., Zhao, X., Tian, Y., Zhou, Z., Wang, W. and Wang, H. (2015) Proteinase-activated receptor 2 promotes cancer cell migration through RNA methylation-mediated repression of mir-125b. *Journal of Biological Chemistry*, 290(44), 26627-26637.

Yang, Q., Underwood, M., Hsin, M., Liu, X. and He, G. (2008) Dysfunction of pulmonary vascular endothelium in chronic obstructive pulmonary disease: basic considerations for future drug development. *Current Drug Metabolism*, 9(7), 661-667.

Yau, J., Teoh, H. and Verma, S. (2015) Endothelial cell control of thrombosis. *BMC Cardiovascular Disorders*, 15(1).

Yokota, N., Koizume, S., Miyagi, E., Hirahara, F., Nakamura, Y., Kikuchi, K., Ruf, W., Sakuma, Y., Tsuchiya, E. and Miyagi, Y. (2009) Self-production of tissue factor-coagulation factor VII complex by ovarian cancer cells. *British Journal of Cancer*, 101(12), 2023-2029.

Zelaya, H., Rothmeier, A. and Ruf, W. (2018) Tissue factor at the crossroad of coagulation and cell signaling. *Journal of Thrombosis and Haemostasis*, 16(10), 1941-1952.

Zhang, N., Hartig, H., Dzhagalov, I., Draper, D. and He, Y. (2005) The role of apoptosis in the development and function of T lymphocytes. *Cell Research*, 15(10), 749-769.

Zhao, P., Metcalf, M. and Bunnett, N. (2014) Biased Signaling of Protease-Activated Receptors. *Frontiers in Endocrinology*, 5.

Zwaal, R. and Schroit, A. (1997) Pathophysiologic implications of membrane phospholipid asymmetry in Blood Cells. *Blood*, 89(4), 1121-1132.